

PETROLOGY OF THE SUPRACRUSTAL ROCKS OF BUNDELKHAND MASSIF, BABINA – MAURANIPUR TRANSECT, UTTAR PRADESH

By

Moirangthem Mourdhaja singh



*Forwarded
21/2/04*

THESIS

SUBMITTED FOR THE DEGREE OF

DOCTOR OF PHILOSOPHY

IN

GEOLOGY

OF THE

BUNDELKHAND UNIVERSITY

JHANSI – 284128

INDIA





बुन्देलखण्ड विश्वविद्यालय, झाँसी
BUNDELKHAND UNIVERSITY, JHANSI

B++ (ABOVE 5 STAR) ACCREDITATION BY NAAC (UGC)

झाँसी (उ.प्र.) 284128

DEPARTMENT OF GEOLOGY
INSTITUTE OF EARTH SCIENCES
BUNDELKHAND UNIVERSITY, JHANSI

Certificate

This is to certify that *Shri Moirangthem Mourdhaja Singh*, has worked under supervision on the problem "*Petrology of the supracrustal rocks of Bundelkhand massif, Babina-Mauranipur transect, Uttar Pradesh*" in the Department of Geology, Institute of Earth Sciences, Bundelkhand University, Jhansi. He completed the research work for the full period as prescribed under clause of the Ph.D. ordinance and the thesis embodies the result of his investigation conducted during the period he worked as a Ph.D. research scholar.

(S.P. Singh)
Supervisor

ACKNOWLEDGEMENTS

I take this opportunity to thank all those who helped and guided me to complete this research work.

It is with a profound sense of gratitude and regard that I expressed my utmost, heart felt thanks to my respected supervisor **Prof. S.P. Singh** (Head), Department of Geology, Institute of Earth Sciences and Dean Faculty of Science; who embodies vast knowledge and performed the task of imparting knowledge to me and moulding my future. His sincerity, enthusiasm, tireless encouragements and clear concept of the subject are some of the qualities that had left a permanent impression on me.

Gratitude has no means of expression and I am at a loss of words when I express the feeling of regards and heartfelt thanks for respected **Prof. S. Santosh Kumar**, Department of Geology, Kumaon University, Nainital, whose sense of precision, deep knowledge, long experience and invaluable suggestions has always helped me.

I extend my sincere thanks to **Dr. Abhimanyu Singh**, Lecturer, Department of Environment Science, who gave his time during research work.

Thanks are also extended to **Dr. H.K. Sachan**, Wadia Institute of Himalayan, Geology, Dehradun, and **Dr. Tamil Ghosh**, Instrumentation Centre, Roorkee for carrying out geochemical and microbe analyses

I record to my admiration for the help extended by my department colleagues **Dr. Ram Chandra, Dr. B.C. Joshi, Dr. S.C. Bhatt** and **Dr. V.K. Singh**.

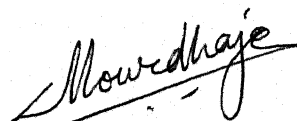
I am also thankful to **Mr. Brajesh Singh**, Dept of Geology, Kumaon University, Nainital who gave time for geochemical data plotting.

I wish to express my heartfelt thanks to my friends, Mr. Aduyat Saxena, Miss Anoobhuti Saxena, Mr. Jitendra Kumar, Saxena, Shiv Kumar, Ms. Yamini Singh, Mr. Shab Singh Yadav and all my department members, for their constant help in various ways to accomplish this research work successfully.

I am sincerely thankful to **Mr. Sumit Kumar** and **Raj Kumar** for typing the script and enhancing the diagrams in computer and giving the final shape to my thesis.

I would be failing in my duty if I do not acknowledge my wife **Smt. Kongbam Chanu Jnanapati** and Madam **Pushpa Singh**, for their continuous inspiration during the research work.

Finally I am highly indebted to my parents for their love, affection and constant inspiration at every moment of my life.



Date :

(Moirangthem Mourdhaja Singh)

CONTENT

	Page
Chapter-I : INTRODUCTION	1-4
1.1 Location and Approach of the Area	4
1.2 Climate and Vegetation	4-5
1.3 Flora and Fauna	5
1.4 A Brief Resume of the Previous Works	5-7
1.5 Nature and Scope of the Present Investigation	8
1.6 Methodology	8-9
Chapter-II : GEOLOGICAL SETTING	10-
2.1 Introduction	10
2.2 Regional Geology	11-
2.3 Bundelkhand Massif Complex (Pre-Bundelkhand Granitoids)	14-
2.3.1 TTG and gneisses	15
2.3.2 Metamorphics of mafic and ultramafic rocks	16
2.3.3 Metasedimentaries	16-1
2.3.3.1 Banded Iron Formation	17
2.3.3.2 Carbonates	17-1
2.3.3.3 Quartzites	18
2.3.3.4 Phyllites and Schist	18
2.4 Acid Magmatism (Bundelkhand Granitoids)	19-2
2.4.1 Hornblende granite/ porphyritic coarse grained granite	19
2.4.2 Biotite granite/porphyritic medium grained granite	20
2.4.3 Foliated biotite granite	20
2.4.4 Coarse grained leucogranite	20-2
2.4.5 Fine grained leucogranite	21
2.5 Post Bundelkhand Granitoids	21-23
2.5.1 Quartz reefs	21-22
2.5.2 Mafic swarms and dykes	22
2.5.3 Bijawar Group	22-23
2.5.4 Vindhyan Supergroup	23
2.5.5 Deccan Traps	23
2.6 Regional Structure	23-26
2.6.1 Structure in migmatite, gneiss, and amphibolite	24
2.6.2 Structures in meta-volcanic and meta-sedimentary rocks	24-25
2.6.3 Structure in granitic and other rocks	25-26
2.7 Regional Stratigraphy	26-28
2.8 Geochronology	28-30
2.9 Geology of the Area	30-39
2.10 Topography and Drainage	30-31
2.11 Rock Types	31-34
2.11.1 TTG, migmatites and biotite gneisses and amphibolites	31
2.11.2 Amphibolites and hornblende-biotite-gneisses	32
2.11.3 Metamorphosed mafics and ultramafics	32
2.11.4 Banded magnitude quartzite	32
2.11.5 Metavolcanics	33
2.11.6 Hornblende granite / gray granite	33
2.11.7 Foliated biotite granite	33

2.11.8	Coarse grain leucogranite	33
2.11.9	Fine grained leucogranite	34
2.11.10	Quartz reefs	34
2.11.11	Dolerite	34
2.12	Structures	34-36
2.12.1	TTG, gneisses and migmatites	34-35
2.12.2	Mafic-ultramafic and banded iron formation rocks	35-36
2.12.3	Granitoids	36
2.12.4	Quartz reefs	36
2.12.5	Dolerite dykes	36
2.13	Mylonites and Shear Zone Structures	37-38
2.13.1	E-W shear zone	37-38
2.13.2	NE-SW shear zone	38
2.14	Lineaments	38
2.15	Faults	38-39
Chapter-III : PETROGRAPHY		40-56
3.1	Older Metamorphic Group (OMG)	40-44
3.1.1	Biotite-gneiss, TTG, migmatite and granite-gneiss	40-43
3.1.2	Amphibolites and biotite-hornblende gneisses	43-44
3.2	Newer Metamorphic Group	44-52
3.2.1	Mafics and ultramafics	44-46
3.2.2	Banded iron formation	46-48
3.2.2.1	Banded- magnetite-quartzite	47
3.2.2.2	Quartzites	47
3.2.3	Metamytonites and metavolcanics	48-52
3.2.3.1	Metamytonites and ultramytonites	48-50
3.2.3.2	Metavolcanics (felsic and mafic)	50-52
3.3	Granitoids	52-55
3.4	Quartz Reefs	55
3.5	Dolerites	55-56
Chapter-IV : GEOCHEMISTRY		57-73
4.1	Introduction	57
4.2	Analytical Methods	57
4.3	Geochemistry	57-73
4.3.1	Geochemistry of granites, migmatites and gneisses	58-65
4.3.1.1	Classification and nomenclature	58-60
4.3.1.2	Tectonic discrimination	60-61
4.3.1.3	Petrogenesis	61
4.3.1.4	Major oxides variation	61-62
4.3.1.5	Trace element geochemistry	62-64
4.3.1.6	Trace element variation	65
4.3.2	Mafic & Ultramafic Rocks	65-73
4.3.2.1	Classification and nomenclature	66-68
4.3.2.2	Tectonic discrimination	68-70
4.3.2.3	Chemical variation of elements	70
4.3.2.4	Major oxides variation	70-72
4.3.2.5	Trace element variation	72-73

Chapter- V : MINERALOGY AND PHASE PETROLOGY	74-86
5.1 Mineralogy	74-79
5.1.1 Electron microprobe technique	74
5.1.2 Sample preparation	74
5.1.3 Advances of EPMA in mineralogy	75
5.1.4 Biotite	75-76
5.1.5 Muscovite	77
5.1.6 Chlorite	77-78
5.1.7 Amphiboles	78-79
5.1.8 Opaque Minerals	79
5.2 Phase Petrology	80-86
5.2.1 Phase relationship in older metamorphic group	81-83
5.2.2 Phase relationships in newer metamorphic group	83-84
5.2.3 Prograde regional metamorphism (M ₂)	84-86
5.2.4 Phase relationship in recrystallised mylonites and metavolcanics	86

Chapter-VI : METAMORPHISM AND EARLY CRUSTAL EVOLUTION	87-95
6.1 Metamorphic Zones	87-89
6.1.1 Chlorite - biotite zone (Lower green schist facies)	88
6.1.2 Almandine zone (Upper green schist facies)	88
6.1.3 Staurolite - almandine zone (Lower amphibolite facies)	88-89
6.2 P-T Conditions	89-90
6.3 Early Crustal Evolution of Bundelkhand Complex	91-95

Chapter-VII : CONCLUSIONS	96-109
REFERENCES	110-124

LIST OF FIGURES

Sl. No.	Plates No.	After Page No.
1.	Fig. 2.1 Location map of the study area.	39
2.	Fig. 2.2 Regional Geology of Bundelkhand Massif.	
3.	Fig. 2.3 Regional tectonic set up and geological and geophysical map of the central India.	
4.	Fig. 2.4 Trend of (a) Quartz Reefs and (b) Mafic Dykes in Bundelkhand.	
5.	Fig. 2.5 Major River trend in Bundelkhand	
6.	Fig. 2.6 Geological map of the Babina-Mauranipur Transect (Study area, District Jhansi, Uttar Pradesh.	
7.	Fig. 2.7 Geological cross-section along X-Y line of the Babina area, western part of the study area.	
8.	Fig. 2.8 Geological cross-section along A-B line of the Mauranipur area, eastern part of the study area.	
9.	Fig. 2.9 Geological cross section along P-Q line of the Dhaurra area, central part of the study area.	
10.	Fig. 4.1 Na ₂ O vs K ₂ O (wt%) plots for gneisses and granites of the study area (Harpum, 1963).	73
11.	Fig. 4.2 (a) Normative An-Ab-Or plots for gneisses of the study area. (After O'Connor, 1965), (b) The normative QAP variation diagram after Le Maitre (1989).	
12.	Fig. 4.3 (a) Normative An-Ab-Or plots for granites of the study area (After O'Connor, 1965), (b) The normative QAP variation diagram after Le Maitre (1989).	
13.	Fig. 4.4 P vs Q diagram for the (a) granites and (b) gneisses of the study area based on Debon and Le Fort (1982).	
14.	Fig. 4.5. (a) A versus B diagram of granites of the study area (After Debon and Le Fort; 1982 and Debon et. al., 1986). (b) A vs B diagram of gneisses of the study area (After Debon and Le Fort; 1982 and Debon et. al., 1986). (c). Shands Index diagram for gneisses of the study area (After Maniar and Piccoli, 1989).	
15.	Fig. 4.6. The chemical classification and nomenclature of granites of the study area using the totals alkali versus silica (TAS) diagram (After Le Maitre et. al. 1989).	
16.	Fig. 4.7 (a) A-F-M diagram plots for the granites (After Irvine and Baragar, 1971) with line separating fields of alkaline and sub alkaline. (b) Total alkali vs Silica diagram for granites of the study area (After Irvine and Baragar 1971).	
17.	Fig. 4.8. Discrimination diagram for the granites of the study are (After Maniar and Piccoli, 1989). (a) SiO ₂ vs K ₂ O, (b) SiO ₂ vs Al ₂ O ₃ , (c) SiO ₂ vs FeO/(FeO+MgO).	

18. Fig. 4.9 Shands Alumina Saturation Index diagram for granites of the study area (After Maniar and Piccoli, 1989).
19. Fig. 4.10 R1 vs R2 multicationic plots of (a) granites and (b) gneisses of the study area (After De La Roche, 1980, Modified by Batchelor and Bowden, 1985).
20. Fig. 4.11 Harker's variation diagrams of SiO_2 vs Na_2O , K_2O , Al_2O_3 , P_2O_5 , CaO , Fe_2O_3 , TiO_2 and MgO for the gneisses of the study area.
21. Fig. 4.12 Harker's variation diagrams of SiO_2 vs Na_2O , K_2O , Al_2O_3 , P_2O_5 , CaO , Fe_2O_3 , TiO_2 and MgO for the granites of the study area.
22. Fig. 4.13. (a) $\text{Al}_2\text{O}_3 - (\text{Na}_2\text{O} + \text{K}_2\text{O} + \text{CaO}) - (\text{FeO} + \text{MgO} + \text{MnO})$ Triangular diagram showing the different modes of magma formation of granites and gneisses of the study area. (b) Rb–Ba–Sr ternary diagram after El-Bouseilly and El-Sokkary (1975) with the distribution of granites of the study area.
23. Fig. 4.14 (a) Rb–Sr (log-log) plots of gneisses and granites with grids for crustal thickness (after Condie, 1973). (b) K–Rb relationship of the gneisses and granites of the study area, after Shaw (1968).
24. Fig. 4.15 Discrimination diagrams for the granites for the study area (After Pearce et. al., 1984).
25. Fig. 4.16 (a) Variation diagram of Normative Orthoclase vs Pb (ppm) for gneisses and granites of the study area. (b) Variation diagram of Sr. (ppm) against model Plagioclase for gneisses and granites of the study area.
26. Fig. 4.17 Harker's variation diagrams of SiO_2 vs Y, Rb, Ba, Sr, Rb/Sr, and Rb/Sr vs Sr. for granites of the study area.
27. Fig. 4.18 Harker's variation diagrams of SiO_2 vs Zr, Nb and TiO_2 vs Zr of granites of the study area.
28. Fig. 4.19 Harker's variation of SiO_2 vs Y, Cu, Rb, Ba, Sr, Rb/Sr and Rb/Sr vs Sr, for gneisses of the study area.
29. Fig. 4.20 Harker's variation diagrams of SiO_2 vs Zr, Ga, Nb, and TiO_2 vs Zr. for gneisses of the study the area.
30. Fig. 4.21 Nomenclature of normal (i.e. non-potassic) igneous rocks from the study area after Cox et. al., (1979).
31. Fig. 4.22 Classification of the mafic and ultramafic rocks based on total alkalis versus silica (TAS), after Le Bas and Streckeisen (1991).
32. Fig. 4.23 (a) The classification of mafic and ultramafic rocks according to their cation percentage of Al, $(\text{Fe}_{\text{total}} + \text{Ti})$ and Mg showing the tholeiite, calc-alkaline and komatiite fields after Jensen, (1976). (b) Major element trending diagram to distinguish continental and oceanic basalts (after Pearce et. al., 1975) shows the maximum concentration of mafic and ultramafic samples of the area in the ocean floor domain.
33. Fig. 4.24 (a) $\text{FeO} - \text{FeO}/\text{MgO}$ variation diagram (Miyashiro and Shido 1975) showing abyssal tholeiite affinity of the mafic and ultramafic rocks of the area. (b) $\text{TiO}_2 - \text{SiO}_2$ variation diagrams (Macdonald & Katsura 1964; Whitehead & Goodfellow 1978) for the mafic and ultramafic rocks of the area. (c) $\text{SiO}_2 - \text{MgO}$ diagram of Redman and Keays

(1985) has been used to classify the mafic and ultramafic rocks of the area.

34. Fig. 4.25 (a) Plot of wt% K_2O versus wt% SiO_2 showing the major subdivision of the island arc volcanics rock suits. (b) Triangular $(Zr + Y) - 100 Ti - Cr$ diagram showing the major differentiation trend of mafics and ultramafic the study area (Davis et. al., 1979).
35. Fig. 4.26 (a) A-F-M diagram plots for the mafic and ultramafics of the study area (after Irvine and Baragar, 1971). (b) Total alkalis vs Silica diagram for mafic and ultramafic rocks of the area with lines separating field of alkaline sub-alkaline (after Irvine and Baragar, 1971).
36. Fig. 4.27 (a) Diagram of Alkali Index (A.I.) versus wt.% Al_2O_3 for the Classification of tholeiitic and high-alumina (calc-alkaline) basalts (after Middlemost 1975). (b) AFM diagram indicates the tholeiitic characters of the mafic and ultramafic rocks of the study area with progressive iron-environment compatible towards tholeiitic trend. (c) $FeO-MgO-Al_2O_3$ diagram (Pearce et. al., 1977) for mafic and ultramafic rocks of the area.
37. Fig. 4.28 (a) K_2O versus Na_2O (wt.%) diagram showing the subdivision of the alkalic magma series into high-K, K, and Na sub-series (Middlemost 1975). (b) Classification of alkalic and sub-alkalic basalts in terms of wt.% Na_2O versus wt.% SiO_2 (after Middlemost, 1975).
38. Fig. 4.29 (a) $Ti/100 - Zr - Y \times 3$ tectonomagmatic discrimination diagram for mafic and ultramafics rocks of the area (after Pearce and Cann, 1973). (b) FeO/MgO vs. TiO_2 diagram (after Jelinek et. al., 1980) for the mafic and ultramafics rocks of the area. (c) Zr/Y vs. Zr diagram (after Pearce and Norry, 1979) showing plots for the mafic and ultramafics rocks of the area.
39. Fig. 4.30 (a). $TiO_2-MnO-P_2O_5$ tectonomagmatic discrimination diagram for mafic and ultramafic rocks of the study area (after Mullen, 1983). (b) $MgO-CaO-Al_2O_3$ triangular diagram for mafics and ultramafics of the study area. (c) SiO_2 vs FeO/MgO variation diagram for mafics and ultramafics of the study area.
40. Fig. 4.31 Plots of the mafic and ultramafics rocks in various discrimination diagrams principally based on immobile minor and trace element. The classification boundaries are as proposed (a) Winchester & Floyd (1977), (b) and (c) Floyd & Winchester (1978) and (d) Pearce & Cann (1973).
41. Fig. 4.32 Harkers variation diagram of SiO_2 vs Na_2O , K_2O , Al_2O_3 , P_2O_5 , CaO , Fe_2O_3 TiO_2 and MgO .
42. Fig. 4.33 (a) Al_2O_3 vs $FeO/(FeO+MgO)$ diagram for mafic and ultramafics rocks of the study area. (b) Alumina vs total alkalis diagram of mafic and ultramafic of studies area.
43. Fig. 4.34 (a) MgO vs CaO , (b) MgO vs FeO (c) $100 \times Mg/(MgO+FeO)$ vs $(Na_2O + K_2O)$ diagram for mafics and ultramafics of the study area.
44. Fig. 4.35 The relation diagram (a) MgO vs Ni and (b) MgO vs Cr for the mafics and ultramafics of the study area (c) Zr/Nb vs Y/Nb diagram for mafics and ultramafics of the study area.

45. Fig. 4.36 Harkers variation diagrams of SiO_2 vs Y, Cu, Rb, Ba, Sr, Rb/Sr and Pb/Sr vs Sr. 73
46. Fig. 4.37 Harkers variation diagrams of SiO_2 vs Zr, Ga, Nb, and TiO_2 vs Zr.
47. Fig. 4.38 Binary plots of (a) Zr vs MgO , (b) Zr vs TiO_2 , (c) Zr vs Ni and (d) Zr vs Y.
48. Fig. 5.1 The EMPA data of the biotite are plotted in the four end member phlogopite, Annite, Siderophyllite and Eastonite. (Deer, Howie and Zussman, 1962). 86
49. Fig. 5.2 The EMPA data of muscovite of investigated area has been shown in Ferrophengite-phengite-muscovite and Ferromuscovite diagram (Deer, Howie and Zussman, 1962).
50. Fig. 5.3 The electron microprobe data of the investigated area are plotted in the amphibole diagram showing the range and composition of amphibole in the $(\text{Na} + \text{K})$ vs Al^{VI} diagram after Leake, (1978).
51. Fig. 5.4 The EPMA data of amphibole from the investigated area is plotted on amphibole diagram (after Leake, 1978).
52. Fig. 5.5 (a) The phase compatibility relation for amphibolites portrayed in ACF diagram. (b) Phase relations for biotite gneisses, tonalite, garnetiferous gneiss and TTG are shown in AKF diagram in the KFMASH system.
53. Fig. 5.6. The phase relation for biotite-hornblende gneisses and amphibolites of OMG group are shown in A'FM projection diagram.
54. Fig. 5.7 (a) Mineral assemblages of coexisting phases of mafics and ultramafics (low- grade metamorphites) are shown in $\text{CaO-MgO-FeO-Al}_2\text{O}_3\text{-SiO}_2\text{-H}_2\text{O}$ (CFMASH) system through ACF diagram (Bowen 1940). (b) The phase relationship for low-grade metamorphosed mafic and ultramafics are shown in ACF diagram.
55. Fig. 5.8 The phase compatibility relations for metamorphosed low- grade schist portrayed in ACF diagrams (a) and (b) in the $\text{CaO-FeO-MgO-Al}_2\text{O}_3\text{-SiO}_2\text{-H}_2\text{O}$ (CFMASH) system.
56. Fig. 5.9 The phase relationship for mylonitised metavolcanics and recrystallised mylonites are shown in (a) ACF diagram (b) AKF diagram, and (c) AFM projection from muscovite.
57. Fig 6.1 P-T conditions diagram showing experimentally determined equilibria to the present study. The triple point and stability of aluminosilicate is after Bohlen et. al., (1991). 95
58. Fig 6.2 A geological cross action along X-Y line of geological map of the investigated area Fig 2.b. The different observed mineral assemblages are shown in pertinent system. The solid circles of the different triangles represent the observed mineral assemblage of the M_1 and M_2 episodes of metamorphism.

LIST OF PLATES

Sl. No.	Plates No.	After Page No.
1-	Field photographs	39
	(a) Gneisses – 1, 2, 3.	
	(b) NMG – 8, 10, 11, 13	
	(c) Granite – 15B, 16	
	(d) Quartz reef – 9, 15A, 17C	
	(e) Shear – 4C, 5, 6, 7, 15B & 15C, 16 A & 16B, 17, 18	
	(f) Fold – 1, 2, 14B	
	(g) Fault – 4, 14C	
	(h) Joints – 14.	
	(i) Gneissic enclave – 12A & 12B	
2-	Micro photographs	56
	(a) Gneisses – II-B & II-C, III, IV	
	(b) Schists – I, II-A, V, VI, VII, VIII, IX, X	
	(c) BMQ – XIII	
	(d) Granite – XI, XII	

LIST OF TABLES

Sl. No.	Plates No.	After Page No.
1.	Table 2.1 Regional Geology of Bundelkhand Craton.	14
2.	Table 2.2 Structures in Bundelkhand massif.	39
3.	Table 2.3 Stratigraphic succession of the Bundelkhand Craton.	
4.	Table 2.4 Radiometric dating of the rocks of Bundelkhand Massif.	
5.	Table 2.5 Relationship between deformation, mesoscopic structure and recrystallization of rocks of the Bundelkhand massif.	
6.	Table 2.6 Tectonothermal activities in the investigated area.	
7.	Table 2.7 Stratigraphy of the area.	
8.	Table 4.1 Major Element Analyses (in wt.%) and CIPW Weight Norms of Granites of study area (Bundelkhand region).	73
9.	Table 4.2 Major Element Analyses (in wt.%) and CIPW Weight Norms of Gneisses of study area (Bundelkhand region).	
10.	Table 4.3 Major Element Analyses (in wt.%) of Mafics and Ultramafics of study area (Bundelkhand region).	
11.	Table 4.4 Trace Element Analyses (in ppm) of Granites of study area (Bundelkhand region).	
12.	Table 4.5 Trace Element Analyses (in ppm) of Gneisses of study area (Bundelkhand region).	
13.	Table 4.6 Trace Element Analyses (in ppm) of Mafics and Ultramafics of study area (Bundelkhand region).	
14.	Table 5.1 Microprobe analyses and structural formulae of Biotite (Granite).	86
15.	Table 5.2 Microprobe analyses and structural formulae of Muscovite.	
16.	Table 5.3 Microprobe analyses and structural formulae of Chlorite.	
17.	Table 5.4 Microprobe analyses and structural formulae of Amphibole.	
18.	Table 5.5 Microprobe analyses and structural formulae of Opaque minerals.	

INTRODUCTION

The knowledge on the assembly, evolution and dispersal of landmasses is one of the fundamental aspect for understanding the continental dynamism and evolutionary history of the earth. The information related to different geological processes, operated within individual continental block in a particular geological time span also provide valuable clues to know the cyclic phenomena of super continents. The sufficient imprints of geological, geochemical, and geochronological and tectonometamorphic events are preserved in the various super continental cycles. These data would be useful in furnishing the evolutionary models of cratonic blocks as well as in correlation of their characters. Apart from this, these evidences may be effectively used for bridging gaps between cratonic blocks and the super continents.

Precambrian shields of the world have become the nerve centers for global research and are meticulously studied by several workers to decipher the early history of the earth. The formation of supracrustal rocks or first landmass is infact an irreversible process in the geological history of earth, which led the processes of initiation of stabilization, continental growth and micro-continent and supra-continental development. The peninsular India is known as one of the prominent Precambrian shield of the world, and is exposed in the south of the Indo-Gangetic alluvial plains. Rogers (1986) divided the peninsular shield into five distinct crustal areas viz. Bhandara, Singhbhum, Aravalli, Easternghat and Dharwar-granulite terrain. Later on they were considered as cartons (Radhakrishna 1989) and have been divided into Eastern Dharwar, Western Dharwar, Bastar, Singhbhum and Bundelkhand-Aravalli Craton. Each craton was perhaps characterized by a central part known as nucleous, which is consisting of extensive outcrop of granite-gneisses and granitoids. These core rocks are commonly associated with large sequences of meta-sedimentaries and meta-volcanics, which were metamorphosed in the low green schist and amphibolite facies. These sequences are represented by common features such as the presence unstratified ultramafic and mafic volcanic rocks showing local acid magmatism, presence of localised-basal oligomietic-polymietic conglomerates and wide occurrence of banded magnetite quartz (BMQ) and cherts in Iron formation. The granite appeared as great batholithic massifs in all cratonic block of Indian shield viz. Closepet granite in the Dharwar, Singhbhum granite in the eastern region, the Bastar granite, the Dongargarh granite of the central India, the Untala, Berach and Gingla granites in Rajasthan and the Bundelkhand granite in Bundelkhand region. These granitoids were found as acidic intrusive in respective cratons. The

relationship of widely exposed older granitoids with the "schistose" formations (metasedimentary and metavolcanic rocks) is a matter of petrological and geochemical interest for exploring the earlier crustal history of earth. The diverse interpretations, and evidences of intrusive relationship characters were matched for the understanding the basement-cover relationship. The recent geochronological data suggest that the bulk of the peninsular crust was perhaps cratonised before 2600 M.a. (Radhakrishna and Naqvi 1986).

The ancient remnants of gneisses and metamorphics (as old as 3400 M.a.) are now being identified from various places in peninsular region. The geochronological and geochemical studies further reveal that the extensive crust-forming event was possibly completed before the 3400 M.a. (Mid. Archaean), which led to evolve the formation of the peninsular gneissic basement (Mahadevan, 1994). The Central Indian shield witnessed two Precambrian orogenic phases between 2600-2000 M.a. and 2000-1600 M.a. The early Proterozoic mobile belt and middle Proterozoic mobile belt were evolved around the early formed supra crusts (>3400Ma) respectively during these orogenic events (Radhakrishna and Naqvi, 1986). Rogers et al (1986) have faced difficulties in solving the existing facts regarding origin of Indian shield (1) whether the peninsular India became a coherent crustal block by accretion of separate cratons along orogenic joins and/or (2) whether it underwent intracratonic orogeny and rifting of a previously coherent shield (super cratons).

Our knowledge about above two basic concepts and regarding crustal evolutionary history of Indian shield is still very meager. Rock types having special petrotectonic significance and related to deep crustal processes have to identify and needed for evaluation. A discrepancy has been found in furnishing the genetic model of cratonic rocks. On the other hand the ultramafic and mafic rocks have association with metamorphics and TTG instead of anorthosites, alkaline rocks and lamprophyres. Contrary to this the charnockitic rocks and granulites were observed to be associated with mafic and ultramafics. These concepts have a special significance in establishment of genetic model and tectonic environment for the evolution of cratonic blocks. The early Archaean komatiites and associated tholeiites have importance inferring the composition of Archaean mantle source areas (Viljoen and Viljoen, 1970). Ultramafic-mafic rocks seem to have widely varying significance and many of them have been found likened to ophiolitic suites. Therefore they can be considered to represent tectonically oceanic crust obducted in many areas.

The Bundelkhand massif occupying an area of 26,000sq.km. lies between 24°N to 27°N latitude and 77°30' E to 81°24' E longitude. The entire massif is dominated by

batholiths of acidic magmatism. The schists and banded iron formations from Baraitha basin of this massif was first reported by Medlicott (1859). Subsequently, Mallet (1869) has also noticed gneisses in this massif. Later on, Mathur (1954), Saxena (1961), Prakash et al; (1975), Mishra and Sharma (1974), Basu (1986), Sarkar et al. (1996), Shukla and Pati (1999), Prasad et al; (1999) Mondal et al; (2002) and several workers have recognized various types of schists and gneisses as lensoidal bodies within the granitic massif. Unfortunately, no significant attempt has been made to study the metamorphic history of schists and gneisses with reference to crustal evolution of Bundelkhand craton. The geophysical investigations suggest that granite massif is widely composed in the northeast and northwest region below the alluvium and in also the southern extremities below the Bijawar and Vindhyan (Shastri et al 1971; Rao, 1968, Banerjee 1987 and Verma and Banerjee 1992). The Bouguer Anomaly Map of India (NGRI, Hyderabad, GPH/5, 1975) shows that the southern contact of the Bundelkhand granite massif with Bijawar and Vindhyan rocks, is marked by steep gravity gradient (Fig 2.3). It envisaged that there might be a sympathetic development of rifting along the Son-Narmada lineament. The northern margins of this craton covered by the Ganga-Yamuna alluvium, exhibit a very gentle gravity gradient. The E-W trend of gneissic foliation in the Bundelkhand massif continues westward and possibly joins with the Berach Granite of Rajasthan before being truncated by the NE-SW Aravalli and Delhi trend. Aeromagnetic study also reveals that the ovoid and elliptical shaped anomaly zones of low intensity are characterized by the Bundelkhand massif where, enclaves of metasedimentary and metabasic rocks are marked by the anomaly zones of contrasting patterns and higher intensity (Gupta and Bhattacharya 1991). Therefore, the current research findings about Bundelkhand craton are only confined to the magmatic evolution of acidic magma (2500M.a.). The crustal evolution and magmatic activities in Bundelkhand in the light of recent researches are still unknown, whereas, significant researches have been carried out on these objectives in Singhbhum, Bastar, Rajasthan and Dharwar cratons. Not only this, a geochronostratigraphic and tectonothermal setup has also been established in these cratons by several workers. Recently, a tectonic model has been proposed for the evolution of Satpura orogenic belt and Central cratonic shield by Basu (2001).

According to Radhakrishna (1989), the junction between the early Proterozoic magmatic terrains (northern Bundelkhand and the southern Bundelkhand terrain) and the southern peninsular terrain is delineated by Central Indian Tectonic Zone (CITZ). This view was partially accepted by Yedekar et.al. (1990). They suggested that the two ancient cratonic blocks represented by Bundelkhand Protocontinent (B.P.) and Deccan Protocontinent (D.P.) (middle to Late Archaean) were separated by a narrow intercratonic basin, which is not existing today, but is marked by the Central Indian Shear (CIS).

Recently, Sharma (2000) has generalised the evolutionary model of Bundelkhand craton with the help of limited geochemical, geochronological and field data. Sarkar et.al. (1996) reported the occurrence trondhjemitic rocks of mid-Archaeon from the Bundelkhand cratonic block in Central Indian shield.

1.1 Location and Approach of the Area

The study area belonging to the northern part of Bundelkhand complex, lies between 78°25'E to 79°10'E longitudes and 25°10'N to 25°20'N latitudes in Jhansi district. The detail geological and structural studies have been carried-out by enlarging the toposheets (No.54K/7, 54K/8 54K/11, 54K/12, 54K/15, 54K/16,540/3 and 540/4) of survey of India.

Jhansi town can be easily approached as it is situated on the main railway line between Delhi to south Indian states via Mathura, Agra, and Gwalior. From Jhansi a metalled road called Jhansi-Lalitpur road (NH26) passes through Babina. Babina is 27km from Jhansi and is the western end of the transect, Mauranipur the eastern end of the transect is on the Jhansi-Khajuraho road and is 60km, from Jhansi.

1.2 Climate and Vegetation

The Bundelkhand region exhibits a particular type of climate and is characterized by excessive heat during the summer months and mild cold during the winter. Thus the Bundelkhand falls under tropical semi-arid climate. During the summer season, high temperature in plain causes low-pressure areas, which includes movement of monsoon. The temperature begins to rise in last week of February and reaches the maximum 50° C in May-June. The hot breeze locally known as 'loo' is common during this period. The normal mean monthly maximum temperature has been recorded as 45.7°C while the peak maximum temperature of 50°C and the lowest temperature of 3°C (Jan.) has been recorded. The best time for the fieldwork in Bundelkhand is from October to February.

The rainfall distribution pattern is irregular. Most of all the rainfall (approximately 90%) is caused by the summer monsoon, falling from June to October in the region. The annual precipitation in Bundelkhand varies from 90cm to 100cm. The region gets the maximum rainfall during the months of July and August.

Northwestern areas of the Bundelkhand region receives nearly 90cm while in southeastern areas receives 120cm. (mean annual rainfall). There is scant winter rainfall in this region. April and November are the driest months of the year.

The soils are generally found shallow to medium depth attaining a thickness ranging from a few cms to as much as 15cm. The thicker sections are being invariably contains a mixture of residual and transported soils. Reddish soils, grayish black soils and yellowish black soils locally known as Rakar, Parwa, Mar and Kabar soils respectively are the important soils have been developed in this region. The latter two appears to be a mixture of lateritic and residual soil over the igneous rocks.

1.3 Flora and Fauna

The important floras of the Bundelkhand region are timber, tendu, mango macca, neem, peepal, bargad, palash and babool. The wood of semal and mango tree in used for matchsticks, tendu for 'bidi' making, khair for preparing katha, gum is also prepared from babool tree. The therapeutic plants such as Rajjia, sprintine and usaka are used in blood pressure (hypertension) and lungs problems.

The major fauna of Bundelkhand region are present as lion, leopard, bear, elephant, neelgai, deer, cheetal, fox, jackal and rabbit etc. and also birds like parrot, koyal, neelkhanth, crow, eagle, vulture etc.

1.4 A Brief Resume of the Previous Works

Bundelkhand craton constitutes various type of rocks ranging from early Archaean to late Proterozoic. It forms the northern part of the Indian peninsular shield, which occupies an area of 26,000 Km². It is flanked by Bijawar and Vindhyan basins in the south and southeastern part, Aravalli ranges in the west and Gangetic alluvium situated in the north and northeastern part.

The first geological account of the Bundelkhand region was given by Medlicott (1859). He described schist and banded iron formations at Barata (Baraitha) in the southwestern part of the massif. Further Wilson (1873-74) has prepared geological map of several parts of the massif but no report is yet available. Mallet (1869) has reported the gneisses and prominent quartz veins in the massif. Hacket (1870) worked mainly in the northwestern part of massif and discussed the detailed geology of the Gwalior and its adjoining areas.

After a long gap, in early forties Chatterjee (1941-42), Mehta (1944-45), Krishnaswamy (1945-46), Roychowdhary (1947-48) and Srivastava (1951-52) all from geological survey of India, worked in different parts of the massif for the search of mineral resources, as mentioned by Basu (Basu1986).

Mishra (1948) has critically reviewed the petrological diversities of the granitic rocks in the massif. Pascoe (1950) first time proposed the regional stratigraphy of Bundelkhand area and opined that the region comprising of crystalline and volcano-sedimentary rocks of Archaean age. These rock units have been designated as "Bundelkhand Granite", "Mahroni Schist", Bijawar series", and "Vindhyan system". Jhingran (1958) summarized the works of geological survey of India and recognized ten types of granite. He also reported the gneisses, quartz reefs, basic dykes, serpentine rocks and various xenoliths in granitoids present in the massif.

Mathur (1954) and Saxena (1961) worked on the petrological evolution of granitoids of the massif. According to them granites are the products of granitisation of intensively deformed and pre-existing metamorphosed sediments. Apart from amphibolites, migmatites, coarse-grained pegmatitic granites, aplites and quartz veins from the Kabrai area. Saxena (1961) have described various types of schist including garnetiferous-muscovite schist and quartzite. Chatterjee et al (1971) proposed a chronostratigraphic sequence of Jhansi-Lalitpur region based on geochronological data provided by Crawford (1970).

Prakash et.al (1975) studied the stratigraphy of the south -western part of the massif, which was mainly confined to Girar-Sonrai area. Mishra and Sharma (1974) carried out detailed work on the stratigraphic and structural setup of the north-central part of the massif. Their classification can be correlated with the works carried out by Prakash et.al (1975). They divided the Bundelkhand sequence into four formations:-

- (1) Kuriacha Formation of high grade metamorphic rocks (equivalent to the Rajaula Formation of Prakash et. al 1975)
- (2) Palar Formation of low-grade metamorphic rocks.
- (3) The Bundelkhand granite and
- (4) The Bundelkhand basic intrusive

Mishra and Sharma (1974) also discussed the petrochemistry of the Bundelkhand Granites and classified them into two groups viz., K-poor granite and K-rich granite. Alam and Zainuddin (1981) reported three types of granite – coarse-grained biotite granite, spotted granite and fine-grained granite in this massif near Mahoba.

Basu (1986) compiled the earlier works along with data of his decadal work and proposed a comprehensive geological and stratigraphic model of economically enriched area of Bundelkhand. Bhattacharya (1985 and 86) explored his investigations on deformation as structures in older metamorphic rocks. He emphasized that the folds

evolved in a particular generation are confined to certain fields. Radhakrishna (1989) outlined Central Indian Tectonic Zone (CITZ), which encompasses the SONATA belt. In his model CITZ marks the tectonic junction between the two early Proterozoic magmatic terrains-the northern Bundelkhand terrain and the southern peninsular terrain. Sarkar et al (1984,1989,1990,1995,1996) gave a detailed account of the geochronology and petrology of this massif. They dated the granitoids and high grade metamorphic rocks of this region and suggested three kinds of granitoids (1) gray granodiorite (2.5Ga), (2) pink leucogranite (2.35Ga) and (3) fine grained regarded as leucogranite (2.27Ga) while high-grade gneisses of Baghora are genetically very old crustal material (3.5Ga).

Roday and his co-workers (1990,1993,1995) worked on kinematics and strain transitions along shear zones and proposal a model for emplacement of quartz reefs along sheer zones in Bundelkhand massif. They described the genetics of numerous sigmoidal tensile fissures produced due to effect of E-W trending sinistral brittle-ductile shears. The inhomogeneous stresses were dominated in the quartz reefs, which emerged as principal tectonic fabric in granitic massif of the central Indian Craton. Pati and Mamgain (1996) observed some orbicular structures in the granites while Shukla and Pati (1999) noted few high-grad metamorphic rocks as enclaves in the granitoids exposed in the north of Babina. Pati and Raju (2001) discussed komatiite type basalt in the great massif. Sharma and Rahman (1995,1996) described the geochemistry and the early Archaean to Palaeoproterozoic crustal growth of the Bundelkhand craton. According to them, the evolutionary history of Bundelkhand craton (early Archaean to Palaeoproterozoic periods) is evidently supported by the occurrences of trondhjemitic gneiss, amphibotites, quartzites, banded iron formation, schists, marble and calc-silicate rocks. Mondal 1995, Mondal and Zainuddin (96,97) and Mondal et al (1998, 2002) have carried out excellent works on geochemistry and geochronology of granites and gneisses of the Bundelkhand massif. According to them, the emplacement of granitoids possibly took place before 2.5Ga within the gneisses of Kuraicha (dated 3.29Ga old and represent the oldest rock unit in the massif). Zainuddin et al (1992), and Mondal et al (2002) described genetically five different types of calc-alkaline granites. They inferred that the emplacement of granitoids appeared as a consequence of collision tectonics. Prasad et al (1999) made on significant attempts to describe the metavolcanics and matasedimentary sequences in this massif. They have critically described the deformation pattern in gneisses and correlated them with the structures found in metavolcanics and sedimentaries.

1.5 Nature and Scope of the Present Investigation

The Archaean-gneisses are broadly characterized by tonalite trondhjemite granodioritic (TTG) in nature. Their geochemistry envisages that the TTG constitutes a significant component, which demarks the existence of an older micro-continent on the earth (Taylor and Mc Lennan 1985, Martin; 1993). The TTG suite has been recently recorded in few Indian localities viz. Kabbaldurga, Champua-Onlajori, Kaptipada, Bonani, Orissa; Gorur-Hassan, Karnataka; Anmod Ghat, Goa; Jhamar Kotra, Rajasthan; Markampara, Bastar, M.P; Baghora, Bundelkhand, U.P. The chronological data suggests that the whole rock isochron age of these TTG ranges from 3000-3500 Ma in the Indian peninsula. These TTG are often associated with low to medium grade metamorphic rocks. These metamorphics are mafic to ultramafic in nature and invariably interbedded with BMQ and ferruginous quartzite. In the present studies, the author is keen to furnish an innovative evolutionary model for evolution of cratonic crust by analyzing huge geochemical, geological data of gneisses, metamorphosed mafics and ultramafics and volcanosedimentary and granitoids rocks of the region. In the proposed investigated area the TTG appear in the form of raft while the banded iron formation are showing an angular relationship with TTG and biotite gneisses. The granitoids have emerged as intrusive in these two rocks. The radiometric data of these gneissic rocks yield 3.5 Ga for TTG, 2.5-2.4Ga for granitoids (Sarkar et al; 1996). However no studies have been carried out for the metamorphic evolution of TTG and banded iron formation as well as metapelites and quartzites. Recently, Sharma (2000) described these rocks are associated with Archaean gneisses of greenstone belt. Keeping this in view, it is thought that the present area has sufficient scope for the petrological studies of these rocks, especially in framing the petrogenic and evolutionary model of Bundelkhand craton.

1.6 Methodology

A brief account of the geological work that has been carried out under present studies in the field as well as in the laboratory is summarized as under:

- (i) A detailed geological mapping on the enlarged toposheet ((No.54K/7, 54K/8 54K/11, 54K/12, 54K/15, 54K/16,540/3 and 540/4) has been carried out and the emphasis is given to the transect zone of iron formation and biotite gneisses and tonalitic gneisses (TTG).
- (ii) A detailed structural mapping at the contact of iron formation and tonalitic gneisses has also been done.

-
- (iii) Based on the available radiometric and regional structural and geological data, a tectonothermal event and geochronostratigraphy has been proposed for the first time.
 - (iv) The textural relationship and reaction texture of different rocks with reference to crystallization, deformation and time relationship has been carried out.
 - (v) Mineral chemistry and involved phase relationship has been discussed in the different pertinent system for the first time.
 - (vi) The metamorphic reactions involved in the formation of different mineral assemblages were discussed through graphical presentation and chemographic relationship in the different pertinent system of ACF, AKF, and AFM diagrams.
 - (vii) Chemical analysis of rocks of petrological interest was analysed. The factual data were effectively used to infer the petrogenesis, tectonic environment and evolution of Mid Archaean crust.
 - (viii) Geothermometry were applied to estimate the P-T conditions of metamorphism.

On the basis of above data recorded in the field as well as in the laboratory, painstaking efforts have been made for retracing the petrogenic and evolutionary history of Bundelkhand cratonic rocks.

CHAPTER- II

GEOLOGICAL SETTING

2.1 Introduction

The 'Bundelkhand massif', the northern part of Indian Peninsula, occupies an area of about 26,000km². It lies between 24° 11' N to 27° 27' N latitude and 77° 30' E to 81° 24' E longitude and covers the southern parts of Uttar Pradesh and the northeastern parts of Madhya Pradesh. Bundelkhand massif comprises different types of crystalline rocks viz. igneous and metamorphic along with the quartz reefs, very low-grade metasedimentaries and mafic dykes swarm (Basu 1986).

Geographically maximum area of Bundelkhand massif is covered by different variety of granites. This acid magmatism was very profound and has almost diminished the earlier geological records. Therefore it is very difficult to describe the geology of the fragile part of Archaean geology in general. On the basis of extensive acid magmatism the Bundelkhand massif has been classified into three events viz. Pre-Bundelkhandgranitoids, Bundelkhand acid magmatic rocks, and Post-Bundelkhand granitoids in the present study.

Contrasting lithounits and polyphase deformational signatures depict a complex geological history of this massif. The relics of the signatures of Pre-Bundelkhandgranitoids are occasionally preserved as a small to large lensoidal bodies within the Bundelkhand granitoids (Basu; 1986, Roday et al; 1995 and Prasad et al; 1999). Geochemical, petrological and structural studies (Basu; 1986, 2001, Mondal et al; 1995, 96, 97, Sarkar et al; 1995 and Sharma; 1998) reveal that there are some oldest crustal components in the Bundelkhand. The present investigated area has a unique place in the massif where Pre-Bundelkhandgranitoid rocks are well exposed.

Lithologically, the study area comprises gneisses, banded-magnetite-quartzite, quartzite, talc-mica schist, chlorite schist, and ferruginous quartzite, ultramafics and volcanosedimentary sequences. Granitoids are the most widely exposed rocks in the area and have an intrusive relation with above litho-units. Quartz reefs trending NE-SW are mainly associated with pink granitoids. Banded-magnetite-quartzite trending in E-W is present as isolated patches of hillock (Plate 8) that has been used as marker band in the present study. Beside this, tonalitic-gneisses occur in the form of raft has been also used as marker band in the present study area. The mylonitised granites, granitoids and pegmatites are exposed at several places as enclave in the pink granite.

2.2 Regional Geology

Bouguer gravity anomaly map prepared by Verma and Banerjee (1992), modified by Jain et al. (1995), a cross section along the Gwalior-Malanjkhand (Fig2.3) revealed that both Bundelkhand and Malanjkhand granite terrain (Baster craton) show low gravity; the northwestern part of the Bundelkhand shows gradual rise in gravity and maximum reached below the Sindh river section mainly covered by alluvium and large masses of basic rocks. Gravity over the Bijawar basin is considerably high, as the high gravity is slightly offset towards the northern margin of the basin. It is presumed that basic rocks invade the shoulder of the rift. Gravity below the Mahakoshal belt is remarkably high though a little offset to the south. It can be envisaged by the reverse North Narmada Fault dipping south / SSE (Basu 2001). There is a small high gravity in the central part of the Vindhyan basin. Mishra et al (2000) recorded high Bouguer gravity anomaly of large wavelength over the Satpura Mountain, suggesting high-density material below the mountain.

The Bundelkhand craton consists mainly of granitoids, migmatites, gneisses, and low-grade metamorphics. The craton is delineated from Aravalli-Rajasthan craton by Great Boundary Fault (GBF) in the west (Agarwal et al; 1995, Basu 2001, Mondal et al; 2002) and is delineated from Bastar and Chhotanagpur craton by EW trending Son Narmada Lineament (SNL) in the south and southeast (Basu; 2001, Banerjee et al; 1987, Verma and Banerjee; 1992, Valdiya; 1982). The northern boundary of this massif is probably deep faulted but extends into the Indo-Gangetic plain and is covered by recent alluvium (Khan et al 1996).

In this massif, the E-W trending low-grade and high-grade metamorphics viz. amphibolites, fuchsite quartzites, banded-magnetite-quartzite, schists, tremolite-chlorite schist, calc-silicates, garnet-sillimanite gneisses, tonalite-trondhjemitic-granodiorite (TTG) rocks has been recorded as sporadic bodies at the low land areas and are profusely intruded by less deformed granitoids (Prakash et al; 1975, Basu; 1986, Sharma 2000, Prasad et al; 1999). The major petrological episodes of late Archean to early Proterozoic is marked by the granite activities, which in fact has diminished all earlier litho-units. Due to subsequent tectonic activities continuous erosion caused the removal of upper part of early-formed crust, thus the geological signature in the massif is very limited. The recent geochronological data (Sarkar et al 1996, Mishra et al; 1998, and Mondal et al; 2002) and polyphase deformation and metamorphism pointed out that various phases of thermal activities have also taken place in North and South of Son-Narmada Lineament

and affected the Bundelkhand craton as well as Baster craton (Fig2.3). Only few patches of older relics are identified and mapped by the earlier workers.

Medlicot (1859) gave the first geological accounts of Bundelkhand area. He described schist and banded iron formations at Baraitha in the southwestern part of the massif and also recorded amphibolites and greenstone at Baraitha and Girar areas. Some gneisses and prominent quartz veins in the massif were reported by Mallet (1869) from the southern part of the massif. Chatterjee (1941-42), Mehata (1944-45), Krishnaswamy (1945-46), Chowdhury (1947-48) and Srivastava (1951-52) of Geological Survey of India carried out geological mapping and preliminary mineral investigations in several parts of the Bundelkhand massif, as mentioned by Basu (Basu 1986).

Mishra (1948) describes the petrological diversities of the granitic rocks of the massif. Mathur (1954) discussed the petrological evolution of the massif as products of granitisation of pre-existing intensively disturbed and metamorphosed sediments. Jhingran (1958) summarized the granite-gneisses of the various parts of the massif. He also described the numerous bodies of hornblende-chlorite-schist and quartz-amphibolite schist at Kuraicha. Saxena (1961) also described various schists including amphibolites, migmatites, coarse-grained pegmatitic granites, aplites, and quartz veins from Kabrai. Prakash et al; (1975) studied the stratigraphy of the massif in southwestern part of the Bundelkhand massif. According to them Archaean sedimentary-volcanic sequence (Rajaula Formation) is followed by the sediments (Berwar Formation), culminated by the emplacement of Bundelkhand granite block in the north, and the fracturing ultrabasic intrusion, Bijawar sedimentation, basic intrusions and lava flows in the granitic block of south.

Mishra and Sharma (1974) described the stratigraphy and structure of the north central part of the massif. They also described the petrochemistry of the Bundelkhand granites, and classified them into (i) Potassium poor and (ii) Potassium rich granites.

Sharma (1982) described the petrography and structure in various parts of the massif. According to him Bundelkhand complex comprises metasediments, meta-acid volcanics, granites and basic rocks and also suggested that schist, amphibolites, quartzites and migmatites exposed in the Saprar river section (near Mauranipur) are the oldest rocks in the Bundelkhand.

Prasad et al (1999) described the metavolcanic and metasedimentary sequences viz. migmatitic orthogneisses, amphibolites, schists, metabasalts, BIF and felsic volcanic-plutonic rocks in the north central part of the massif. Shukla and Pati (1999) also observed some older enclaves viz. hornblende-biotite schist, diorite, amphibolite, hornblende

tonalite, crystalline limestone, quartzite, biotite-gneiss, and migmatite-gneiss in the Bundelkhand massif from Bijouli (Jhansi). Pati and Mamgain (1996) reported orbicular granite around Banda for the first time.

Zainuddin et al (1992) carried out the detailed fundamental work on the Bundelkhand granitoids and identified five different phases of granites from the massif. According to them hornblende granite is the oldest phase followed by foliated biotite granite. Porphyritic biotite granite is intrusive into foliated biotite granite. Coarse-grained leucogranite has intruded into porphyritic biotite granite and the youngest fine-grained leucogranite is intrusive into all the older types of granites. On the other hand, three types of granitoids, viz. hornblende, biotite and leuco-granitoid have been identified within the massif on the basis of mineralogy (Mondal et al; 2002).

Bijawar outcrops occur sandwiched between Bundelkhand complex in the north and Vindhyan rocks to the south. The rocks of the Bijawar Group are exposed in the type area near Bijawar. In general Bijawars forms a monoclinical south dipping unit with flat, open WSW-plunging folds in the eastern part (Banerjee 1982). The Bijawar basin extends for about 80 km in ENE-WSW direction and the rocks are exposed in the form of a broad synclinorium over the basement of Bundelkhand granite-gneiss complex. In the south, Vindhyan Supergroup of rocks overlies Bijawar group of rocks. Kumar et al; (1990) revised the stratigraphy of Bijawar Group rocks proposed by the different earlier workers (Wilson; 1873-74, Mathur; 1960, Mani; 1969 and Haldar and Ghosh; 1981). According to them the Bijawar Group is divided into two subgroups- (i) the lower Moli Subgroup, which comprises sandstone, volcanic traps, chert, breccia, conglomerate and dolomite and (ii) the upper Gangu Subgroup which comprises ferruginous breccia, shale, sandstone, phosphorite, sandstone and quartzite.

Towards northwest of Bundelkhand massif, the lower-Proterozoic Gwalior Group of sedimentary rocks are exposed. The main rock type around Gwalior city is made up of shales, sandstones, cherts, conglomerates and grits and has been considered equivalent to Bijawar Group.

The Vindhyan supergroup covers an area of 104,000 km² in central India, forming a vast semicircle and envelops about half of the outcrop of Bundelkhand complex. The Vindhyan Supergroup of rocks overlies the Bundelkhand complex in SE, S and SW sides. The Vindhyan Supergroup constitutes an unmetamorphosed column of calcareous, arenaceous and argillaceous sediments. The lower part of the supergroup is made up of calcareous and argillaceous sediments while the upper part on the other hand is made up of arenaceous rocks of estuarine or fluvial origin.

All these rocks discussed above have left enough imprints of different episodes of magmatism, metamorphism, sedimentation and deformations. The Bundelkhand granitoids are nearly unmetamorphosed except the NE-SW trending quartz reefs and E-W trending shear zones. Therefore, it can be concluded that the metamorphic rocks present as lensoidal body within the granitoids received metamorphism and deformation before the granitic activities. Further Bijawar Group followed by Vindhyan Supergroup and Deccan volcanics, which exposed in the southern part of the massif overlay these rocks and are devoid from the NE-SW trending quartz reefs and also from NW-SE trending mafic dykes. This inference points that the Bundelkhand granitoid rocks have received at least two phases of deformation prior to the deposition of Bijawar Group and Vindhyan Supergroup. But little attention has been given for the relationship of metamorphics of different grade as well as with deformations, and different thermal activities occurred so far. In the present work emphasis will be given in time relationship with metamorphism and crystallization of the different metamorphic rocks, which were deformed and metamorphosed before the great batholith of Bundelkhand granitoids.

The Regional geology of the Bundelkhand craton has been presented as follows:

Table 2.1 : Regional Geology of Bundelkhand Craton

Post-Bundelkhand rocks	Deccan Traps Vindhyan Supergroup Bijawar and Gwalior Group Mafic Dykes and Swarms Quartz Reef
Syn Bundelkhand granitoids (Acidic Magmatism)	Fine-grained leuco granite Coarse grain leucogranite Foliated biotite granite Biotite granite Hornblende granite
Pre- Bundelkhand granitoids (Bundelkhand massif complex)	Metavolcanics of mafics and felsic Banded Magnetite Quartzite, Micaceous quartzites, commingtonite - grunerite - garnet - magnetite schist Talc-chlorite schist, actinolite-tremolite- talc schist, hornblende-chlorite -epidote schist, garnet chlorite-actinolite schist Biotite- gneiss, hornblende-biotite gneisses, sillimanite gneisses, amphibolite Tonalite-trondhjemite gneisses, granite-gneisses, migmatite.

2.3 Bundelkhand Massif Complex (Pre-Bundelkhand Granitoids)

A few years ago, the geology of Pre-Bundelkhand granitoids was mainly based on the small lensoidal xenoliths of gneisses, mafics-ultramafics, metasedimentaries, and metavolcanics (Mallet; 1869, Jhingan; 1958, Basu; 1986, Saxena; 1961, Sharma; 1982), which occur in the granitoids. It is known that TTG constitutes a significant component of Archaean craton throughout the world. So nowadays geologists of all over the world are paying an attention to find out this early component of crust from different parts of the

shield blocks. There are several localities in the Indian shield where the TTG have been reported (Sarkar et al; 1996). Sarkar et al (1996) reported this rock from the Bundelkhand craton for the first time and compared it with other TTG rocks reported from south Indian shield. Besides this, the relics of other older crustal component were identified and reported from Bundelkhand massif. These rocks are present as lensoidal body within the granitoids. These xenoliths can be broadly classified into three categories.

1. TTG and biotite gneisses
2. Metamorphics of mafics and ultramafics
3. Meta sedimentaries.

2.3.1 TTG and gneisses

Mid-Archaean (3500 Ma) crustal materials viz. tonalite and trondhjemitic rocks were identified for first time from Bundelkhand massif by Sarkar et al (1996), and Sharma et al (1998) and is named after type area Baghora trondhjemitic gneisses and Lodapahar trondhjemitic gneisses respectively. Subsequently Sharma and Rahman (1995) also reported the occurrences of large relict blocks of trondhjemitic gneisses from Kabrai and Rampura areas, on Mahoba-Charkhari road. Rampura gneisses are highly deformed and closely associated with amphibolites, metasedimentary rocks and BIF. These deformed gneisses have been intruded by an undeformed hornblende-granite. Grey to pink and medium to fine-grained trondhjemitic gneisses is found intrusive into highly deformed basic host rocks (early crust) in Loda Pahar, Kabrai area. TTG rocks of Bundelkhand are medium grained, leucocratic and comprise chiefly oligoclase, quartz and biotite. In general gneisses are well foliated with steep northerly dips and with an ESE-WNW strike and show evidence of polyphase folding (Plate2). Mesoscopic isoclinal folds are also common in gneissic rocks (Plate 3). Major NE-SW trending quartz reef of Post-Bundelkhand granite age bounded the gneissic raft along the western margin of the massif.

Prakash et al (1975) marked the migmatites and gneisses, from various places of southern part of Bundelkhand massif. Prasad et al (1999) reported the migmatitic gneisses at north of Simra from Tikamgarh District, Madhya Pradesh. Grey, Pink, banded (stromatic) to streaky (schlieric) gneissic enclaves is also noticed from many places of the north of Simra area. The trend of the gneissic banding varies from NW-SE to E-W. Mondal et al (2002) mentioned the five large lensoidal gneissic bodies in the massif (fig 2.2). Besides the gneisses the granulites were also reported from this massif. Jhingran (1958) describes about granulites as inclusions in the Bundelkhand massif without giving any specific location. Das (1959-60) describes a 30m x 30m exposure of garnetiferous granulites from 1.6 km north of Pandara.

2.3.2 Metamorphics of mafic and ultramafic rocks

The older metamorphic enclaves of mafic and ultramafic rocks and metavolcanosedimentaries are observed in lensoidal form at many places. Medicott (1859) recorded amphibolite and greenstone rocks in associations with the Bundelkhand crystallines at Baraitha and Girar. The enclaves of hornblende-chlorite schists and amphibolites were also mentioned by Jhingran (1958).

Chlorite-biotite-schists and metabasalts, conformable with quartz-feldspar-biotite gneisses in the area around Madaura, are reported by Prakash et al (1975). Mishra and Sharma (1974) established the high-grade metasedimentary rocks as Kuraicha Formation, which formed the oldest crust in Bundelkhand, and the low-grade metamorphics as Palar Formation, which includes pelites, semipelites, volcanogenic metasediments and meta-arkoses. They also considered hornblende schist and quartz-amphibolites schist as the main constituent of Kuraicha Formation and basic dykes transformed into talc-schist in the Kuraicha area.

In general metabasic and metaultrabasic enclaves occur as small sized isolated bodies throughout the granitoids and are mostly foliated and devoid of any lineation. Magnetite-bearing gabbros occur to the south west of Kakarwaha village (Basu; 1986). Basu (1986) identified three principal metaultrabasic and metabasic rocks from Bundelkhand massif. Metaultrabasic rocks are represented by large bodies of talc-tremolite schist, which occur around Balwantgarh and tremolite-actinolite schist to the southeast of Kakarwaha. Gabbroic rocks of metabasic rocks are observed towards south west of Kakarwaha or east of Madaura.

Epidiorites (metabasic rocks) are the most widespread among metabasic rocks; occur in small patches within the granitic rocks. They can be seen on Haidarpur-Kakarwaha track. A body of metadolerite has been reported by Srivastava (1970-71) in the north west of Baghora. This E-W trending thin body exhibits compressed filled vesicles, and it traverses the axial region of an E-W trending antiformal fold in the migmatites. Mani and Bhattacharya (1969-70) reported a large body of basic-ultrabasic rock to the north and northeast of Baraitha village.

2.3.3 Metasedimentaries

Medicott (1859) reported metasedimentary enclaves, "ribboned (alternate thin layers) iron-oxide and quartz schist" from Barata (Baraitha) and adjoining Girar area. Jhingran (1958) reported quartzite, magnetite-quartzites, slate, carbonates and sandstone enclaves from Bundelkhand granites. Prakash et al (1975) postulated Archean sedimentation and volcanism, which was later on subjected to metamorphism and

described as Berwar Formation of 300 m thick metasedimentaries exposed near Berwar village in southernmost part of the massif. Basal lenticular quartz conglomerate, fuchsite-quartzite, grey to green chloritic shales and banded magnetite hematite-quartzites of Girar are the main rock types of Berwar Formation. The fuchsite quartzites described by Prakash et al (1975) are the same rocks mentioned by Wilson (1868-69, c.f. Basu 1986) and Mehta (1944-45, c.f. Basu 1986) as pyrophyllite schist.

Mishra and Sharma (1974) put the iron formation above at the top of Kuraicha Formation and describe red beds followed upwards by glauconitic quartzite to the north and northwest of Mauranipur Railway Station. Prasad et al (1999) described three suits of volcanics and metasedimentaries along with gneisses at Dhaura. These volcanic sedimentary and gneissic rocks occur in the form of a NW-SE to E-W trending belt and bordered by intrusive pink biolite granite towards north and south. They also noted inclusions of amphibolites, schists and BIF in the gneissic complex.

2.3.3.1 Banded iron formation

Banded Iron Formation has been recorded from many parts of the Bundelkhand massif- (i) at Baraitha and Girar by Medlicott (1859), (ii) between Babina and Papaoni; Wilson (1873-74), (iii) near Gora and Balyara; Das (1959-60), (iv) at Kamla Sagar Dam; Mishra and Saxena (1959), (v) west and north of Mauranipur Railway Station; Srivastava (1970-71) and (vi) at Chanro; Goyal and Jain (1972-73).

In general iron-formation consists mainly of banded quartz-magnetite rocks, banded magnetite amphibolite and amphibole-bearing Banded-magnetite-quartzites. The banded-magnetite-quartzites of Girar-Baraitha and Chanro are hard and compact, while those of Babina, Papaoni, Gora-Balyara and NW of Mauranipur are fragile. They are well banded with alternating gray and white bands of magnetite and quartz (Plate 13a). At places the magnetite and quartz bands show wavy boundary generally symmetrical, which indicates that these iron formation have suffered low-grade metamorphism. Not only this pencontemporaneous deformational sedimentary structure were also noted from BMQ at many places. Most of the iron formations in this massif have the general E-W strike and are tightly folded synclinal structures with axial planes dipping on the average 65° to the north.

Actinolite, cummingtonite, grunerite, garnet, hornblende, chlorite, epidote, biotite and hercynite, magnetite are the main silicates in these iron formations.

2.3.3.2 Carbonates

Jhingran (1958) recorded limestone as inclusions in Bundelkhand massif at Gairwar and Magur. Basu (1986) found some carbonate rocks about 0.6 km south of the

Berwar village. Singh and Kumar (1970) reported lenticular calcite outcrops at Khajraha in Jhansi District. They considered these rocks as carbonatites. Mukherjee (1973-74) considers these as calcareous metasediments. Mishra and Sharma (1974) also considered these as carbonatites with magnetite and siderite bands.

2.3.3.3 Quartzites

Jhingran (1958) mentions small quartzites bands as inclusion in granites at several places but does not specify any locality. Das (1959-60) recorded biotite quartzite inclusions within the medium to coarse grained pink granite at west of Kuryankhirk and east of Gailwara, about 0.8 km west of Laron, and to the NW of Pandra. Saxena (1961) mentions a number of bands of quartzite in the Kabrai area. Basu (1986) noted the quartzites from shear bands in granite. Mukherjee (1973-74) recorded lens of quartzites, in Rajpur and Jaswantpura, trending NE-SW and well foliated. Goyal and Jain (1972-73) records schistose and fine grained quartzite about 2.5 km east of Patha in the river Jamni. Mukherjee and Senthappan (1973-74) records quartzites, at Garhmau, Palar and Gaurari areas in the Jhansi district.

2.3.3.4 Phyllite and schists

Jhingran (1958) describes inclusions of slaty rocks in Bundelkhand granites at NE of Nadgaon (in the Chhatarpur distt). Mishra and Sharma (1974) include black shales but they did not specify any locality of occurrence. Pascoe (1950) mentioned talcose schist, hornblende schist, chlorite schist, quartzose schist and "argillaceous schist" in areas around Mahroni in the southwestern part of Bundelkhand. Jhingran (1958) mentions quartz schists and feldspathic schists in the Sadhri nadi about 12km WNW of Basatgawan. Puri (in Basu; 1986) reported various schistose rocks including chlorite, hornblende, mica, talc-quartz and feldspathic schists in a narrow region between the granites and the Vindhya near Marla.

Saxena (1961) described biotite-muscovite schists interbedded with flaggy micaceous quartzites and garnetiferous muscovite schist at Kabrai. He also described greenish white quartzite and muscovite schist at the same place. Mishra and Sharma (1974) mention phyllites and low-grade schists in association with quartzites (quartz reefs) in the Palar formation. Srivastava (1970-71), Basu (1986) and Mukherjee (1973-74) located some stringers of schistose rocks with sillimanite occurring at 4Km milestone on Jhansi-Mauranipur Road from Jhansi. Jain and Goyal (1973-74) also found a band of sillimanite schist in the east of 7.6 km milestone from Jhansi on the Jhansi-Orchha Road.

2.4 Acid Magmatism (Bundelkhand Granitoids)

On the basis of mineral composition, texture, colour and location, the granites of the Bundelkhand have been classified into different types viz. Jhansi granite, Matatila granite, Garhmau granite, pink granite, porphyritic granite, hornblende granite, foliated biotite granite etc. Jhingran (1958) first time compiled the occurrences of Bundelkhand granitoids and classified ten types of granites in Bundelkhand. Saxena (1961) grouped the granite into pink and gray and suggested that the granites of the massif are result of transformation of quartzites and other metasediments. Prakash et al (1975) divided the granite into four categories and opined that the granites of north Lalitpur originated as a result of regional granitisation of metasedimentary. Basu (1986) recognized three main types of granites viz. (i) the porphyritic coarse-grained granite, (ii) porphyritic medium grained granite, (iii) non-porphyritic to sparsely porphyritic medium to fine grained leucogranite and he further divided them into six types (Basu; 2001). Sharma (1982) divided the granites on the basis of the location- (i) Garhmau granite and (ii) Matatila granite and further classified into three phases.

The above said divisions of the granite were mainly based on texture, structure and location. Due to similarity and overlapping characters, these classifications could not be satisfactorily functional for the purpose of geological study. Therefore, Zainuddin et al; (1992) and Mondal et al; (1996) proposed genetical classification based on geochemical character, colour index and mineralogy beside the texture and structure of rocks. They classified the granitoids batholith into five types- (i) hornblende granite, (ii) porphyritic-biotite granite, (iii) foliated-biotite granite, (iv) coarse-grain-leucogranite, and (v) fine-grain leucogranite.

2.4.1 Hornblende granite/porphyritic coarse grained granite

The rock is commonly pinkish red to light pink in colour and is dark red on weathered surface. The feldspar phenocrysts are tabular in form. The hornblende is an essential mineral, which is usually associated with biotite. High packing of feldspar phenocrysts is noted at many places. Massive exposures around Jhansi, extending upto 14km stone on Jhansi-Lalitpur Road in the south, across the Jhansi-Lucknow Road on the east and upto the quartz reef north of the Jhansi Railway station, between the Betwa river at Jhararghat and upto 6km south of Talbehat. It is also exposed around Mauranipur, Mahoba, Khajuraho, and many other places. Sharma (1982) described this granite as Garhmau granite.

2.4.2 Biotite granite/porphyritic medium grained granite

Porphyritic medium grained granite recorded specially to north east of Karesra Kalan, 47km south of Jhansi on Jhansi-Lalitpur Road. This rock becomes coarser near the contact with Jhansi granite (Porphyritic Coarse Grained Granite). Compared to Jhansi granite, the rock is dull in colour with the smaller feldspar phenocrysts. At few places like Agori, the quartz grains are larger than the feldspar phenocrysts. In this granite microcline is dominant as phenocrysts. The biotite is one of an essential component. The hornblende may exist with this rock. This granite is more or less equivalent to porphyric medium grain granite proposed by Basu (1986).

2.4.3 Foliated biotite granite

The foliated biotite granite is commonly dark pink to light pink in colour and exhibits local foliation, and also shows coarse-grained porphyritic texture. The phenocrysts of feldspar are prismatic and are highly packed.

2.4.4 Coarse-grained leucogranite

Small veins and patches of syno-granite rocks are commonly seen in the Jhansi granite and to a lesser extent in the Karesra granite (Basu; 1986). Some lenses are recorded at Jhararghat on the Betwa River. These granitoid bodies exhibit a blocky habit. These are reddish pink to chocolate coloured rocks with phenocrysts of microcline orthoclase and perthite in a groundmass of albite, minor quartz and biotite. Basu (1970-71) first recorded this porphyry to the south of Jhansi on Jhansi-Lalitpur Road south of Ghurari Nala. A prominent zone can be seen from Khajraha Buzurg also be seen to the south east of Manpur Tal. The rock is of light fawn colour with tiny phenocrysts of white feldspar.

Granite porphyry dykes with coarse-grained feldspar phenocrysts are noticed in various parts of the massif. To the south of Talbehat, there are discontinuous parallel bodies upto 20m wide and 50m to 200m long. Many traceable bodies are recorded across the Jhansi-Lalitpur Road between 53km and 58km milestones from Jhansi. Several bodies of coarse porphyry are recorded from Birdha, southern bank of Dukwan Reservoir.

A light grey variety is commonly seen only in the coarse grained Jhansi granite occurring in the NE of Barora near 34.6km milestone on Jhansi-Lalitpur road, 3.6 km south of Jhararghat, 0.6 km north of Matatila Railway station and along the west bank of the Jamni River to the east of Birdha.

A large outcrop of medium to fine coarse-grained non-porphyritic leucogranite occurs on the western flank of Chhikahra. It is a massive rock with a pegmatitic structure and is intruded by the Kabrai leucogranite.

Large composite bodies are also found in Jhansi town (Gwalior Road), in the Sonagir hills, to the west of Nathikhera, in the Kuraicha hill forming the east abutment of the Kamla Sagar Dam, on the Jamni Dam right canal and scores of other places. It is a grayish white to grayish pink rock with moderate proportion of dispersed ferromagnesian constituents. A number of prominent medium grained leucogranite bodies are seen at Kabrai (Basu, 1986).

2.4.5 Fine grained leucogranite

A small fine-grained leucogranite body was encountered on the southern flank of a hill to the west of Ratauli village. The younger fine-grained leucogranites have lower content of ferromagnesian minerals and they are conspicuously devoid of hornblende. Basu (1986) found out a body of fine-grained leucogranite from west of Nathikhera trending in a NNW-SSE direction upto the Dukwan reservoir on the Betwa River for about 9 km. It is moderately dark with dominant fawn fine-grained groundmass and sparse small sized phenocrysts of cream-colored feldspars. Another 1.6 km extension of the body to the south was noticed by Mukherjee (1973-74) and describes as porphyrite. A similar body is noted across the Jhansi-Mauranipur Road at the Ghugwa Rest House 23 km from Jhansi. Fine-grained leucogranites are widely exposed in Lalitpur.

2.5 Post-Bundelkhand Rocks

2.5.1 Quartz reefs

Quartz Reefs are the characteristic features of parallel ridges of quartz, trending NE-SW in Bundelkhand massif. They rise about 175m above the surrounding land. Jhingran (1958) mentioned that sometimes quartz give out small offshoots and coalesce into one. He also mentioned that the cataclasites and the granulated nature of cherty reef rock together with the presence of schistose structures. It represents long narrow zones along which intense mylonitisation had taken place. According to Basu (1986) there are eleven major quartz reefs in Bundelkhand massif and spaced at 12 km to 19 km apart, the average widths of reefs vary from 50 m to 60 m and lengths from 35 km to 40 km. The longest ridge passes through Nivari is traceable almost continuously for 100km.

Quartz is the main mineral constituent in most of the reefs. The pyrophyllite and diaspore are mainly associated with quartz reefs. At places quartz reefs exhibit disseminated crystals of pyrite, secular hematite and rarely chalcopyrite. Grayish white

coloured quartz reefs are dominant in the massif. At many places reefs show pinkish white and milky white colour. Dark grey, rosy and black patches are also observed rarely. Maximum quartz reefs occur in the NW of Jhansi, SE of Chhatarpur and SE and SW of Tikamgarh. At many places the wall rocks bordering the quartz reef show signatures of crushing. Basu (1986) suggested that reefs do not relate with any sedimentary phase they are purely epigenetic manifestations and products of shearing and mylonitisation. Roday et al (1995) pointed that quartz reefs were emplaced along brittle ductile shear zones, and their associated polymetallic sulphide and pyrophyllite-diaspore mineralisation, mark an end-stage of hydrothermal fluid activity after the crystallization of the granite plutons. They also mentioned that these events coincide with the stabilization of the Bundelkhand massif.

Roday et al (1995) have developed a kinematic model attributed to the geometry of the quartz reefs and the mafic dykes in Bundelkhand massif. According to them mafic dykes and quartz reefs were emplaced along the fractures developed due to changes in maximum compressive stress from an initial NE-SW trend to a final NW-SE trend.

2.5.2 Mafic swarms and dykes

Mafic dykes, trending NW-SE, are more frequent near eastern and southwestern margins of the Bundelkhand massif. These dykes have a cross cut relation with the most prominent NE-SW trending quartz reefs. However, at places ENE-WSW and E-W trending dykes are also observed in the Bundelkhand massif. The maximum width of dyke (45m) is recorded near Kakarwao. In general the dykes are doleritic in nature. They are usually dark grayish green in colour. Basu (1986) recognized three generations of dykes. Coarse-grained variety is cut across by a medium grained variety, which in turn includes transverse bodies and lenticels of a very fine-grained aphanitic dolerite. Medium grained variety is more widespread and named after Mahoba as great dolerite dyke of Mahoba. This is about 11km long ENE-WSW and forms a prominent ridge. Coarse-grained variety has a gabbroic appearance and is recorded as Kakarwao Dolerite. The fine-grained variety, which resembles the Malwa plateau basalts lying immediately to the southwest of the Bundelkhand massif, is designated as the Chhikahra dolerite.

2.5.3 Bijawar Group

Bijawar Group of rocks occur as low hills on the southern fringe of the Bundelkhand massif. Exposures of these rocks are in two sectors. The eastern one lies mainly in the Chhatarpur and Sagar districts of Madhya Pradesh and Lalitpur district of Uttar Pradesh. Western part of Bijawar Group is seen after a gap of 250 km from eastern sector in Uttar Pradesh (Mirzapur Distt.). Another exposure is seen in the Harda inlier in

the Narmada Valley 275 km SW of the type area. The Harda and Mirzapur Bijawar are now known as Mahakoshal Group. Bijawar rocks lie above the Bundelkhand Massif and below the Vindhyan Supergroup of rocks. They are exposed along the south-southeastern edge of massif between Sonrai to Chitrakoot in the two-separate basins. Bijawar Group of rocks consists of pebble bed, quartz arenite, mafic trap, bedded chert and dolomite, chert Breccia, phosphatic shale, highly ferruginous shale and sandstone. Quartz veins, basic sills, stromatolite bands, are found.

2.5.4 Vindhyan Supergroup

Vindhyan rocks overlie the Bundelkhand massif on all sides except in northern part of it. The Vindhyan Supergroup forms a vast semicircle pattern extending in Rajasthan, Madhya Pradesh, U.P. and Bihar, and is delineated by Son-Narmada fault in south. The Yamuna-Ganga alluvium in the north conceals both the Bundelkhand massif and the Vindhyan. The basal conglomerates, limestone, porcellanite, shale, glauconite sandstone, quartzite and fawn sandstone etc. are the main rock types of the Vindhyan supergroup. Alternate layers of sandstone, shale, limestone and quartzite are the characteristic feature of Vindhyan Supergroup. The Vindhyan Supergroup is widely exposed in south of Bundelkhand massif (Fig 2.3) and has been lithologically divided into Semri, Kaimur, Rewa and Bhandar Groups. The carbonate facies dominates in Semri and Bhandar.

2.5.5 Deccan Traps

In Bundelkhand region Vindhyan rocks are directly overlain by Deccan Traps towards south south west of granitic massif. Deccan Traps covers an area of about 500,000 square kilometers in the northern and western parts of the Indian Peninsula. The lava flow some times reported at massif also. The extensive lava flows which give rise flat-topped mountains and plateau with step like terraces are believed that they have erupted sub-aerially through the fissures in the earth's crust. Eastern and southern parts of the Deccan Plateau is composed of uniform horizontal tholeiitic flows representing the quiet type of eruptions and represents the lower unit. The upper unit exposed in the northern part of the Deccan Plateau, which having numerous inter-trappean beds is characterized by an explosive activity.

2.6 Regional Structure

Bundelkhand complex is ornamented by several regional structures like quartz reefs, dykes, folds, faults, shear zones etc. The different rock types of the complex have undergone several generations of deformation episodes. The contacts between Granitic terrain (massif), Bijawar Group and Vindhyan Supergroup in south, and Indo Gangatic

towards north are demarcated by faults or unconformity and are most important for the study of the structural evolution of terrain.

Major and Minor Structures viz. lineaments, folds, joints, schistosity and foliation, bedding plane structures are observed in the Bundelkhand Complex and has been discussed separately.

2.6.1 Structures in migmatite, gneiss and amphibolite

Gneissic structure exhibits well developed banding represented by melanosomes and leucosomes of variable thickness. The leucosomes are mainly of quartzo-feldspathic with minor biotite. The melanosomes are granodioritic to dioritic where biotite and minor amphibole are embedded. In the streaky gneisses, bands of biotite and rarely amphibole are interlayered with quartzo-feldspathic leucosomes. Basu (1986) described that the gneissose structure exhibits a general WNW-ESE strike with moderate to steep (35 to 65) dips in many parts of the complex.

Five phases of deformation were recorded from the migmatite gneisses and amphibolites (R.P. Sharma; 1982), which are represented by various types of foldings. The F1 folds are tight isoclinal, their hinge generally trend E-W. F2 folds are open to tight upright and coaxial to F1 folds and trending E-W. The F3 folds are subvertical and vertical, the fold axis is steeply plunging, F4 folds are upright to steeply incline and F5 folds are upright. Recently Prasad et al (1999) also reported five phases of deformation in the gneisses. They suggested that isoclinal to tight reclined and open folds (F1, 2,3) were developed during first, second and third phase of deformations and in the fourth phase deformation sinistral shear zones were developed in NE-SW direction while in the fifth phase deformation dextral shear zones were developed in NW-SE direction.

Shukla and Pati (1999) also mentioned that migmatites, and gneisses show NW-SE strike trend, moderate to subvertical dip due north. They also noted that F2 folds plunging northwest are observed in migmatite gneiss.

2.6.2 Structures in meta-volcanic and meta-sedimentary rocks

In many parts of the Bundelkhand complex metabasalt/amphibolite, BMQ, gneisses and minor schists are found in association with granitoids. Metabasalts and schists exhibit well-defined schistosity. In many parts of the complex schistosity shows orientations of strike at NW-SE and NE-SW.

Prasad et al (1999) have described three phases of deformation in the volcanic and metasedimentary rocks exposed near Prithivipur. The first phase deformation resulted

in tight to isoclinal and reclined folds with schistosity. The axial surfaces of the first phase folds trend WNW-ESE to E-W with steep NW plunging fold axes ($>50^\circ$). The second phase deformation produced reclined type folds (F2 folds). They are co-axial and co-planar with F1 folds. The third phase deformation produced tight to open folds (F3 folds) with axial surfaces at high angle to those of F1 and F2 folds. The axial surfaces of the third phase folds trend NW-SE to NE-SW and the fold axes plunge 25° - 60° N. They also compared these three phases of folding in the volcanic and sedimentary rocks with orthogneisses. They also mentioned that an intense schistose fabric developed in metabasalts near the northern contact.

Slump structures and flowage of unconsolidated material resulting in podlike masses are common in Banded-magnetite-quartzite rocks of Chanro and Girar areas (Basu; 1986). Similar slump structure and penicontemporaneous structure were reported by other workers (Shukla & Pati 1999 and Sharma; 1998). Similar tight isoclinal folds are common in the banded iron formations of Bundelkhand complex; at places open folds are also observed. Generally fold axes are parallel to the strike of the iron bodies, i.e. east west and axial planes dip towards north.

The supracrustal rocks (metabasic and metaultrabasic rocks, meta-cherts, banded iron formations, fuchite-bearing quartzites, quartzites) of southern part of Bundelkhand region are folded generally on E-W axes into tight to isoclinal folds overturned to the south (Prakash et al. 1975, Roday et al 1995). These authors also mentioned that the F1 folds in these supracrustal rocks are generally variably oriented and coplanar folds and F2 fold structures lie at high angle to early structures and they appear to have been formed after the emplacement of granite.

2.6.3 Structures in granitic and other rocks

At many places, granitoids exhibit foliation, which is marked by the parallelism of tabular grains of feldspar phenocrysts in Bundelkhand Massif (Plate16). Basu (1986) mentioned that foliations in granites do not possess a regional control but are possibly the result of local stresses. The regional trend of foliation is WNW-ESE. Prakash et al (1975) described that most of the ductile shear zone in the granitoids were developed towards the end phase of late kinematic diapirs and this is generally abundant in contiguity with supracrustal rocks, or in proximity with adjoining diapirs. Two sets of shear zones in granitoids have been described by many workers (Basu; 1986, 2001, Sharma; 1988 and Roday et al; 1995). Both the sets of shear zones are generally steeply dipping or vertical. The EW trending sinistral shear zones are more ubiquitous than their NW-SE trending dextral counterparts. Shear zones are generally located at the boundary of supracrustal rocks; sometimes they are also located at the boundaries of individual diapirs.

There is no doubt in saying that the Bundelkhand massif is traversed by two prominent sets of lineaments one having the general NE-SW trend and another trending NW-SE (Fig 2.4). The NE-SW one is observed as quartz veins and reefs, the NW-SE one as mafic dykes. Quartz reefs have slightly sigmoidal geometry, characteristic of the tensile veins, generated by a brittle - ductile inhomogeneous simple shear. They are at very definite periodicity and lie subperpendicular to ESE trending cleavage within the ductile shear zones.

Basu (1986) described three principal sets of lineaments based on the study of LANDSAT-I imageries. They are trending NE-SW, ENE-WSW, and NW-SE (Fig 2.4). The southwestern part of the massif has more density of lineaments than others. At places lineaments intersect each other and at places occur as curvilinear or parallel to each other. Basu also mentioned that low density of lineaments in the massif indicates absence of intense tectonism.

In general, granite exhibits three sets of joints in which two are trending NE-SW and NW-SE with steep dips and the third one horizontal. Commonly joints are observed in open forms. The gaps of the joints rarely exceed 10cm in width and the length of the individual joints are also do not exceed 50m. At places pegmatite veins have filled up some of the joints.

Bundelkhand massif is also well ornamented by fractures. The massif granite, rocks are extremely fractured at places and other dykes have followed particular sets of fractures. Granites show ENE-WSW trending fractures, pegmatites and quartz reefs followed the NE-SW trend while dolerite has followed the NW-SE trending fractures. The fractures within massif are commonly observed as straight but at places zigzag fractures are also observed.

2.7 Regional Stratigraphy

The Bundelkhand massif mainly comprises granitoid rocks of different episodes, gneisses, migmatites, metabasics, schists, and volcano-sediments. Quartz reefs and mafic dykes are represented by NE-SW and NW-SE trending lineaments through out the massif. Number of workers has been attempted to describe the geology and stratigraphy of the Bundelkhand massif (Table 2.3).

Medlicott (1859) described the occurrence of greenstone, dykes and quartz reefs for the first time on the maiden investigation in Bundelkhand craton. Fermor (1936) described the age of the gneisses as post Dharwar. Pascoe (1950) and Chatterjee (1971) attempted to set up a stratigraphic column of Bundelkhand. According to them Mehroni Schist Belt is Archaean in age, and granite is considered as Pre Dharwar.

Jhingran (1958) mentioned that relicts of metasediments are equivalent to Dharwar. Granites, quartz reefs and basic dykes respectively are of younger episodes. Saxena (1961) also attempted to describe the lithostratigraphy of the Bundelkhand. Saxena (1961) added an unconformity between granitoids & schist in the stratigraphic sequences proposed by Jhingran (1958).

Prakash et al (1975) have classified the stratigraphic sequences of Bundelkhand massif as (i) Rajaula Formation, consisting of metamorphosed volcano-sedimentary, is unconformably overlain by (ii) Berwar formation consisting of ferrogneissous metasediments and mafic and ultramafics. They put these two formations under Mehroni Group. Above the Mehroni Group (after a gap of deposition) they put (iii) Bundelkhand Granite Formation which consists variety of granites including migmatites and (iv) Madaura Formation on the top which consists dolerite dykes, quartz veins, pegmatite, gabbro, pillow lava etc.

Mishra and Sharma (1974) proposed a four fold classification of Bundelkhand Massif and suggested that (i) Kuraicha Formation, which is comparable to Rajaula Formation of Prakash et al (1975), as the oldest formation of the region. It consists of migmatites, gneisses, schists, quartzites etc. Kuraicha Formation is unconformably overlain by (ii) Palar Formation, which consists of quartzites, phyllites, schists, diaspore, ferruginous quartzites etc., it is followed by (iii) Intrusive of Bundelkhand granitoids and (iv) Mafic dykes and Swarms.

Basu (1986) proposed a lithostratigraphic succession of this region after a long time field investigation in Bundelkhand region. According to him Banded Iron Formations and metabasites are the oldest rock types in the region and also opined that they are of Pre-Bundelkhand after a gap of deposition Bundelkhand Granitic Complex existed. Basu put the gneisses as oldest followed by various phases of granites of different episodes. He also considered quartz reefs and dolerites as the youngest lithounit.

Sharma (1982) also proposed the lithostratigraphy of the Bundelkhand complex. They placed the (i) Kuraicha Formation as the oldest unit which comprises migmatite, gneisses, amphibolites, chlorite - biotite schist, quartzites etc. Kuraicha Formation is unconformably overlain by Bundelkhand Group, which comprises six formations having different lithology. They are (i) Palar Formation, (ii) Paron Meta-acid volcanics, (iii) Garmau Granite, (iv) Matatila Granite, (v) Mahoba Dolerite, and (vi) Madaura Ultrabasics. Sharma (1998) proposes the stratigraphy of Bundelkhand in terms of the tectonic events. They proposed the following stratigraphic sequences of Bundelkhand (i) Mahroni Formations of Archaean is conformably overlain by Bundelkhand granitic complex

(2600 Ma), (ii) Bijawar and Gwalior Groups (2400-2300Ma), (iii) the Vindhyan Supergroup (1500-550 Ma), and (iv) Malwa (Deccan) Traps (Cretaceous-Eocene).

On the basis of field observations, geochronological data available from literature and detailed structural review, the following stratigraphic sequences of Bundelkhand Complex is proposed (i) Tonalite-Trondhjemitic Gneisses (TTG) (>3100 Ma) suggested as older metamorphic group (OMG), is overlain by (ii) Newer Metamorphic Group (NMG), which comprises low-grade metamorphosed mafic and ultramafic suits followed by Banded Iron Formation. It is unconformably overlain by volcano-sedimentary rocks. (iii) Bundelkhand granitoids were emplaced and deformed at late Archaean to early Proterozoic (2500-2300 Ma). The quartz reefs were emplaced at late stage. (iv) Bijawar and Gwalior volcano meta-sedimentaries were laid over Bundelkhand Granitoids after a prolong gap of depositions. (v) Mafic and Ultramafic dykes and swarm (1600Ma) emplaced before the deposition and recrystallization of Bijawar Group of rocks. Vindhyan Supergroup is deposited after the recrystallization and deformation. Finally, Vindhyan Supergroup is unconformably overlain by Malwa Traps, which is the topmost/youngest lithounit of the Bundelkhand microcontinent.

2.8 Geochronology

The Bundelkhand Massif, lies in the central part of the Indian peninsula and is separated from the south by the Son-Narmada lineament, the Great Boundary Fault in the west of the Aravallies, and the Himalayas in the north. The Son-Narmada lineament has been considered as one of the oldest sources of thermal pool in Central Indian Craton since late Archaean times. Therefore, multiphases of tectonic and igneous activities have been taken place in and around this lineament. The signatures of these activities can be also recorded in the older crustal material in the form of reset date or disconchorded ages. The Satpura orogeny (1600 Ma) has been considered as the last strongest orogenic phase of Precambrian in Central Indian craton so far (Pandey et al; 1995).

The review of the geochronological data in Bundelkhand massif and Central part of Indian Peninsula (Fig 2.3) suggest that Bundelkhand and Baster Craton were the two oldest Archaean nucleus in the north and south of SONATA respectively. To update and understand the various geological events of Bundelkhand massif, several attempts have been made by different workers from time to time. The published geochronological data of different workers has been compiled and presented in table 2.4.

The oldest age 3500 ± 99 Ma has been obtained from the banded gneisses of tonalite-trondhjemitic affinity of Baghora area of Bundelkhand by Sarkar et al (1996). This age is comparable to the other tonalitic-trondhjemitic greisses reported from the other part

of Indian shield viz. (Beckinsole et al 1980, Moorbath et al 1986, Dhoundial et al 1987, Sarkar et al 1990, 95).

Age of Bundelkhand intrusive granite activity is supported by the Rb-Sr whole rock isochron age of 2560 ± 106 Ma (Crawford; 1970) from the Jhansi, khajarahho granitoid of Bundelkhand and also radiometric date of Pb/Pb age 2518 ± 6 Ma (Mondal; 1998), 2492 Ma (Mondal et al; 2002). These granites have been divided into three distinct intrusive phases (Sarkar et al; 1984, 89, 90 and 1995) viz. (i) Gray granodiorites and granites (ca. 2400 Ma) or Biotite granitoid (2521 ± 6 Ma) (ii) Pink leucogranites (ca. 2350 Ma) and (iii) Fine-grained leucogranites (ca. 2270 Ma) or Hornblende-granitoids (2516 ± 9 Ma), Leucogranite (2492 ± 10 Ma), suggested by Mondal et al (2002). Xenolithic enclaves of deformed metasedimentary rocks and silicic gneisses within undeformed granitic batholith (2521 Ma to 2492 Ma) thus, represent the presence of gneiss rocks before of the Pre-Bundelkhand granitoid (>2500 Ma).

The zircon ages of Kuraicha gneisses (3297 ± 8 Ma) and Mahoba gneisses (3270 ± 3 Ma) Lodhapahar, 3300 Ma (Sm/Nd) obtained by Mondal et al (2002), represent the minimum crystallization ages of the silicic protolith that were transformed into TTG gneisses during deformation and metamorphism after their emplacement. They have also obtained different discordance dates for the gneisses viz. 3100 Ma. For Kuraicha and Mahoba gneisses, 2700 Ma for Babina gneisses and 2500 Ma for Karera gneisses. These radiometric data indicate the presence of multiple phases of thermal activities within the massif after the M_1 metamorphism. The oldest event of granitic magmatism in the region took place at 3297 Ma as indicated by the TTG gneisses folded with amphibolites and metasediments from Kuraicha and Mahoba. The other discordance age viz. 2700 Ma may be related to M_2 metamorphism while 3200 Ma age may be correlated in mafic and ultramafic eruption for NMG. The 2500 Ma discordance date of gneisses may be correlated with emplacement of massive granitoids, which is intermingled with granite-gneisses during the M_1 metamorphism.

The younger gneiss dates of Karera and Panchwara (2500 Ma, Mondal et al; 2002) may be discordance age, which is either cooling or recrystallization age formed during reactivation of shears or may be related with large scale granitic magmatism in this region. Three suits of granitoids; hornblende granitoid (2500 Ma), Biotite granitoid (2520 Ma) and Leucogranitoid (2490 Ma) suggest their emplacement in quick succession at 2500 Ma within a few tens of million years.

Gray granodiorites and granites (Ca 2400 Ma), pink leucogranites (Ca 2350 Ma), and fine-grained (aplitic) leucogranites (Ca 2270 Ma) have been dated by Sarkar et al (1984, 1989, 1990, 1996). These Rb/Sr dates point prolong acid magmatism in the Early-

Proterozoic time. They may be correlated with Bundelkhand continental growth and subsequent late stage pegmatitic and hydrothermal activities.

Crowford and Compston (1970) obtained the Rb-Sr isochron age of 1830 ± 200 Ma for the mafic volcanic rocks associated with Gwalior Group of sedimentary. Pandey et al (1995) reported Rb-Sr isochron age of 1691 ± 180 Ma for the Kurrat volcanic rocks. Sarkar et al (1997) reported Rb-Sr age of 1789 ± 71 Ma for mafic rocks of the Dargawan sill of Bijawar basin. The clustering of these geochronological data around 1800 Ma points that last thermal activities perhaps took place due to release of tension & extensional tectonics in the massif.

On the basis of above discussion tectonothermal events and their relation with different metamorphic, magmatic and sedimentation along with deformational history have been proposed (table 2.5) for the first time for the evolution of Bundelkhand craton.

2.9 Geology of the Area

The study area Babina-Mauranipur transect covers about 1000sq km, of the central part of northern block of Bundelkhand massif. The area is consisting high grade metamorphics represented by TTG, biotite gneisses, migmatites and amphibolites, low-grade metamorphics represented by mafics and ultramafics, banded iron formation, and metavolcanics and mylonites, the massive exposures of different types of granitoids, quartz reef and mafic dykes. The study area has been mapped for detailed study of petrogenesis of different rocks and their structural relationship. The field investigations could be completed during several field sessions covering with a period of about two years. The geological map of study area is prepared after detailed fieldworks on the enlarge toposheet of the Survey of India and some lab works, and is presented in Fig. 2.6.

2.10 Topography and Drainage

The entire study area is characterized by more or less plateau type topography where E-W trending small-detached hillocks of banded iron formation and NE-SW trending quartz reef are exposed. Quartz reefs are generally raising about 100 m above the surrounding plain while small ridges of iron formation are raising about 60m above the surrounding plain. Both the ridges are symmetrical and gentle slope and are occasionally characterized by dextral or sinistral displacement structure. The older metamorphic rocks are usually present at the low-level topography. At places granites terrain giving small hillocks of dome like structure. Geomorphologically, the study area has been divided into two parts.

- Plateaus with hillocks and ridges
- Plains with large valleys.

Regional drainage system of the study area shows dendritic pattern. Betwa (Nadi) river is the only major perennial stream in the study area, which follows NW direction. Yamini, Sukhanai and Saprar are also important rivers flow from south to north in the study area.

2.11 Rock Types

*dhjenite gneiss -
Tonalite Trondhjemite*

2.11.1 TTG, migmatites, biotite gneisses and amphibolites

Good exposures of gneisses have been observed at Jaunpur, Ghisauli, Mankuan, Baghora, Dhaura, Gora and Mauranipur villages (Fig.2.6). They are characterized by leucocratic to melanocratic, medium to coarse grained with well-developed gneissose texture (Plate-2). Sometimes the bands of leucosome and melanosome varying in thickness (Plate-3) and sometimes the partial melting characters were observed. Feldspars, quartz, mica, sericite, apatite, zircon, opaque and epidote are the important mineral constituents of this rock unit. In general foliation in the gneisses are trending in NW–SE to WNW–ESE direction and steeply dip ($> 75^\circ$) towards NE and NNE direction. Xenoliths of the gneisses have been found in the granites at many places, particularly at Jaunpur (Plate-2). A strip of small lensoidal, highly deformed migmatite-gneissic enclave is also observed at Kamalasagar Dam, Mauranipur in the medium to fine grained granite. In the study area majority of the gneisses are highly deformed (Plate-1 and 2). At Jaunpur area, streaky gneisses are also observed (Plate-4b). They are observed as gray in colour, medium grained hard and compact. In this area both the well-banded gneisses and streaky gneisses are exposed (Plate-3) and it seems that the banded gneisses are changing into gray granite due to partial melting and recrystallisation during the advance stage of metamorphism and deformations. Coarse-grained porphyritic leucogranite intrusion is observed at the contact of gneisses and mafic-ultramafics (Plate-8a). Gneisses are also observed directly at the contact of the iron formation and sometimes with mafics and ultramafics. At Dhaurra area the waxing and winning patterns of gneissic bands are also observed. Augens of feldspars are observed in all the sections of the study area but south of Mauranipur and Jaunpur it is notable (Plate- 6a, b & c). The size of feldspar varies from 3.5 cm X 2cm to 1.5cm X 0.8cm at these places.

2.11.2 Amphibolites and hornblende-biotite-gneisses

In the study area amphibolites are observed in all the sections but Dhaurra and Jaunpur (Babina) areas are the best examples. Amphibolite is hard and compact, massive, fine to medium grained and dark coloured. The constituent minerals are hornblende, biotite, plagioclase, quartz and chlorite. In Dhaurra section, hornblende and plagioclase minerals are dominant while in Jaunpur section, hornblende and biotites are dominant. Amphibolites are usually observed in the form of lenticular patches in gneisses. They have also undergone different deformational events. At Jaunpur a thick folded band of amphibolite is observed (Plate- 1b,c). Sometimes the biotite-gneisses and amphibolites seem to be co-folded (Plate 2.2), which indicates that both the rocks were deformed and subjected to high-grade metamorphism during the same event.

2.11.3 Metamorphosed mafics and ultramafics

Mafic and ultramafic schist (hornblende–chlorite schist, talc–chlorite schist etc.) are mainly found at the contact of the BMQ and gneisses. Notable exposures are found at Babina, Dhaurra, and Mauranipur. They are medium to fine grained and gray to dark grayish green in colour. Foliation planes are generally in ENE–WSW, steeply dipping north word westerly ($> 75^{\circ}$) (Plate 11b) and parallel to the banded iron formation. These mafics and ultramafics are generally observed as highly weathered form (Plate-11b). Talc, chlorite, amphibole are the main constituent minerals.

2.11.4 Banded magnetite quartzite

Banded magnetite quartzites are hard, compact and heavy, fine-grained brownish black in colour (Plate 10). The constituent minerals are magnetite, quartz, cummingtonite, garnet, magnetite and quartz (Plate 13a). Thick magnetite bands are also present in some sections.

Quartzites are observed generally in association with BMQ. Fuchsite bearing quartzite is observed at Mauranipur near the railway crossing (Plate -17c). It is fragile in nature, and dull green in colour. The quartzites observed in Babina are dirty pinkish white in colour, fine-grained, massive and compact. The BMQ display a linear pattern trending ENE–WSW having steep dip ($>60^{\circ}$) in NNW direction. This rock unit is also showing deformational events of the geological past. Two stages of folding in BMQ are observed at Mauranipur section (Plate14b). Tight to open folds are observed in Dhaurra section. Penicontemporaneous sedimentary structures were also recorded.

Near Pura Village BMQ display the NE–SW and E–W trending joints, which are parallel to the trend of quartz reef.

2.11.5 Metavolcanics

Very low grade metamorphosed mafic and felsic volcanic rocks (Plate 11b,c) are observed at Dhaurra and Babina in the study area. At Dhaurra mafic volcanics are observed in a narrow zone. Sometimes pillow type structures (Plate -11b) were found. Mafics rocks are dark gray in colour, very fine-grained, massive, very hard compact and at places, it is observed as pillow type structure (Plate-11b), at Dhaura (North of Simara) section. Plagioclase feldspars, quartz, amphiboles are the main constituent minerals of this rock type.

Felsic rocks are light pink in colour, fine grained, massive, hard and compact. The best section can be severed at Dhaura. Rhyolitic flow structures are also observed (Plate-14a) at Dhaurra where K-feldspar stretched rotated phenocrysts and elongated. Quartz, biotite and magnetite epidote, sericite are the main minerals constituents observed in this rock types. Both, the basalts and rhyolites are showing the same trend i.e. NW–SE to E–W. It is worth to describe that these metavolcanics along with metasedimentary subjected to strong deformation and shearing (Plate-14a,17a,b,18) during low-grade metamorphism.

2.11.6 Hornblende granite / gray granite

Hornblende granite at Uprar (Plate 9a) and near Katera is dark gray in colour, medium grained hard and compact. Phenocrysts of feldspar are also observed (Plate 16). Hornblende granite has a contact with pink porphyritic granite without any deformation. This granite usually contains the xenoliths of metamorphites of different size and shape.

2.11.7 Foliated biotite granite

At Katera reserve forest (temple site) foliated biotite granite is observed. It is coarse to medium grained, pink in colour, hard and compact. Along the foliation plane feldspar phenocrysts are oriented in E–W direction and NE–SW fabric is clearly developed (Plate-12 b), and also observed two stage deformation signatures.

2.11.8 Coarse grained leucogranite

Observed as pink in colour, coarse grained, hard and compact. Phenocrysts of K-feldspar are commonly observed (Plate-13 c). Another very coarse-grained porphyritic granite, pink in colour is also observed. Quartz, feldspar and biotite crystals can be clearly identified by naked eye. Biotite is common in all leuco-granites but hornblende may be or may not be present. Very coarse variety is more common. It also occurs at the contact of iron formation and gneisses.

2.11.9 Fine grained leucogranite

It is fine-grained, light pink to pinkish white in colour, non-phorphyric hard and compact. This granite is observed mainly at Mauranipur, SW of Kamla Sagar dam. The mineral constituents of fine-grained leucogranite are similar to that of coarse grained, but it is non porphyritic in general; hornblende is almost absent.

2.11.10 Quartz reefs

In the study area quartz reefs show different types of colour viz. grayish white, milky white, pinkish white, hard and compact. Quartz is the main constituent of reef minerals but feldspar, epidote, chlorite and opaque minerals are also observed. The reefs are generally trending in the NE–SW direction. However NNE–SSE and E–W trending reefs were also noticed. Seven major reefs trending in NE–SW direction have been mapped in the investigated area.

2.11.11 Dolerite

Dolerites are observed as dark green in colour, medium grained, very hard and compact. Pyroxenes, plagioclase, magnetites uralite, biotite, epidote, quartz and chlorites are the main mineral constituents observed in these rocks.

2.12 Structure

Large and small-scale structures observed in the investigated area are discussed in the following paragraphs. The detailed field study points out that the study area represents a long and narrow east-west trending major synform structure (Fig. 2.7) where the highly deformed low grade metamorphics (NMG) occur in the core part and coarse to medium grained, folded gneisses (OMG) on the flanks. The monotonous northerly dips and small-scale structures reveal large synclinal structure.

2.12.1 TTG, gneisses and migmatites

Migmatites and gneisses trending in WNW–ESE to NW–SE are characterized by vertical to moderate dips due NNE to NE. Different kind of complex structures have been observed in the gneisses. Tight to isoclinal folds (F1), axial plane NW–SE to E–W and plunging towards NW are observed from the biotite-gneisses (Plate 1 and 2). Tight to inclined fold (F2), sometimes coaxial and co-planar with F1 folds are also observed (Plate-1c). Open cross folds (F3) are also observed (Plate 1a), which postdate the gneissosity. The presence of sheath fold (plate 5c) and S–C fabric (Plate 4a & b) in the gneisses

indicate a strong deformation event after the high-grade metamorphism. The rotation of fabrics, presence of sheath and S-C fabrics in the gneisses suggest that the shearing and thrusting processes in Archean period cannot be ruled out. Moreover the rotation of porphyroblasts of feldspar in the gneiss (Plate 6&7) suggests sinistral shearing processes in shear zone. The structural studies revealed that these high-grade metamorphics have undergone at least two phases of deformation before the shearing and metamorphism and at least four phases of deformation after the metamorphism.

Most of the gneissic rocks of the study area preserve the deformational signatures of different phases. The rotation of feldspar phenocrysts (Plate 4, 6 b, 12c), S-C fabrics (Plate 2 a, b), sheath fold in E-W trending shear zones and mylonites point that a north-south directed stress, D4 deformation across the gneissosity was active after the crystallization of high grade metamorphites. The presence of mylonites and ultramylonites indicate ductile to brittle-ductile environment for the mylonitisation. It is also supported by shear zone mineralogy.

The fifth phase deformation structures are related with NE-SW trending shears (Plate 4a). This may be related to emplacement of quartz reef. In NE-SW direction is also observed in this rock unit as minor faults (Plate 1a). The last phase of deformation is recorded by dextral displacement of quartz reefs and NW-SE trending faults.

2.12.2 Mafic-ultramafic rocks and banded iron formation

Metamorphosed rocks of mafics, ultramafics and metasedimentaries (NMG) trending ENE-WSW overlies NW- SE trending high-grade metamorphics (OMG). The gneisses trending in NW-SE direction were found to swing in the E-W direction at the contact, which points that the rocks of these two groups have discordant relationship with each other and should have been formed at the two different events and then coarse to medium grained –folded at one stage. They are present at Mauranipur and Dhaurra. The contact between these two metamorphic rocks at Babina, Dhaurra and Mauranipur is found to be mylonitised and sheared.

The tight to open folds, axial surface trending NW-SE, related to D3 deformation, plunging towards north is recorded. The ENE trending banded iron formation exposed in a linear pattern is used as a marker band (plate 8) to find out the mafics and ultramafics and high-grade metamorphics in the study area. The structural study points that NMG rocks have subjected to at least three phases of deformation. These shears are nearly vertical and mostly confined to hornblende and biotite granitoids. The leucogranite found as intrusive in this unit is also involved in the shearing at many places. The fine-grained

granitoids of this phase are least affected. In the shear zones, the rocks are highly mylonitised. The presence of epidote, chlorite, sericite etc points that they were developed in the brittle -ductile conditions.

A thick E-W trending shear zone is found in the north of NMG, exposed at Babina, Jhankari dhaura, Gora kalan (2.6) where felsic, mafic and volcanosedimentaries were affected. These mylonites and ultra-mylonites of this zone are generally observed as medium to fine grained, and light pink to whitish green in colour. The ultramylonites observed at Jhankri Village (Mauranipur) comprise folded alternate bands of quartzofeldspathic and mafics rocks (plate 16 (a), (b) and 17 plate 18). The minerals constituents in this zone intensely folded bands of quartzofeldspathic materials are chlorite, amphibole, K-feldspar, quartz, and magnetic etc.

2.12.3 Granitoids

E-W trending dextral and sinistral shear zones have been observed at Babina, Katera, Dhaurka and Mauranipur areas. Thin to thick shear zones trending is E-W and NE-SW were observed at many places. The NNE-SSW trending shear was also noticed. S-C and S-C' fabrics are observed in granitoids (plate 12 (b)).

2.12.4 Quartz reefs

Emplacement of quartz reefs along NE-SE direction is undoubtedly related to major tectonic activity. The study point that they were emplaced after deformation received by the metamorphics and granitoids in the study area (plate 18). Sinistral displacement of older metamorphic group and newer metamorphic group is recorded at many places in the study area viz. at Babina, at Orchha etc. At Babina the displacement is very distinct (Plate 8 b, c), even the contact observed at Mankua (plate 8(c)). The signatures of the emplacement due to the quartz reef in the older and newer metamorphic rocks, and the granitoids are marked by fault (plate 1(a) 11(c) and joints (plate 10(b)).

2.12.5 Dolerite dykes

The dolerite dykes emplaced is also observed in the study area at Babina and Dhaurra area (plate 15(c)). These NW-SE trending mafic dykes displaced the quartz reefs dextrally and sinistrally. Dextral displacement is observed at Nayakhara (Near Prithvipur) and sinistral displacement at Laron (South of Katera). So at present study this mafic dyke emplacement is considered as the last phase (6th phase) deformation phase.

2.13 Mylonites and shear zone structures

Mylonites can be defined as strongly deformed rocks in which the strains are localized into a relatively narrow planar zone. The zone in which mylonitization occurs is called shear zone / mylonites zone. The grain size reduction usually occurred and recrystallization of crushed grains commonly observed in the form of foliation in the shear zone. Sense of shear can be easily deduced in the field when the displaced marker is present. It is possible to observe the variation in orientation of new foliation with respect to zone boundaries in the narrow shear zones.

In the study area, numerous thick to narrow shear zones of different types have been observed from all the litho-units. These shear zones are a few cm. wide to 100m long marked by bands of mylonites (plate no.) The mylonites at places vitreous appearance where commonly sinistral and rarely dextral displacement of pre existing elements upto a meter have been observed. The border of shear zone with undeformed rock is quite sharp and at places wall rock granite react by fracturing and flattening of quartz grains. Some of the shear bands of the granite exhibit pink and gray laminations. It is unfortunate that many earlier workers have recognized the features as sedimentary origin. In the investigated area mainly three types of shear zones have been recognized. The E-W trending shear zone is very thick and exposed throughout the area. Its thickness varies from 100-200m. It was contemporaneous to E-W shear deformation. A NE-SW trending shears are mainly visible in the granite gneisses and are co-terminus with quartz reefs. Mylonites bands of this shear zone are few cm to few meter wide and 100m to 1 km long. The incipient lines of shears seem to have been occupied by the quartz veins. The third type sheared is NNE-SSW and has displaced all the earlier marked shear zones. These shears are less prominent are early hair type zone. This is few cm in width and 10-15 m in length.

2.13.1 E-W shear zone

These shear zone is marked in the gneisses, granite and volcanosedimentaries. The sense of shearing is marked by rotated porphyroblasts of feldspar crystals (plate 6) in the gneisses and granite. Besides this, small-scale sense of shearing features are also observed such as S-C fabric near Sukuan (plate 4,5).

A thick zone of mylonites trending in E-W is observed at Jhankri (Mauranipur) in the low grade metamorphic (plate 17 and 18) where S-C fabrics are clearly demarked the rotation and displacement structures. Intense schistosity is observed within the bands. It indicates E-W trending sinistral shear zone. At Dhaurra a thick mylonitised sheared zone is also observed in the felsic volcanic rocks of the NMG, where rotation of feldspar

phenocrysts and quartz ribbons can be seen (plate 14a). Besides this at Dhaurra the banded iron formation follows a S-type structure due to E-W shearing (Fig 2.6)

At Katera reserve forest a narrow E-W trending mylonitised zone passing through the leucogranite is observed (plate 16).

2.13.2 NE-SW shear zone

Shear zones are observed at Mankua, and Bindrapura, east of the Sukuwan (Fig 2.6). Numerous NE-SW shear zones also observed at the north of Mauranipur railway station in the NMG. The NE-SW trending shear zones are mainly confined along the quartz reefs. They are 10-15 meter in thickness and 200-500 meters on length. Most of the shears are sinistral in nature and formed in the ductile to brittle –ductile in nature. The alteration and hydrous minerals are very frequent in these shears.

The structural study points that shear zone trending in E-W is the oldest mylonites which is followed by NE-SW trending shear. The NNE-SSW trending shears less prominent in the area and it has displaced the E-W and NE-SW trending shears.

2.14 Lineaments

The study area is characterized by three types of lineaments orientation (i) NE-SW (plate a) (ii) NW-SE and (iii) E-W (plate 8a). The first and the third are the predominant linear features observed in the area. Along NE-SW trending lineaments, mainly quartz reefs are observed and this lineament displaced the E-W trending lineament, which is represented by banded iron formation (plate 8b). The NW-SE lineament is represented by the most prominent mafic dyke swarms in the massif but in the present investigated area it is not so prominent like NE-SW and E-W lineaments. This NW-SE lineament has truncated the NE-SW trending quartz reefs. Therefore it is suggested that this NW-SE lineament, along which the mafic dykes were emplaced; is the youngest lineament observed in the study area, while E-W trending lineament represented by the Iron formation is the oldest lineament.

2.15 Faults

Faults of different trends are observed in many places of the study area and their mode of displacement are also different, but NW-SE faults are predominant (Fig. 2.6). These faults are more or less parallel to the older lineaments as well as to the older shear zones. Different faults observed in the area have been demarcated in geological map (Fig 2.6). At Nayakhera the prominent quartz reef trending NE-SW is dextrally displaced by the NW-SE trending fault. In contrast near Laron toward southwest of the NE-SW trending

quartz reef in synistrally displaced by the NW-SE trending fault. In the northern side of Mauranipur the E-W trending iron formation is faulted by parallel series of faults along NE-SW direction.

Tectonic, metamorphic and igneous activities of the study area in different lithounits are summarized in table (2.6). On the basis of field relationships, structural data, geochronological information, macroscopic and petrological studies of the metamorphics and igneous rocks of the study area, a geochronostratigraphy of has been proposed for the first time and is presented in table 2.7.

Table 2.2 Structures in Bundelkhand massif

DEFORMATION AND MESOSCOPIC STRUCTURE				
Litho unit	Sharma 1982	Basu, 1986	Roday, et. al., 1995	Prasad et. al. 1999
	Present Study			
POST BUNDELKHAND	Basic Dykes	NW-SE dolerite dykes cutting across NE-SW quartz reefs. Phyllonitic structure and enechelon fractures observed.		Dolerite dykes in the form of swarms emplaced in the massif is the evidence of extensional tectonic and last phase of thermal activity. General trend NW-SE and displaced the NE-SW trending quartz reefs.
	Quartz Reefs	NE-SW trending reef, secondary quartz veins observed.	Cataclastic & mylonitic nature, & have sigmoidal characteristics of veins brittle-ductile shear displaced sinistrally the BIF	Emplaced in all rocks. Trend of quartz reef is NE-SW, in the massif. Related to is brittle ductile in nature. Sigmoidal quartz veins developed within the main body in the late stage deformation. Displaced older and newer metamorphic rocks sinistrally. At places quartz reef displaced sinistrally by NW-SE trending faults. (D ₅ Deformation).
SYN BUNDELKHAND	Granitoids	Two phases of deformation (D4&D5). Upright to steeply inclined folds (F4) trending between W& NW	Two-phases of deform shear zones. Both steeply or vertical dip. E-W sinistral shearing and N15° NE-SW dextral shearing slow brittle ductile nature. Minor sinistral and dextral strike slip faults observed.	The hornblende granitoids and biotite grained emplaced among E-W trending fracture zones. E-W trending dextral and sinistral shear zone are observed. S-C and S-C' fabrics developed in granite and felsic volcanics. E-W trending dextral & sinistral shear zones indicates brittle ductile nature. Augen structure and subhorizontal lineation occurred in D ₃ and D ₄ deformation. Shear zones are ductile to brittle ductile in nature. Three phases of deformation recorded.
PRE BUNDELKHAND GRANITOIDS	Palar/Bervar Formation, Meta-volcanics, NMG	Two phases of deformation (D4&D5). Upright to steeply inclined folds (F5) trending between W and NW. Alternate bands of magnetite and quartz observed. The schistosity in metamorphics	Bedding in the form of alternate magnetite - Quartz layers. Trending E-W with steep dip (65°) due North. Tight similar fold, axes parallel to the strike of the body, plunging NE, joints are common. Quartz sericite - schist trending NW-SE & NE-SW observed.	Development of S ₁ and S ₂ schistosity in the meta-sedimentaries and meta-volcanics. E-W trending dextral shear (D ₄) zones observed, sub-horizontal stretching lineations mylonites and ultra mylonites observed. Intense schistosity at the contact between meta-sedimentary and meta-volcanics indicate sinistral shearing. Tight to open folds, axial surface trend NW-SE to NE-SW, folds axes plunging towards north. N 80° trending (BIF) beds steeply dip towards north. Four phases of deformation recorded.
	Rajaula/Kuraicha Formation : Migmatites, Gneisses, Metroni schists, Amphibolites etc. OMG	Five phases of deformation (D ₁ , D ₂ , D ₃ , D ₄ and D ₅). F ₁ folds - Tight isoclinal, hinge trending E-W. F ₂ folds open to tight upright, coaxial to F ₁ , hinge E-W trending. F ₃ folds sub-vertical and vertical steeply plunging. F ₄ folds upright steeply inclined F ₅ folds - upright	F ₁ fold observed initial developed in diorite to tonalitic rocks and developed sinistral shear zones.	Tight to isoclinal fold (F ₁), axial plane NW-SE to E-W trend and plunging towards NW are observed. F ₂ folds - tight to reclined, co-axial and co-planar with F ₁ , tight to open fold (F ₃), axial plane trending NW-SE to NE-SW are plunging towards north. Sheath and quartz ribbons observed in the shear zone of gneisses. Six phases of deformation recorded

Table : 2.3 Stratigraphic Succession of the Bundelkhand craton

Pascoc, 1950	Prakash et. al. 1975	Sharma, 1982	Basu, 1986	Present Study
Peridotites, pyroxenites (partially altered to serpentinites and talc-actionite dolerite-trap dykes)	Deccan Traps Vindhyan Supergroup Bijawar and Gwalior Group	Bundelkhand Group Madura ultrabasic : Pyroxenites, gabbro, serpentine, metabasic. Mahoba Dolerite : Dolerite dyke keratophyres, lamprophyres, carbonate. Matatila Granite : Pink granite, coarse to fine, massive. Garhmau granite : Grey, coarse to fine, massive, parphyroblastic gneisses. Paron meta-acid volcanics : Porphyroblastic, compact, sheet like granitic rocks. Palar Formation : Quartzite, phyllite, spotted phyllite, black shale, limestone, ferruginous quartzite with trace of chalcopyrite, galena, malachite, secondary. ---- Unconformity ---- Kuraicha Formation : Migmatites, gneisses, para-, ortho- and augen gneisses, amphibolite, chlorite and biotite schists, quartzites, meta-arkose, garnet-biotite gneisses.	Deccan Traps Vindhyan Supergroup Bijawar and Gwalior Group Dolerites Quartz reef (with pyrite, chalcopyrite, pyrophyllite and diaspore) Aplite Esmeraldite Porphyries Pegmatite Leucocratic granites Migmatites & Syenites Medium grained porphyritic granites Coarse grained porphyritic granite Coarse biotite granite Gneisses. ---- Unconformity ---- Rajaula Formation : Banded iron-formation Metabasites, gneisses, marble, schists, Metamorphosed mafics and amphibolite.	(Post-Bundelkhand Granitoids) Deccan Traps Vindhyan Supergroup Bijawar and Gwalior Group Mafic Dykes and Swarms Quartz Reef Bundelkhand Granitoids Fine grain leucogranite Coarse grain leucogranite Foliated biotite granite Biotite granite Hornblende granite (Pre-Bundelkhand Granitoids) Newer Metamorphic Group Metavolcanics Banded Magnetite Quartzite, Micaceous quartzites, commingtonite-grunerite-garnet magnetite schist. Talc-chlorite schist, actinolite-tremolite- talc schist, hornblende-chlorite -epidote schist, garnet chlorite-actinolite schist Older Metamorphic Group Biotite- gneiss, hornblende-biotite gneisses, sillimanite gneisses, amphibolite Tonalite-trondhjemitegneisses, granite-gneisses, migmatites.
Pre-Dharwar, Bundelkhand granite Complex with quartz reef, and with inclusions of Mahroni schist.	Bundelkhand, granite Formation: Dull pink, dense fine grained to porphyritic granite : coarsely crystalline pink un-foliated granites and migmatities. ---- Unconformity ---- Berwar Formation : Iron-formation, carbonate rock, grey green slates, Fuschsite quartzsite and conglomerate. ---- Unconformity ---- Rajaula Formation : Sedimentation- volcanism (amphibolites, biotite-feldspar foliated gneisses.)			

Table 2.4 Radiometric dating of the rocks of Bundelkhand Massif.

S. No.	Location & Rock Type	Method	Age in M.a.	Reference
1.	Majhgawn Kimberlite plug	K-Ar	1140±20	Crawford & Compston, 1970 and Mathur, 1960
2.	Vindhyan Sedimentary Rocks	K-Ar	~1400	Sharma and Rahman, 1990
3.	Alipura Mafic Dyke	K-Ar	1523	Sarkar et. al., 1990
4.	Kurat Volcanic rocks	Rb-Sr	1691±180	Pandey et. al., 1995
5.	Dargawan Mafic rocks as Sill (Bijawar Basin)	Rb-Sr	1789±71	Sarkar, 1997
6.	Kalinjar Fort Mafic dyke	K-Ar	1799	Sarkar et. al., 1990
7.	Mafic volcanics (associated with Gwalior Sedimentary Rocks)	Rb-Sr	1830±200	Crawford & Compston, 1970
8.	Quartz Reef		2000	Sharma & Rahman
9.	Bdera Gneissic migmatite	Rb-Sr	2130±102	Sarkar et. al., 1984
10.	Coarse grain granites, granite porphyry and Aplite (Babina Talbehat)	Rb-Sr	2246±78	Sarkar et. al., 1984
11.	Grey granodiorite near Jhansi	Rb-Sr	2359±53	Sarkar et. al., 1984
12.	Granodiorite near Jhansi	Rb-Sr	2402±70	Sarkar et. al., 1990-1996
13.	Bansi Rhyolite	Pb ²⁰⁷ /Pb ²⁰⁶	2517±7	Mondal et. al; 2002
14.	Lalitpur Biotite Granitoid	Pb ²⁰⁷ /Pb ²⁰⁶	2521±6	Mondal et. al; 1998.
15.	Bansi Rhyolite	Pb ²⁰⁷ /Pb ²⁰⁶	2521±7	Mondal et. al; 1998.
16.	Granites	Rb-Sr	2560±106	Crawford, 1970
17.	Karera Gneisses	Pb ²⁰⁷ /Pb ²⁰⁶	2563±6	Mondal et. al; 2002
18.	Pillow lava (near Bijawar)		2600	Crawford & Compston, 1970
19.	Bansi Rhyolite	Pb ²⁰⁷ /Pb ²⁰⁶	2517±7	Mondal et. al; 2002
20.	Lalitpur Biotite Granitoid	Pb ²⁰⁷ /Pb ²⁰⁶	2521±6	Mondal et. al; 1998.
21.	Bansi Rhyolite	Pb ²⁰⁷ /Pb ²⁰⁶	2521±7	Mondal et. al; 1998.
22.	Granites	Rb-Sr	2560±106	Crawford, 1970
23.	Karera Gneisses	Pb ²⁰⁷ /Pb ²⁰⁶	2563±6	Mondal et. al; 2002
24.	Pillow lava (near Bijawar)	Rb-Sr	2600	Crawford & Compston, 1970
25.	Migmatitic Gneisses	Pb ²⁰⁷ /Pb ²⁰⁶	2696±3	Sharma; 1998
26.	Babina Gneisses	Pb ²⁰⁷ /Pb ²⁰⁶	2697±3	Mondal et. al; 1998.
27.	Panchwara Gneisses	Pb ²⁰⁷ /Pb ²⁰⁶	3189±5	Mondal et. al; 1998.
28.	Lodhaphar gneisses	Sm-Nd	3200	Sharma & Rahman; 1995
29.	Mahoba Amphibolites	Pb ²⁰⁷ /Pb ²⁰⁶	3249±5	Mondal et. al; 2002
30.	Mahoba Gneisses	Pb ²⁰⁷ /Pb ²⁰⁶	3270±3	Mondal et. al; 2002
31.	Kuraicha Gneisses	Pb ²⁰⁷ /Pb ²⁰⁶	3297±8	Mondal et. al; 2002
32.	Lodhaphar gneisses	Sm-Nd	3300	Sharma & Rahman 1995, 1996
33.	Baghora Gneisses (TTG)	Rb-Sr	3503±99	Sarkar et. al; 1996

Table 2.5 Relationship between deformation, mesoscopic structure and recrystallisation of rocks of the Bundelkhand massif

		Deformation	Mesoscopic structure	Metamorphic
POST BUNDELKHAND	Mafic Dykes	D ₆ (1800 Ma to 1600 Ma)	Giant dolerite dykes throughout the Bundelkhand massif is the evidence of extensional tectonic and last phase of thermal relaxation. They generally trend NW-SE and displaced the NE-SW trending quartz reefs.	At the contact of basic dyke a narrow zone of alteration and hydrothermal activities. chlorite, sericite, epidote, pyrite, calcite, tremolite, actinolites, pyrophyllite, and diasporite developed at the contact.
	Quartz Reef	D ₅ (2300 Ma to 2000 Ma)	Emplacement quartz reefs in NW-SW trending direction in brittle and ductile deformational environment. Sigmoidal veins developed at the late stage deformation. It displaced the older and newer metamorphics sinistrally.	The retrogression and alteration of feldspar and amphibole minerals observed. Hydrothermal and pegmatite activities were common. The prophyllite, diasporite, clay, epidotes, kaolinite minerals developed along NNE-SSW trending reefs. The base metals, molybdenum and other ore fluid emplaced along fracture and shear zone.
SYN BUNDELKHAND	Granitoids	D ₄ (2500 Ma to 2300 Ma)	E-W trending dextral and sinistral shear zones are observed S-C and S-C' fabrics developed in granite gneisses, and volcano-sedimentaries. Sheath folds and quartz ribbons developed. Shear zones are few meters to up to 1 km recorded thick and developed in ductile to brittle ductile environment. The new E-W trends fabrics in the gneisses.	Local thermal metamorphism, specially in the mylonites zones, recorded. Mortar texture, recrystallization of chlorite, biotite, feldspar, hornblende developed in mylonites at the contact of hornblende/ biotite granite. Crystallization of epidote, chlorite, sericite in the granite and gneisses are the indication of hydrothermal activity and retrograde metamorphism at the late stage emplacement Bundelkhand granitoids. In the granitoids, NMG and OMG, E-W trending mylonites, blastomylonites, ultramylonites developed.
PRE BUNDELKHAND GRANITOIDS	Newer Metamorphic Group	D ₃ (3200 Ma to 2600 Ma)	Tight to open folds, axial surface trending NW-SE to NE-SW folds axis plunging towards north recorded N 80° trending beds are steeply dip (> 65). Alternate bands of magnetite and quartzite points two phases of deformation and metamorphism. Mafics, ultramafics Iron formation, ferrogneiss quartzite, deposited in E-W trending epicontinental basin. The OMG metamorphics folded, rotation of strike from NW to EW.	Prograde M ₂ metamorphic minerals of green schist facies to lower amphibolite facies developed. Metamorphism (M ₂) recorded in the mafic ultramafic, ferruginous quartzites and volcanosedimentaries.
	Older Metamorphic Group	D ₁ and D ₂ (3500 Ma to 3200 Ma)	F ₁ fold tight to isoclinal and reclined, axial surface trending NW-SE to E-W, folds axis plunging NW. F ₂ fold – tight to reclined, co-axial and co-planer with F ₁ folds.	3500 Ma old TTG were emplaced at 3200 Ma during the metamorphism (M ₁). Gneisses, migmatites and formations of upper amphibolite facies. M ₁ metamorphism recorded. Biotite granites, Gray granites, streaky gneisses, Biotite hornblende gneisses, clac-silicate granulites, garnet - silliminite gneisses were developed.

Table 2.6 Tectonothermal activities in the investigated area

	Litho Unit	Deformation	Tectonics, metamorphism and magmatism
POST BUNDELKHAND GRANITOID (2300-1600Ma)	Basic Dykes	D ₆ Ma to 1600 (1800 Ma)	General trend of dyke is NW-SE, displaced sinistrally the quartz reefs trending NE-SW. Alteration along the shear zones, crystallised the minerals chlorite, muscovite, seriate, epidote, pyrite, pyrophyllite and diaspore. No metamorphism at the contact of basic dyke and country rock. Dolerite dykes in craton spread over the massif in the form of swarms is the evidence of extensional tectonic and last phase of magmatism in the region
	Quartz Reefs	D ₅ Ma to 2000 Ma (2300 Ma)	NE-SW trending quartz reef, formed in the brittle - ductile deformational environment. Alteration of feldspars and amphibole minerals. Development of phyrophyllite, diaspore, kaolinite, epidote, chlorite, sericite are the indication of hydrothermal activity. Sigmoidal veins developed within the main body of reef at the late stage of deformation. Quartz reefs displaced the older rocks, marks the dextral shearing. Quartzite and Pegmatite emplaced in NE-SW direction
SYN BUNDELKHAND (2500-2300Ma)	Granitoids	D ₄ Ma to 2300 Ma (2500 Ma)	Mortar texture, recrystallization of chlorite, biotite, feldspars, andalusites developed in E-W trending mylonites zones suggests thermal metamorphism on the local scale. Dextral and sinistral shearing, E-W trending shear zones in the brittle ductile environment, augen structures and sub-horizontal lineation were also occurred in gneisses, TTG rocks of OMG. E-W trending dextral shearing. Sub-horizontal stretching lineation, mylonites and ultra-mylonites developed along E-W in NMG E-W trending shear zone with S-C and S-C' fabrics are observed in dextral and sinistral shears developed in granite OMG and NMG. Hbl. Granite, Bio Granite, deformed granite, Leucogranites observed.
PRE BUNDELKHAND (3500-2600Ma)	Newer Metamorphic Group	D ₃ Ma to 2600 Ma (3200 Ma)	The NW-SE trending fabrics in the gneisses rotated to E-W. Prograde (M ₂) metamorphic rocks of green schist to lower amphibolites facies developed in NMG (mafic and ultra mafics with volcano-sedimentary rocks). Act-Tre-schist, micasceous, quartzite, BMQ, Qtz. schist, Com-Gru schist formed. Tight to open folds with axial surface trending NW-SE to NE-SW, plunging towards north recorded in NMG. M2 event of metamorphism recorded. Deposition of banded iron formation, ferruginous quartzite, mafics and ultramafics, volcanosedimentary rocks in epicontinental sea.
	Older Metamorphic Group	D ₁ & D ₂ Ma to 3200 Ma (3500 Ma)	Hook folds, tight to isoclinal fold F ₁ , F ₂ folds coaxial with F ₁ plunging towards NW, axial plane trending NW-SE to E-W. Tight to open fold F ₃ , plunging north, axial plane trending NW-SE to NE-SW developed in D ₂ deformation. F ₃ fold post date the metamorphism M ₁ , formed during D2 deformation. Gneisses, migmatites, granite-gneisses, streaky gneisses, biotite-hornblende gneisses, calc silicate granulites, garnet-sillimanite gneisses were formed (M ₁ metamorphic event).

Table 2.7 : Strtigraphy of the study area

Tectonic -Unit	Litho -units
Mafic Dykes (1800-1600Ma)	Dolerites, gabbro, metadolerites, lamprites
Quartz Reefs (2300-2000Ma)	Pegmatites, quartz veins, quartzite, mylonites
Bundelkhand Granitoids (2500-2300Ma)	Hornblende granites, biotites granites, coarse grained leucogranites, deformed granites, medium to fine grained leucogranite, syenogranite, microgranites, aplites
Newer Metamorphic group (3200-2600Ma)	Meta mylonites and Metavolcanics: mylonites and ultramylonites, rhyolites and, basalt. Banded magnetite quartzites (BMQ), Quartzites, commingtonites-grunerite-magnetite quartzite micaceous quartzite, quartzite, mica schist, garnet mica schist etc. Garnet-chlorite-actinolite schist, tremolite-talc- actinolite schist, talc-chlorite schist, hornblende- epidote chlorite schist, actinolite-chlorite schist.
Older Metamorphic Group (3500-3300Ma)	Tonalite- Trondhjemite-gneiss (TTG), gneiss amphibolite

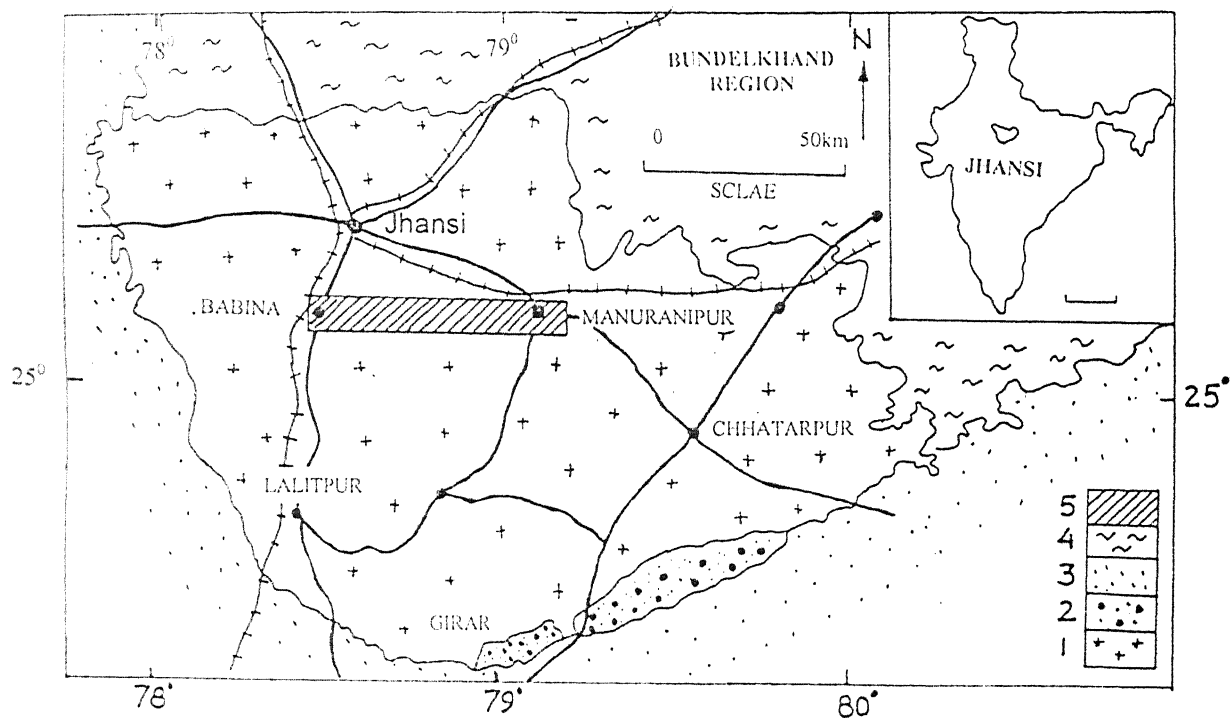


Fig. 2.1. Location map of the study area. 1: Granite Massif, 2: Bijawar, 3: Vindhya, 4: Alluvium, 5: Study area. Inset locates the Bundelkhand Craton in the map of India.

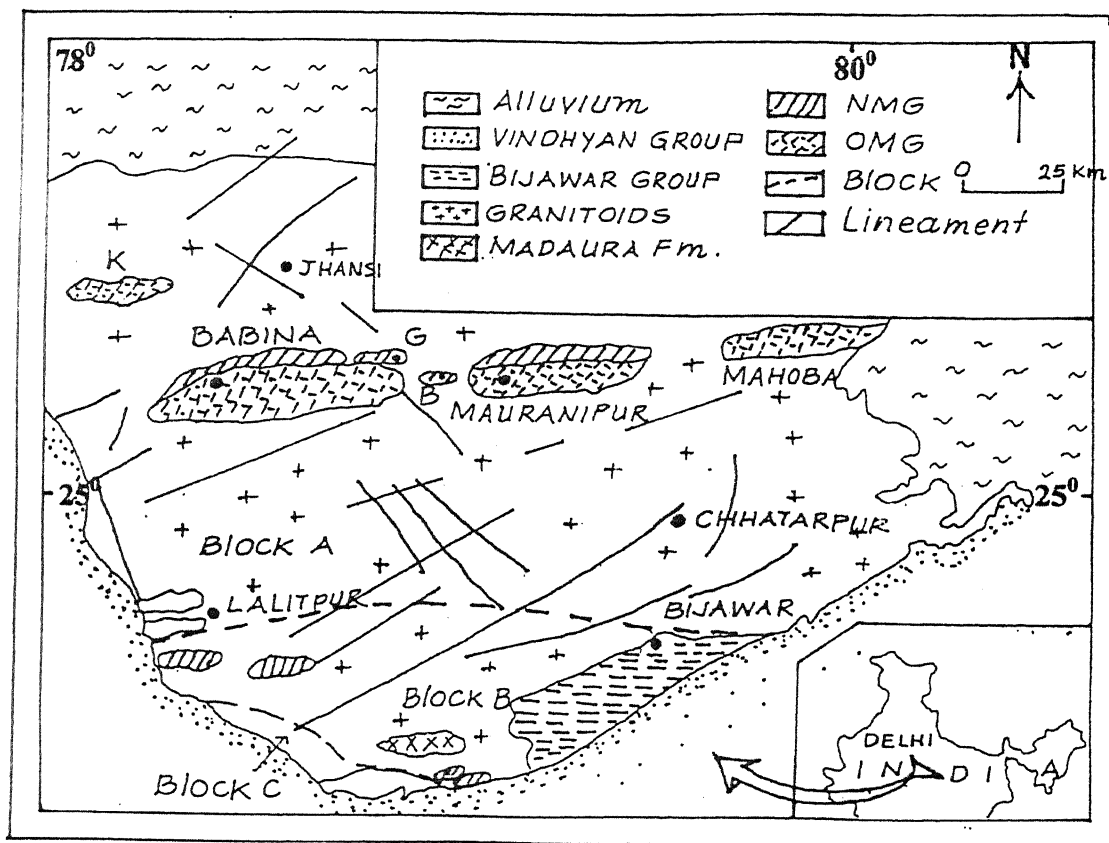
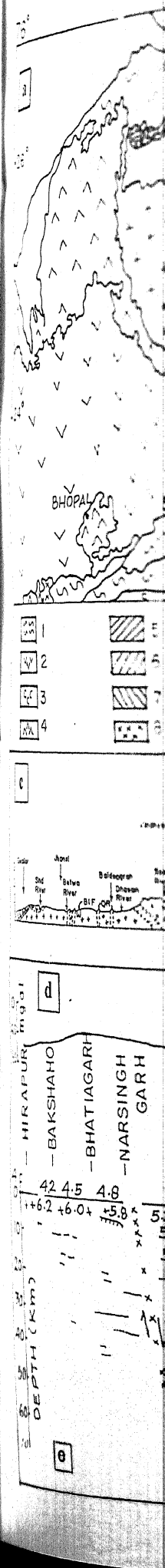


Fig. 2.2 Regional Geology of Bundelkhand Massif (Modified after Mondal et. al. 2002, Basu 1986 and Prakash et.al. 1975).

The older Metamorphic Group (OMG) and Newer Metamorphic Group (NMG) of rocks are exposed in E-W direction and are mainly confined in central part of the massif. Blocks A, B, and C are based on topography. Inset locates in Bundelkhand craton in the map of India.

Fig 2.3. Regional tectonic set up and geological and geophysical map of the central India.

- (a) Geological map of Northern Part of Central India (after Basu 2001).
1: Alluvium, 2: Deccan Volcanics, 3: Gondwana, 4: Vindhyan supergroup, 5: Gwalior group, 6: Bijawar Groups, 7: Mahakaushal Group, 8: Intrusive Granite, 9: Bundelkhand Granite, 10: Sidhi Gneiss, 11: Chhotanagpur Gneiss, 12. Madaura Group.
- (b) Proterozoic mobile belt in the Indian shield. Map showing the boundary of Bundelkhand craton and granulite rocks of Eastern Ghats and its relation with other Indian provinces. The abbreviation are BKC: Bundelkhand Craton, AC: Aravalli, Craton, SG: Sothern Granulite Belt, EGB: Eastern Ghats Belt, EDC: Eastern Dharwar Craton, BTC, Bastar Craton, DEC: Deccan Basalt, D: Delhi.
- (c) Geological Cross-section from Gwalior to Malanjkhanda (for lithological symbols an horizontal scale see figure (a) (after Basu 2001).
- (d) Bouguer Anomaly Between Hirapur and Manda (after Ramakrishna, 1995).
- (e) Crustal Depth Section from DSS along Hirapur-Jabalpur-Mandla (after Ramakrishna, 1995). 1: Refractor with velocity km/sec, 2: Reflector segments, 3: Reciprocal Reflection Segments, 4: Crystalline Basement 5: Moho segments, 6: Fault with direction of throw.



sical map of

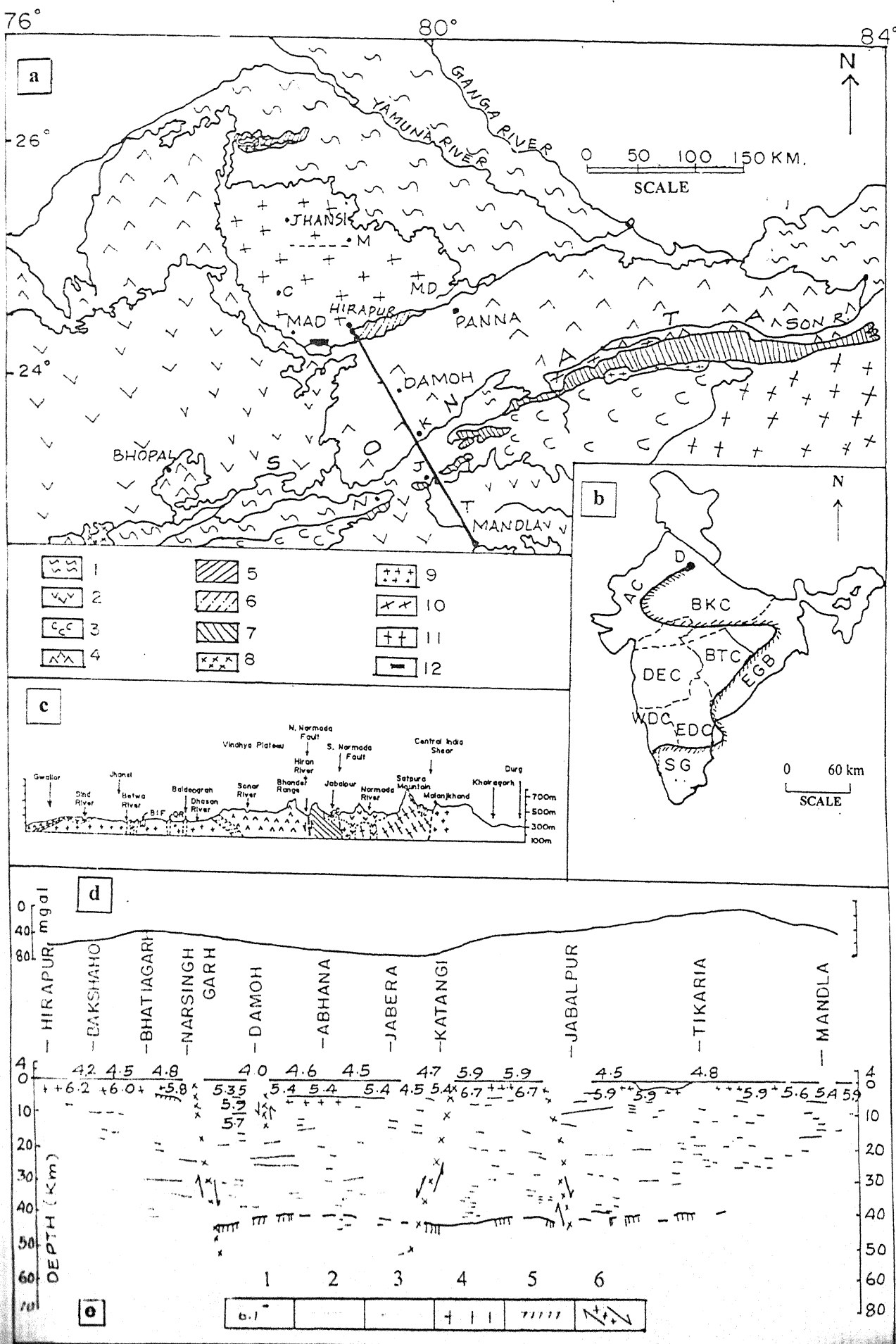
after Basu 200
na, 4: Vindhya
7: Mahakaush
ranite, 10: Sit
oup.

Map showing
rocks of Eastern
The abbreviat
ton, SG: Sothe
Eastern Dhan
D: Delhi.

Malanjkhanda
e (a) (after Basu)

Manda (a)

Jabalpur-Mand
velocity km/sec.
Segments,
with direction



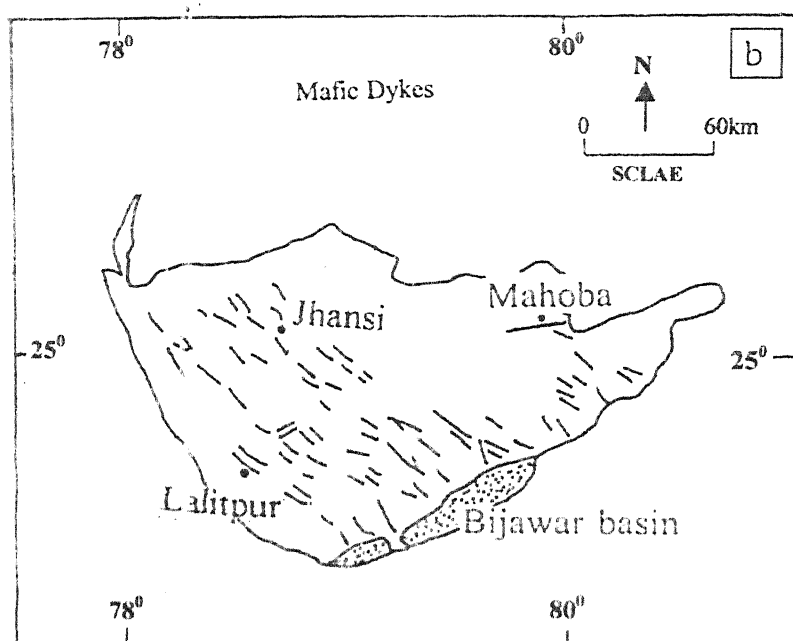
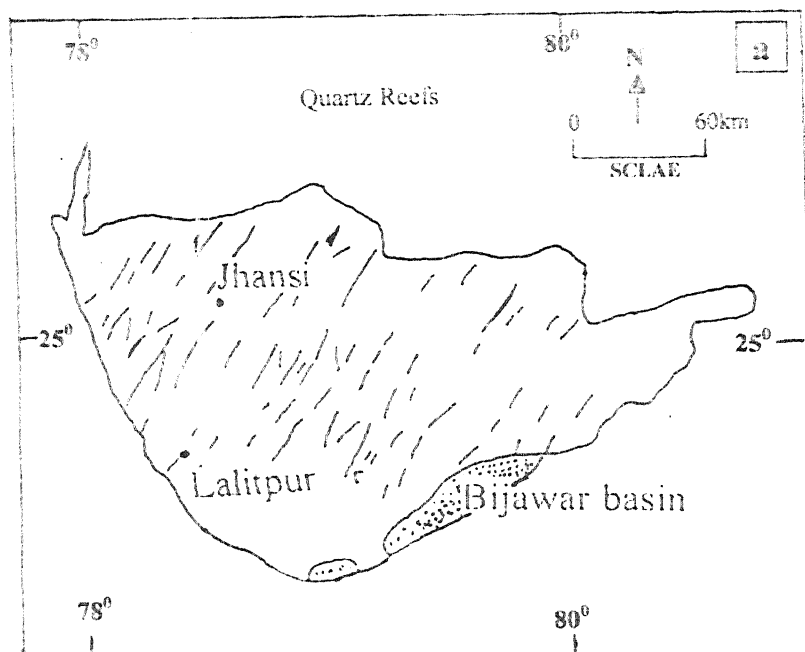


Fig 2.4. Trend of (a) Quartz Reefs and (b) Mafic Dykes in Bundelkhand (after Sharma 2000)

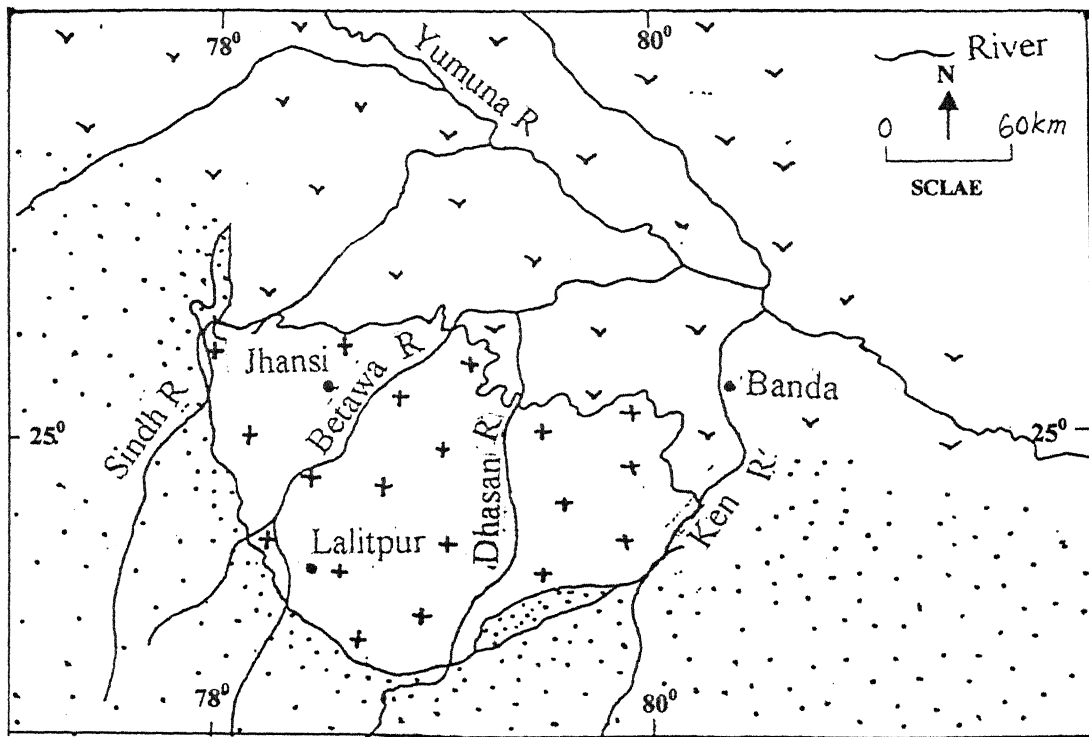


Fig 2.5. Major River trend in Bundelkhand Region

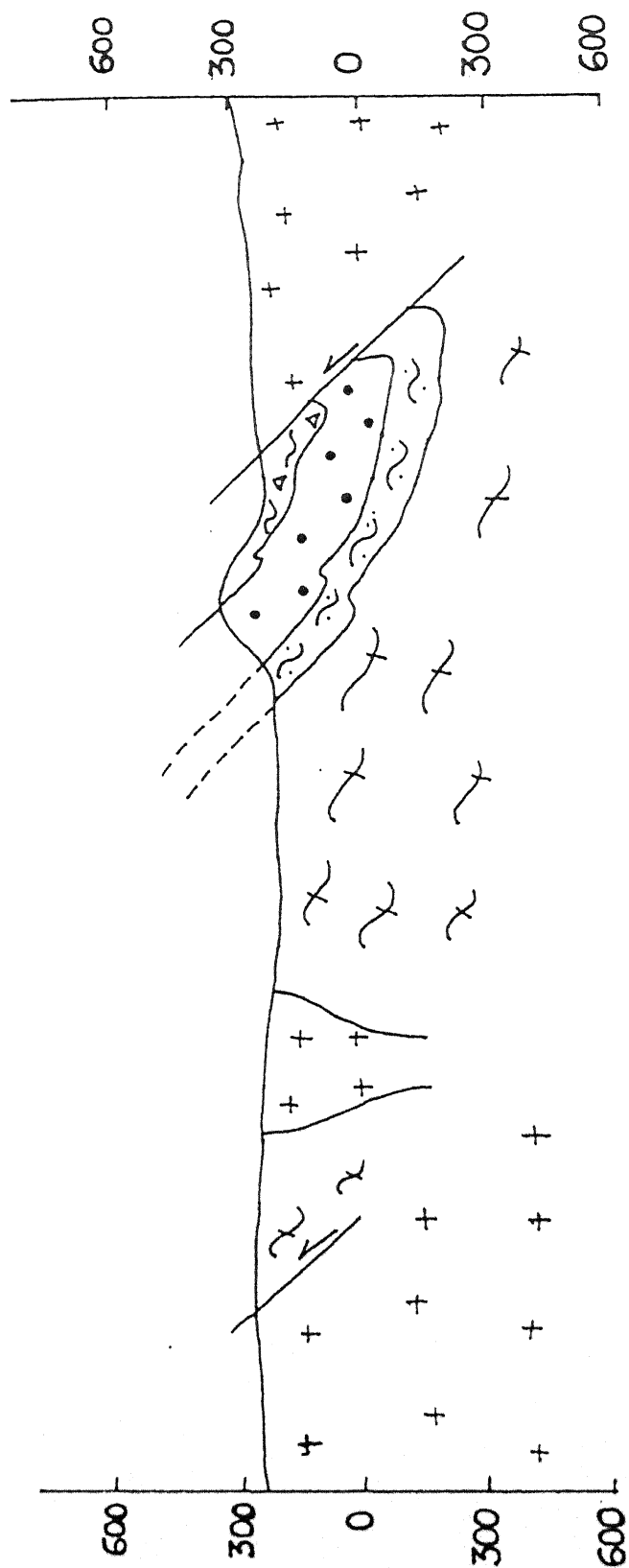


Fig. 2.7 Geological cross-section along X-Y line of the Babina area, western part of the study area.

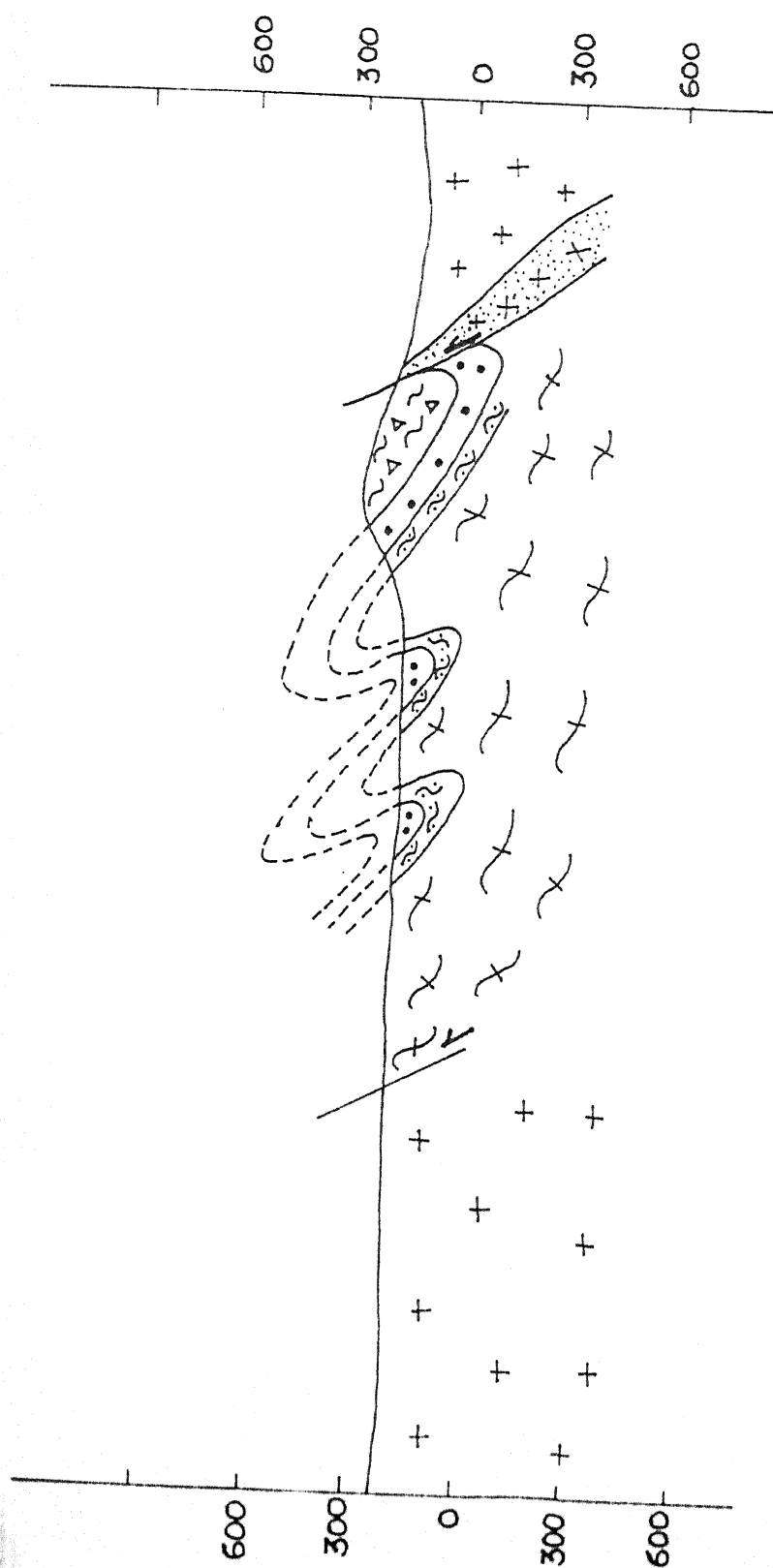


Fig. 2.8 Geological cross-section along A-B line of the Mauranipur area, eastern part of the study area.

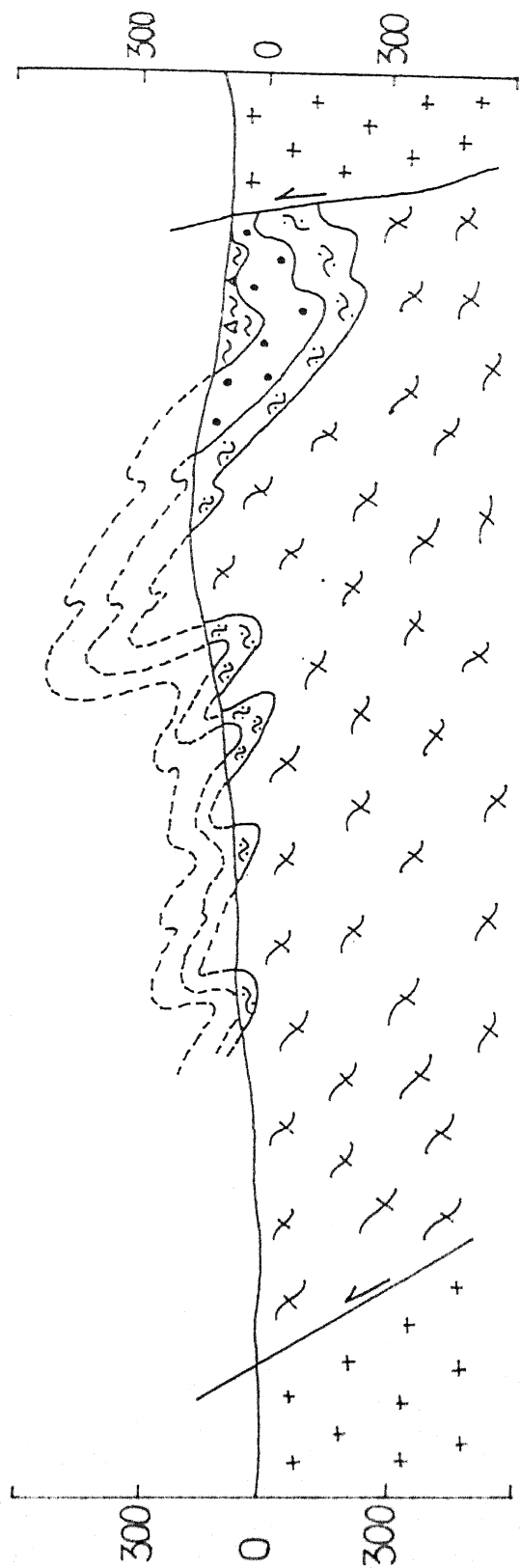


Fig. 2.9 Geological cross section along P-Q line of the Dhaurra area, central part of the study area.

PLATE – 1

Fig. (A) Hand specimen photograph of gneiss showing F_1 and F_3 folds. Sample collected from Gneisses exposure at Lakardevi, Babina.

Fig. (B) Hand specimen photograph of gneiss and amphibolite showing co-folding (F_1 and F_2 folds). Sample collected from Jounpur, Babina.

Fig. (C) Hand specimen photograph of gneiss and amphibolite showing co-folding and developed hook fold (F_1 and F_2 folds). Sample collected from Jounpur, Babina.

PLATE - 1

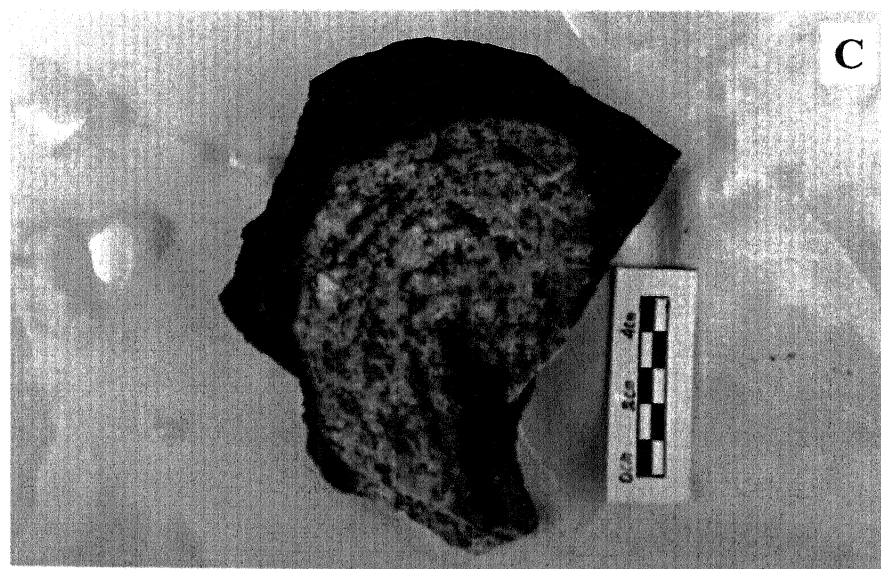
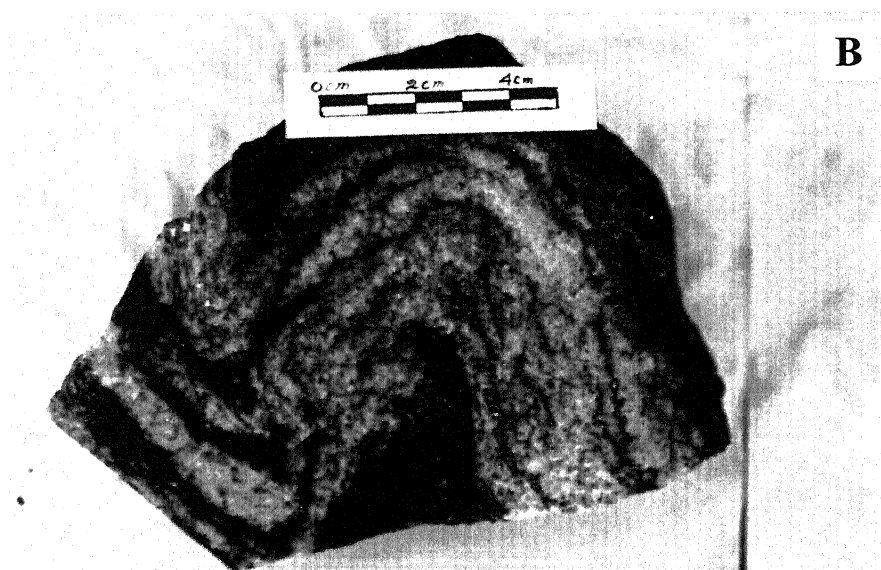
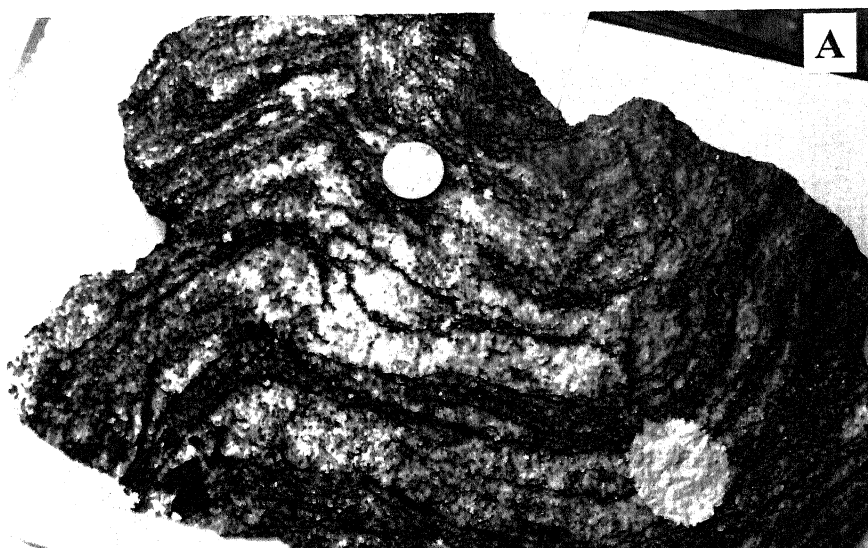


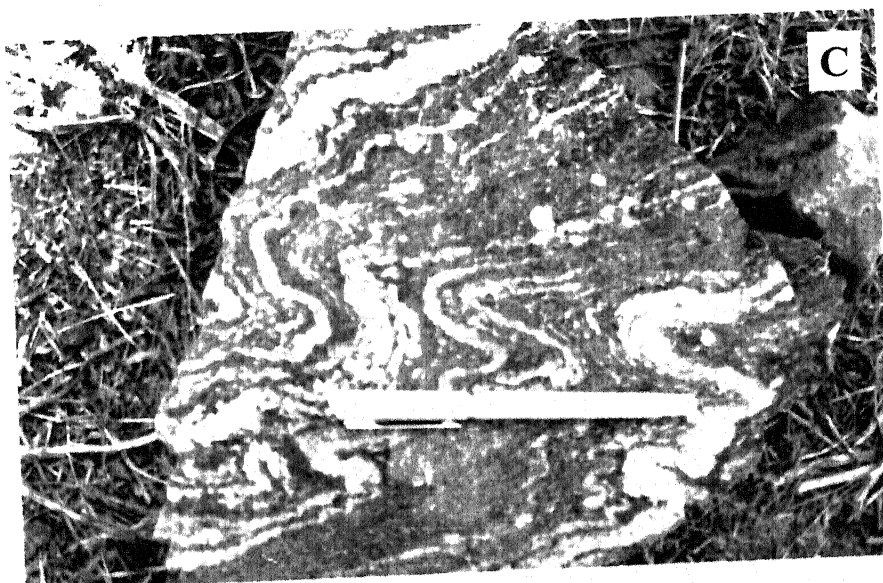
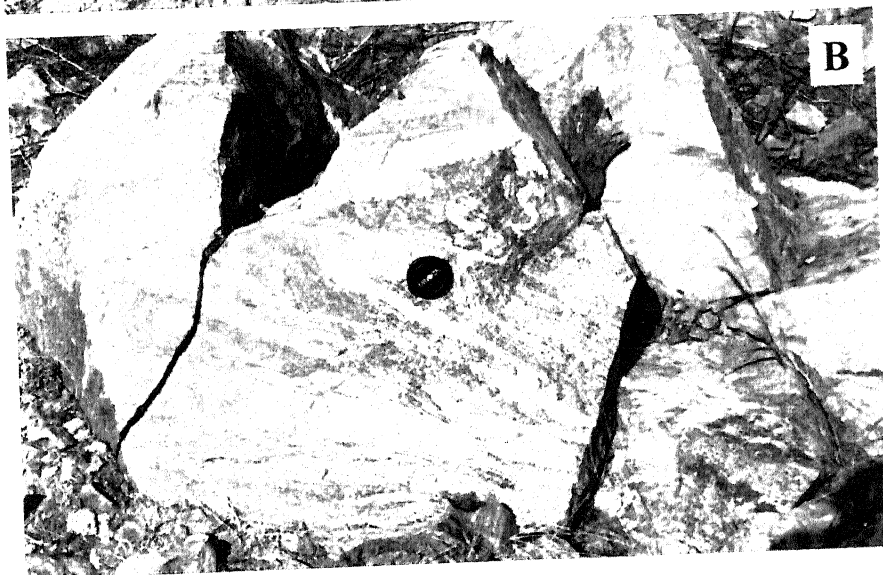
PLATE – 2

Fig. (A) Field photograph shows the gneiss observed at Jounpur, Babina. It shows the alternate bands of leucocratic and melanocratic minerals. It also shows folding.

Fig. (B) Field photograph of gneiss at Jaunpur showing folding and partial melting.

Fig. (C) Field photograph showing intense folding (ptygmatic fold) in gneisses at Gora. The thickness of the bands is irregular.





observed at Jounpur &
melanocratic

showing folding at

ptygmatic fold) in
regular.

PLATE – 3

Fig. (A) Field photograph of gneiss at Jounpur, showing partial melting and recrystallization, and also showing development of augens of quartz feldspathic masses.

Fig. (B) Field photograph of gneisses at Gora showing recrystallization and development of augens of quartzofeldspathic masses. The thickness of the leucosomes decreases with increasing thickness of melanosomes. Augen structures are also showing the E-W shearing.

Fig. (C) Field photograph of gneiss showing development of streaky gneiss converting to the gray granite.

PLATE - 3



PLATE – 4

Fig. (A) Field photograph showing minor faulting bands of gneiss along NE-SW direction near Babina iron formation.

Fig. (B) Field photograph of streaky gneiss at Jounpur, Babina showing the development of gray granite and also showing the S-C fabric indicating E-W trend.

Fig (C) Field photograph of seeth fold in gneiss near Babina iron formation shows the development of S-C fabric and indicating E-W shearing.

PLATE - 4

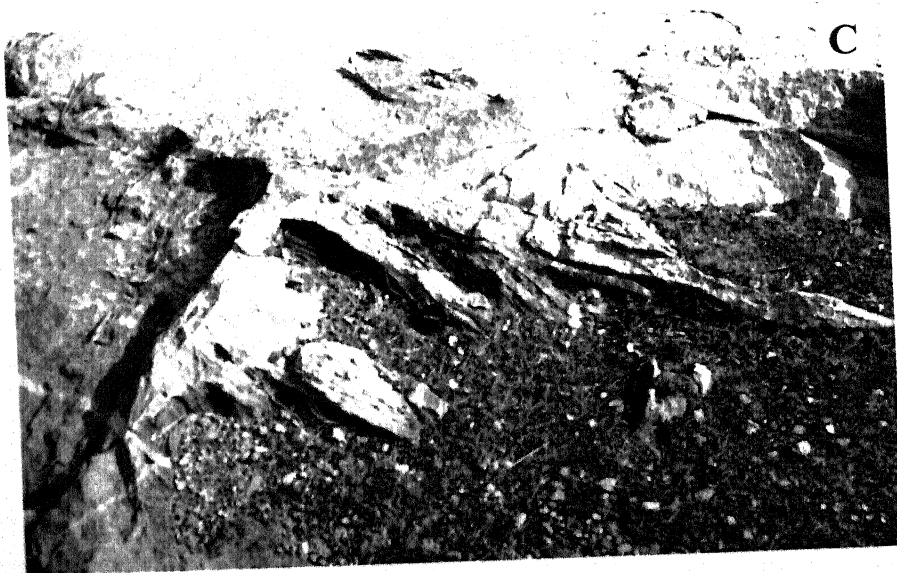
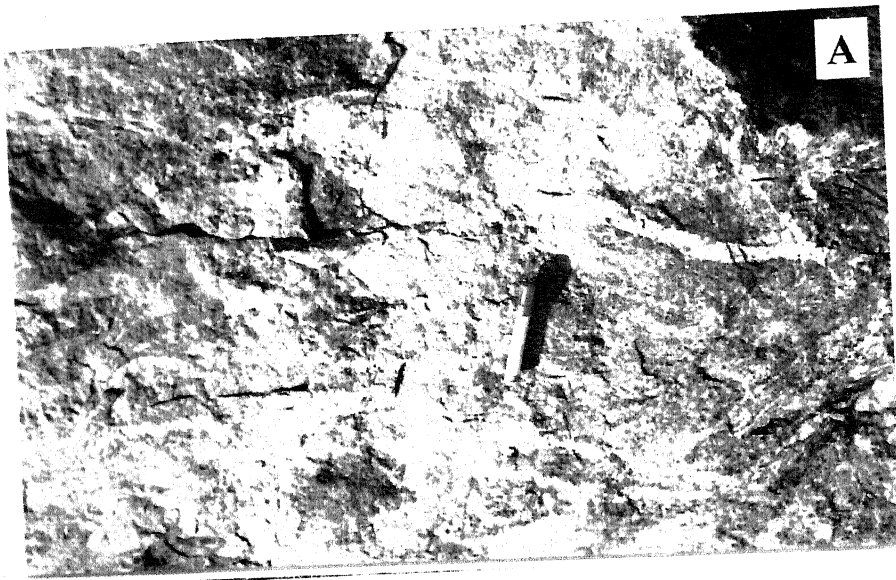


PLATE – 5

Fig. (A) Field photograph showing S and C plane, indicating E-W shearing in gneiss at the road head of Babina Sukwa road near Babina iron formation.

Fig. (B) Field photograph of gneiss at the road head of Babina – Sukwa road near Babina iron formation. Relict of S-C fabric is also observed.

Fig. (C) Field photograph of gneiss near Babina iron formation showing sheath fold structure developed due to intense deformation.

PLATE - 5

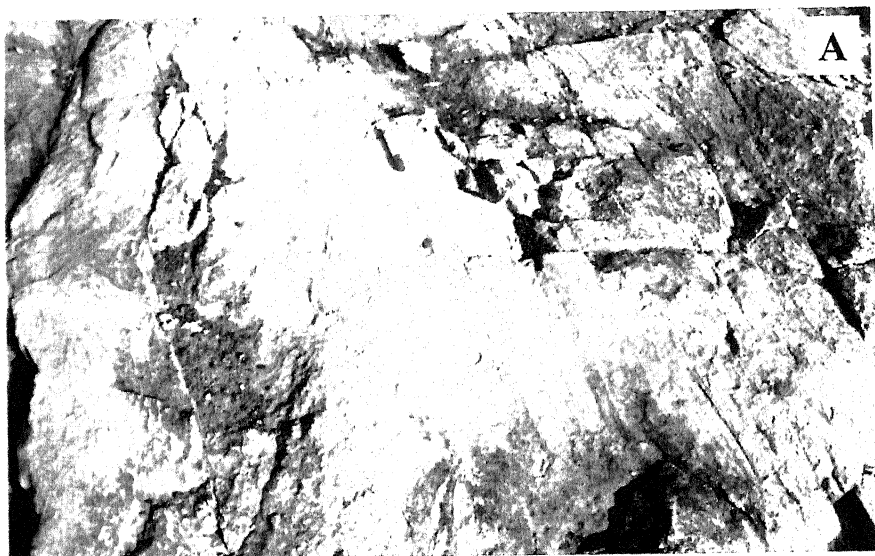
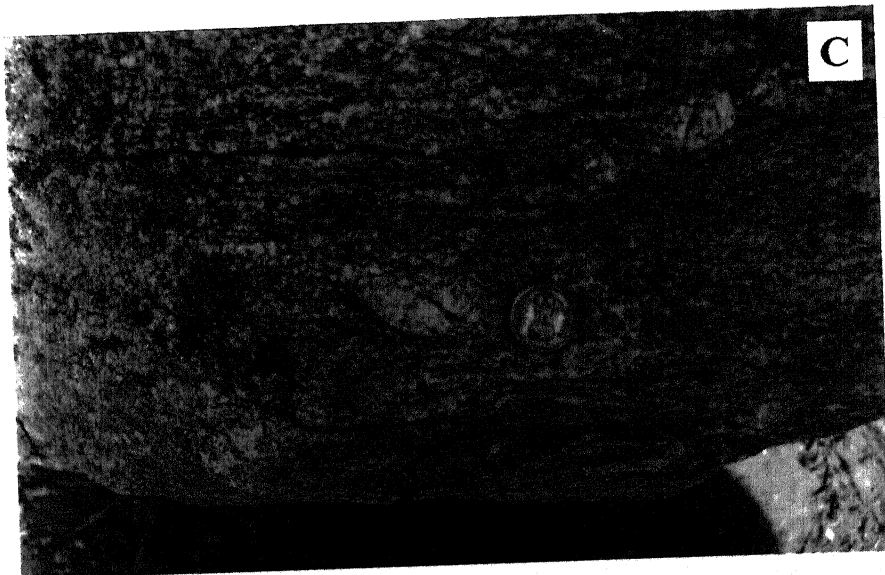
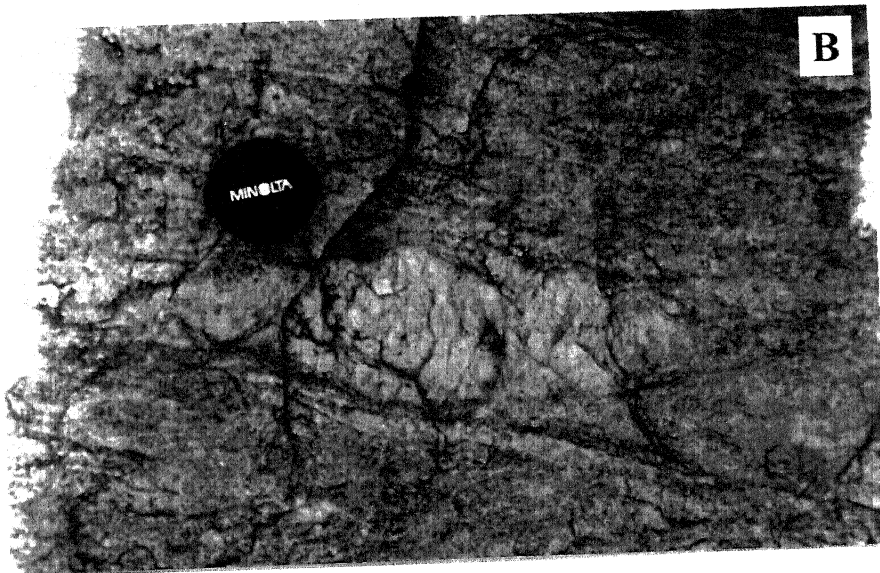
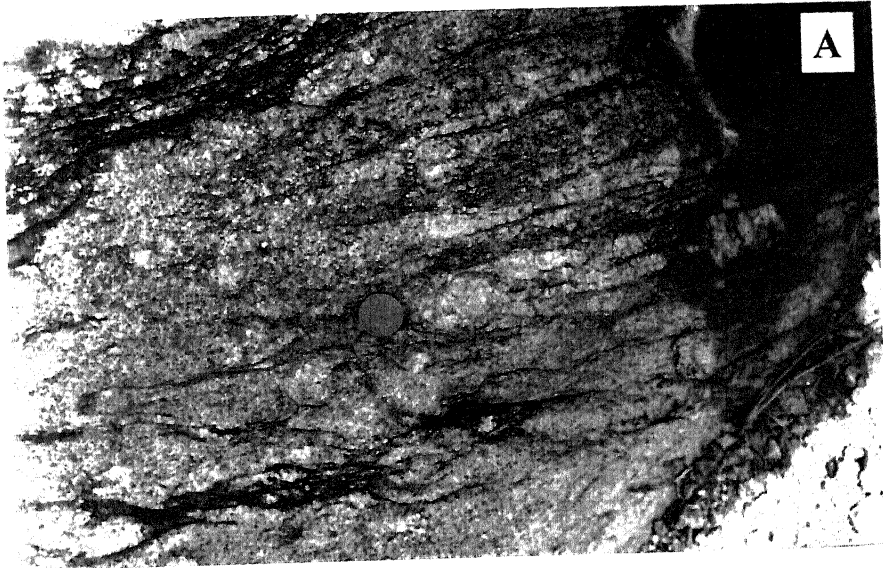


PLATE – 6

- Fig. (A) Field photograph of gneiss at the south of Mauranipur village showing the development of augens of quartzofeldspathic masses and also showing the reducing the melanosomes.
- Fig. (B) Field photograph shows the augen structure in gneiss. This photograph also showing the E-W shearing at Mauranipur
- Fig (C) Field photograph of gneiss at south of Mauranipur showing the development of augen structure and reducing of melanocratic and leucocratic bands.



uth of Mauranipur
quartzofeldspathic
somes.

structure in gneiss
g at Mauranipur

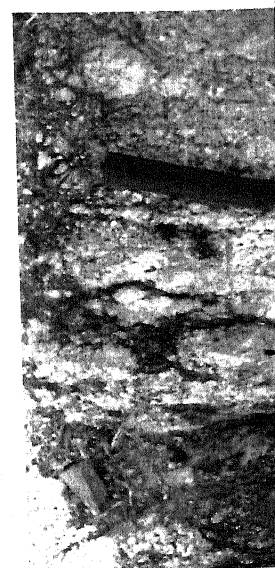
Mauranipur showing
cing of melanocrystic

PLATE – 7

ig. (A) Field photograph of gneiss at Dhaurra showing the S-C fabric and development of augens of quartzo-feldspathic masses.

ig. (B) Field photograph of mylonitised granite orientation of feldspar phenocrysts shows E-W shearing and NE-SW fracture developed due to deformation near Dhaurra.

ig. (C) Field photograph of porphyritic granite of Dhaurra showing E-W shearing by the rotation of feldspar phenocrysts and NE-SW trending fracture.





TE - 7

Dhaura showing the SO
to-feldspathic masses

white orientation of
NE-SW fracture

Dhaura showing
and NE-SW

PLATE – 8

Fig. (A) Field photograph showing the panoramic view of the contact of ENE-NSW trending iron formation and older gneissic terrain at lower relief at Babina.

Fig. (B) The field photograph showing the panoramic view of iron formation, which is synistrally, is displaced in NE direction.

Fig. (C) Field photograph showing the panoramic view of contact of ENE-NSW iron formation and the NE-SW trending quartz reef, which displaced the iron formation.

PLATE - 8

A



B



C



PLATE – 9

Fig. (A) Field photograph showing the panoramic view of the contact of prominent NE-SW trending quartz reef and hornblende, biotite-gneiss at Bangra.

Fig. (B) Field photograph showing the panoramic view of ENE-WSW trending quartz reef and NE-SW trending quartz reef at Bangra.

Fig. (C) Field photograph showing the panoramic view of the contact junction of ENE-WSW and NE-SW quartz reef at Bangra.



PLATE - 9

A



B



C

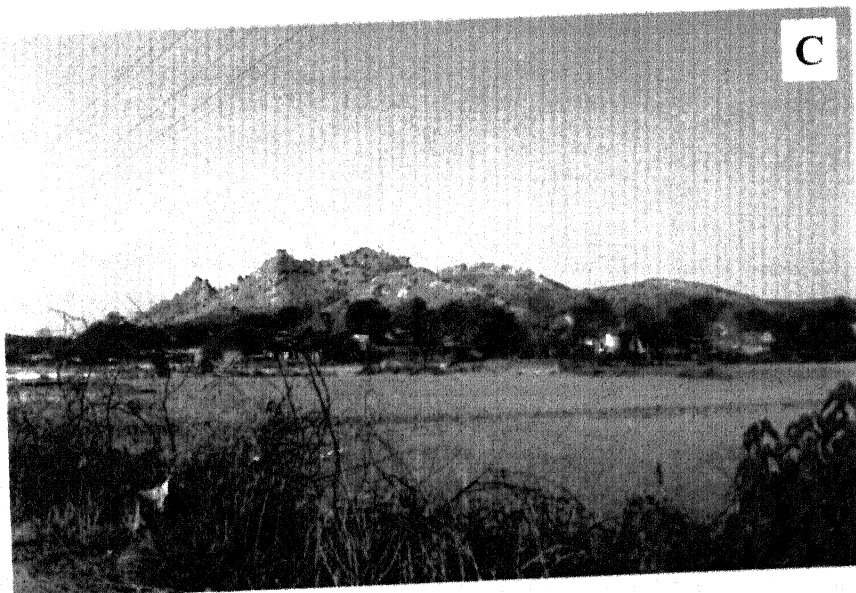


PLATE – 10

Fig. (A) Field photograph showing the northerly dipping fuchsite quartzite bed on the foot hill of BMQ at Mauranipur, near railway track.

Fig. (B) Field photograph showing the exposure of ENE-WSW trending mafics and BMQ at Kamla Sagar dam, Kuraicha. Photograph shows veins of later stage of late stage magmatism.

Fig. (C) Field photograph of iron formation at Mauranipur shows the banded magnetite quartzite dipping NNW.

PLATE -10

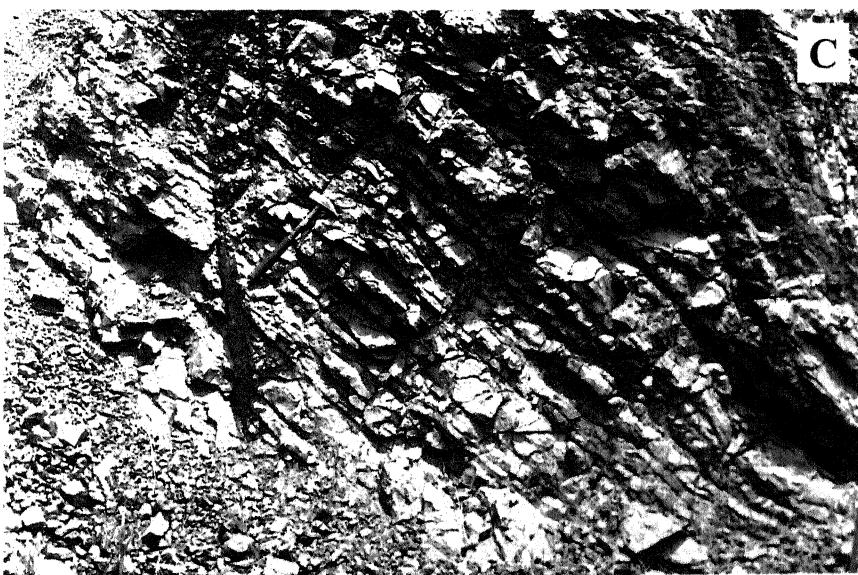


PLATE – 11

Fig. (A) Field photograph showing the high angle dip in metamorphosed ultramafics, trending ENE-WSW at Dhaurra.

Fig. (B) Field photograph showing spheroidal weathering in metavolcanic to the north of Dhaurra iron formation.

Fig. (C) Field photograph showing the exposure of metavolcanic near Dhaurra.

PLATE - 11



PLATE – 12

Fig. (A) Field photograph shows the older gneiss enclave within medium grained leucogranite near Pura Village, Babina.

Fig. (B) Field photograph showing an enclave of migmatite gneiss within fine grained pink granite at Kamla Sagar dam, Kuraicha.

Fig. (C) Field photograph showing the contact of older deformed (mylonitised) biotite granite and later phase undeformed pink granite at Katera reserve forest.

PLATE - 12

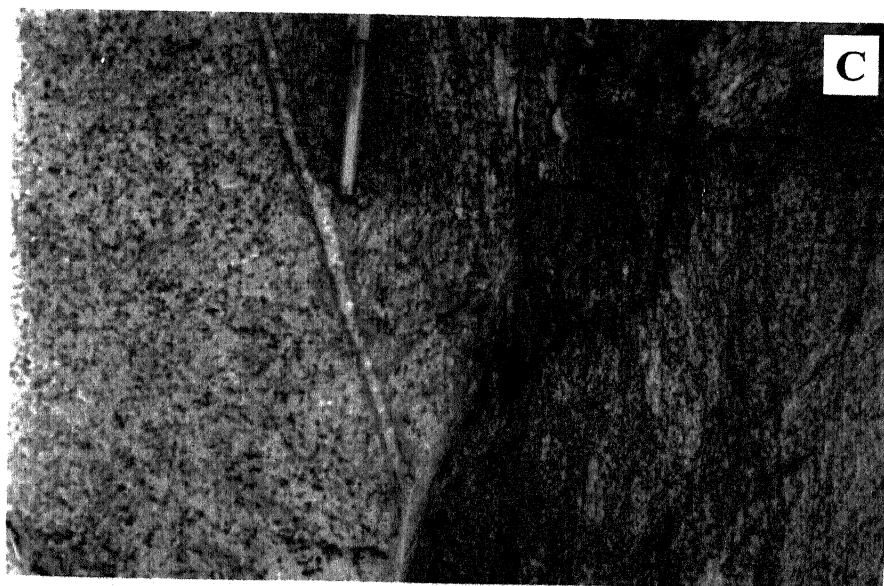
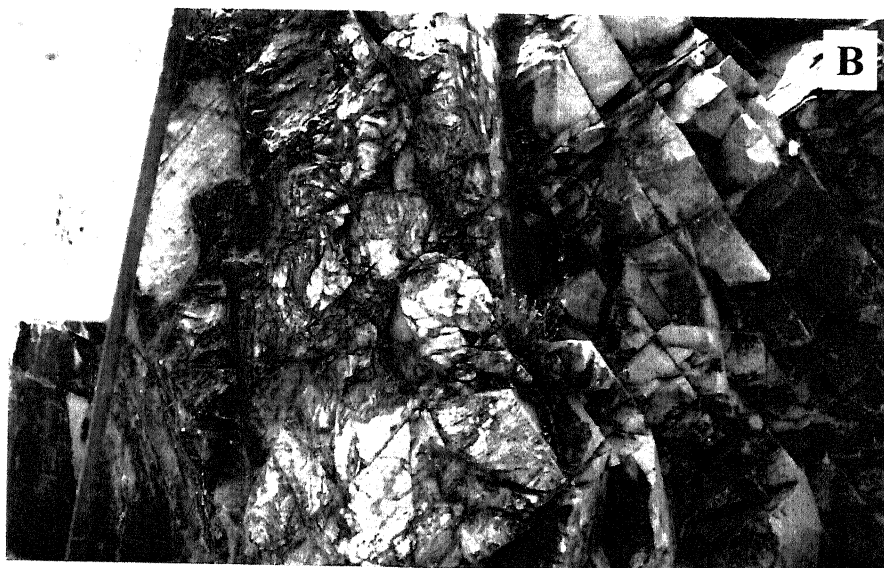


PLATE – 13

Fig. (A) Field photograph showing the exposure of banded magnetite quartzite at Babina.

Fig. (B) Field photograph showing the two sets of joints trending E-W and NE-SW, developed due to deformation received by the iron formation near Pura Village.

Fig. (C) Field photograph felsic-volcano sedimentary (rhyolitic) rocks showing E-W and NE-SW trending fractures, which indicates deformation undergone by this rock unit.

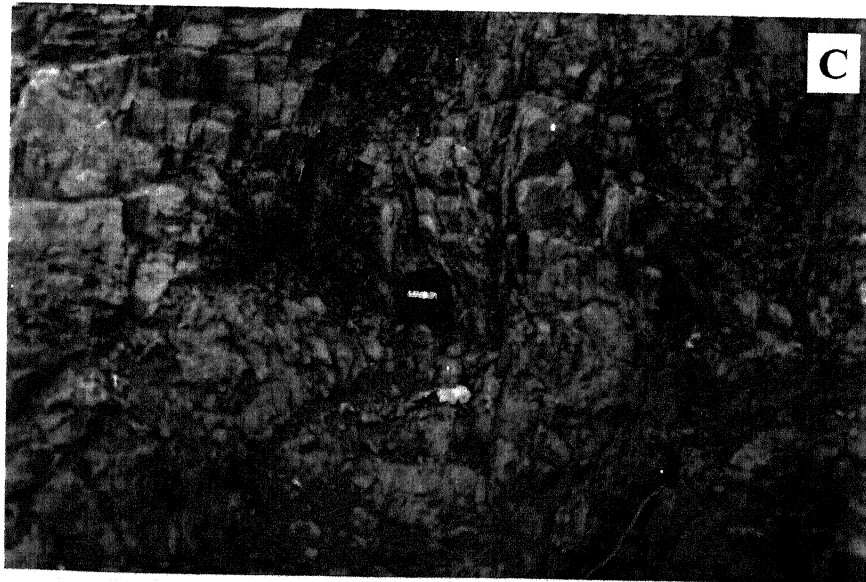
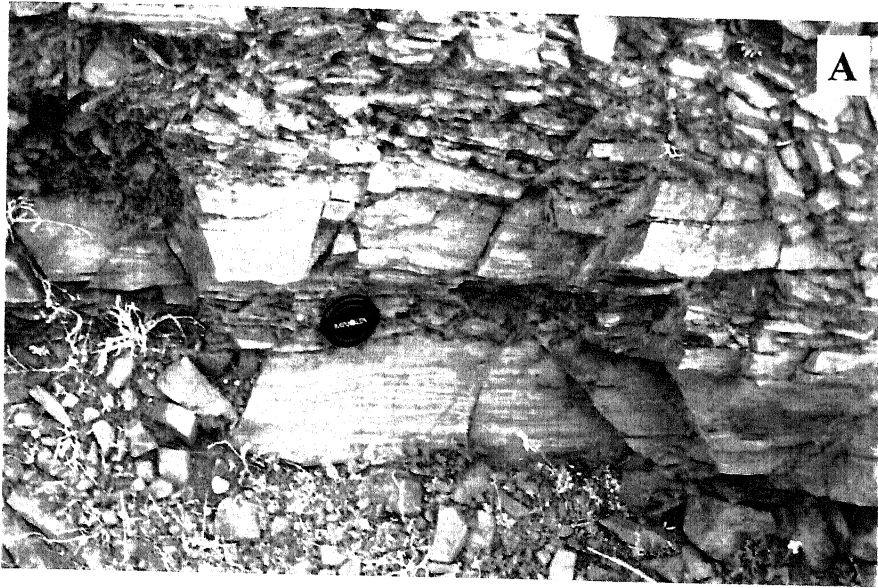


PLATE – 14

Fig. (A) Field photograph felsic volcano-sedimentary (rhyolitic) rocks showing E-W and NE-SW trending fractures, which indicates deformation this rock unit has undergone.

Fig. (B) Field photographs showing the folded quartz veins in iron formation at Kauraicha (Kamla Sagar dam).

Fig. (C) Field photograph showing the NE-SW trending minor fault, which displaced the bands of gneiss, near Babina iron formation.

PLATE - 14

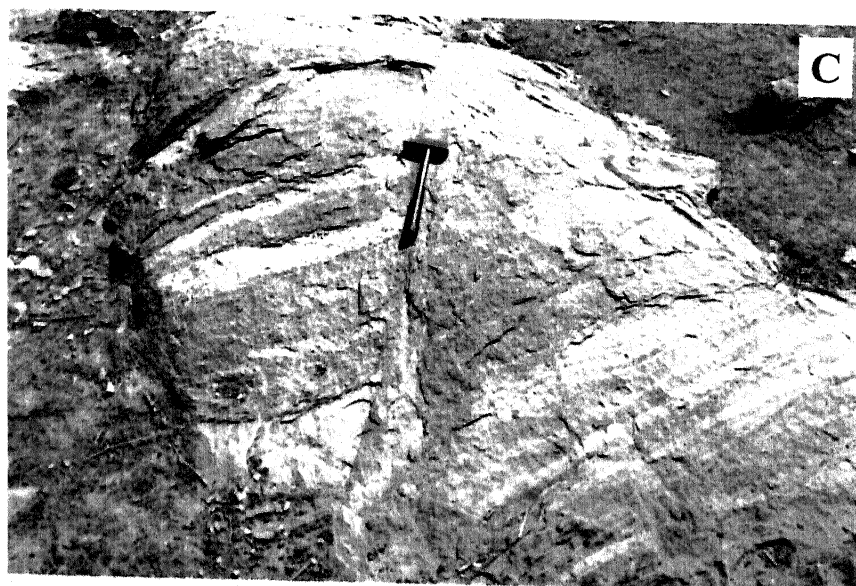
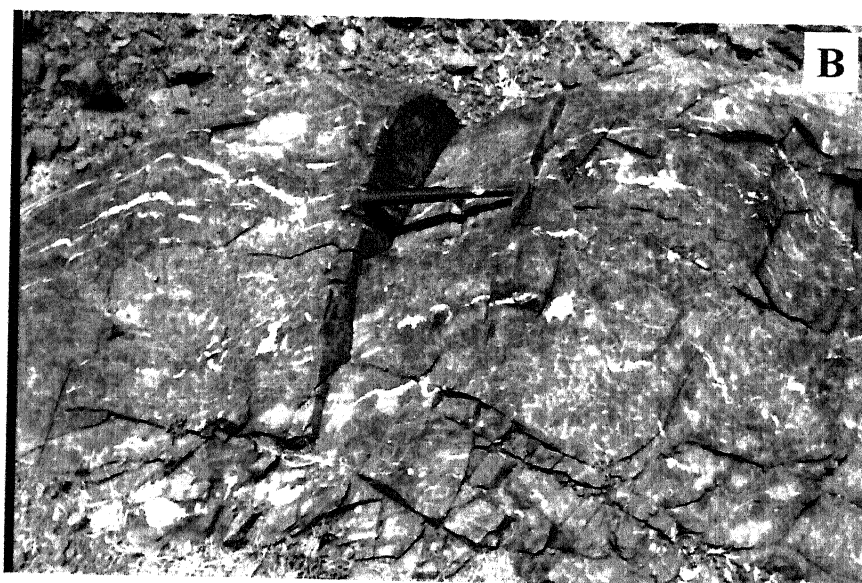
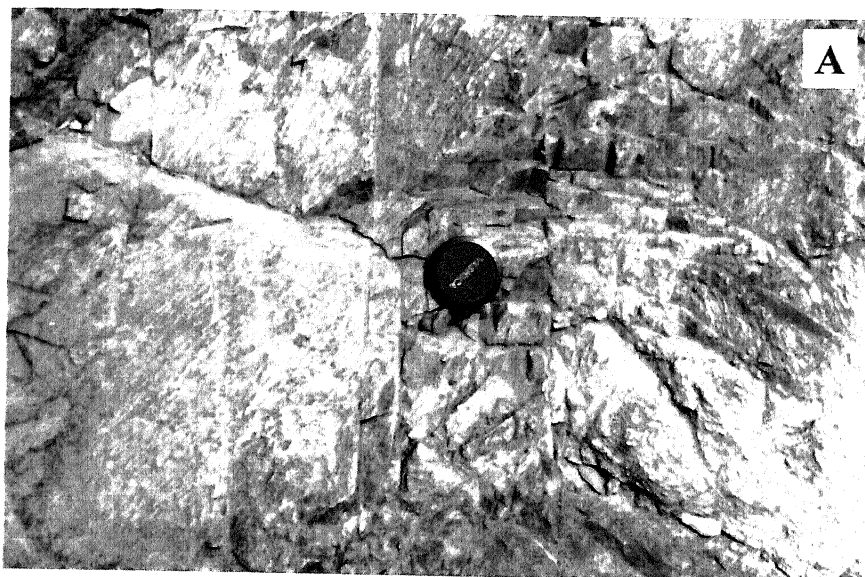


PLATE – 15

- Fig. (A)** Field photograph showing the panoramic view of quartz vein within iron formation at Jhankari (Mauranipur).
- Fig. (B)** Field photograph showing the deformed granite in which S-C fabric is clearly seen, indicating dextral shearing along E-W direction in the north of the investigated area.
- Fig. (C)** Field photograph of gneiss at the south of Mauranipur showing the crystals of feldspars in rotation.

PLATE - 15

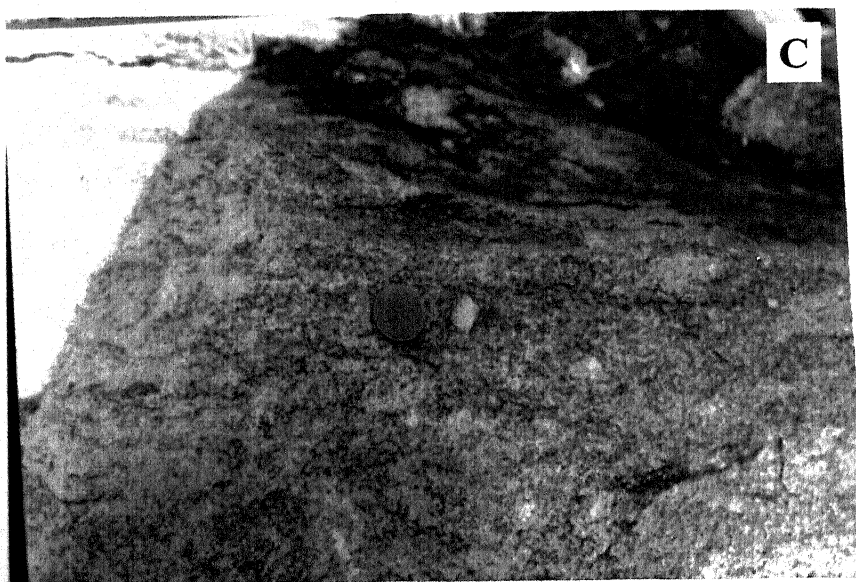
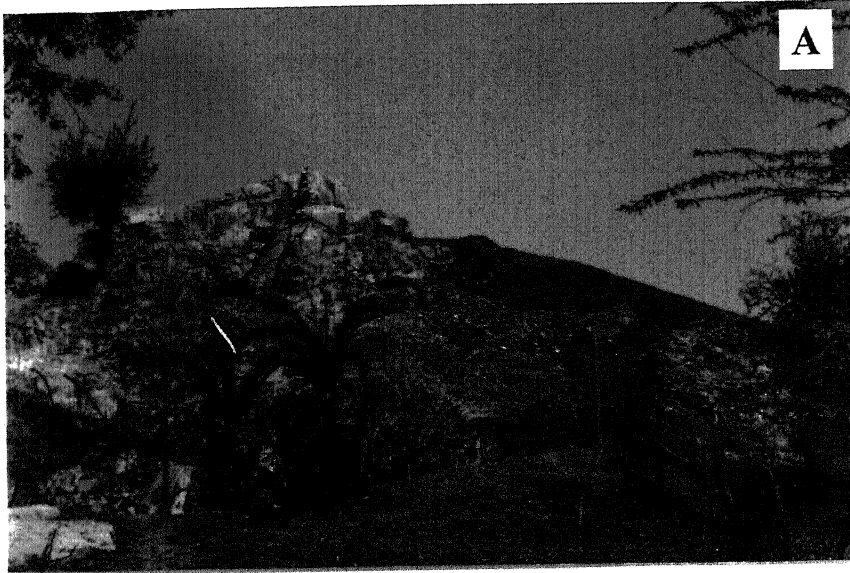


PLATE – 16

Fig. (A) Field photograph showing E-W and NE-SW shearing developed due to deformations in granite at Katera reserve forest.

Fig. (B) Field photograph showing the S-C fabric developed in deformed granite and showing E-W trending shear at Katera reserve forest.

Fig. (C) Field photograph of porphyritic granite; shows feldspar phenocrysts at Katera reserve forest.

PLATE - 16

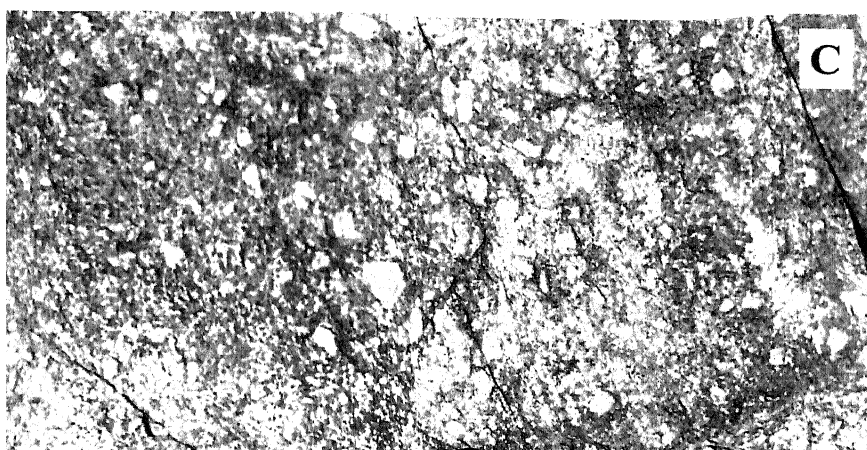
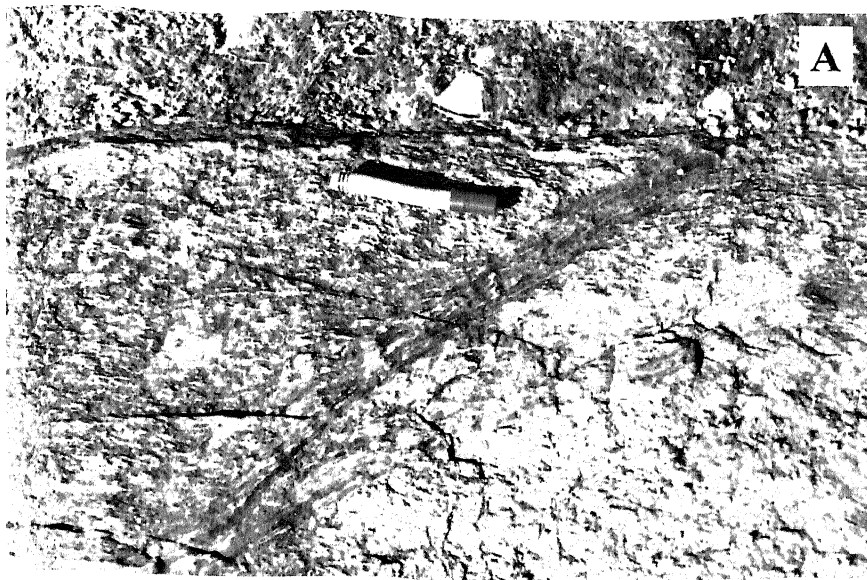


PLATE – 17

Fig. (A) Field photograph of mylonites of Jhankari shows bands of quartzo-feldpathic masses.

Fig. (B) Field photograph showing ptigmatic folds developed in mylonites at Jhankri (Mauranipur).

Fig. (C) Field photograph showing the fuchsite quartzite vein within iron formation at Jhankri (Mauranipur).

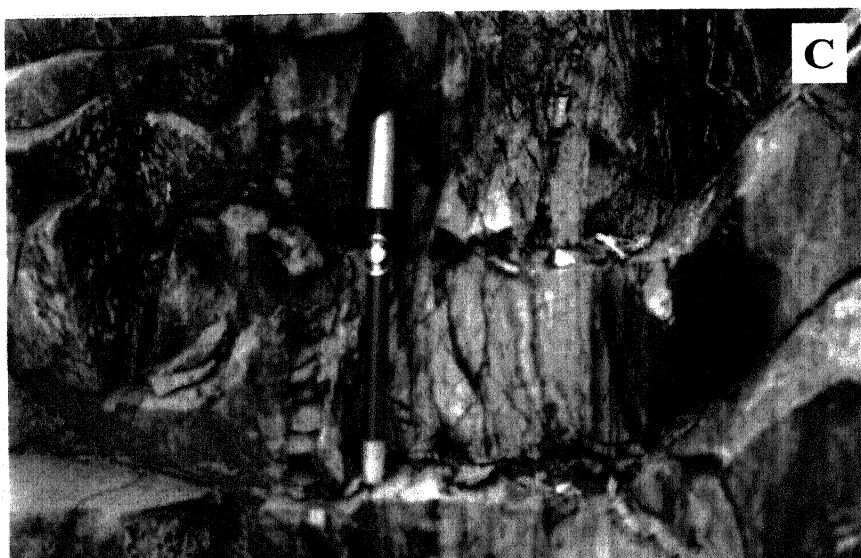
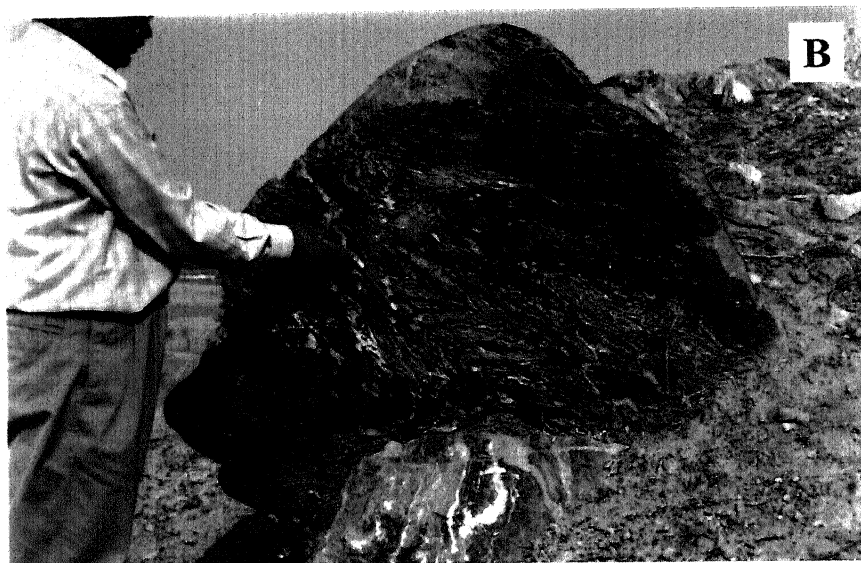
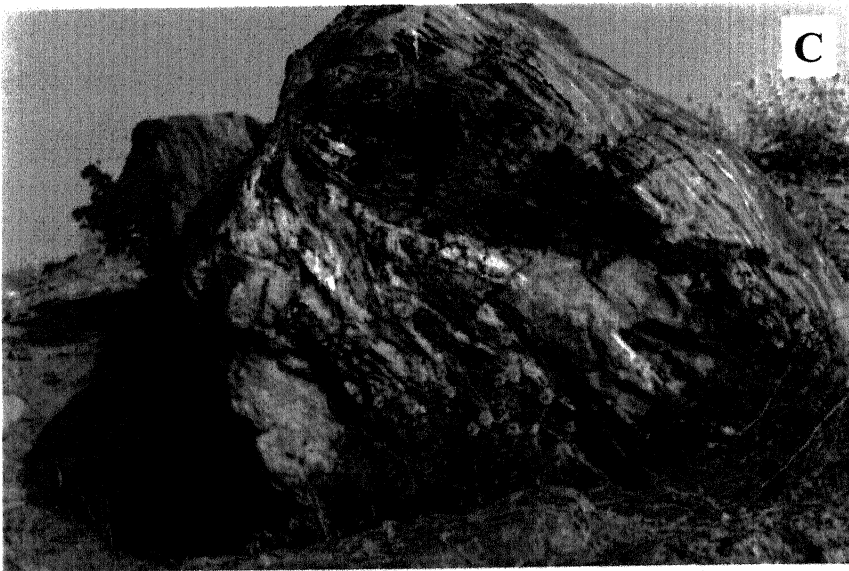
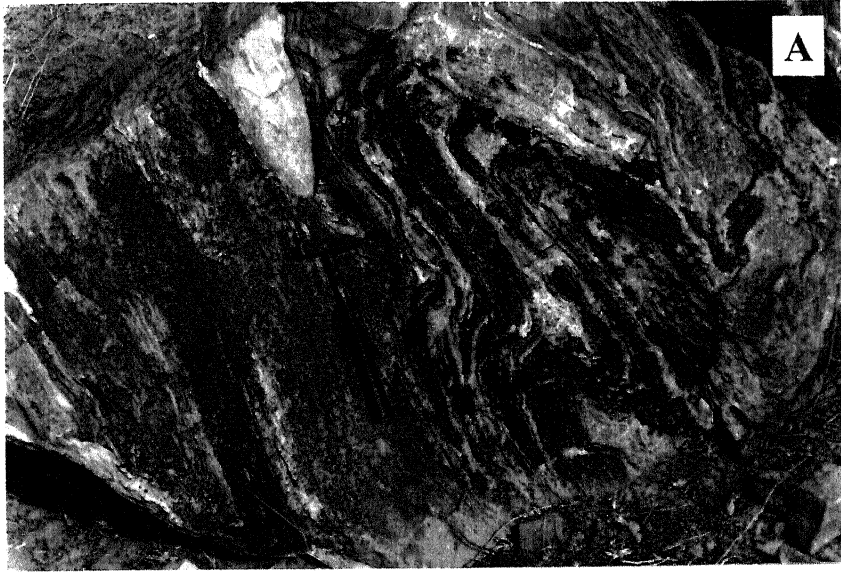


PLATE –18

Fig. (A) Field photograph of mylonite showing dip towards north and high intensity of folding at Jhankari (Mauranipur).

Fig. (B) Field photograph of mylonite showing shearing of folds at Jhankari (Mauranipur).

Fig. (C) Field photograph showing lensoidal quartzo–feldspathic masses developed within the bands of mylonites indicating sense of shearing at Jhankari (Mauranipur).



PETROGRAPHY

The chronological study of crystallization and deformation is based mainly on relations between the time and fabrics of rocks i.e. external foliation (Se) and the internal foliation (Si) within the porphyroblast (Spry 1969). Almost all the metamorphic rocks are normally subjected to various stages of deformation and crystallization in their evolutionary history. The metamorphic rocks associated with different types of granitoids and mafics of Bundelkhand have been also subjected to polyphase deformation and metamorphism in the Precambrian. During these stages, the rocks of NMG and OMG were formed and preserve the different episode of metamorphism displayed during the cratonic evolution of Bundelkhand block. To avoid the repetition of megascopic and microscopic characters, the rocks of investigated area have been divided into older metamorphic group and newer metamorphic group, granitoids, dolerites and quartz reefs.

3.1 Older Metamorphic Group (OMG)

Older metamorphic group of rocks are exposed in low land topography, generally in the south of Banded Iron Formation. They generally show NW-SE and E-W foliation trend. The rocks are well exposed at Jaunpur, Ghisauli, Katera Gora, Dhaurra, Kuraicha and south of Mauranipur (Fig. 2).

The older metamorphic group of rocks are represented by dark gray to light gray colour bands of tonalite-trondhjemite-gneiss (TTG), migmatite, biotite gneiss, and granite-gneiss. The amphibolite and biotite rich amphibolite (biotite-hornblende gneiss) are also found in association with the above mentioned rock types and is exposed as small lensoidal bodies in the gneisses. They are sometimes cofolded with biotite gneiss also. The older metamorphic group of rocks can be lithologically divided into two i.e. (I) gneiss, TTG, migmatite, granite-gneiss, and (II). amphibolite and hornblende-biotite gneiss for the petrographic study.

3.1.1 Biotite-gneiss, TTG, migmatite, and granite-gneisses

In general the trend of gneissic band, observed in the Bundelkhand region, varies from NW – SE to WNW – ESE and steeply dipping ($< 75^\circ$) towards north. Refolding of folded bands indicate that these gneisses had experienced polyphase deformation (Fig 2). The tight to isoclinal folds (F_1 folds) are found to be refolded by reclined folds (F_2 folds) and open to tight F_3 folds at many areas.

Megascopically, these rocks appear to be medium to coarse grained, gray to light gray in colour, but at places coarse-grained variety with poor bandings were also observed. They show well-developed alternate bands of quartzo-feldspathic masses and ferromagnesian minerals showing the gneissose structure (Fig 2). In general gneissic bands are commonly showing complex folding in the study area. Sometimes, the thickness of the melanocratic bands is more than the leucocratic bands but in general, they are of equal thickness (Fig 2). The waxing and waning patterns of bands are also observed in few areas. In many of the places augens of feldspars are observed and their size vary from 3.5 cm X 2cm to 1.5cm X 0.8cm. The aggregate of granite melt and their partial melting signature are also recorded. Different varieties of gneissic rocks are observed in the investigated area. The presence of S-C fabric and local micro faults observed in the area indicates the sense of shearing and stress developed subsequent to metamorphism. The minerals identifiable in hand specimens are quartz, plagioclase, and biotite from melanocratic bands and quartz and K-feldspars from leucocratic bands. Microscopically these rocks give typical granulose structure in which is leucosomes (feldspars, quartz) and melanosomes (biotite, chlorite and chloritoids) developed alternate gneissose bands. Feldspars, quartz, mica, sericite, apatite, zircon and opaque minerals are the mineral constituents of this rock unit. The mineral assemblages and textural relationship of individual minerals of gneisses, migmatites and TTG are described below.

- (i) K-feldspar – perthite- plagioclase-biotite-quartz (K-feldspar < plagioclase)
- (ii) K-feldspar – perthite- plagioclase – quartz
- (iii) K-feldspar – perthite- antiperthite – biotite - quartz (plagioclase < K-feldspar)
- (iv) K-feldspar – biotite – quartz
- (v) K-feldspar – plagioclase – biotite – quartz
- (vi) K-feldspar – plagioclase- biotite- hornblende – quartz (plagioclase >> K-feldspar)

K-feldspars are representing by orthoclase, microcline, and perthite feldspars. In many of the thin sections sericitised orthoclase represents the twinned to untwinned nature and occasionally shows the carlsbad twinning. In general, microcline is observed as fresh, medium to fine grained and also shows cross-hatch twinning distinctly (Plate II b). In few thin sections microcline perthites are also recognized, at places hair perthite is identified in the orthoclase feldspar (Plate IIc). The leucocratic host minerals other than quartz in gneisses are represent by plagioclase (oligoclase), microcline and orthoclase (Plate II c). In large orthoclase crystals the albite lamellae represent the lamellar twinning.

Foliation and folding of bands are commonly observed in all the thin sections. Rotation of phenocrysts of feldspars is also commonly recognized (Plate I a).

Most of the thin sections of rocks of shear zone show intense alteration of K-feldspars (Plate IV a,b) specially orthoclase feldspars changed into sericite. Albitisation and microclinalisation of orthoclase feldspar is also recorded at places in the granite-gneisses (Plate IV b) and deformed gneiss

Plagioclase grains are present as medium to coarse, and prismatic form. They show colorless in thin sections with low relief. They are recognized by polysynthetic twinning (Plate IVa). At places mirmackitic intergrowth (Plate VI B) of quartz and plagioclase are also recorded. Inclusions of zircon, apatites and K-feldspar (antiperthite texture in TTG) observed within the coarse grain plagioclase crystals. Alteration of plagioclase to chlorite and epidote is also recorded.

Quartz is a predominant mineral constituent in this rock unit. It has subhedral to anhedral in shape and grain size varies from medium to fine grained. It shows undulose extinction due to polyphase deformation and crystallisation.

Biotite is also one of the important mineral constituents in this rock type. Under the microscopic study two types of biotite are noted (i) the commonly found brown coloured biotite, (Plate IIIa) and (ii) green coloured biotite. Both the types are strongly pleochroic. The brown coloured biotite usually contains pleochroic haloes and crystals of Zircon. The green coloured biotite is associated with retrograde minerals of granite-gneisses. The alteration of biotite to chlorite and sericite is common. It is worth mentioning that muscovite was never been noticed with gneisses, granite and muscovite. In general grain size shows medium to fine grained, tabular form. Most of them are well oriented in a particular direction in the plane of schistosity. They are characterized by one set perfect cleavage in prismatic sections. The different stages of secondary chlorite have developed due to variable alteration of biotite.

Sericite is the most predominant constituent of all secondary mineral observed in gneisses. Intense sericitisation of the core part of K-feldspar is commonly observed in some thin sections. It observes as tiny, flaky crystals in a haphazard and random fashion in all the gneissic samples collected from the investigated area.

Apatite is occasionally observed as colourless in thin sections and represented by small six sided prismatic crystals with moderate to high relief. At times elongated prismatic grains show first order gray colour. Apatite is also occurs as inclusions in feldspars and biotites.

Zircon usually occurs as minute, circular, short prismatic crystals. It is distinguished from apatite by higher relief and stronger birefringence. It is very common as inclusion in biotite and orthoclase of biotite gneisses.

Opaque minerals are usually observed as subhedral to anhedral in shape and present as accessory mineral. Majority of them appear to be equidimensional. Occasionally magnetites give sieve structure. In many thin sections patchy irregular masses of magnetite is also observed. It is also found as inclusions in feldspars and biotite.

Chlorite generally occurs as secondary product which is altered from biotite. It is observed as patchy masses, at places as subhedral-elongated crystals, bluish green in colour and also show pleochroism and berlin blue interference colour.

Epidote is usually found as an aggregate of anhedral elongated grains in association with quartz and feldspars as alteration product. It is observed as colourless in plane polarized light but in cross nicol it gives light pink in colour.

3.1.2 Amphibolites and hornblende-biotite gneisses

Megascopically, amphibolites are medium to fine grained, generally dark in colour, very hard and compact. Amphibolites are exposed at Babina, Prithvipur, and Mauranipur. The best amphibolites exposure is in Jaunpur (Babina).

Microscopically, amphibolites are massive but when associated with biotite, it show schistosity. It is characterized by the coarse grained minerals. The hornblende, biotite, plagioclase, quartz and magnetite can be easily seen in hand specimen. On the basis of mineral constituent they have been divided into three rock types- (1) hornblende plagioclase gneiss and (2) hornblende-biotite gneiss, and (3) hornblende-biotite-diopside gneiss.

Hornblende is one of the predominant mineral constituents of amphibolites. It occurs as medium to fine grained, subhedral prismatic crystals. It is characterized by two sets of perfect cleavage, second order interference colour. Extinction angle varies between $10^{\circ}/20^{\circ}$. Hornblende shows pleochroism having the following characters, X (pale green), < Y (green), < Z (dark green). Alteration of hornblende into chlorite is also recorded in some thin sections. Small inclusions of biotite (Plate VI c), magnetite (Plate VI a), hornblende, quartz, and plagioclase (Plate I a, c) have been recorded in hornblende. In few sections, the inclusion of orthopyroxene and clinopyroxene are also observed (Plate V a).

Plagioclase is observed as medium to fine grained, subhedral laths form. It shows low relief, colourless and polysynthetic twinning (Plate I a). Plagioclase is mainly oligoclase and labradorite in composition.

Biotite is observed as medium to fine grained and brown in colour (Plate I a,b,c). It shows pleochroism from dark brown to colourless, and third order interference colour. It shows straight extinction and one set perfect change in prismatic sections. In general biotite crystals are aligned in the plane of schistosity with the hornblende. Sometimes biotite shows the replacement texture in amphibole and pyroxene (Plate VI a). The inclusion of hornblende and quartz in coarse grain biotite is very common (Plate V b).

Quartz is present as subhedral to anhedral in shape, medium to fine grained. It shows low relief and undulose extinction due to strain effect; it also occurs as inclusions in hornblende and biotite.

Chlorite is observed in general as secondary mineral, altered from hornblende. It is identified as patchy masses in random fashion. It shows berlin blue colour and weak pleochorism.

Iron oxide minerals are observed as brownish red to black in colour, subhedral to anhedral in shape and present as accessory mineral. Occasionally magnetite shows sieve structure. Rutile is medium to coarse grained and shows light brownish red.

Pyroxene : it is medium to coarse grained. The clinopyroxene is most common mineral. The relic of orthopyroxene in diopside and hornblende is noticed in few sections (Plate V a). The inclusion of magnetite and hornblende is common (Plate VI c).

3.2 Newer Metamorphic Group (NMG)

The NMG rocks consist of tremolite – actinolite-chlorite schist, talc- schist, epidote-chlorite-tremolite schist, hornblende-chlorite schist, cummingtonite-actinolite-magnetite schist, magnetite-quartzite, phyllonite, metavolcanics (mafic and acidic). These rocks can be represented by metamorphosed product of mafics and ultramafics, banded iron formation, mylonites and metavolcanics.

Megascopic and microscopic findings in these three major rock units are individually descried below:

3.2.1 Mafics and ultramafics

Metamorphosed rocks of mafic and ultramafic unit are generally observed at lower stratigraphic level of iron formations (BMQ). In general they are highly weathered and at places, they are covered by thick soil. But still good exposures are also found at many

places. Megascopically they occur as grayish green to dark dirty greenish with white tint in colour. The hornblende, radiating actinolite, tremolite, and talc are the minerals easily recognized in hand specimen. These rocks show two schistosity.

The following mineral characterizes these mafic and ultramafic schistose rocks. The schistosity in mafic and ultramafic and NMG is marked by the alignment of chlorite, tremolite, actinolite and talc minerals. Some minerals (hornblende, cummingtonite) crystallized at the late stage and are marked by S₂ schistosity. The garnet shows syntectonic to late tectonic crystallization growth. The following mineral assemblages have been obtained in the study area.

- (a) Hornblende – magnetite – quartz
- (b) Hornblende ± tremolite – actinolite – chlorite – quartz
- (c) Tremolite ± phlogopite – chlorite – magnetite – quartz
- (d) Garnet – chlorite – actinolite – epidote-quartz
- (e) Talc – chlorite ± serpentine – magnetite ± quartz ± phlogopite
- (f) Chlorite – talc – tremolite ± actinolite ± hornblende ± phlogopite

The textural relationships of minerals are discussed below.

Hornblende is present as medium to fine grained, green in color. It shows strong pleochroism, perfect cleavages and high relief. The alteration of hornblende into actinolite and chlorite is also recorded. Epidote, chlorite, magnetite, tremolite are the common minerals present as xenoliths in hornblende. The hornblende usually aligned on the S₂ schistosity. The shearing and rotation of hornblende also found.

Actinolite is present as light green in colour and acicular form. Relief is fairly high and gives second order interference colour. In few thin sections alteration of actinolite into talc is also observed (Plate VIII c). It is mainly associated with elongated quartz, phlogopite, tremolite, talc on S₁ plane.

Chlorite occurs as small patches in few thin sections as scaly masses usually light green with fair relief. The colorless chlorite is also notice in few sections. It shows gray blue interference colour of first order. Some of the thin sections show chlorite as altered from amphiboles (Plate IX a). The prograde chlorites were noticed as inclusion in hornblende and tremolite. The magnetite is common inclusion.

Talc present as medium to fine grained, colorless. It occurs as platy or fibrous aggregates having more or less parallel arrangement (Plate VIII c). In many of crystals

boundaries are not clear. Extinction is more or less parallel. In few thin sections talc is observed as altered mineral from actinolite.

Quartz is represented by subhedral to euhedral shape and size vary from medium to fine grained undulose extinction indicates the strain effect due to deformation.

Tremolite is present as pale green in colour, long prismatic crystals commonly fibrous aggregates. It shows weak pleochroism, high to moderate relief. In few thin sections shows alteration to talc (Plate X b).

Epidote is observed as small anhedral elongated crystals, at places as aggregates. It shows berlin blue in colour, high relief. The relics of epidote crystals were noted in hornblende.

Serpentine is represented by antigorite. It observed as pale green in colour, aggregates of fibrous-lamellar structure. It shows low relief, first order interference colour and parallel extinction.

Phlogopite is present as medium to fine grained, light brown in colour, slightly pleochroic. It is distinguished from biotite by lighter colour.

Magnetite is subhedral to anhedral in shape, black to brown in colour. The other types of iron oxides are also present in few thin sections as pale brownish colour.

3.2.2 Banded iron formation

The rocks of banded iron formation are exposed from Babina to Mauranipur in the discontinuous hillocks along the E-W direction in the investigated area. Mankuan, Dhaurra, Gora are important localities for iron formation of rocks. At Mankuan village, the E-W trending BMQ is transverse by a NE-SW trending quartz reef.

Megascopically these metamorphosed ferruginous rocks shows alternate bands of quartzite and magnetite, at places hematite bands are also recorded in the field, in few places specially at Babina, commingtonite-grunerite bands of whitish green in colour were also identified. It shows well-developed schistosity with needles of amphibole. Quartzite rocks are also identified along with banded magnetite quartzite (BMQ). Quartzites are light pink to pinkish white in colour; show fine-grained massive and compact nature. Thickness of the quartzite and magnetite bands ranging from 0.25 cm to 1cm. Grunerite - commingtonite bands are very thin with compared to quartzite and magnetite bands.

The metamorphics of banded iron formation comprises magnetite, quartz, commingtonite, grunerite, actinolite, garnet, tremolite, biotite, chlorite, epidote etc with different proportion. They all show medium to fine grained, and well-developed schistosity.

The banded iron formation has been divided into two litho-units i.e. (i) Banded –magnetite-quartzite and (ii) Quartzite.

These two rock units show the following mineral assemblages.

3.2.2.1 Banded - magnetite - quartzite

- (i) Magnetite – quartz
- (ii) Stilplomalane – chlorite – magnetite – quartz
- (iii) Magnetite – epidote – actinolite – quartz
- (iv) Cummingtonite – hornblende – garnet – chlorite – magnetite – quartz
- (v) Cummingtonite – grunerite – magnetite – quartz

3.2.2.2 Quartzites

- (i) Muscovite – sericite – biotite – quartz
- (ii) Chlorite – epidote – quartz
- (iii) Magnetite – actinolite – tremolite – epidote – chlorite – quartz
- (iv) Garnet – chlorite – muscovite – microcline – magnetite – quartz

Individual mineral characteristics from microscopic study are described below.

Magnetite is the most dominant mineral of BMQ. It is observed as coarse to fine grained and black in colour. Magnetite inclusions are also found in biotite, stilplnomelane, garnet, amphiboles, chlorite and quartz. The other types of iron oxides such as limonite is characterised by brownish yellow and occurs as patchy form.

Quartz is present as medium to fine grained, subhedral to anhedral in form. At places secondary quartz veins, which cut across the magnetite-quartz bands are also observed. Undulose extinction in quartz is showing the strain effect.

Cummingtonite is observed within the bands of quartz and magnetite. They are present as prismatic, colourless crystals, aligned on S_2 plane and show second order of interference colour. The presence of magnetite aggregate is characteristic of this mineral.

Actinolite is present as light green, acicular form, at some places showing radiating pattern. It shows weak pleochroism in shades of green with high relief and second order interference colour.

Chlorite occur as small elongated patches. In some thin sections it is also observed as scally masses. It shows green in colour, fair relief, and weak pleochroism. Extinction is almost parallel.

Biotite is present as medium to fine grained, characterised by one set perfect cleavage in prismatic sections and greenish brown to colourless in colour. It shows strong pleochroism from light brown to dark brown. In few thin sections alteration of biotite to chlorite is also observed.

Apatite is observed as colourless or silvery white, small six sided prismatic crystal with low relief. In few thin sections apatite is found as inclusion in biotite.

Epidote is generally occurs as medium grain and is aligned in particular orientation. Usually epidote veins cut across the quartzite and magnetite bands. They are found as colourless in plane-polarised light but under crossed nicols it shows light green to bluish colour.

Grunerite is represented by prismatic, banded forms, and sometimes acicular to fibrous in nature. It is observed as colourless with high relief in plane polarised light and shows second order interference colours. Prismatic crystals show parallel extinction. In general it is found in association with magnetite and quartz.

Garnet is observed as medium to coarse grained, commonly associated with chlorite and hornblende. The magnetite is commonly observed as inclusions (Plate VIII a, IX C). The coarse grains show retrogression into chlorite, while smaller crystals associated with hornblende is prograde type.

3.2.3 Metamylonites and metavolcanics

Recrystallised mylonites and ultramylonite rocks, metavolcanics of felsic and mafic suits represent the rocks of this unit. These rocks are exposed in north of iron formation (BMQ). Best exposures are found at Babina and Dhaurra village. Megascopically these rocks are medium to fine-grained but at places coarse-grained variety is also observed. These rocks have diverse physical appearance, texture and mineral composition. The rocks of this unit have been discussed in two different heads:

3.2.3.1 Metamylonites and Ultramylonites

Metamylonites and Ultramylonites are generally observed at the contact of BMQ. Megascopically they are found as medium to fine-grained. Foliation and schistosity are well developed. Colour is varying from dark gray to light pink or whitish green, with patches of whitish spots of feldspars and epidote.

Microscopically they are medium to fine grained. The development of schistosity indicates deformation and recrystallisation of mylonites. Quartzofeldspathic masses and biotite flakes have enveloped the rotated feldspar phenocrysts.

Following mineral assemblages have been observed on the basis of detailed texture, structure and mineral constituents identified in thin sections of the recrystallised, mylonites and ultramylonites

- (i) Hornblende – chlorite – biotite – quartz – K-feldspars
- (ii) Actinolite – hornblende – K-feldspars – plagioclase – quartz
- (iii) K-feldspars – quartz – chlorite – magnetite – epidote \pm biotite
- (iv) Chlorite – epidote – K-feldspars – andalusite-quartz
- (v) Chlorite – chloritoid – muscovite – K-feldspar – quartz – magnetite

Texture and structure of individual minerals are described below.

Hornblende is present as medium to fine grained, at places few coarse grained crystals are also observed. Hornblende crystal shows green in colour, strong pleochroism in shades of green, second order interference colour with high relief. Two set perfect cleavage hornblende are also observed in tiny crystals. Subhedral, elongated prismatic crystals are commonly inclined with the foliation plane.

Actinolite occurs as fine-grained fibrous aggregates. It shows pale green colour, faint pleochroism and high relief. Actinolite crystals are generally oriented within the schistosity plane but in some thin sections they also distributed in random fashion.

Chlorite is present as a bluish-green to green, medium to fine-grained subhedral elongated scaly masses. Chlorites are weakly pleochroic but shows fair relief. In some thin sections chlorite is found as an alteration product of hornblende.

Chloritoid occurs as greenish gray and prismatic grains. It shows high relief and almost parallel extinction. Chloritoid distinguished from chlorite by its higher relief, bluish to colourless pleochroism and polysynthetic twinning.

Plagioclase is observed as medium to fine grained, subhedral laths and colourless crystals. At places tiny crystals of plagioclase feldspar occurs within the groundmass along with quartz. Within this quartzofeldspathic mass elongated ferromagnesian minerals lie in a preferred orientation so it gives schistosity structure. Plagioclase feldspars show lamellar twinning. In few thin sections alteration of plagioclase feldspar is also observed.

K-feldspars are represented by medium to fine grained, subhedral to anhedral crystals of orthoclase and microcline. At places phenocrysts of orthoclase are showing rotation, indicating the sense of shearing. Both the orthoclase and microcline shows colourless and low relief. Orthoclase shows Carlsbad twinning but microcline shows

crosshatched twinning. It is worth noting that orthoclase is usually subjected to shearing while microcline is medium to coarse and not affected by shearing.

Quartz is observed as medium to fine grained, anhedral crystals. Sometimes aggregates of quartz across the mylonite plane have been observed. Quartz is colourless, shows low relief and absence of cleavage. It commonly shows undulose extinction due to strain effect. The porphyroblastic and blastoporphyratic texture of quartz is noted from many thin sections.

Biotite occurs as a brown coloured, medium to fine grained, subhedral-elongated crystals. It shows strong pleochroism from light brown to dark brown and one set of perfect cleavage in prismatic sections. Biotite flakes lie in a preferred orientation so the schistosity can be identified easily. Most of biotite is unaffected by shearing having crystallized after mylonitization.

Muscovite is present as colourless, aggregates of scaly masses. In few thin sections it shows one set perfect cleavage. Muscovite crystals are aligned in a preferred orientation oblique to mylonite planes, which in turn developed schistosity.

Epidote is present as colourless, anhedral elongated, medium to fine grained crystals. It shows high relief, is colourless in plane-polarised light but under crossed nicols it shows second order interference colours. In some thin sections it is found as an alteration product of feldspar.

Magnetite is commonly identified as medium to fine grained irregular patchy masses. Other iron oxides are also observed in some thin sections.

3.2.3.2 Metavolcanics (felsic and mafic)

The exposures of felsic volcanics have been identified at Babina and Dhaurra. Rhyolites are found in association with mylonites and ultramylonites. At many of the places flow structures were also recorded. Felsic and mafic volcanics are best exposed north of Dhaurra iron formation. Megascopically these rocks show light gray to pink color, are massive, very hard and compact. At places elongated thread like phenocrysts of K-feldspars were also observed along the foliation plane and shows rotation of crystals due to later phase of deformation in thin sections. These types of rocks are found generally at low height and dome like structure may be due to high viscosity of silicious lavas.

Amphibole : Hornblende is the predominant mineral but is present as small relics. Beside hornblende, actinolite, tremolite are also present along with epidote. Hornblende shows light green colour, subhedral elongated crystals, two sets of perfect cleavage, pleochroism and high relief. The maximum extinction angle in longitudinal sections varies from 15° to 30° . Hornblende differs from augite by its in maximum extinction angle and

cleavage. Alteration of hornblende to chlorite is also observed. In some thin sections actinolite is also recorded giving acicular fine-grained prismatic form. It shows weak pleochroism and light green colour.

Microscopically rhyolites are medium of fine-grained. The crystals of feromagnesian minerals are aligned in a preferred direction. So far as the mineral constituents of the rhyolites are concerned, the following minerals have been identified.

1. Predominant and essential minerals – K-feldspar and Quartz
2. Accessory minerals – biotite, magnetite, zircon and apatite; rarely hornblende and plagioclase
3. Secondary minerals – sericite, epidote and chlorite

The microscopic characteristics of individual mineral constituents of felsic and mafic rocks are described below:

Feldspars are represented mainly by orthoclase and microcline and sometimes by plagioclase

Orthoclase is present as coarse to medium grained subhedral rectangular crystals. It shows common simple twinning in Carlsbad law. In many of the thin sections alteration of orthoclase to sericite is also observed. It is usually presented in the groundmass as poorly developed crystals with quartz.

Microcline is present as medium to fine grained subhedral to anhedral crystals. It shows typical cross-hatched twinning (polysynthetic twinning), low relief and inclined extinction ranging from 13° to 15° .

Plagioclase is present as medium to fine grained subhedral crystals. At places tiny laths of plagioclase, in association with quartz and biotite, enclose the orthoclase phenocryst. Plagioclase phenocrysts are also observed. It shows lamellar twinning. Plagioclase laths generally represent lineation and biotite flakes the schistosity are aligned in a particular flow direction. In the plagioclase phenocrysts inclusions of apatite & zircon are also observed.

Quartz is observed as predominant mineral constituent varying in grain size from medium to fine grained but coarse-grained quartz phenocrysts are also observed. It is characterized by anhedral shape, low relief and less alteration. It shows undulose extinction due to strain effect.

Biotite is present as secondary mineral constituent in medium to fine grained prismatic crystal. It shows brown color; pleochroism in biotite is defined by brown to dark

brown. In some thin sections alteration of biotite into chlorite has also been observed. It is usually associated with apatite and opaque minerals.

Augite is present as select form characterized by small short prismatic crystals, colourless to light green in colour, exhibiting second order interference colours. The epidote, plagioclase, chlorite and calcite are the common mineral associated as secondary alteration.

Opaque minerals are present in all the thin sections as medium to fine grained, subhedral to anhedral, crystals. In some of thin sections they are observed as patchy irregular masses.

Zircon is present as colourless minute crystals of shorts prismatic habit. It shows high relief parallel extinction and absence of cleavage. Zircon is distinguished from apatite by stronger birefringence and higher relief. In some thin sections it shows zoning.

Apatite is commonly observed as small six sided crystals and sometimes as anhedral, silvery white prismatic crystals. It shows low relief in contrast to zircon. Apatite is commonly observed as inclusion in Orthoclase feldspar and biotite.

Sericite is generally observed as secondary mineral. It is represented by, nonpleochronic, tinny scaly aggregate and parallel extinction. Sericite is altered from orthoclase feldspar through sericitisation process.

Epidote is generally observed as an aggregate of anhedral elongated crystal in association with feldspar and quartz. It is present as altered product of feldspar and shows high relief, light pink in color and weak pleochroism (fig).

Chlorite is found as secondary minerals altered from biotite. It shows bluish green colour, medium to fine grained, scaly masses. It is characterized by fair relief, weak pleochroism and parallel extinction.

3.3 Granitoids

On the basis of texture, structure, mineral composition and field relationship, the granitoids of the study area have been classified into five types viz. (i) Hornblende Granite, (ii) Biotite Granite (iii) Coarse grained Leucogranite, (iv) Fine grain Leucogranite, and (v) Deformed Granite.

Texture and structure of granite

Magascopically the granites of the investigated area are varying in grain size from coarse to fine grained, leucocratic to mesocratic hard and compact in nature. Leuco granitoids (pink granite) are the most common type in the study area. The phenocrysts of

feldspar are very frequent in fine-grained leucogranite. Such grains are found as intrusive along the shear zones trending in E-W direction. In hand specimen feldspar, quartz, biotite and rarely hornblendes can be identified easily. The deformed granite bands contain quartzofeldspathic masses and show preferred orientation with alternate ferromagnesian minerals bands in biotite rich variety. At places bands of mica are continuous as waning and waxing pattern along the direction of foliation planes and quartzofeldspathic masses from small lenticular patches along these planes in the biotite granite.

Microscopically the texture of Bundelkhand granites are represented by coarse to fine-grained, holocrystalline, equigranular, hypidiomorphic to allotriomorphic. In many of the thin section porphyritic texture is also observed where phenocrysts of feldspar are embedded in groundmass of feldspar and quartz.

The minerals constituents of the granitoids, which are identified in thin section, are as follows

1. Predominant (essential) minerals – feldspar, quartz
2. Accessory minerals – biotite, hornblende, zircon, apatite, opaques, allanite and sphene
3. Secondary minerals – sericite, epidote and chlorite.

Characteristics of individual minerals

Orthoclase is one of the most predominant minerals constituents in granite, which is as coarse to medium grained, euhedral to anhedral in shape, and commonly shows intense alteration to sericite. It also shows intergrowth with microcline (Plate XII b). At places zoned orthoclase is also observed, where the core consists perthite that is followed by plagioclase (Plate XI b).

In some thin sections antiperthite feldspar is also recorded. Apatite and zircon is commonly found as inclusion in the orthoclase feldspar. At places quartz inclusions are also observed. Orthoclase phenocrysts are also found occasionally as fresh less altered and shows Carlsbad twinning, low relief. At places untwined to twinned altered orthoclase feldspar are also observed (Plate XII a, b).

Microcline is commonly observed as less altered coarse to fine-grained, euhedral to anhedral shape crystals but at times alteration from orthoclase through microclinisation is also recorded. At some places microcline-perthite is also recorded. In plane polarized light sometimes it is very difficult to differentiate but in cross nicol it gives distinct crosshatched twinning, which is not observed in quartz.

Plagioclase is observed as coarse to fine grained. The fine-grained variety shows subhedral small laths. It gives lamellar twinning. At times antiperthite is also observed in which small grained of orthoclase feldspar are present within the plagioclase lamellae (Plate XII b). In some thin sections alternation of orthoclase feldspar to albite is also recorded. Rarely in few sample phenocrysts of plagioclase feldspar are identified and zoned plagioclase is also observed MK6, KT-23.

Quartz is also one of predominant minerals constituent among essential minerals. It occurs as coarse to fine grained anhedral in shape. Quartz is characterized by low relief, sharp extinction and less alteration. At places quartz show undulose extinction due to strain effect. It is also observed as inclusions in feldspars and biotite (Plate XI a, b).

Biotite is present as one of the predominant minerals constituents among accessory minerals in the investigated area and as essential mineral in the biotite granites. It is observed as coarse to fine grained, tabular crystals. Two types of biotite are recognized in thin section studies, the common one is brown in colour and another green in colour. Both are strongly pleochroic. Alternation of biotite to chlorite is occasionally found in the study area (Plate XI a). Biotite shows high relief, one set perfect cleavage in prismatic section, aligned in deformed granite and parallel extinction. Inclusions of zircon surrounded by pleochroic halos are also observed in biotite.

Hornblende occurs as an essential mineral. It shows medium to fine grained subhedral prismatic crystals green in color, pleochroism in shades of green and second order interference colours. In many of the thin sections hornblende crystals having two sets of perfect cleavage are observed. Sometimes the xenoliths of biotite or hornblende minerals are found in coarse crystals of hornblende (Plate XII c).

Zircon is occasionally found as inclusion in biotite & hornblende. It is observed as minute short prismatic crystal, having very high relief and shows parallel extinction and absence of cleavage.

Apatite is occasionally found as small crystals. It shows high relief and observed commonly as inclusions in biotite and feldspar.

Opaque minerals (usually magnetite, ilmeno-magnetite and ilmenite) occur in some of the granites of study area. It is found as medium to fine grained subhedral to anhedral in shape at places as patchy. Irregular masses, occasionally magnetite, show sieve structure. In many of the thin sections they are found as inclusions in quartz, feldspar, biotite and hornblende.

Allanite rarely occurs as brown colored crystals and shows pleochroism, high relief and parallel extinction.

Sphene is found as colorless, euhedral, acute rhombic crystal and shows high relief.

Sericite is the most predominant mineral constituents among secondary minerals. Intense sericitisation of K-feldspar is very common in all the thin sections. Sericite is observed as tiny, flaky /scaly aggregates (Plate XII a).

Epidote is found as granular aggregate of anhedral elongated crystals in association with feldspar (Plate XI a). It is colorless in plane-polarised light but under crossed nicols it gives pink colour. It shows weak pelochroism and high relief chlorite is observed as bluish green in color scaly masses. It shows high relief and berlin blue interference colour. In general chlorite are found as secondary product, which altered from biotite and hornblende.

3.4 Quartz Reefs

Quartz reefs are the only predominant structure standing high above the granite massif in Bundelkhand. In the study area quartz reefs cut across the banded iron formation, gneisses and granitoids, and sinistrally displaced them. Megascopically quartz reefs show dirty white color but at places gray, milky white, pinkish white color varieties are also found in the investigated area. Quartz reefs are hard and compact nature.

Microscopically quartz reefs show mono-mineralic type. Feldspar, opaques and chlorite are also observed. Epidote veins are also observed in some thin section. The microcline is medium to coarse grained, altered to fresh, twin to crosshatched twinning. Quartz and sericite are common inclusion in microcline.

The boundaries of quartz crystals are not clear generally. It shows sharp extinction but at times undulose extinction is also observed due to strain effect.

3.5 Dolerites

Dolerites are observed at Babina and Dhaurra. Megascopically dolerites are dark green or melanocratic in color, medium grained, hard and compact. Granular black prismatic crystals of pyroxenes can be identified in hand specimen but at places grayish white patches of feldspar are also recognized.

From the microscopic study the following minerals are identified:

1. Essential minerals – pyroxenes and plagioclase feldspar

2. Accessory minerals – magnetite, hornblende
3. Secondary minerals – epidote, uralite, biotite, epidote, quartz, chlorite.

Pyroxenes are the predominant mineral constituents of this rock. Intense alteration of pyroxenes is very common in all the thin sections.

Clinopyroxene (Augite) is less altered in comparison to plagioclase. It shows light green color, subhedral, and short prismatic crystals. It gives high relief, second order interference colors and shows high extinction angle. Alteration of clinopyroxene to uralite is also noticed in few sections.

Plagioclase is observed as long laths of subhedral crystals. It shows polysynthetic twinning, low relief and inclined extinction. The plagioclase laths are in general highly saussuritized with the formation of epidote and quartz.

Magnetite is present as opaque mineral black in color, coarse grained to medium grained generally along the cleavage planes of pyroxenes. At places less subhedral magnetite crystals are also observed as an inclusion in biotite.

Uralite is found as an alteration product of clinopyroxene. The formation of uralite includes fibrous, yellowish brown amphibole but it does not show pleochroism, which is common in amphiboles.

Epidote is found as secondary product, which altered from plagioclase feldspar through saussuritisation. It is medium to coarse grained. It is observed as granular aggregate. It shows high relief, colorless in plane polarized light, but in cross nicols it shows pink color.

Quartz is also found as a secondary product of plagioclase feldspar formed by the process of saussuritisation. Quartz is not frequently found in all the thin sections. It occurs as medium to fine anhedral grains and shows sharp extinction.

PLATE - I

- A. Coarse grained hornblendes are aligned along the gneissosity (S_2 plane). Plagioclase crystal S_1 schistosity present. K-feldspar is sometimes sericitised.
- B. Coarse grained Hornblende crystals aligned along S_1 schistosity are present. Two set perfect cleavage hornblende crystals are aligned along gneissosity (S_2 plane). Altered plagioclase feldspars is present within hornblende crystals (S_2 plane). Inclusions of clinopyroxene in hornblende are present.
- C. Hornblende crystals are aligned along a preferred orientation. Altered plagioclase feldspar is present. Quartz and phlogopite mica are present.

PLATE - I

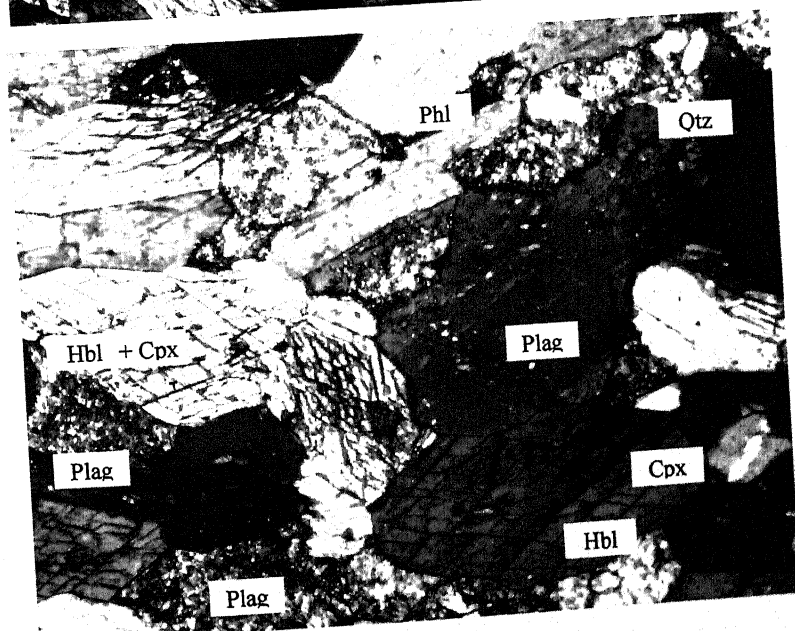
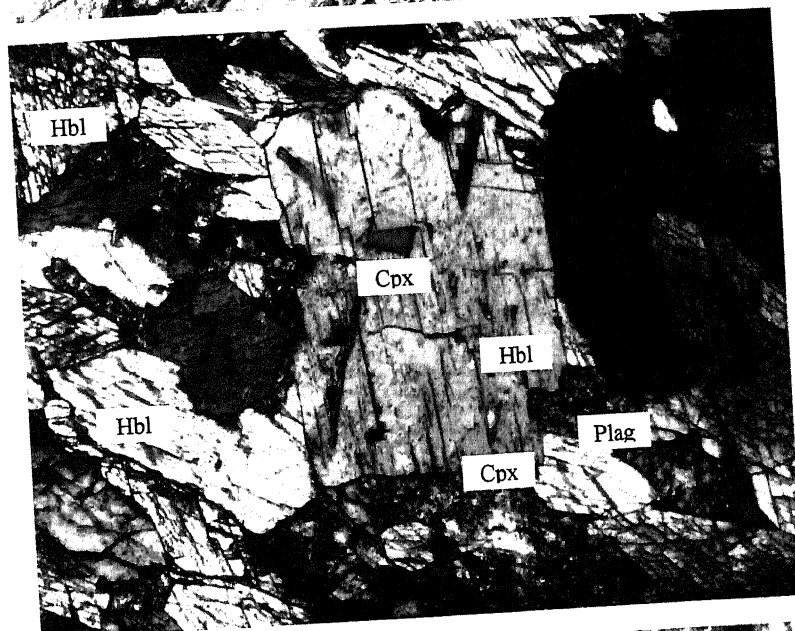
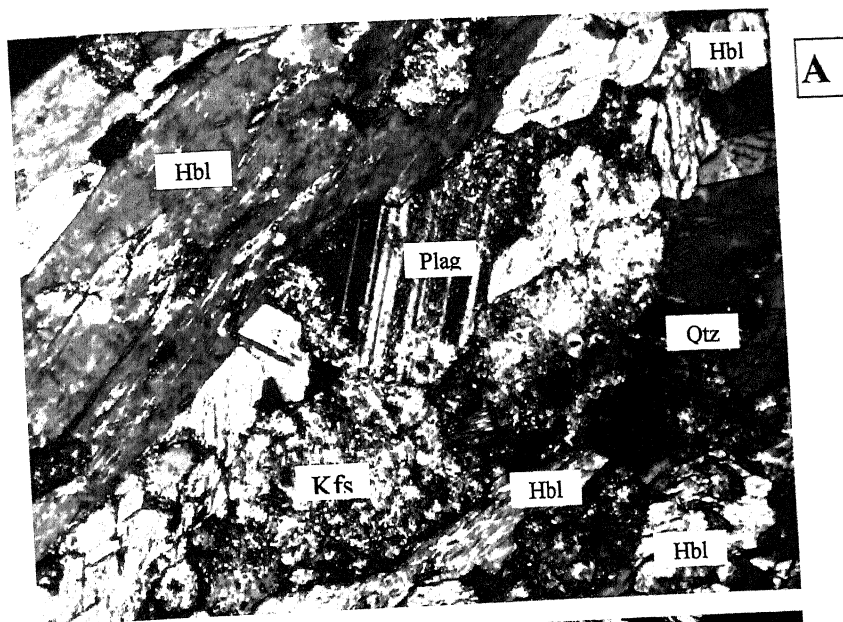


PLATE – II

- A. A coarse grained hornblende crystal is present and is inclined to the two set perfect cleavage crystal of hornblende aligned along gneissosity. Quartz and altered plagioclase crystals are present.
- B. Perthitic texture is present. Coarse grained perthite crystals are present in association with quartz and plagioclase.
- C. Coarse grained K-feldspar and plagioclase crystals are present. Biotite and quartz crystals are also seen.

PLATE - II

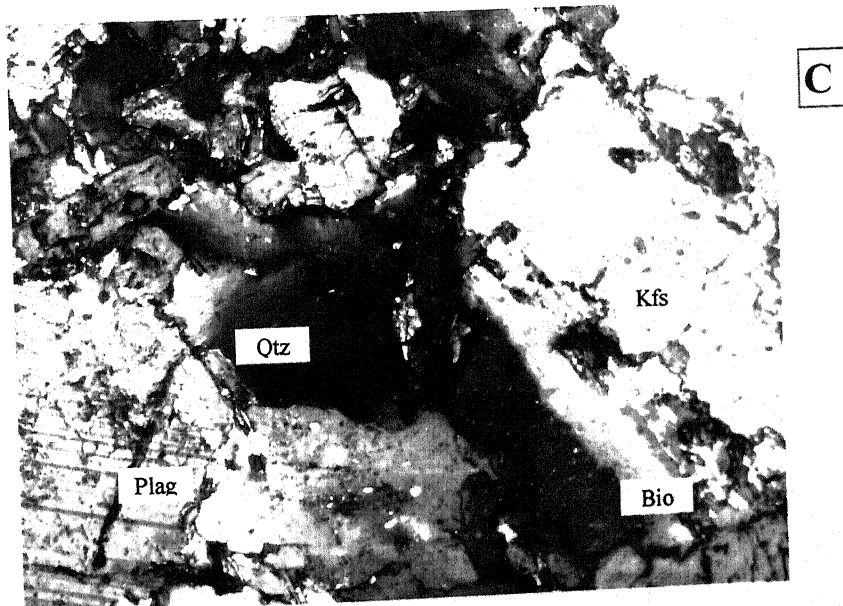
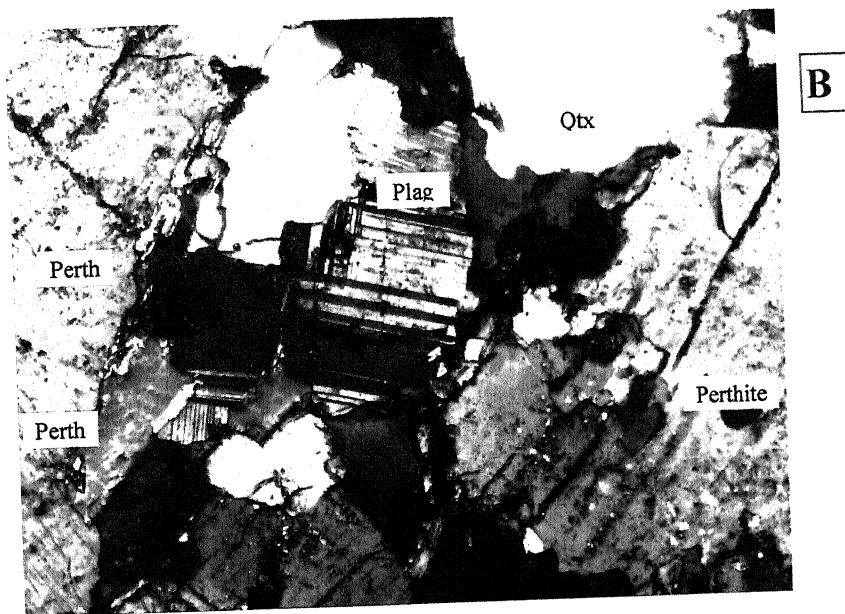
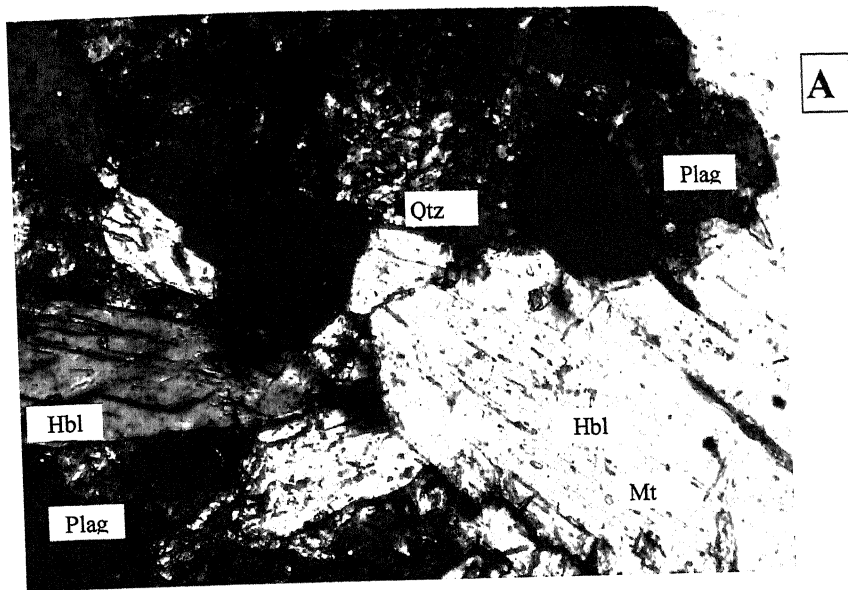
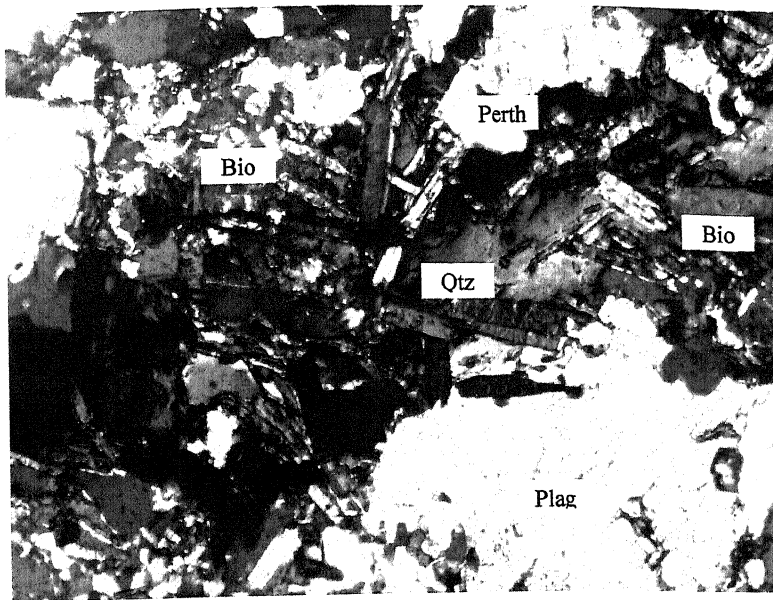


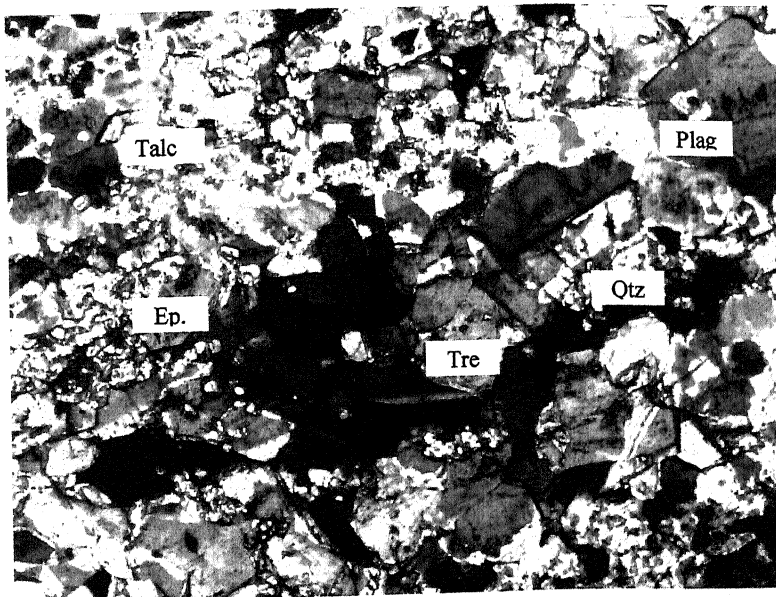
PLATE – III

- A. Coarse grained plagioclase and medium grained elongated biotite are recorded. Perthitic texture is also observed.
- B. Photograph shows medium grained quartz, plagioclase, tremolite crystals. Talc and epidote are also recorded.
- C. Photograph shows that perthitic texture is present. Chlorite, epidote, K-feldspar and quartz are also seen.

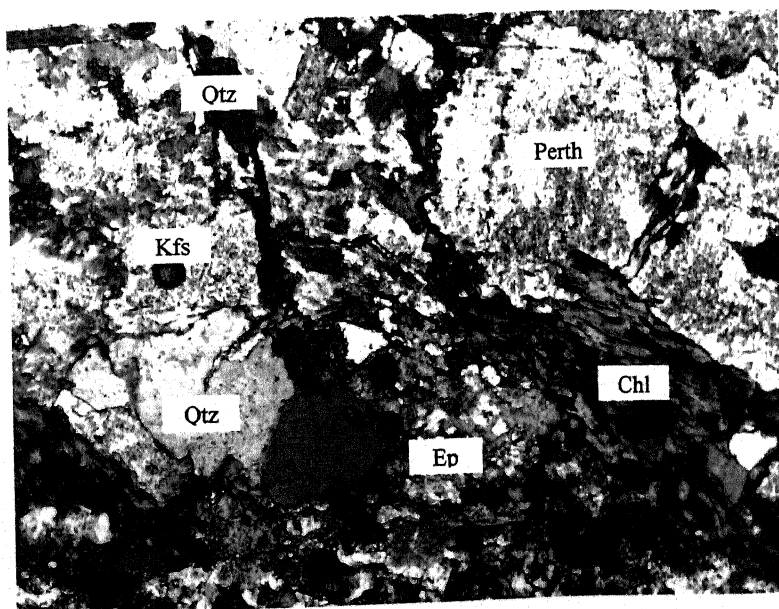
PLATE - III



A



B

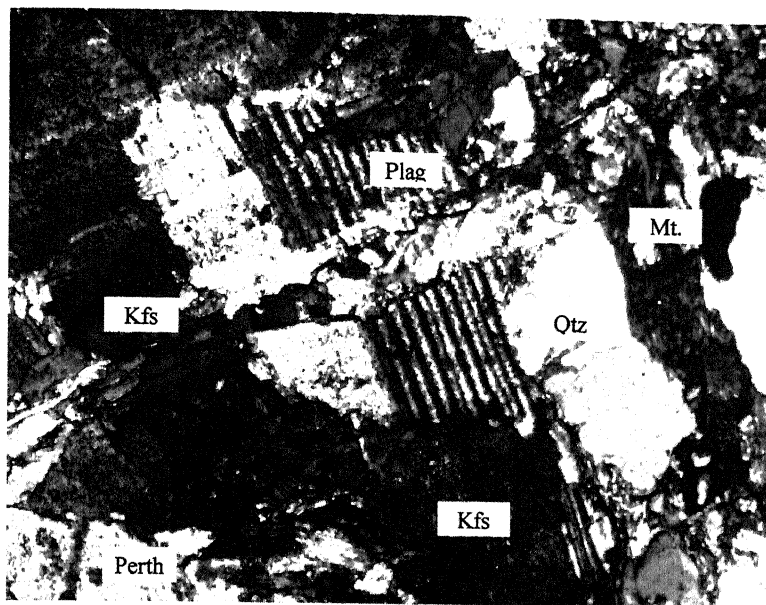


C

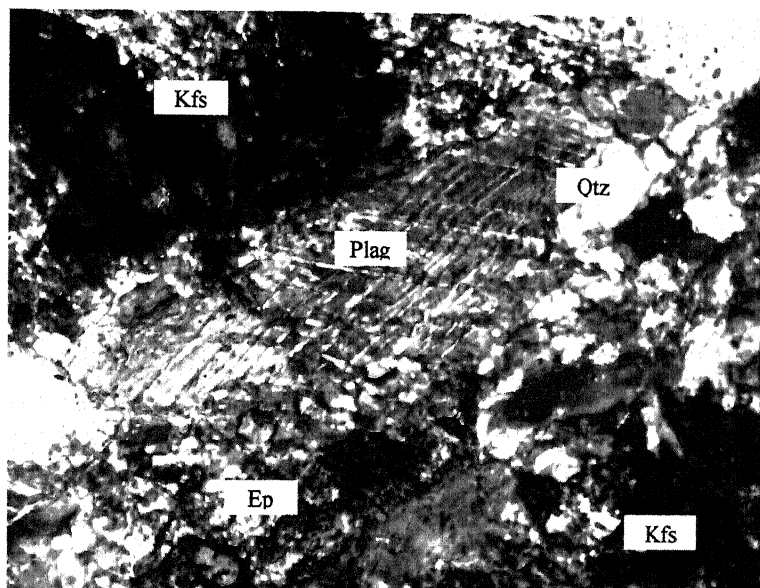
PLATE – IV

- A. Coarse grained, plagioclase, K-feldspar and quartz are observed. Perthitic texture and magnetite is also recorded.
- B. Coarse grain plagioclase feldspar and quartz, K-feldspar and epidote are seen.
- C. Coarse to medium grained plagioclase, K-feldspar and quartz crystals are present. Sericite is also observed.

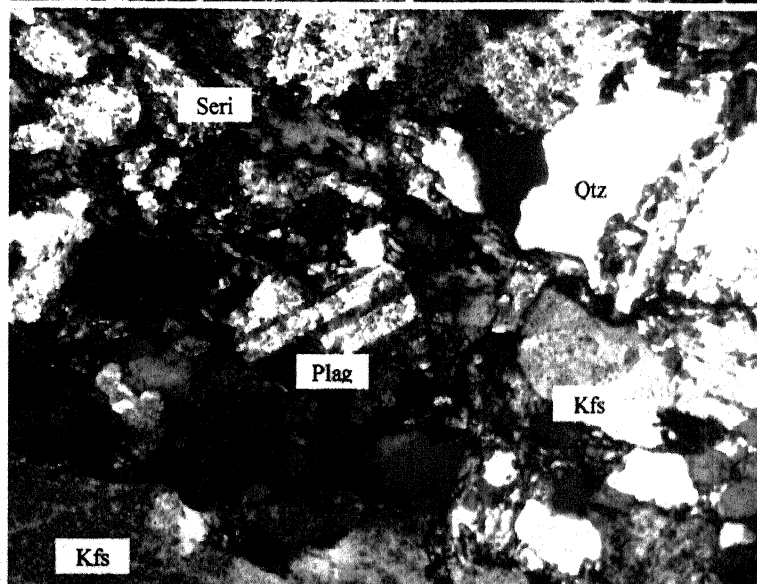
PLATE - IV



A



B

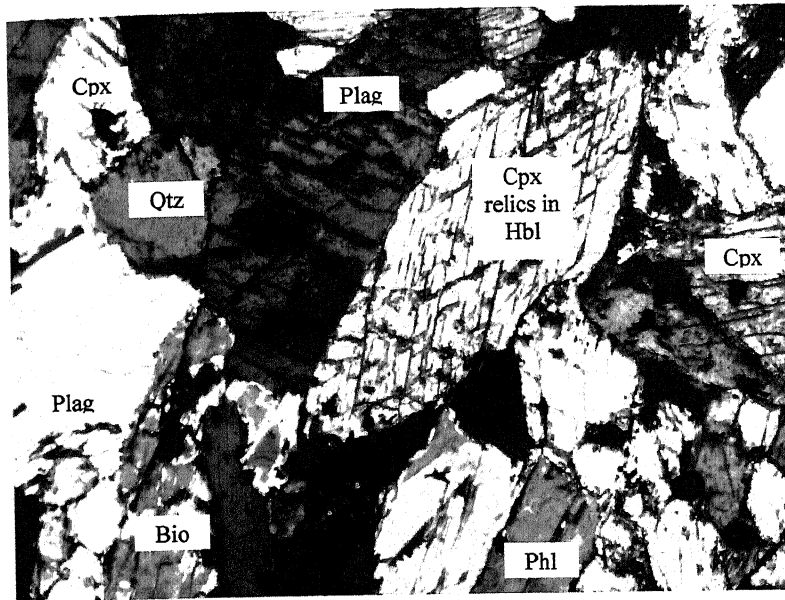


C

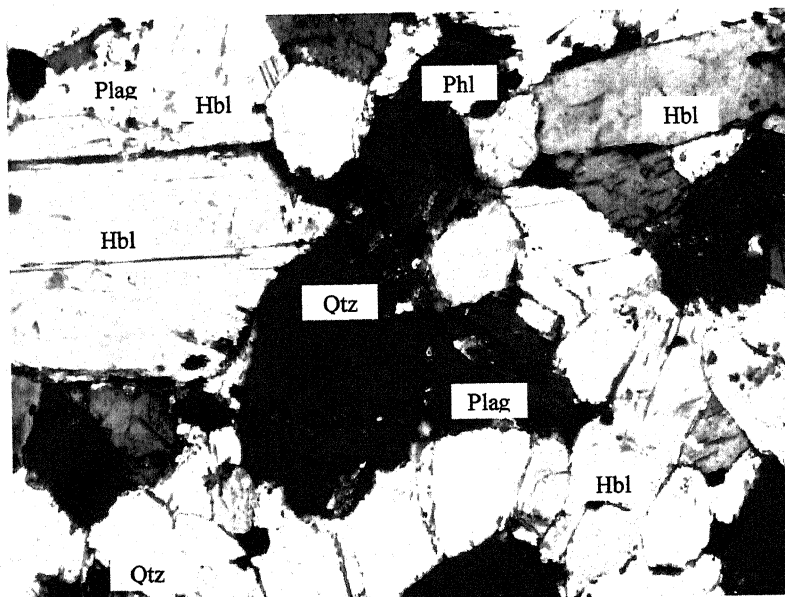
PLATE – V

- A. Coarse grained hornblende crystals are present. Clinopyroxene, plagioclase, and phlogopite are present.
- B. Coarse grained quartz and hornblende crystals are present. Plagioclase is also present.
- C. In coarse grained hornblende crystals biotite inclusions are present. Coarse grained magnetite, phlogopite and quartz are present.

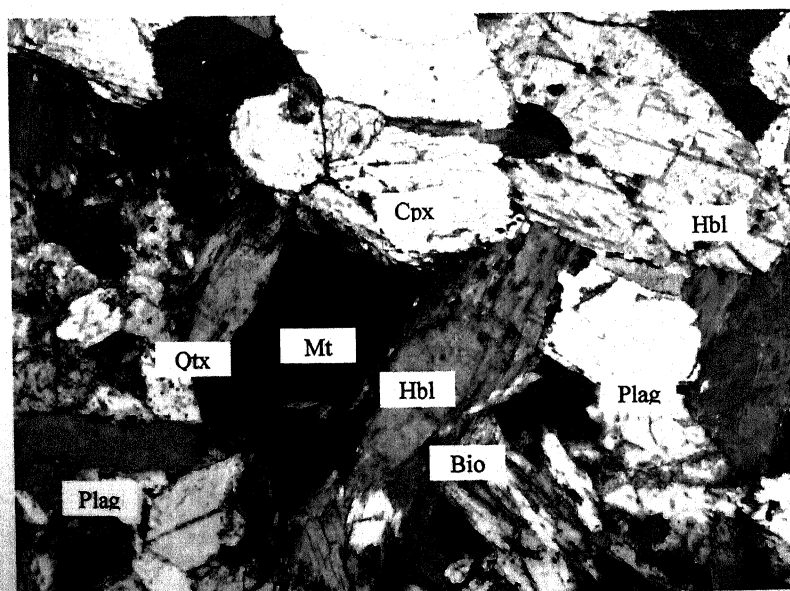
PLATE - V



A



B



C

PLATE – VI

- A. Hornblende crystals are present, medium grained biotite, plagioclase and clinopyroxene are also present.
- B. Coarse to medium grain clinopyroxene and hornblende crystals are present in association with plagioclase.
- C. Very coarse grain hornblende crystals are aligned along a preferred orientation. Coarse to medium grained quartz crystals are also been. Biotite is seen as altered from hornblende

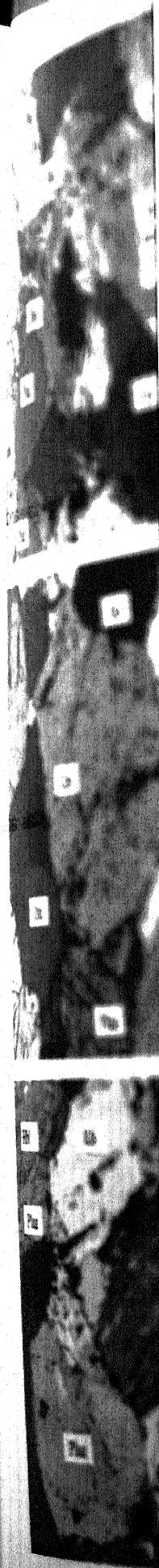
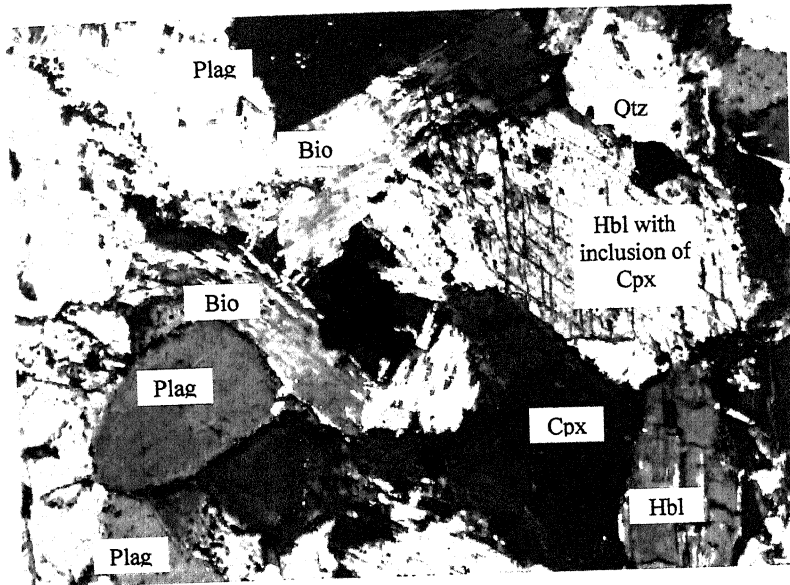
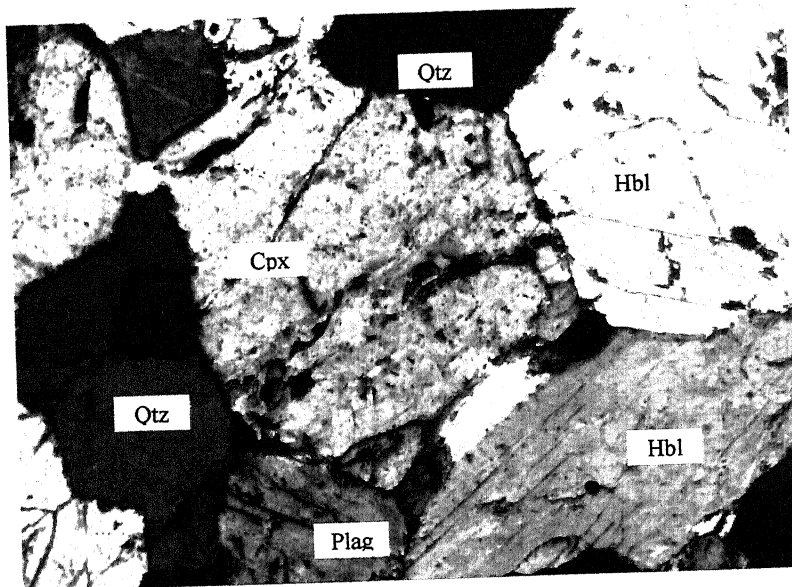


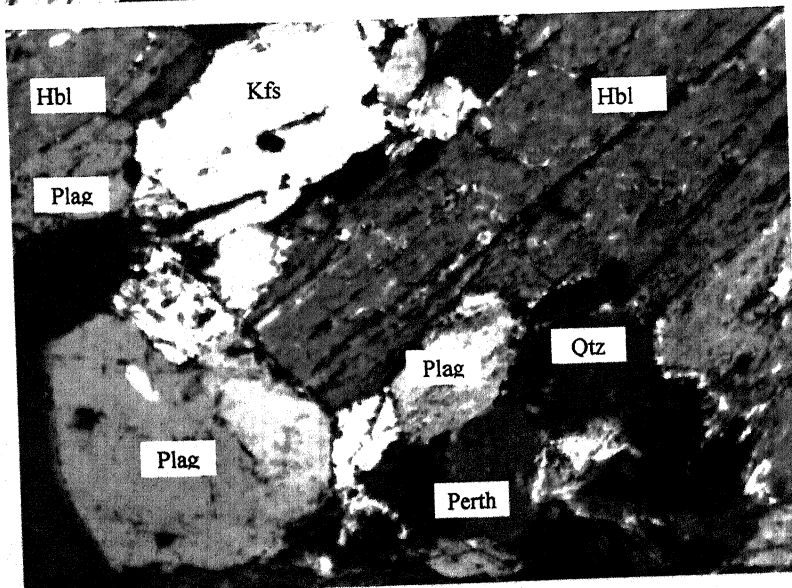
PLATE - VI



A



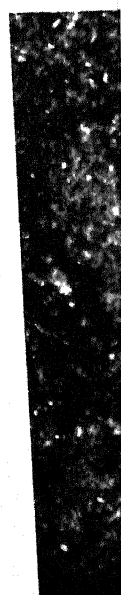
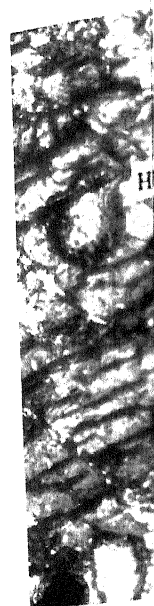
B

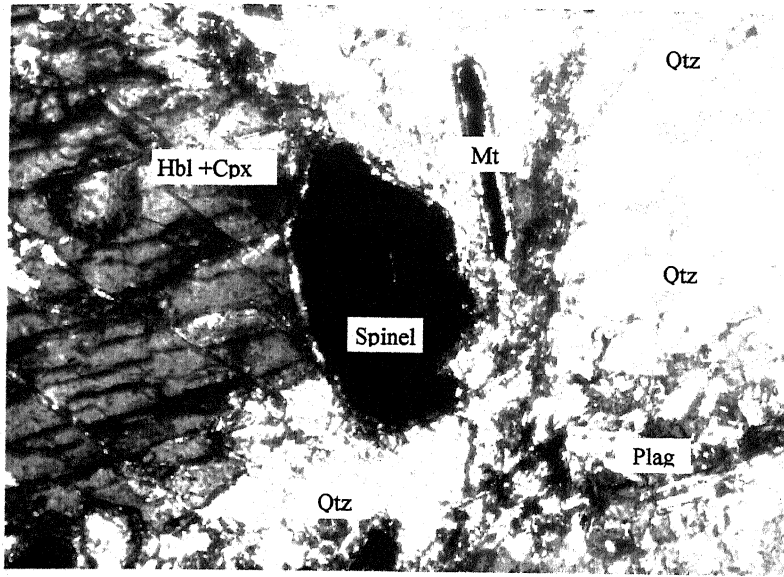


C

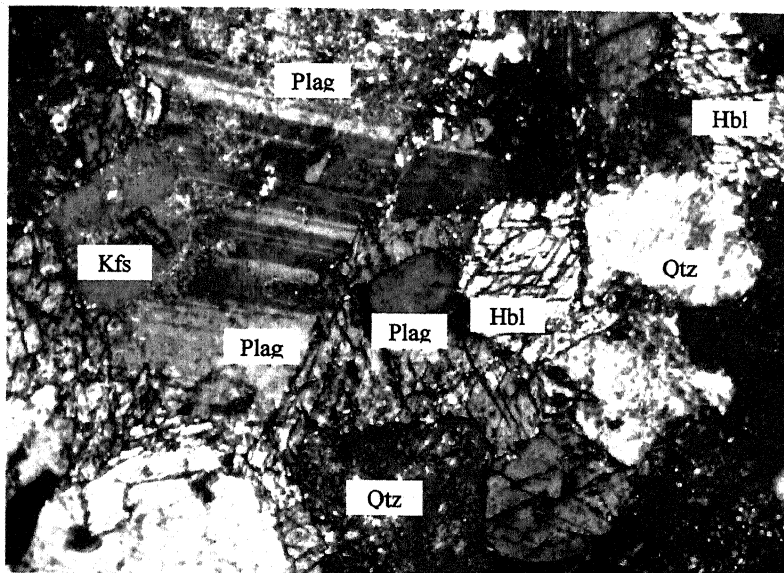
PLATE – VII

- A. Zoned magnetite crystals are present. The outer rim is sillimanite. Coarse-grained hornblende crystals are aligned along a preferred orientation. Quartz crystals are also seen.
- B. Hornblende crystals are present. Coarse grain plagioclase feldspar is also seen. Apatite is present as inclusion.
- C. Chlorite and quartz crystals are present with talc, actinolite and magnetite.

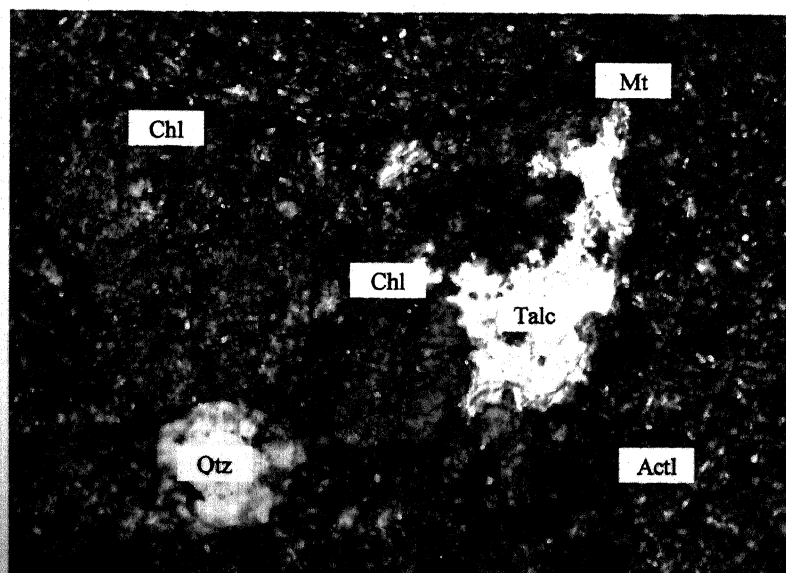




A



B

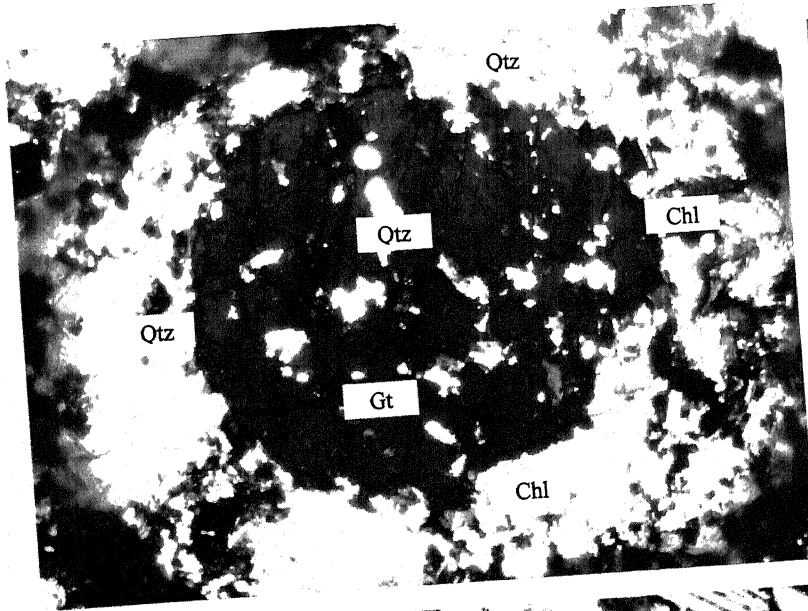


C

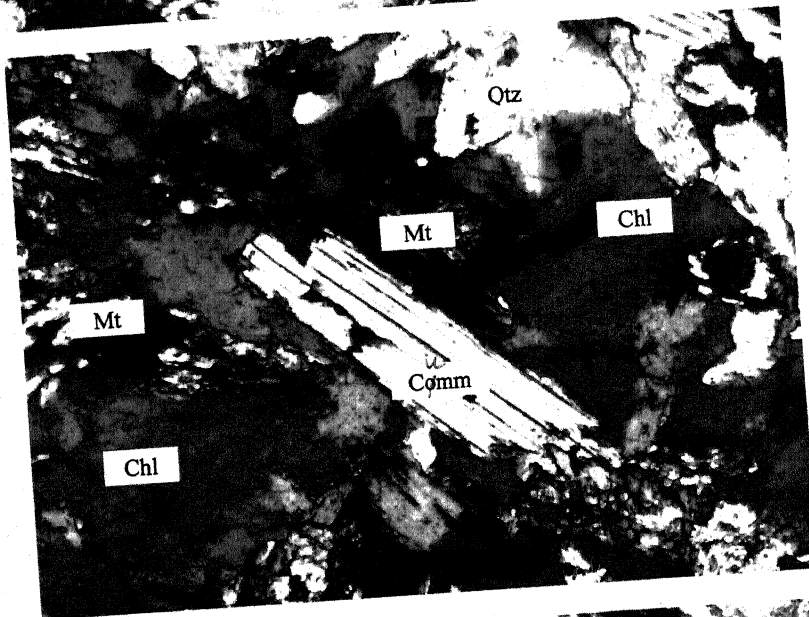
PLATE – VIII

- A. Fractured coarse grained garnet crystal is present and around it fine grained muscovite chlorite and quartz crystals are present. Within garnet quartz is seen as inclusion.
- B. Schistose structure is present. Coarse grain elongated muscovite crystals are also recorded along the schistose plane. Coarse grained patches of chlorite are also recorded.
- C. Elongated tremolite and actinolite shows schistosity. Talc and chlorite are also observed along with biotite and magnetite.

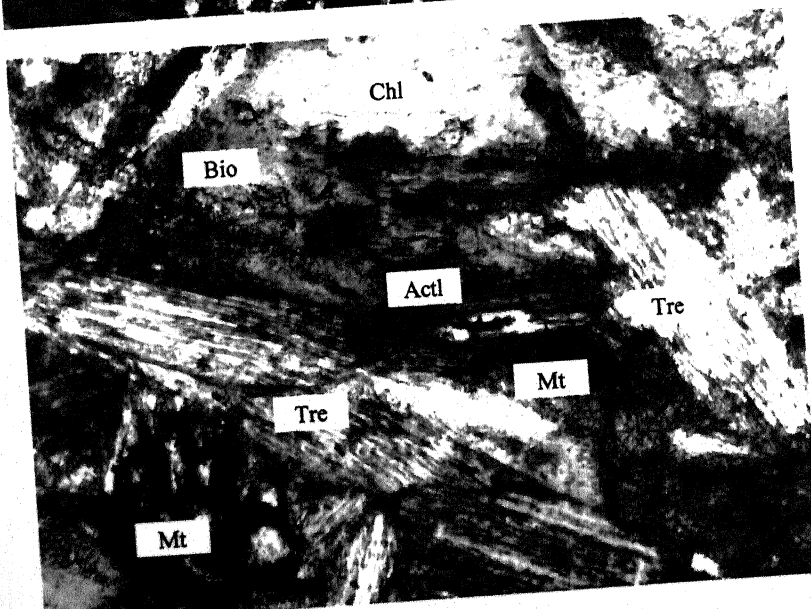
PLATE - VIII



A



B

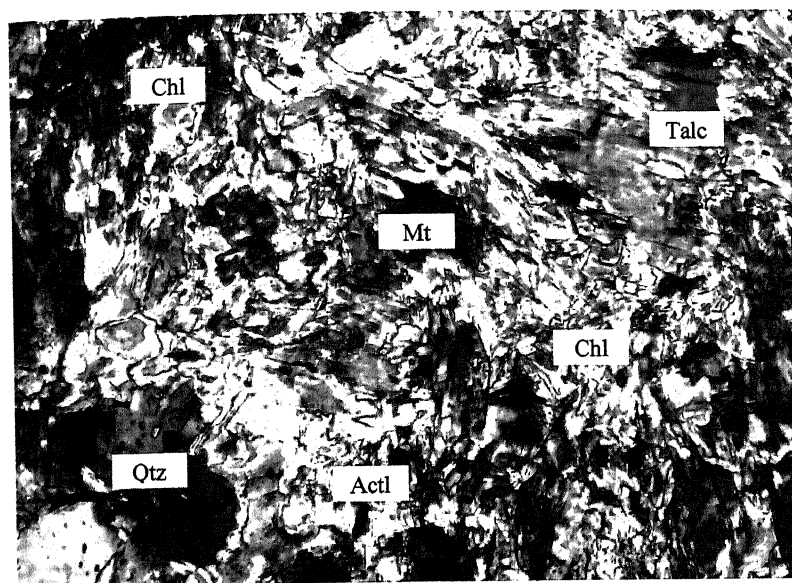


C

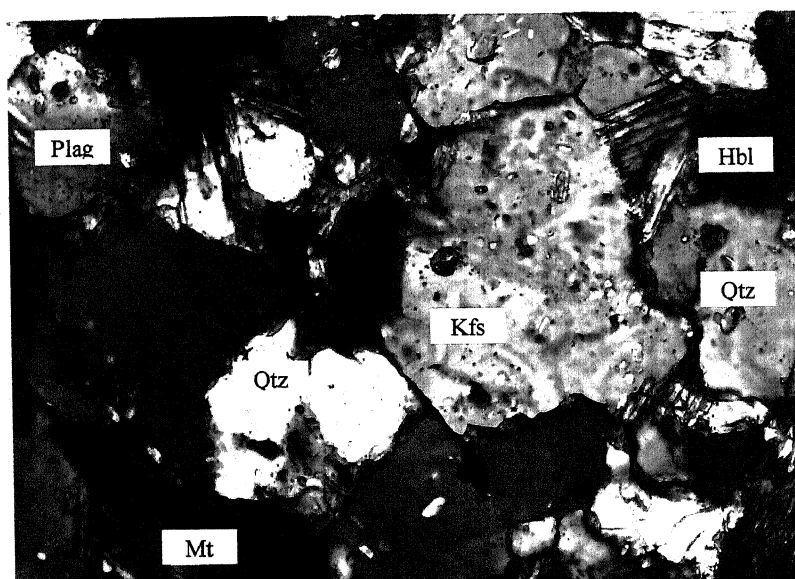
PLATE - IX

- A. Coarse to medium grained talc crystals and fine-grained elongated tremolites are recorded. Epidote is also observed.
- B. Photograph shows coarse to medium grained quartz crystals. Muscovite and Biotite are also present along with K-feldspar, plagioclase and magnetite.
- C. Photograph shows the fractured coarse-grained garnet and coarse to medium grained quartz. Chlorite and elongated needle shape Muscovites are also recorded. Fine-grained quartz fills the fractures of garnet.

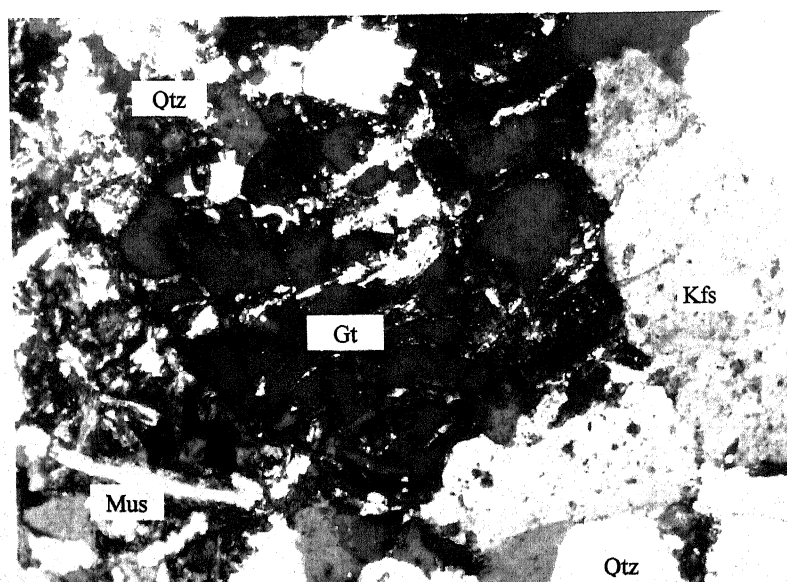
PLATE - IX



A



B



C

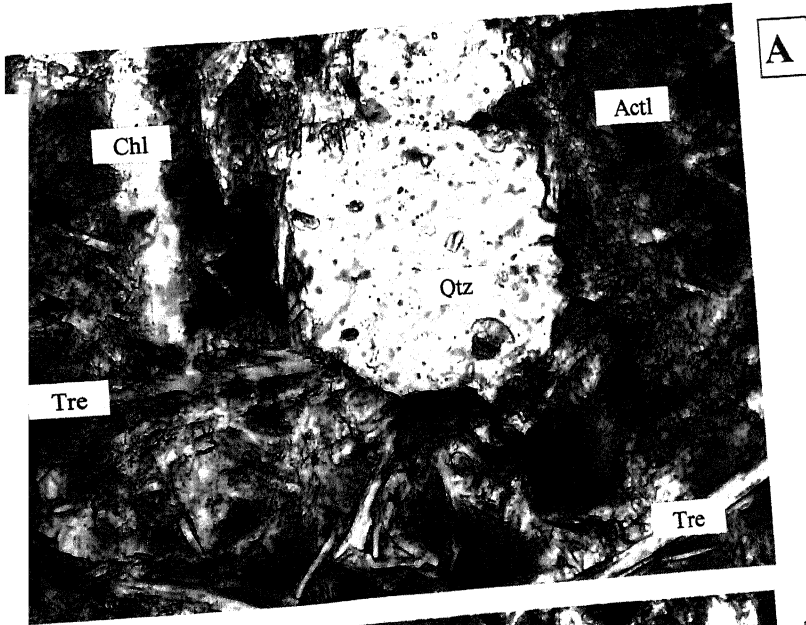
PLATE - X

- A. Photograph shows the coarse grained quartz and elongated tremolite crystals. Chlorite is also recorded.

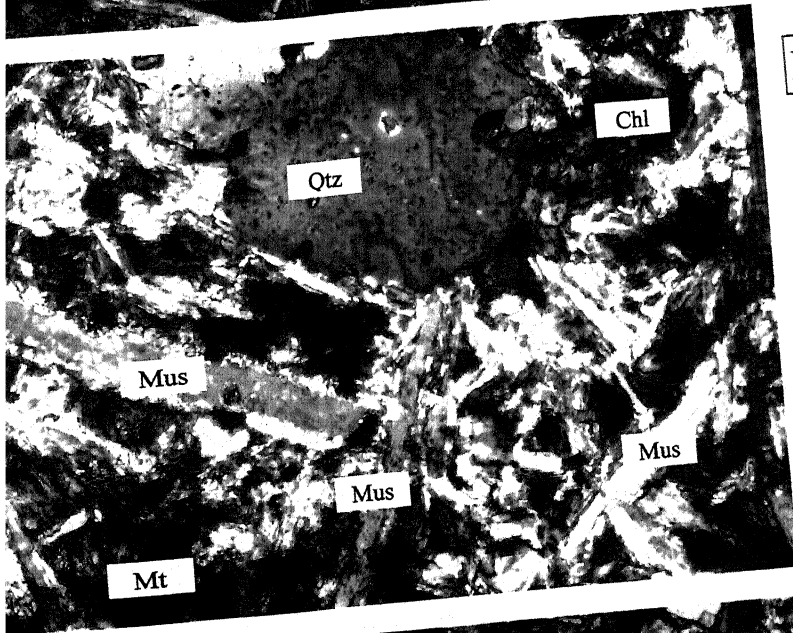
- B. Photograph shows elongated needle shape Muscovite and Biotite crystals. Anhedral coarse-grained quartz crystal, and chlorite are also observed.

- C. Photograph shows fine-grained equigranular chlorite, muscovite, plagioclase, quartz and epidote with opaque magnetite.

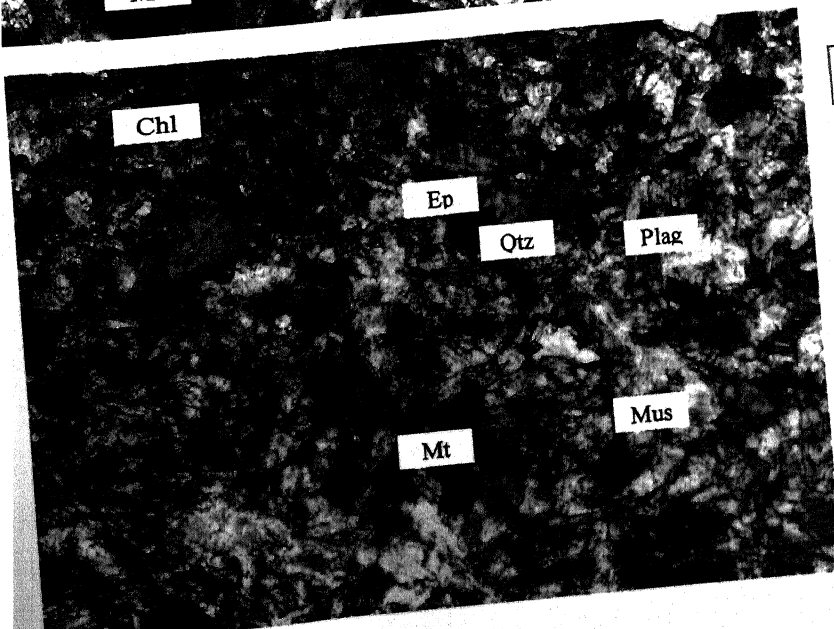
PLATE - X



A



B



C

PLATE – XI

- A. Coarse to medium grained quartz, biotite hornblende, K-feldspar, plagioclase, feldspar are observed. Biotite and Hornblende are aligned along a preferred orientation, which showing mild deformation. Within the ferromagnesian schistose plane zircon is also recorded.
- B. Photograph shows medium grained zircon crystal. Coarse-grained orthoclase, medium to fine grained quartz, elongated, biotite and hornblende are also recorded.
- C. Coarse grained K-feldspars and quartz crystals are present. Zircon is also observed. Large plate of chlorite is distinctly seen.

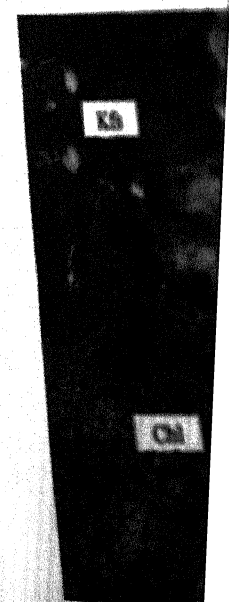
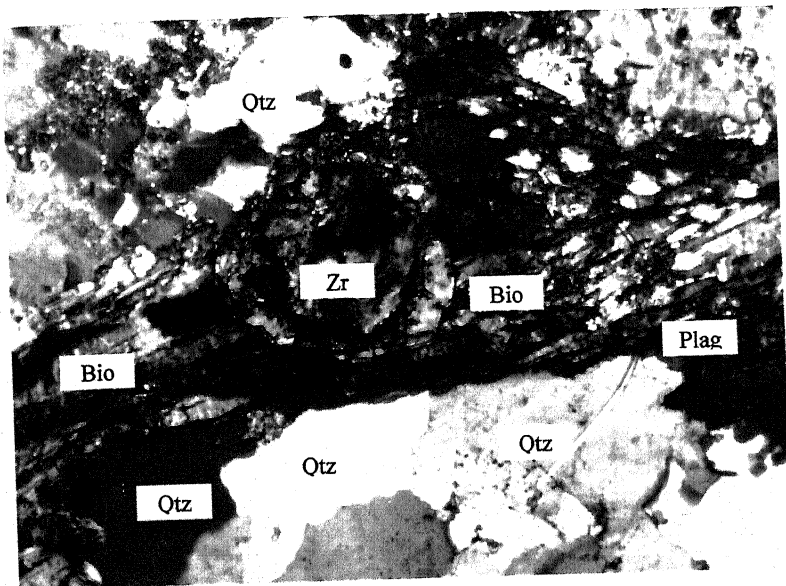
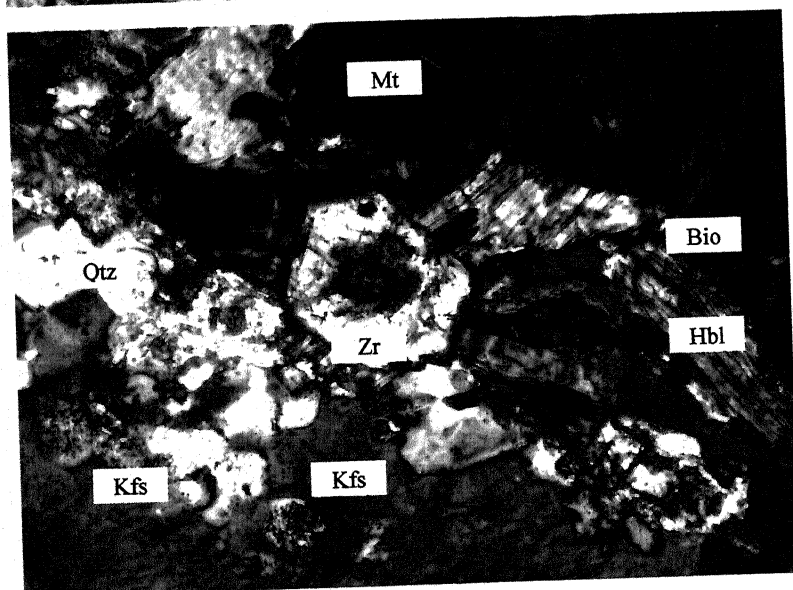


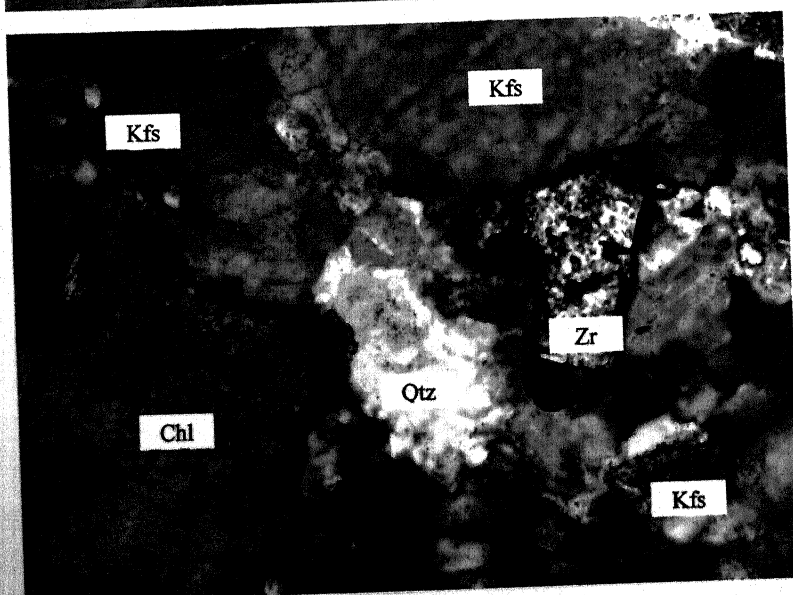
PLATE - XI



A



B



C

PLATE – XII

- A. Photograph shows plagioclase and K-feldspars. Saussuritisation of feldspar is also seen.
- B. Photograph shows porphyritic texture. Plagioclase and quartz are observed. Deformed plagioclase is also recorded.
- C. Photograph showing the inclusion of fine-grained magnetite and plagioclase within coarse grained amphibole crystals. Coarse to medium grained quartz crystals are recorded.



PLATE - XII

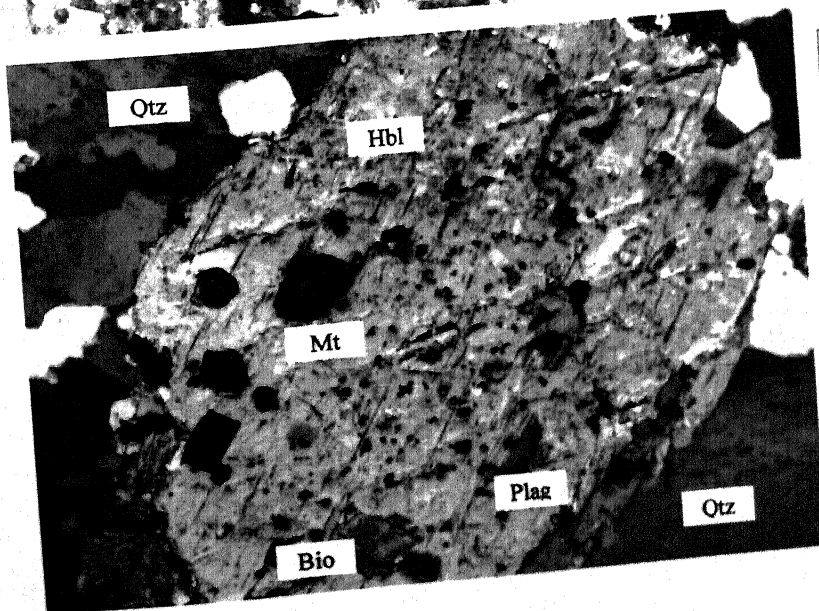
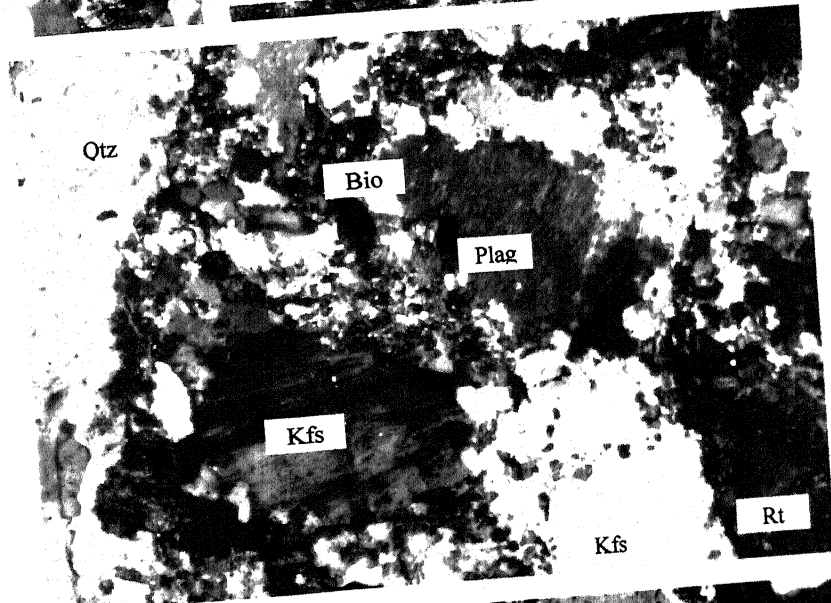
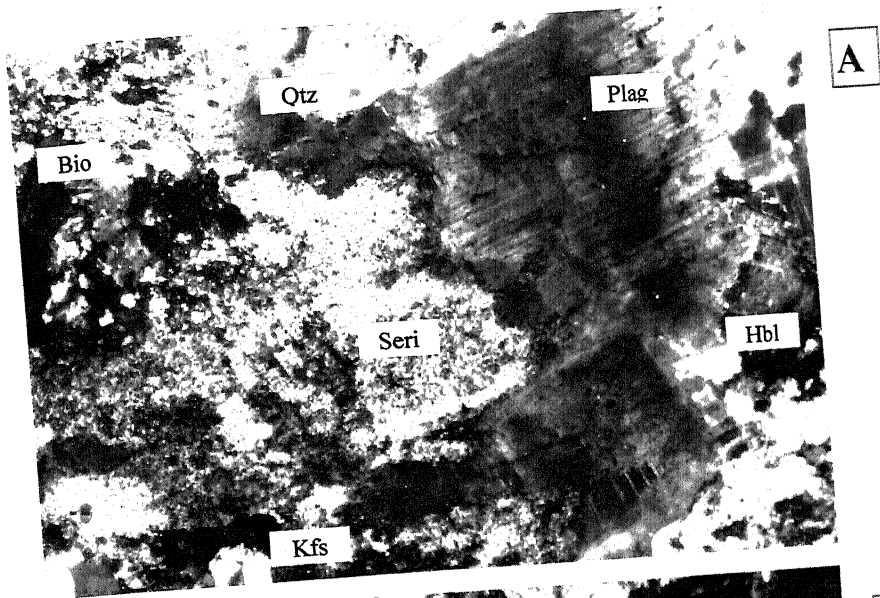
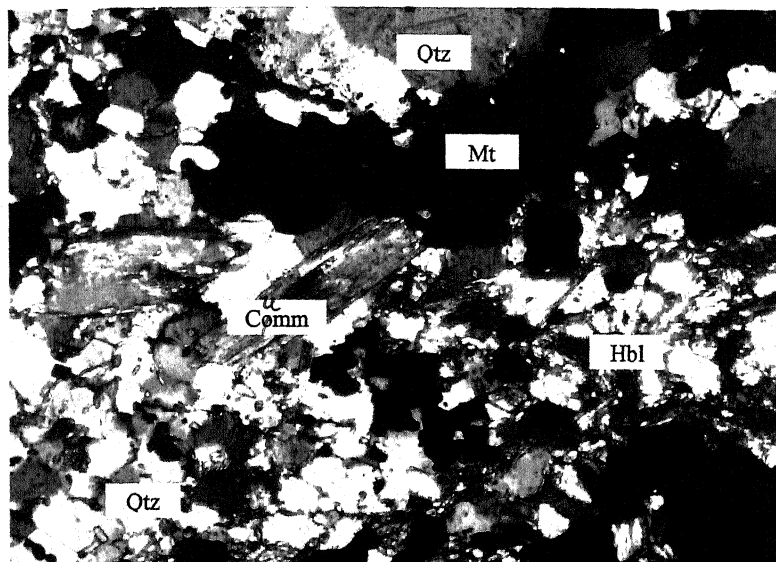


PLATE – XIII

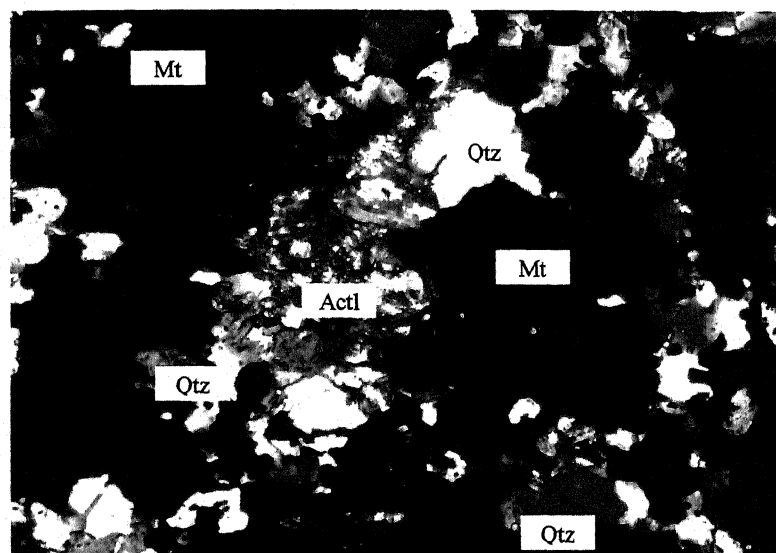
- A. Magnetite and quartz bands are present. Fine grained cummingtonite-grunerite and medium grained. Actinolite is also recorded.
- B. Photograph shows magnetite and quartz with actinolite and epidote.
- C. Quartz and magnetite with elongated actinolite crystals are recorded.



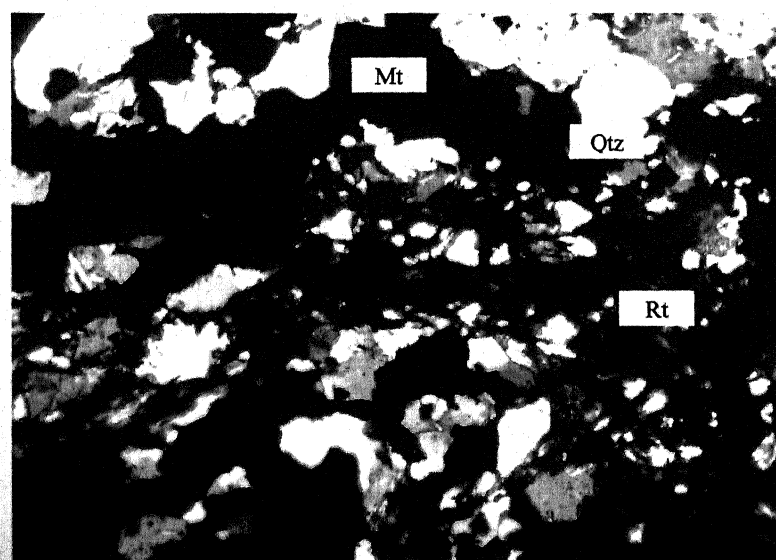
PLATE - XIII



A



B



C

CHAPTER- IV

GEOCHEMISTRY**4.1 Introduction**

In this chapter, analyses of the rocks of petrological interest and their results have been evaluated and presented on different diagrams and their possible interpretation and application for petrogenesis and tectonic environment of Bundelkhand massif have been discussed in view of the behavior of major and trace elements. The obtained geochemical data and their importance in geological processes of mid Archaean to early Proterozoic time in northern part of peninsular India has been discussed in detailed. Granites, gneisses, amphibolites and metavolcanosedimentary rocks are the major rock types in the study area. The exposed rocks in the investigated area have been divided into two parts viz. Part A: migmatites, gneisses and granites and Part B: mafics and ultramafics, for the presentation and discussion of different geochemical data.

For geochemical analyses, twentyfour representative samples have been chosen for petrological and tectonic interest of the study area. Weighing about 1Kg, each sample was reduced to chip size in a jaw crusher. The resulting samples were ground to 2000-mesh size in grinding mill, fitted with hard chrome steel grinder to avoid contamination. The powders were further coned and quartered, and desired quantities were used for analyses. Sample pellets of 40mm diameter were prepared in collapsible aluminum cups, using Herzog Hydraulic pressure at 20kb.

4.2. Analytical Methods

On the basis of the field relationship of the different litho-units and their petrographic studies under the microscope, the chosen twenty five representative rock samples of the migmatites, gneisses, granites, mafics and ultramafics of the study area were analyzed by X-ray fluorescence spectrometer Phillips exam six and PV 9100 at Wadia Institute of Himalayan Geology, Dehradun. The major element (wt%) and their calculated CIPW weight norm for the above-mentioned rock types are represented in Table No 4.1, 4.2, and 4.3.

4.3 Geochemistry

The analytical geochemical data were calculated as CIPW weight norms, trace elements and ratios of various major oxides of different rock types are presented in table no 4.4, 4.5 and 4.6.

Migmatites, gneisses, amphibolites, mafic, ultramafic, and meta-volcano-sedimentaries are the main rocks of the study area. On the basis of the field relationship, available geo-chronological data, structural and petrographic studies, the above-mentioned rock types were grouped under three heads for the geochemical study.

1. Older metamorphic Group: Migmatites, TTG, gneisses and amphibolites
2. Newer metamorphic Group: Mafic, ultramafic and metavolcanosedimentary rocks.
3. Bundelkhand granitoids: hornblende granite, biotite-granite, coarse-grained leucogranite, fine-grained leucogranite and deformed granite.

Five samples of granite of petrochemical interest and six samples of gneisses were analysed for major and trace element. The obtained analytical data have been presented in the pertinent diagrams to obtain the genetic interpretation.

The major element data (Table No. 4.1 and 4.2) of the gneisses and the granites of the study area indicate the following characteristics:

1. Both, the gneisses and granites are the highly silicic having 55.97 to 77.49-wt% SiO_2 and 68.76 to 89.52-wt% SiO_2 respectively.
2. The alumina (Al_2O_3) content in gneisses is moderate and ranging from 12.80 to 15.38wt%, while in granites it is present as low to moderate, ranging from 5.88 to 16.39wt%. Alumina content (Av. 14.25wt% in gneiss and 12.95wt% in granite) is greater than the total alkalies ($\text{K}_2\text{O} + \text{Na}_2\text{O}$) (Av. 6.84wt% in gneiss and 8.26wt% in granite) in gneisses and granites.
3. The potash content in gneisses ranges from 1.24 to 5.00wt% K_2O while in granites ranges from 0.14 to 13.75wt% K_2O . Potash content is less than the soda content (3.20 to 5.34 -wt% Na_2O) in majority of the gneisses but in contrast to this the K_2O content is greater than the Na_2O content (0.08 to 5.32-wt% Na_2O) in majority of the granite samples.
4. The Titania (TiO_2) content in gneisses and granites are low ranging from 0.04 to 1.76wt% TiO_2 and 0.03 to 0.44wt% TiO_2 respectively.

4.3.1 Geochemistry of granites, migmatites and gneisses

4.3.1.1 Classification and nomenclature

The gneisses and granites have been chemically classified on the basis of different oxides, norms and cationic parameters. The classification schemes based on Na_2O vs K_2O (Harpum, 1963), An-Ab-Or (O'Connor 1965), Q-A-P (Streckeisen, 1967 and

Le Maitre 1989), P-Q (Debon and Le Fort, 1982) etc. have been considered for the geochemical classification of granites and gneisses of the present study area.

Based on Na_2O vs K_2O diagram (Fig. 4.1) a majority of gneiss samples falls in the tonalite field while Granite samples plot in the fields of adamellite and granodiorite.

The ternary (An-Ab-Or) diagram (Fig. 4.2a, and 4.3a) is developed by O' Connor (1965). A majority of the gneisses fall in tonalite, trondhjemite fields while a majority of granites fall in granite field. Pressure boundaries suggested by Whitney (1975) points that average composition of gneisses are plotted in the field above 10 kb pressure, while granites plot in the field between 2Kb and 12 Kb. It suggests that possible pressure during the metamorphism of gneisses could be above 10 Kb. The variation in granites plot mostly between 1.5 to 12 Kb. Boundaries suggesting a multiphase emplacement of acid magmatism and crystallization at different depths.

Q-A-P diagram

The normative Q-A-P triangular diagram (Fig. 4.2b and 4.3b) developed by Lameyre and Bowden (1982) and Le Maitre (1989) has been used for classification of gneisses and granitoids. When plotted on these diagrams the majority of gneisses fall in the granodiorite, and tonalite fields while the majority of granites fall in the monzogranite and granodiorite fields. Gneisses forms a poor calc-alkaline trend, on the other hand granite forms a typical intermediate K_2O and Na_2O rich trend.

P-Q diagram

The P-Q diagram proposed by Debon and Le Fort 1982 ($P=[K - (Na + Ca)]$ and $Q=[Si/3 - (K+Na + 2Ca/3)]$) for the classification of gneissic rocks reveals that majority of the gneisses are fall in the tonalite field (Fig. 4.4b) while majority of granites are plot in the field of granite and adamellite (Fig. 4.4a).

A versus B diagram

$A=[Al - (K + Na + 2Ca)]$ versus $B=(Fe + Mg + Ti)$ diagram is proposed by Debon and Le Fort (1982) and Debon et al; (1986). They described that the chemical-mineralogical change are mainly based on multi-cationic parameters. They suggested that peraluminous and metaluminous characters mainly depend on its negative value of 'A'. A-B diagram (Fig. 4.5b) clearly shows that most of the gneisses occupy the delineated IVth fields of the metaluminous domain. This view also supported by the presentation of geochemical data of gneisses in Shand's alumina Saturation Index diagram (Fig. 4.5c). The geochemical data of granites in A-B diagram indicates that they belong to the association of biotite \pm hornblende \pm clinopyroxene \pm orthopyroxene \pm olivine \pm (Fig. 4.5a)

TAS diagram

Total alkalis versus silica diagram (Fig. 4.6) is developed by Middle Most (1985). In this diagram, majority of the granites are plot in the alkali granite field. Alkalinity ($\text{Na}_2\text{O}+\text{K}_2\text{O}$) of these samples does not exceed more than 10%, which reveals that local metasomatism may not be ruled out in the study area.

A-F-M diagram

The analyzed granite samples were plotted in the A-F-M diagram, (Fig. 4.7a) developed by Irvine and Baragar (1971). Based on this diagram, it is clearly depicted that the granite samples represent the calc-alkaline differentiation trend and evolved toward the alkali corner. In this case, analyses of granitoids of Bundelkhand were also examined to get the ultimate result of evolution trends (Fig. 4.7a). Most of the samples lie in the calc-alkaline trend. Rahman and Zainuddin (1993) also described that the Bundelkhand granites probably have calc-alkaline affinity.

SiO_2 vs $\text{Na}_2\text{O} + \text{K}_2\text{O}$ diagram

The analyses of gneisses and granites are plotted on the SiO_2 versus $\text{Na}_2\text{O}+\text{K}_2\text{O}$ diagram (Fig. 4.7b) proposed by Irvine and Baragar (1971). The diagram indicates two distinct fields calc-alkaline viz. alkaline and sub-alkaline. All the analyzed samples of gneisses lie in the sub alkaline field while granites fall around the line of alkaline and sub alkaline field but majority of them lie in the sub-alkaline field.

4.3.1.2 Tectonic discrimination

Sarkar et al; (1996) and Mondal et al; (2002) obtained the age of TTG and migmatite, gneisses as 3200 M.a. to 3500 M.a. while granites were dated from 1800 M.a. to 2500 M.a. The geochronological study points that the granite-gneisses and Bundelkhand granitoids were the two events, which might have occurred under two different tectonic environments. Therefore in the present study, we discussed them both for comparison.

To classify the tectonic environment of the granites of the study area, different discrimination parameters proposed by Maniar and Piccoli (1989) are applied. They distinguished seven types of granitoids based on their tectonic setting:

1. Island Arc Granitoids (IAG)
2. Continental Arc Granitoids (CAG)
3. Continental Collision Granitoids (CCG)
4. Post – Orogenic Granitoids (POG)
5. Rift-Related Granitoids (RRG)
6. Continental Epeirogenic Uplift Granitoids (CEUG)

7. Ocean Plagiogranites (OP)

IAG, CAG, CCG and POG are considered as orogenic granitoids, whereas RRG CEUG and OP are believed to be anorogenic granitoids. They have grouped the granites according to different tectonic setting as IAG, CAG, CCG (group I) and RRG, CEUG and POG (group II)

It has been noted that the chemical signatures of granites of Bundelkhand massif do not follow single and firm tectonic environment.

All the granites samples fall into the field of orogenic granites distinctly away from the field of anorogenic granites in the discrimination diagram (Fig. 4.8a) and also majority of the granite of the study area fall in the orogenic granite field (Fig. 4.8b and c). Shand's alumina saturation Index diagram (Fig. 4.9) points that the majority of granites falls in metaluminous field where A/CNK value ranges from 0.8 to 1.2. It suggests that granites of the study area resulted from magmatic origin of POG.

4.3.1.3. Petrogenesis

De La Roche's R1-R2 plots, cationic proportion of major oxides (modified by Batchelor and Bowden; 1985) have been used for discrimination of cationic environment. Majority of granites of the study area plots in the syn-continental collision field (Fig. 4.10). The values of the molar ratio $Al_2O_3 / (CaO + Na_2O)$ of granites of the study area in Shands index diagram, have metaluminous composition ($A/CNK = 0.85-1.05$) suggesting that granites were derived from igneous sources (I type granites). Zainuddin et al (1992). Mondal and Zainuddin (1996) suggested that Bundelkhand granites is characterized by I type affinity.

4.3.1.4 Major oxides variation

To understand the role of differentiation process in the formation of gneisses and granites of the study area, the variation diagrams of Harkers (Fig. 4.11 and 4.12) were studied.

Silica versus Other Oxides

Calcium and magnesium oxides: CaO and MgO show a sympathetic relationship with one another in gneisses of the study area but CaO content is always more than MgO. Same trend is also observed in granites. CaO content in gneisses varies from 0.62 to 4.44-wt% while in granite it varies from 0.23 to 2.8-wt%. MgO content varies from 0.32 to 4.14-wt% in gneisses while in granites it varies from 0.17 to 1.32-wt%. In both gneisses and granites, CaO and MgO show antipathic relationship with SiO_2 (Fig. 4.11 e, h and 4.12 e, h).

Alkalies

In gneisses Na_2O varies from 3.20 to 5.34-wt% while in the granite it varies from 0.08 to 5.32-wt% and K_2O content varies from 1.24 to 5wt% and 0.14 to 13.75wt% respectively. In both gneisses and granites Na_2O and K_2O bear an inverse relationship to each other. Further $\text{K}_2\text{O}/\text{Na}_2\text{O}$ ratio varies from 0.25 to 1.20 in gneisses while this varies from 0.78 to 171.87wt% in granites. When silica content is plotted against Na_2O and K_2O individually (Fig. 4.11a, b and 4.12a, b). It is seen that there is a tendency for concentration of SiO_2 around 70wt% in both gneisses and granites but Na_2O around 5wt% in gneisses and 3 to 4wt% in granites. In gneisses of the study area, K_2O concentrates around 1.5wt% while in granites it concentrates around 4wt%.

Alumina

In gneisses of the study area, Al_2O_3 contents vary from 12.80 to 15.38wt % while in granites varies from 5.88 to 16.39wt%. Alumina content increases with decreasing silica content (Fig.4.11c and 4.12c) and the ratio of the Al_2O_3 and SiO_2 shows inverse relationship. Total alkalies and alumina for both gneisses and granites bear a more or less antipathic relationship. There is no definite trend in combined alkalies or alumina though the later show a tendency to decrease with increase in SiO_2 . P_2O_5 , CaO , Fe_2O_3 , TiO_2 , and MgO has a tendency to increase with decreasing SiO_2 contents Fig. 4.11.

Al_2O_3 - ($\text{Na}_2\text{O}+\text{K}_2\text{O}+\text{CaO}$)-(FeO+MgO+MnO) -Triangular Diagram

The gneisses and granites of the study area were plotted on a triangular Al_2O_3 - ($\text{Na}_2\text{O} + \text{K}_2\text{O} + \text{CaO}$) - (FeO + MgO + MnO) diagram (Fig. 4.13a), which indicates a distinct field viz. anatectic and magmatic nature. The majority of the analyzed gneisses and granites sample are plotted in the field of magmatic region (magma of anatexial origin), which shows affinity towards cotectic. This means that the granite rocks of the study area have been formed due to remobilization and partial melting of these gneisses and they are enclosed as lensoidal patches within the gneissic rocks.

Rubidium versus Potassium Diagram

The Rb- K_2O contents of granites of the study area plotted on Rb Vs K_2O diagram (Fig. 4.14b), which shows positive correlation as they have similar ionic behavior. This type of behavior is called the pegmatitic-hydrothermal trends emphasizes the part played by the field phase (Shaw 1968). It is concluded that alkali field circulation has taken place and played an important role during the crystallization of magmatic fluids.

4.3.1.5 Trace element geochemistry

The study of trace elements is very useful for understanding the evolutionary history of the rocks. The distribution of trace elements is similar to that of major elements.

The proportion of the elements in the rocks depends on mineralogy, fluid composition, volume of fluid and pressure temperature conditions (Hanson 1978; Rollinson et al 1981).

For trace elements analysis, powder samples were pelletized and analysed by XRF-ED (X-ray fluorescence - energy dispersive) for Cu, Zn, Zr, Ga, Rb, Y, Ba, Sr and Nb using Philips Exam Six and PV 9100 spectrometer (Perkins- Elmer 4000) after total composition with an HF-HClO₄-HNO₃ and acid mixture. The analytical results are shown in Table 4.4 and 4.5.

Rb – Ba – Sr diagram

El Bouseilly and El Sokkary (1975) described the usefulness of Rb-Ba-Sr ternary diagram in tracing the evolutionary trends of granite rocks. This diagram can also be used to classify the granites, evaluated fraction trends and nature of granites.

In Rb-Ba-Sr ternary diagram (Fig. 4.13b), granites of the study area are plotted. Considerable variation has been recorded from analysed sample. They lie in the fields of granodiorite, quartz, diorite, granite and strongly differentiated granite. It reveals that granites of the study area is magmatic source and have been emplaced and crystallized at different depth with varying physiochemical conditions.

The granites plot in normal granite field (Fig 4.13b) point that high Ba concentration is typically associated with high temperature (least differentiate) K-feldspar (Taylor et al; 1960). Here, the increase in Ba is accompanied by decrease in Rb. Granite plot in strongly differentiated granite field is indicated by the Ba/Rb ratio, which characterizes the change from normal granite to strongly differentiated type. Rubidium enrichment has been known to occur in highly differentiated granite (Ahrens et al; 1952, Taylor et al; 1956).

Condie (1973) has developed Rb vs Sr (log-log) variation diagram (Fig. 4.14a) to estimate the crustal emplacement depth for granites. The gneisses and the granites of the study area are plotted in this diagram.

All the Rb/Sr ratio values of gneisses lies between 0.3 and 2.0 while granite show scattering and fall to the range of 0.3 and above 10.0 on the defined line Fig. 4.14a. It is noted that the granite melt might have been generated at depths around 23-35 Kms. Temperature of about 750° C can be expected at such depths at a universally accepted geothermal gradient of about 30°C per km.

Pearce et al; (1984) described the discrimination of granites in Rb-Y + Nb and Nb-Y (in ppm) space. The relative trace element characteristic of the granites in the study area can not be assigned collectively of any one tectonic regime when plotted on Y+Nb

versus Rb log-log (ppm) and Y versus Nb log-log (ppm) diagram (Fig. 4.15), all the samples cluster near the triple junction demarcating lines of volcanic arc granitoids (VAG), syn-collisional granitoids (syn-COLG) and within plate granitoids (WPG) field.

Behavior of Potassium –Rubidium –Strontium

The high grade metamorphics and granite shows high K, Rb, Sr. The K-Rb relationship shows that granite of the study area plotted above the main trend (MT) is defined by Shaw (1968) for continental igneous rocks. The plot in general shows a positive correlation with wide variation in K /Rb ratios (Fig.4.14b). In the majority of the cases, the data shows that K/Rb ratio of the amphibolite zone have value greater than 1000. It is generally accepted that this is related to the upper amphibolite facies metamorphism (Heier 1965 and Tarney et al, 1979). However, the granites are enriched in Rb (maximum up to 417 ppm) as compared with the value of 150 ppm given by Taylor et al (1956) for granite. This suggests that these granites were subjected to late stage differentiation.

The plot of Rb vs Sr (Fig. 4.14a) points that the gneisses and granites of the study area show the positive relations. Rb concentration ranging from 72 to 1416 ppm in gneisses while granites ranging from 21 to 417 ppm. The Rb/Sr value of gneisses (0.928) and granite (9.28) are much higher than the value of the continental crust as a whole (0.12) and lower crust (0.047) (Taylor and Mc Lehmann, 1979).

The high Rb/Sr ratio of the metamorphic may be due to chemical variation during metamorphism of feldspar minerals appears to be the dominant controlling factor for the abundance of Sr. This is quite evident from the positive correlation shown by gneisses of the study area when Sr plotted against normative plagioclase (Fig. 4.16b). The granite of the study area has also positive correlation.

Behavior of Lithium and Lead

The Pb and Li abundance in rocks is generally controlled by the presence of K-feldspar and biotite minerals in the rocks. According to the Moorbath et al, (1969), indicating that the metamorphics of high grade facies terrains are generally depleted in Pb and Li in comparison to the low grade facies terrains. The positive relationship has been shown by Pb with normative orthoclase (Fig. 4.16a) in gneisses suggesting that the elements preferentially occupy the lattices of K-feldspar in the rock.

4.3.1.6 Trace element variation

The average distribution of trace elements in the gneisses and granites of the study area are shown in Table 4.4 and 4.5. The gneisses have higher Rb (416ppm), Ba (220 to 706ppm), Sr (80-442ppm), Zr (85 to 445ppm) and Cr (271 to 592 ppm) content while in granites, Rb ranges from 21 to 417 ppm, Ba (232 to 1017 ppm), Sr (3 to 423), Zr (9 to 368ppm) and Cr (151 to 502ppm).

The gneisses and granites of the study area is plotted on Harkers variation diagrams (Fig. 4.17 to 4.20). The trace elements of gneisses and granites plotted against SiO_2 show some genetically similar relationship with gneisses and granites. However, a majority of them does not show a distinct trend. Ga, Zr, and Nb show a tendency to increase with decreasing SiO_2 . However, Ga shows distinct trend. Y, Cu, Rb, Ba and Sr do not show any marked variation with increasing SiO_2 in the gneisses and granites (Fig. 4.17 and 4.18).

4.3.2 Mafic & ultramafic Rocks

In order to classify the mafics and ultramafics of the study area and further to understand the genesis and tectonic environments. The major and trace element geochemistry of representative litho-units of mafics and ultramafics have been discussed below.

Nine representative samples of mafic and ultramafic of the study area were analysed by X- ray fluorescence spectrometer Philips exam six and PV 9100at Wadia Institute of Himalayan Geology, Dehradun. The major elements (wt%) is given in the Table 4.3.

The mafics and ultramafics of the study area are characterized by moderate SiO_2 , Al_2O_3 , K_2O , Na_2O and TiO_2 content. Al_2O_3 content is greater than total alkalies ($\text{Na}_2\text{O}+\text{K}_2\text{O}$). MgO and FeO (T) have been noticed considerably high in two samples contain very high value of MgO (28.24%), Cr (3121ppm) and Ni (975ppm).

The major oxides data presented in Table 4.3 depict the following characteristics of the mafics and ultramafics of the study area:

- The mafics and ultra mafics having silica contents 36.56-55.15-wt%. Alumina content ranges form 6.58 to 13.07-wt%.
- The soda content ranges from 0.06 to 2.82-wt%, which is greater than the potash content (0.02 to 1.48-wt%).

- The iron content (FeO total) in mafics and ultramafics ranges from 11.89 to 24.30-wt% FeO (T).
- The Titania content ranges from 0.19 to 2.22-wt% TiO₂.
- The Magnesium content varies from 5.66 to 28.24-wt% MgO. In some samples it reached up to 78% MgO.

Fundamentally, it has been universally accepted that distribution of basaltic rocks and generation of various type of parent basaltic magma are related to different tectonic environment, not only on a global scale but to some extent in smaller tectonic provinces also (Bose 1997). Basalts are universal and are manifested in a wide variety of tectonic environment in general.

4.3.2.1 Classification and nomenclature

Mafics and ultramafics of the study area have been chemically classified on the basis of different oxides, norms and cationic parameters. The classification schemes based on total alkalis versus silica (TAS) diagrams (Le Maitre et al; 1989), and Cox et al; (1979), AFM diagram (Jensen, 1976), TiO₂-K₂O-P₂O₅ diagram (Pearce et al; 1975).

FeO-FeO/MgO, TiO₂-FeO/MgO diagram (Miyashiro and Shido 1975), TiO₂-SiO₂ diagrams (Macdonald & Katsura 1964, Whitehead and Good fellow 1978) etc. have been used to obtained the magmatic characters of the of these low-grade metamorphosed mafic and ultramafic rocks.

The total alkalis (Na₂+K₂O) versus silica diagram proposed by Cox et al; 1979 (Fig. 4.21) depicts that analyzed samples of the study area are of the basaltic nature and are characterized by sub alkali basalt. Similarly TAS diagram (Fig. 4.22) of Le Maitre et al; (1989) also propose that these rocks are of basalt andesite type.

The Jensen's classification schemes (Jensen 1976) using the millication parameters have been described for metamorphic rocks. The element were selected for their variability within sub-alkaline rocks for the way in which they vary in inverse proportion to each other and for their stability under low order of metamorphism. As the samples selected from the study area are metamorphosed, this classification schemes is very helpful in present study.

The scheme of classification is based on the proportions of the millicationic values of (Fe²⁺+Fe³⁺+Ti), Al, and Mg, and is further recalculated to 100% for triangular diagram. The analyzed samples were plotted in this triangular diagram, which fall in the fields of Komatiite, Komatiitic basalts and high Fe tholeiite basalt (Fig. 4.23a). The plotted values in

triangular diagram point that the parent magma compositions of present metamorphites were perhaps komatiite in the initial stage and subsequently it changes to komatiitic basalt and Fe-tholeiitic composition due to fractionation, contamination and metasomatic activities.

The triangular diagram ($\text{TiO}_2 - \text{K}_2\text{O} - \text{P}_2\text{O}_5$) proposed by Pearce et al; (1975) shows that majority of the analyzed samples are of oceanic floor basalt (OFB) character (Fig. 4.23b). On the other hand $\text{FeO} - \text{FeO}/\text{MgO}$ and $\text{FeO} - \text{FeO}/\text{MgO}$ diagrams Fig. 4.24a suggested by Miyashiro and Shido (1975) showing tholeiite affinity. It is also recorded a linear trend for FeO/MgO vs. FeO wt%.

Using $\text{TiO}_2 - \text{SiO}_2$ (wt%) diagram Fig. 4.24b of Macdonald and Katsura (1964), Whitehead and Goodfellow (1978) classifies that the analysed samples of the study area indicate the Ocean Floor tholeiites, in character (Fig. 4.23b).

$\text{MgO} - \text{SiO}_2$ (wt%) diagram (Fig. 4.24c) of Redman and Keays (1985) has been used to find out the nature of parent magma of mafic and ultramafic metamorphics of the study area. It is observed that all the values are characterized by high to low Mg-tholeiites basalts, where majority of them showing low Mg Basalt.

K_2O versus SiO_2 diagram

Wilson (1989) divided the island arc volcanic suites of high alumina basalts into three distinct magma series viz. low K-series, calc alkaline, high K-series. He suggested that low-K-series is synonymous with the island arc tholeiite series of Jakes and Gill (1970) and shoshonite series can also be referred to as an alkaline series. Basaltic members of the calc-alkaline series are sometimes referred to as high alumina basalts. Within each of these series (Fig. 4.25a) the relative proportion of basalts varies widely with respect to more evolved magma types (Baker 1973)). Plot of wt% K_2O versus wt% SiO_2 showing that the analyzed samples of the study area defines both a calc-alkaline and a low-K series (Fig 4.25a).

A $(\text{Na}_2\text{O} + \text{K}_2\text{O}) - \text{F}(\text{FeO}) - \text{M}(\text{MgO})$ diagram of Irvine and Baragar (1971) is also used to understand differentiated trend of parent magma. All the samples lie in the tholeiitic field (Fig. 4.26a). The distinct trend in the diagram suggests that initially the magma was rich in MgO (Komatiitic) and finally evolved in the Fe rich tholeiites with little alkaline enrichment.

Another total alkali ($\text{Na}_2\text{O} + \text{K}_2\text{O}$) versus silica (TAS) diagram proposed by Irvine and Baragar (1971) depicts that the mafics and ultramafics of the study area are of subalkaline nature (Fig. 4.26b).

Alkaline Index $(\text{Na}_2\text{O} + \text{K}_2\text{O})/(\text{SiO}_2 - 43) \times 0.17$ versus Al_2O_3 , showing the subdivision between tholeiitic and high alumina (calc-alkaline) basalts. All the analysed samples of the study area display tholeiitic characters (Fig. 4.27a).

Triangular plots of $(\text{Zr} + \text{Y}) - 100\text{Ti} - \text{Cr}$ (Fig. 4.25b) also reveal that the parent magma was initially high Mg rich (komatiitic) basalts and later on fractionated into the diverse fields (Davis et al; 1979).

K_2O versus Na_2O (wt%) diagram (Fig. 4.28a) is showing the subdivision of the alkali magma into high K-series, K-series and Na-series (Middle Most, 1975). Analysed samples are characterized by K and Na series in which majority of samples lies in the K-series.

Na_2O versus SiO_2 (wt%) diagram is also used to differentiate the basaltic members into the alkaline and sub-alkaline series (Middle Most 1975). All the analysed samples of mafics are plotted in the sub-alkali basalt field (Fig. 4.28b).

4.3.2.2 Tectonic discrimination

Bose (1997) has described the mode of occurrence of ultramafic rocks in eight heads; (i) ultramafic zones in layered intrusions tectonic environment; (ii) ultramafic rocks of ocean floor in zoned of crustal extension, (iii) ultramafic intrusions in orogenic belts and ophiolite suites within zones of plate convergence, (iv) Alkaline-ultramafic complexes, lamprophyre and dyke intrusions, Kimberlite diatremes in atectonic environment, (v) ultramafic mantle xenoliths/nodules, (vi) Peridotitic-Komatiites and picrites in volcanics and subvolcanic association (vii) ultramafic iron meteorites, (viii) non-silicate ultramafics including carbonatites etc. He also mentioned that ultramafics rocks might also occur in other associations; as a minor intrusions within granite batholith, as a member of sheeted dyke system and as back-arc basin (marginal basin) ophiolites etc.

So to understand the tectonic environment, the petrogenesis of mafics and ultramafics of the study area are discussed.

Bulk of the magma generated in global scale appears to be associated with plate margins but at the same time intraplate setting also has characteristic magma types. Three major magma series have been recognized based on petrology viz. tholeiite, calcalkaline and alkaline series (Bose 1997). These magma series have distinct distribution when considered in terms of plate tectonic environments. However, the possibility of overlapping relations between the different series in terms of lithomembers may not be ruled out. The plate margin and the intraplate setting are the chief environment of magma generation. This can be further described into six distinct settings.

The tholeiitic magma commonly developed at the divergent plate boundaries including the system of mid-oceanic ridges and back-arc (marginal basin) developing miniature spreading at centers or local lithospheric attenuation. The tholeiitic magmas generated in these setting are very low in alkali (particularly in K) and incompatible elements (which preferred the melt phase than the solids in equilibrium). The convergent plate boundaries include the island arcs and active continental margins, which commonly manifest calc-alkaline series. The basaltic end members of calc-alkaline series can be distinguished from the island arc-tholeiite (IAT) on the basis of Al_2O_3 content. The former (embracing high Al- basalt) has a range of 16-20 wt% Al_2O_3 whereas for the tholeiitic type it is 12 to 16 weight percent. Calc-alkaline basalt may further be divided into low, medium and high-K types. Alkali magma series may contain sodic, potassic and high-potassic.

Low K-sub alkaline basalts are manifested in many within plate continental flood basalt (CFB) provinces and also show subordinate alkaline lithology. On the other hand, in continental rift zone (CRZ) provinces, alkaline rock types constitute a significant fraction of magma products besides the tholeiites i.e. CRZ magma show compositional bimodality. Volcanic rocks of the ocean basin reveal similar compositional diversity. Alkali basalts and their differentiation products are therefore common in intra-plate oceanic and continental settings. Keeping these ideas, different discrimination diagrams have been proposed along with geochemical characters to find out the suitable environment for generation of magma.

Mafics and ultramafics of the study area can be discriminated on the basis of relative proportion of MgO - FeO - Al_2O_3 (Pearce et. al. 1977). The tholeiitic basalt of the study area plotted on this diagram (Fig. 4.27c) indicates an oceanic island setting.

$\text{Ti}/100\text{-Zr-Y} \times 3$ diagram of Pearce and Cann (1973) reveals that the analyzed samples of study area are mainly island arc tholeiitic type (IAT). But the over printing with mid oceanic ridge basaltic (MORB) type cannot be ruled out (Fig. 4.29a).

Based on the FeO/MgO versus TiO_2 diagram (Jelinek et. al, 1980) shows that the majority of analysed samples of the study area fall in the island arc tholeiitic (IAT) field (Fig.4.29b).

Zr/Y versus Zr diagram of Pearce and Norry (1979) is also used to discriminate the mafics and ultra-mafics of the study area. All samples plot in the IAT and MORB fields (Fig.4.29c).

$\text{TiO}_2\text{-Mn O} \times 10\text{-P}_2\text{O}_5 \times 10$ triangular tectono magmatic discrimination diagram (Fig. 4.30a) of Muller (1983) is also used to discriminate for the mafics and ultramafics of the

study area. Majority of samples plot in the IAT field. One sample lies in the oceanic island alkalic andesite (OIA) field.

TiO₂ versus Zr/P₂O₅ diagram (Fig. 4.31a) of Winchester and Floyd (1977) depicts oceanic tholeiitic type condition for mafic and ultramafic rocks.

TiO₂ versus Zr/TiO₂ (Fig. 4.31b) and Zr/TiO₂ versus Ga (Fig. 4.31c) diagram of Floyd and Winchester (1978) also reveal ocean floor tholeiite affinity for these rocks.

The analysed samples of mafic and ultramafic of the study area are plot in the islands arc basalt fields (Fig. 4.31d) in the Ti/100 versus Zr diagram of Pearce and Cann (1973).

The analysed samples tested in different discrimination diagram point that the mafics and ultramafics of the study area are IAT type configuration for the magmatism.

4.3.2.3 Chemical variation of elements

A variation diagram is a display of chemical and trace elements differences and their trends shown by a related suite of rocks due to compositional variation and its consequences of crystal-liquid fractional processes, related either partial melting or due to fractionation crystallization (Jensen, 1976). They may be plotted in terms of major elements or trace elements, or combination of both. Variation diagrams provide a useful way of synthesizing a large volume of analytical data, which is clearly difficult to compare in table form. They can also provide the basis for the derivation of models to explain the petrogenesis of a particular suite. In the following paragraphs different kind of variation diagrams have been used to find out the exact causes of changing rock composition and genesis of mafic and ultramafic rocks.

4.3.2.4 Major oxides variation

One of the most commonly used variation diagram in igneous petrology is the Harker diagram (Harker, 1909), in which the weight percent of a constituent oxide is plotted against wt% SiO₂ as abscissa (Fig. 4.32). Na₂O varies from 0.06 to 2.82 wt% and K₂O content varies from 0.02 to 1.48 wt%, when silica content is plotted against Na₂O and K₂O individually (Fig. 4.28b and 4.25a), it is noted broadly that, there is a general trend towards increase in K₂O and Na₂O content with increasing silica. Alumina content varies from 6.58 to 13.07-wt%. The data could not define any linear trend but majority having a tendency to concentrate around 11wt% Al₂O₃ and silica around 50wt%.

The plot of Na₂O+K₂O versus SiO₂ is used to classify the members of the alkaline and sub-alkaline magma series. It gives a tendency to increase total alkalis with

increasing silica and compositional it is characterized by typical sub-alkaline trend (Fig. 4.26b).

P_2O_5 versus SiO_2 (Fig. 4.32d) shows a broad positive trend. CaO vs SiO_2 diagram also shows a broad positive trend. CaO have a tendency to concentrated 8 to 12-wt% and silica around 50-wt%.

FeO (T), TiO_2 and MgO versus SiO_2 diagrams (Fig. 4.32, f-h) show Fe and MgO enrichment in the melt. MgO show a broad negative trend suggest that Mg and $FeO(T)$ have an antipathic relationship.

Al_2O_3 versus $FeO/(FeO+MgO)$ diagram (Fig. 4.33a) shows a general positive trend and also indicates that the magnesium rich early magma was subsequently fractionated and finally evolved a Fe and Al rich tholeiitic basalt. Alumina versus total alkalis (Na_2O+K_2O) diagram (Fig. 4.33b) shows a position linear trend. Alumina is always greater than total alkalis but they have sympathetic relationship as alumina increases with increasing total alkalis.

Bulk compositions of the mafics and ultramafics of the study area is plotted in $MgO-CaO-Al_2O_3$ (wt%) (Fig.4.30b). The analysed samples do not show any distinct trend. The MgO 30%, CaO 35%, Al_2O_3 55% depicts meta-tholeiitic type while samples containing high MgO indicate Komatiitic nature.

FeO/MgO versus SiO_2 diagram (Fig. 4.30c) depicts that silica is restricted around 50wt% but FeO/MgO ratio continuously increasing means that Mg was continuous fractionated from the melt and Fe rich melt developed at the end and represented by tholeiitic basalt.

The analysed data show considerable scatter, in the variation diagram of CaO versus MgO (Fig. 4.34a) for basaltic rocks from the study area. Crystal-liquid differentiation is controlled by Ca -rich clinopyroxene and plagioclase either during the partial melting or crystal fractionation (Cox 1980).

FeO versus MgO wt% variation diagram (Fig. 4.34b) is showing characteristic tholeiitic differentiation trend in due course of FeO enrichment with fractionation, progressive differentiation trend in due course of FeO enrichment with fractionation.

$100 \times Mg/(MgO+ FeO)$ versus total alkalis (Na_2O+K_2O) diagram (Fig. 4.34c) shows the late stage of evolution but the metasomatic activities can't be ruled out.

Nickel is a sensitive indicator of olivine fractionation from basic magmas because of its large mineral / melt partition coefficient. NiO & MgO display a good relations (Fig.

4.35a,b), indicating the importance of olivine fractionation/accumulation. Cr also shows a good correlation with MgO possibly due to the concurrent crystallization of olivine and a Cr-rich spinel phase.

4.3.2.5 Trace element variation

Table 4.6 shows the distribution of trace elements of mafics and ultramafics of the study area. They have higher Zr ranging from 7 to 808ppm. The increase in Y, Rb, Ba, Sr and Ga with increase in SiO_2 content (Fig. 4.36, 37) suggest the role of differentiation in the formation of these mafics and ultramafics of the study area.

Fig. 4.38 illustrates simple bi-element relationships using Zr as an index of fractionation. Zr is one of the most immobile elements during low-grade metamorphism and alteration of basaltic rocks and is essentially an incompatible element in basaltic systems (Tarney et al; 1979). MgO ranges from 5 to 12wt%. High range in Zr would necessitate at least 80% fractional crystallization if all the rocks were derived from the same or similar parental magma. Wide range of Zr content at constant MgO (Fig. 4.38d), point out that more than one batch of magma was involved at the late stage of mafic magmatism.

The plots of Ni versus Zr (Fig.4.38c) exhibit essentially similar features, which are consistent with magmatic processes discussed in preceding lines.

Plots of Y versus Zr (Fig. 4.38a) and TiO_2 versus Zr (Fig. 4.38b) show a good positive correlation and define a typical basaltic trend. The ratios Y/Zr and Ti/Zr normally change very little with moderate degrees of crystal fractionation of basaltic magma but are quite sensitive to differences in degree of partial melting of the mantle source or to compositional heterogeneity in the source. Fig. 4.35c shows the variation of Y/Nb versus Zr/Nb a linear trend, which is simply explained in terms of two components mixing, between slightly heterogeneous depleted asthenosphere and low Zr/Nb plume component. A good linear trend, of TiO_2 vs Zr (Fig. 4.38b) point the fractionation of magma.

The Harker's variation diagram for trace elements against SiO_2 (Fig. 4.36 and 4.37) yield some genetic features. Y, Sr, Zr, Nb, Rb and Ga increase with increasing SiO_2 showing their similar differentiation trend which supports the view that these mafics and ultramafics were of the same in nature and possibly have got same petrogenetic history. Cu, Rb/Sr, Ba do not show any marked variation with SiO_2 . Sr versus Rb/Sr diagram (Fig. 4.36g) also does not show any correlation but shows low variation in Rb/Sr ratio.

The positive correlation trend suggests the fractionation of komatiitic magma, and development of tholeiitic character in the later stage of crystallization.

The positive correlation trends in different variation diagrams suggest that komatiitic magma of early stage fractionated in simple way and subsequently changed to tholeiitic composition and finally metasomatised in the late stage.

Table No 4.1 Major Element Analyses (in wt.%) and CIPW Weight Norms of Granites of study area.

Sl. No.	1	2	3	4	5	6	7
Sample	MK4	B17	KTX	KT20	MK12	U2b	Mk13
SiO ₂	89.52	68.76	75.68	70.38	75.74	71.98	71.03
TiO ₂	0.03	0.33	0.11	0.44	0.16	0.33	0.14
Al ₂ O ₃	5.88	16.39	13.06	13.20	13.11	13.62	15.48
Fe ₂ O ₃ (T)	1.95	2.98	1.98	4.37	2.22	3.78	0.85
MnO	0.01	0.04	0.03	0.07	0.05	0.06	0.00
MgO	0.45	0.72	0.20	1.18	0.37	1.32	0.17
CaO	0.32	2.84	0.59	1.66	0.68	2.34	0.23
Na ₂ O	0.11	5.32	4.37	3.44	3.98	3.68	0.08
K ₂ O	0.14	4.17	5.28	3.92	5.39	4.07	13.75
P ₂ O ₅	0.02	0.08	0.01	0.16	0.03	0.11	0.03
SUM	98.43	101.63	101.30	98.82	101.73	101.29	101.77

CIPW WEIGHT NORMS

Quartz	88.15	15.34	28.35	30.20	29.39	27.94	16.80
Corundum	5.10			0.56			0.07
Orthoclase	0.85	24.33	30.90	23.57	31.50	23.85	80.05
Albite	0.95	44.36	36.53	29.52	33.14	30.80	0.67
Anorthite	1.48	8.44	0.40	7.66	1.92	8.55	1.01
Hypersthene	1.93	0.43	0.09	4.17	1.05	3.37	0.52
Magnetite	1.44	2.13	1.42	1.42	3.21	0.62	1.58
Ilmanite	0.06	0.62	0.21	0.85	0.30	0.62	0.26
Diopside		4.32	2.09		1.13	1.98	
Chromite		0.05	0.08		0.09	0.11	0.03
Apatite	0.05	0.19	0.02	0.40	0.07		0.26
Zircon		0.05	0.05	0.08	0.04	0.03	0.07

Table No4.2 Major Element Analyses (in wt.%) and CIPW Weight Norms of Gneisses of study area.

Sl. No.	1	2	3	4	5	6
Sample	J2a	CM4	MK7	J6	017	J2b
SiO ₂	68.94	72.88	77.49	64.65	68.61	55.97
TiO ₂	0.42	0.37	0.04	0.67	0.54	1.76
Al ₂ O ₃	15.29	12.80	12.88	15.38	13.77	15.38
Fe ₂ O ₃ (T)	4.44	3.40	0.97	6.51	4.39	11.27
MnO	0.06	0.04	0.01	0.08	0.07	0.16
MgO	1.05	1.24	0.32	1.35	1.32	4.14
CaO	3.25	1.91	0.62	4.08	2.49	4.44
Na ₂ O	5.07	4.91	4.15	3.80	5.34	3.20
K ₂ O	1.24	1.84	5.00	1.84	1.60	3.02
P ₂ O ₅	0.15	0.06	0.01	0.30	0.15	0.62
SUM	99.91	99.44	101.50	98.66	98.28	99.95

CIPW WEIGHT NORMS

Quartz	26.06	31.64	32.05	25.15	24.98	10.90
Corundum	0.03	---	---	0.40	---	0.21
Zircon	0.3	0.09	0.02	0.04	0.04	0.05
Orthoclase	7.38	10.99	29.21	11.11	9.81	18.04
Albite	43.03	41.84	34.61	32.70	46.07	27.24
Anorthite	15.26	7.54	1.71	18.72	9.02	18.20
Hypersthene	3.88	3.22	0.56	5.15	3.31	12.41
Magnetite	3.23	2.48	0.69	4.80	3.25	8.22
Ilmanite	0.80	0.71	0.07	1.29	1.05	3.36
Apatite	0.36	0.15	0.02	0.73	0.37	1.48
Diopside	---	1.47	1.09	---	2.25	---
Chromite	---	0.13	0.09	0.07	0.08	0.06

Table No 4.3. Major Element Analyses (in wt.%) of Mafics and Ultramafics of the study area.

Sl. No.	1	2	3	4	5	6	7	8	9	10	11
Sample	S3	S4a	P57	D2b	D13	J3a	014	016	S2a	37	38
SiO ₂	49.58	55.15	42.40	51.31	50.92	47.81	44.23	36.56	48.06	49.72	49.18
TiO ₂	2.01	2.22	2.52	0.79	1.53	0.61	0.19	1.56	0.51	1.03	1.36
Al ₂ O ₃	11.53	13.07	11.56	9.61	14.25	10.86	9.15	10.37	6.58	11.72	10.87
Fe ₂ O ₃ (T)	17.76	12.28	23.50	14.22	14.98	13.63	11.89	24.30	12.51	16.11	19.98
MnO	0.23	0.18	0.19	0.17	0.23	0.24	0.22	0.35	0.27	0.24	0.28
MgO	6.91	5.66	11.55	9.62	6.90	12.21	28.24	14.99	21.29	7.74	6.26
CaO	9.55	6.75	1.22	13.95	8.77	10.94	6.35	4.70	11.11	9.04	9.85
Na ₂ O	1.60	2.82	0.95	0.06	2.60	1.44	0.33	BDL	0.42	2.48	1.72
K ₂ O	0.27	1.48	0.47	1.00	1.61	1.00	0.06	0.02	0.10	0.62	0.44
P ₂ O ₅	0.24	0.35	0.13	0.11	0.17	0.07	0.04	0.21	0.09	0.11	0.14
SUM	99.68	99.96	94.48	100.84	101.97	98.82	100.71	93.07	100.96	98.81	100.08

Table No. 4.4 Trace Element Analyses (in ppm) of Granites of the study area.

Sl. No.	1	2	3	4	5	6	7
Sample	MK4	B17	KTX	KT20	MK12	U2b	Mk13
Cu		8	15	16	12	14	5
Zn		43	15	62	23	51	5
Co		3.2	bdl	10.4	bdl	6.9	Bdl
Ni	18	7	5	12	11	23	3
Ga		18.7	16.8	19.6	20.3	18.5	10.5
Rb	21	119	168	181	403	140	417
Ba		1015	232	1081	476	589	297
Sr	3	423	29	196	97	271	9
Y		23	35	54	31	21	27
Zr	9	232	259	368	193	153	331
Nb	2	11	18	29	23	14	20
Th		15.7	33.8	118.6	89.3	33.2	39.6
K ₂ O/Na ₂ O	1.272	0.783	1.208	1.139	1.354	1.105	171.87
K/Rb	47.27	248.47	222.85	153.57	94.83	206.14	233.81
Rb/Sr	7.00	0.281	5.793	0.923	4.154	0.516	46.33
Ba/Rb		8.529	1.380	5.972	1.181	4.207	0.712
Sc		7.1	4.4	8.5	4.6	8.3	1.8
Pb		27	44	40	51	28	30
U		5.6	6.2	11.6	23.9	8.2	15.7
Cr		251	385	293	410	502	151

Table No 4.5 Trace Element Analyses (in ppm) of Gneisses of the study area.

Sample No.	1	2	3	4	5	6
Ref. No.	J2a	CM4	MK7	J6	017	J2b
Cu		14	71	20	68	72
Zn		40	13	99	57	149
Co		7.7	bdl	18.2	11.9	37
Ni	15	20	3	27	17	21
Ga		19.5	15.8	22.2	21.2	24.7
Rb	72	102	198	143	416	209.6
Ba		706	220	223	259	259
Sr	178	108	80	187	442	128
Y		223	21	16	20	45.6
Zr	130	445	85	211	201	242
Nb	15	20	8	17	9	36.9
Th		50.3	37.2	0.5	8.3	2.5
K ₂ O/Na ₂ O	0.244	0.374	1.204	0.484	0.299	0.94
K/Rb	122.22	127.91	179.06	91.23	27.27	102.16
Rb/Sr	0.404	0.944	0.9	0.764	0.941	1.637
Ba/Rb		6.921	1.11	1.55	0.622	1.235
Sc		8.9	3.0	12.8	9.4	14
Pb		28	44	13	16	9.5
U		6.6	21.2	1.7	8.9	6.5
Cr		592	415	337	384	271

Table No 4.6 Trace Element Analyses (in ppm) of Mafics and Ultramafics of the study area.

Sample No.	1	2	3	4	5	6	7	8	9	10	11
Ref. No.	S3	S4a	P57	D2b	D13	J3a	014	016	S2a	37	38
Cu				28	175	47	39	20	99	85	31
Zn				83	105	101	72	130	131	120	131
Co				51	59	60	73	80	78	59	75
Ni	75	31	51	69	93	255	900	118	975	63	34
Ga				20.5	17.5	12.1	7.4	26.9	8.7	15.9	16.7
Rb	18	81	13	34.9	48.2	61.3	2.7	3.5	5.8	42.5	8.1
Ba				492	135	44	45	102	114	129	68
Sr	140	208	9	174	163	82	12	299	68	144	106
Y				21.7	25.4	16.1	9.7	34.6	14.0	23.7	30.5
Zr	166	277	199	77	110	35	7	808	30	89	102
Nb	11	18	7	4.1	7.0	2.8	1.0	67.3	2.7	4.7	5.0
Th				2.0	0.5	2.5	1.6	49.2	3.3	1.9	5.8
K ₂ O/Na ₂ O	0.168	0.524	0.494	16.66	0.619	0.694	0.181	----	.233	0.25	0.255
K/Rb	106.36	129.56	256.36	203.17	236.85	115.67	157.57	40.51	122.25	103.44	385.18
Rb/Sr	0.128	0.389	1.44	0.200	0.295	0.74	0.225	0.011	0.085	0.295	0.265
Ba/Rb				14.09	2.80	0.71	16.66	29.14	19.65	3.03	8.39
Sc				58	43	45	40	36	24	51	60
Pb				9.8	2.8	8.0	14.6	27.5	19.1	11.7	10.0
U				1.1	1.4	1.8	0.3	1.9	0.5	1.4	0.3
Cr				370	170	908	3121	743	2441	67	105

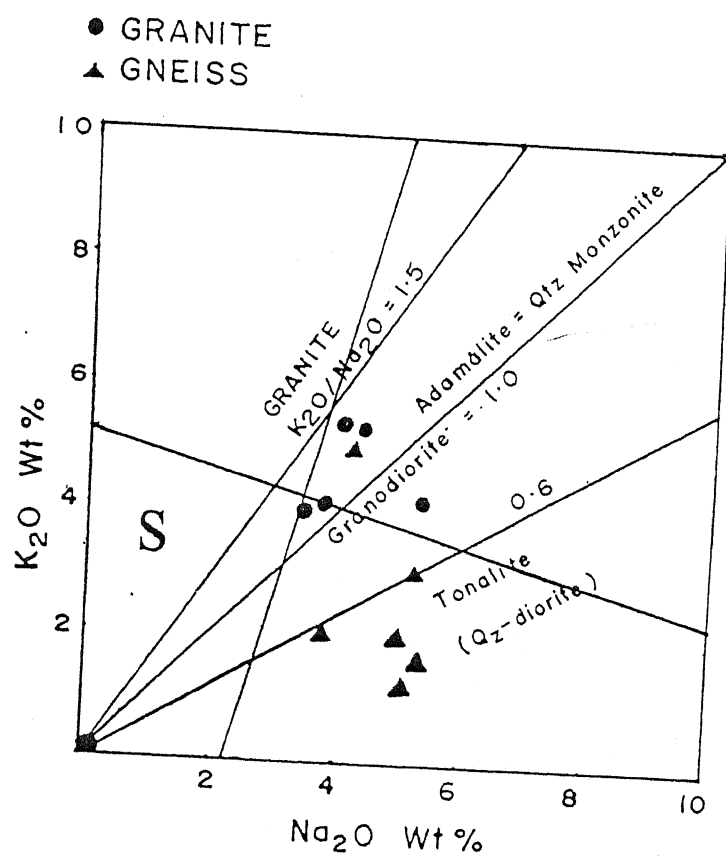


Fig.4.1. Na₂O vs K₂ (wt%) plots for gneisses and granites of the study area (Harpum, 1963).

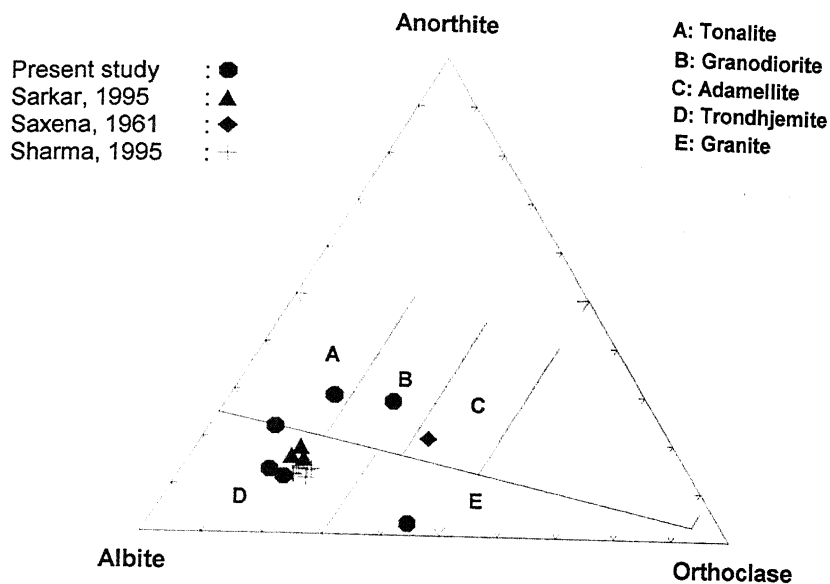


Fig.4.2. (a) Normative An-Ab-Or plots for gneisses of the study area. (After O'Connor, 1965).

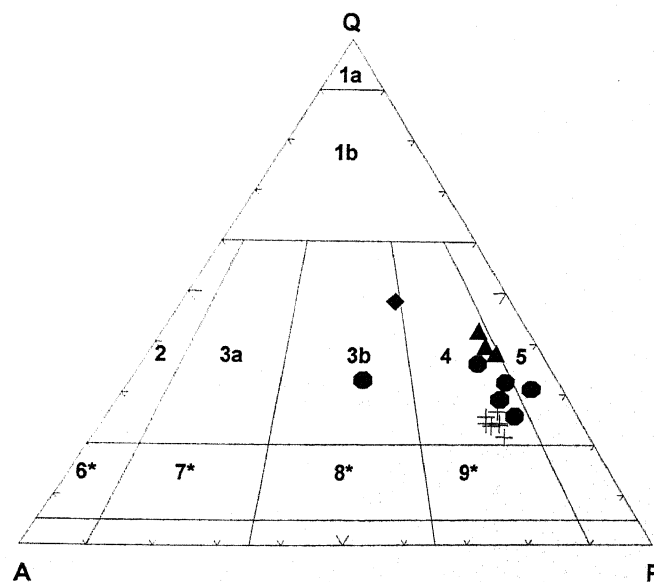


Fig.4.2. (b) The normative QAP variation diagram after Le Maitre (1989) showing field of variation of the gneisses of the study area. 1a : Quartzolite, 1b : Quartz-rich Granitoids, 2 : Alkali Feldspar Granite, 3a : Syno-Granite, 3b : Monzogranite, 4 : Granodiorite, 5 : Tonalite, 6* : Quartz-Alkali Feldspar syenite, 6 : Alkali Feldspar syenite, 7* : Quartz Synite, 7 : Syenite, 8* : Quartz Monzonite, 8 : Quartz Monzonite, 9* : Quartz-Monzodiorite and Monzogabbro, 9 : Monzodiorite and Monzogabbro, 10* : Quartz- Diorite / Quartz- Gabbro/ Quartz - Anorthosite, 10 Diorite/ Gabbro/ Anorthosite

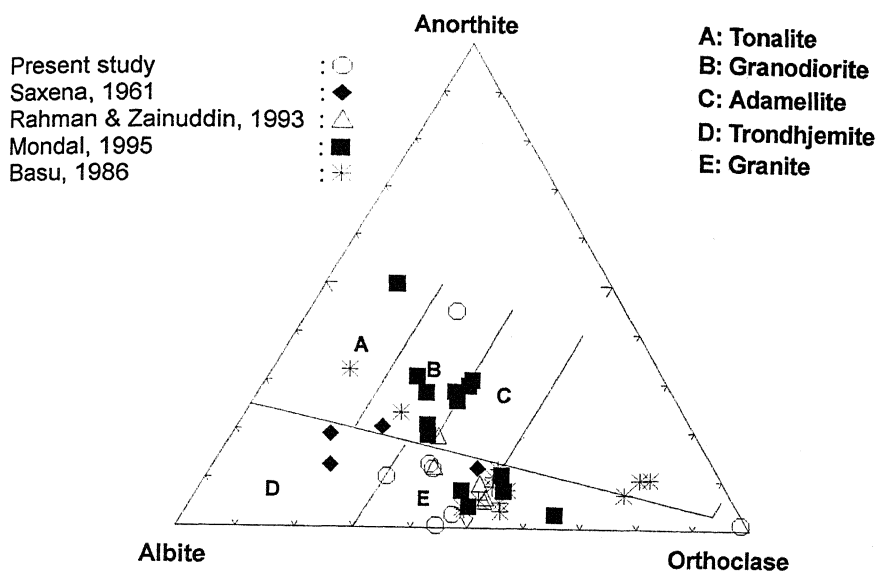


Fig. 4.3. (a) Normative An-Ab-Or plots for granites of the study area (After O'Connor, 1965).

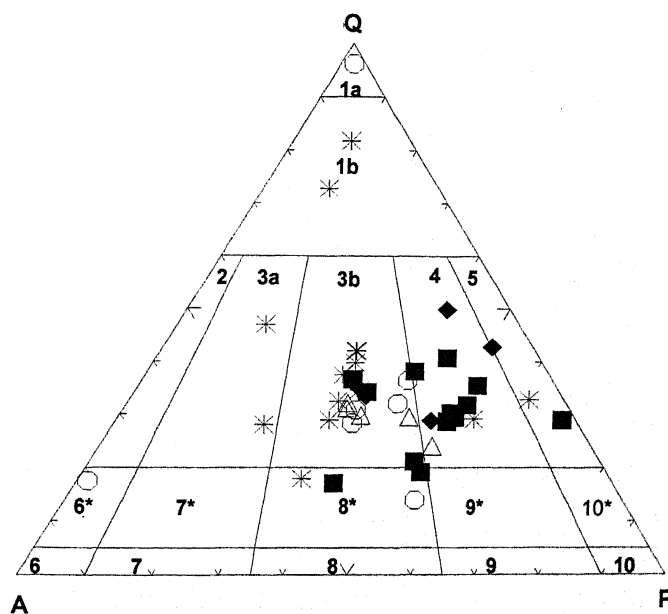
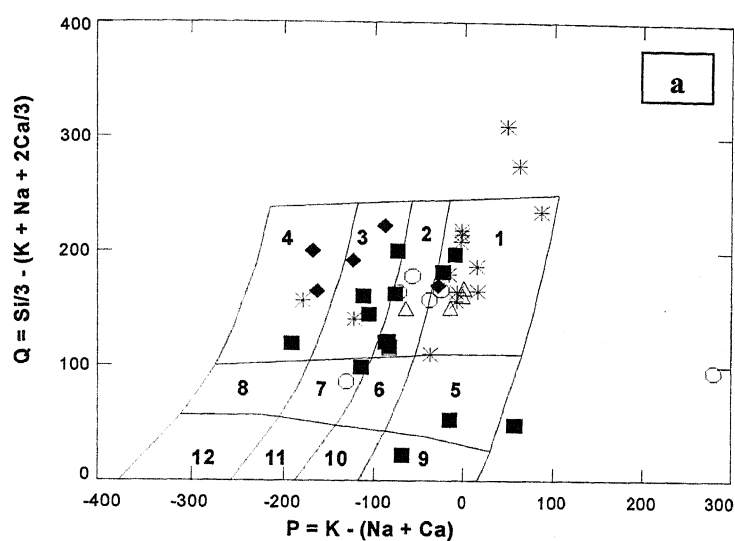
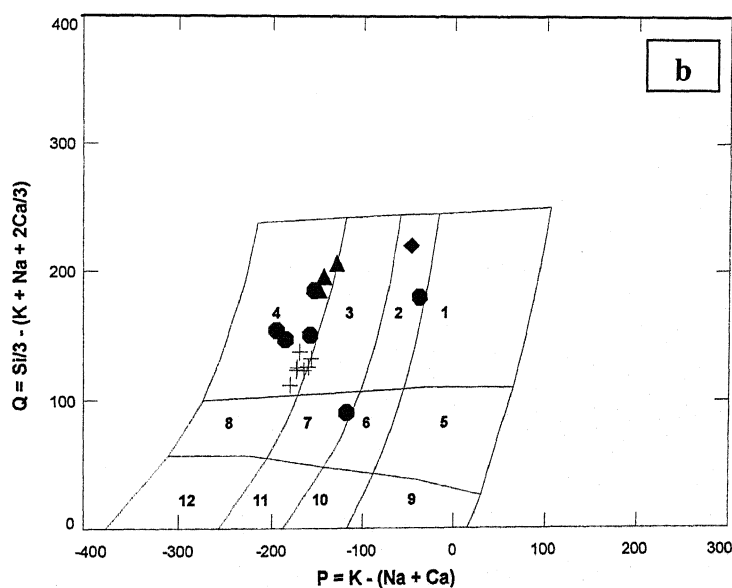


Fig. 4.3. (b) The normative QAP variation diagram after Le Maitre (1989) showing field of variation of the granites of the study area. 1a : Quartzolite, 1b : Quartz-rich Granitoids, 2 : Alkali Feldspar Granite, 3a : Syno-Granite, 3b : Monzogranite, 4 : Granodiorite, 5 : Tonalite, 6* : Quartz-Alkali Feldspar syenite, 6 : Alkali Feldspar syenite, 7* : Quartz Syenite, 7 : Syenite, 8* : Quartz Monzonite, 8 : Quartz Monzonite, 9* : Quartz-Monzodiorite and Monzogabbro, 9 : Monzodiorite and Monzogabbro, 10* : Quartz-Diorite/Quartz-Gabbro/Quartz-Anorthosite, 10 : Diorite/Gabbro/Anorthosite

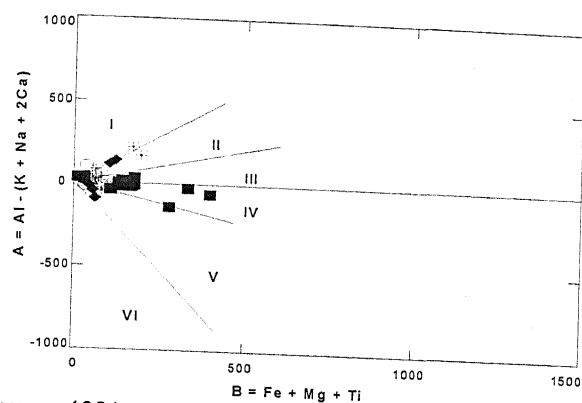


Present study : \circ , Saxena, 1961 : \blacklozenge , Rahman & Zainuddin, 1993 : \triangle , Mondal, 1995 \blacksquare , Basu, 1986 : $*$



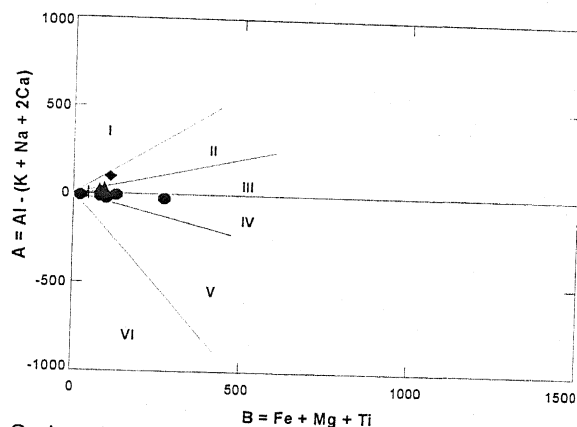
Present study : \bullet , Sarkar, 1995 : \blacktriangle , Saxena, 1961 : \blacklozenge , Sharma, 1995 : $+$

Fig. 4.4 P vs Q diagram for the (a) granites and (b) gneisses of the study area based on Debon and Le Fort (1982). The parameters are expressed as gram atoms into 10^3 of each element in 100 gm of material. Each pigeonhole of the classification grid corresponds to a petro-graphical group (1 to 12). 1 : Granite, 2 : Adametallite, 3 : Granodiorite, 4 : Tonalite, 5 : Quartz Syenite, 6 : Quartz Monzonite, 7 : Quartz Monzodiorite, 8 : Quartz Diorite, 9 : Syenite, 10 : Monzonite, 11 : Monzogabbro, 12 : Gabbro.



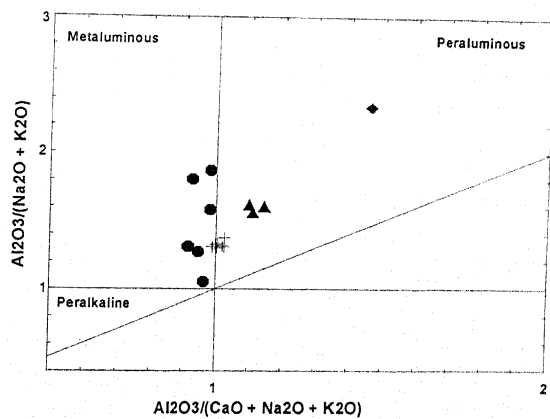
Present study : \circ , Saxena, 1961 : \blacklozenge , Rahman & Zainuddin, 1993 : \triangle , Mondal, 1995 \blacksquare , Basu, 1986 : $*$

Fig. 4.5. (a) A versus B diagram of granites of the study area (After Debon and Le Fort; 1982 and Debon et. al., 1986). The diagram is divided \times six sectors numbered from I to VI. I. $Mu > Bi$, II. $Bi > Mu$, III. $Bi \pm$, IV. $Bi \pm Hbl \pm Cpx \pm Opx \pm Ol \pm$, V. $Cpx \pm Hbl \pm$, VI. $Di \pm$.



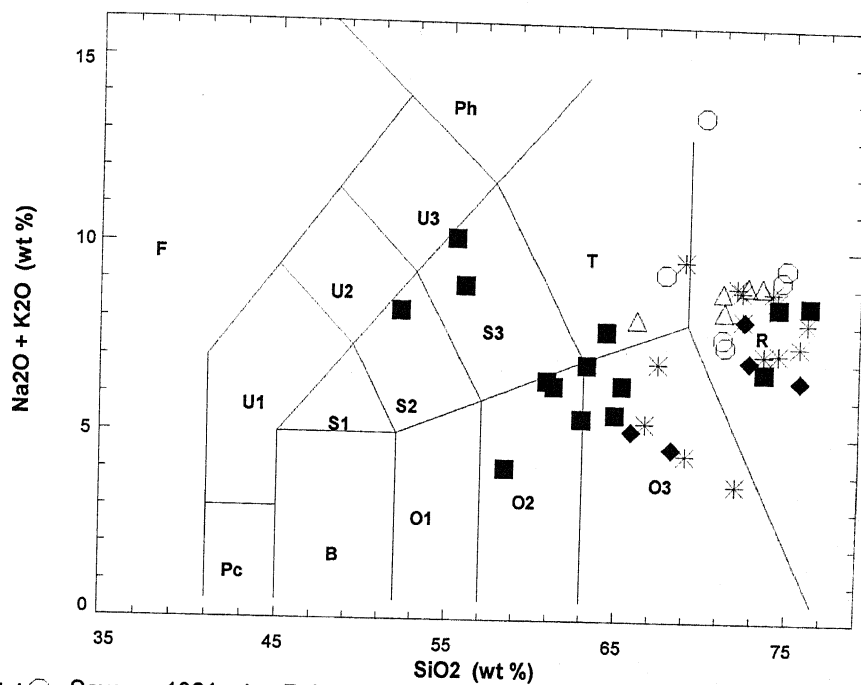
Present study : \bullet , Sarkar, 1995 : \blacktriangle , Saxena, 1961 : \blacklozenge , Sharma, 1995 : $+$

Fig. 4.5. (b) A vs B diagram of gneisses of the study area (After Debon and Le Fort; 1982 and Debon et. al., 1986). The diagram is divided \times six sectors numbered from I to VI. I. $Mu > Bi$, II. $Bi > Mu$, III. $Bi \pm$, IV. $Bi \pm Hbl \pm Cpx \pm Opx \pm Ol \pm$, V. $Cpx \pm Hbl \pm$, VI. $Di \pm$.



Present study : \bullet , Sarkar, 1995 : \blacktriangle , Saxena, 1961 : \blacklozenge , Sharma, 1995 : $+$

Fig. 4.5. (c) Shands Index diagram for gneisses of the study area (After Maniar and Piccoli, 1989).



Present study : \circ , Saxena, 1961 : \blacklozenge , Rahman & Zainuddin, 1993 : \triangle , Mondal, 1995 : \blacksquare , Basu, 1986 : $*$

Fig. 4.6. The chemical classification and nomenclature of granites of the study area using the totals alkali versus silica (TAS) diagram (After Le Maitre et. al. 1989). Pc : Microbasalt, U1 : Tephrite/Basanite, U2 : Phonotephrite, U3 : Tephriphonolite, Ph : Phonolite, B : Basalt, S1 : Trachybasalt, S2 : Basaltic trachyandesite, S3 : Trachyandesite, T : Trachite/Trachydacite, O1 : Basaltic andesite, O2 : Andesite, O3 : Dacite, R : Rhyolite.

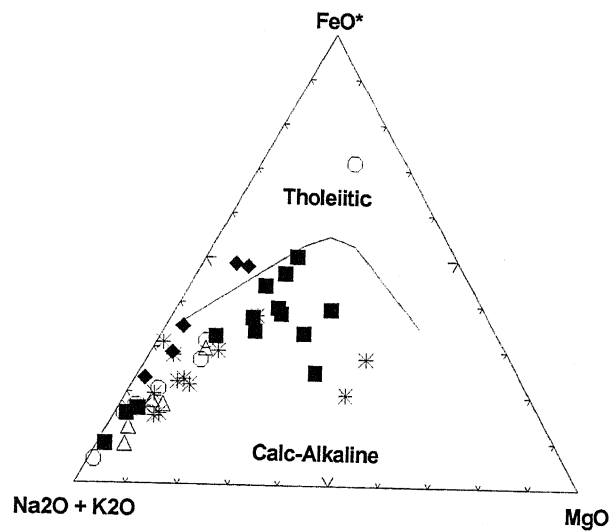
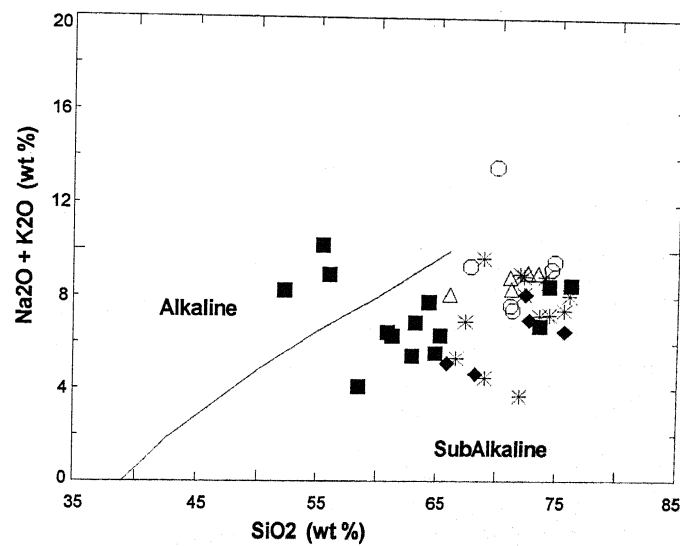
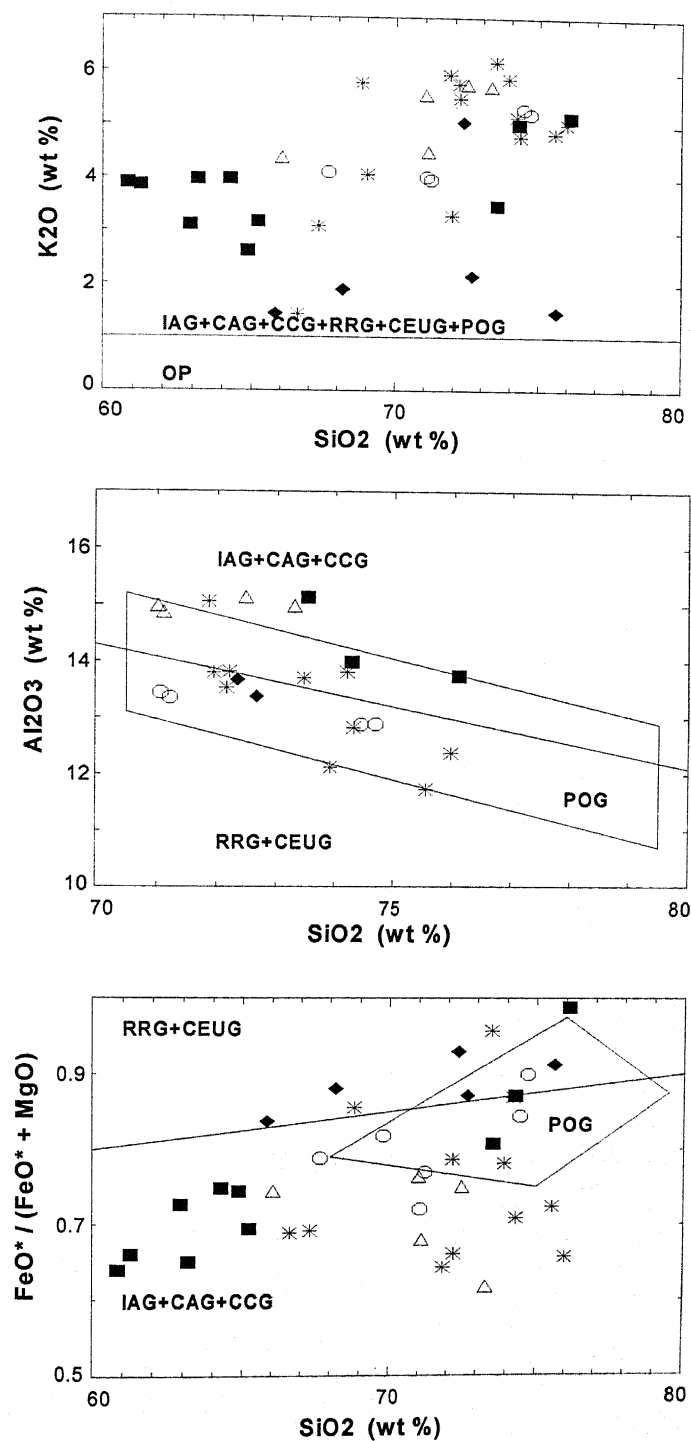


Fig. 4.7. (a) A-F-M diagram plots for the granites (After Irvine and Baragar, 1971) with line separating fields of alkaline and sub alkaline.



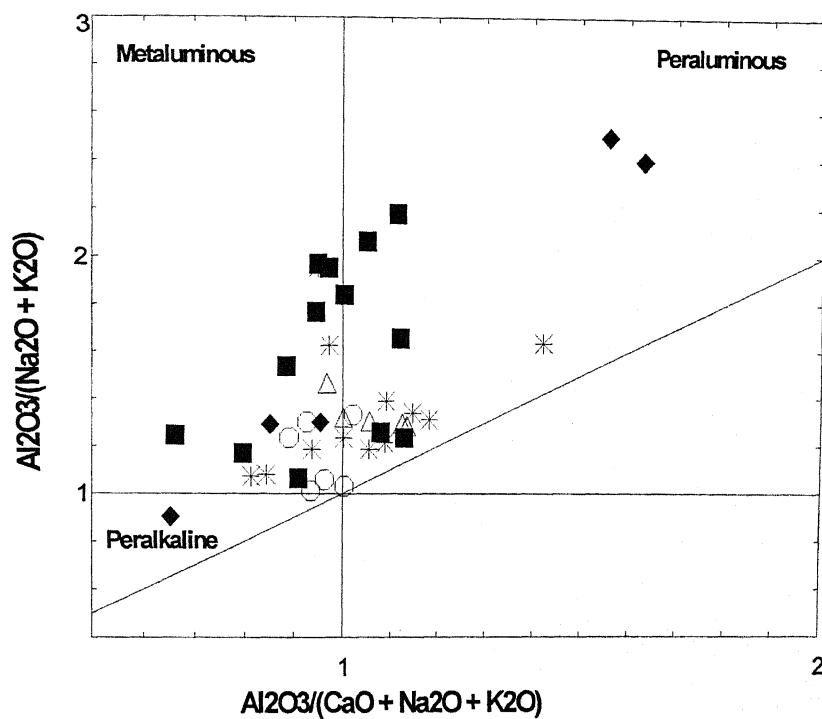
Present study : \circ , Saxena, 1961 : \blacklozenge , Rahman & Zainuddin, 1993 : \triangle , Mondal, 1995 \blacksquare , Basu, 1986 : $*$

Fig. 4.7. (b) Total alkali vs Silica diagram for granites of the study area (After Irvine and Baragar 1971).



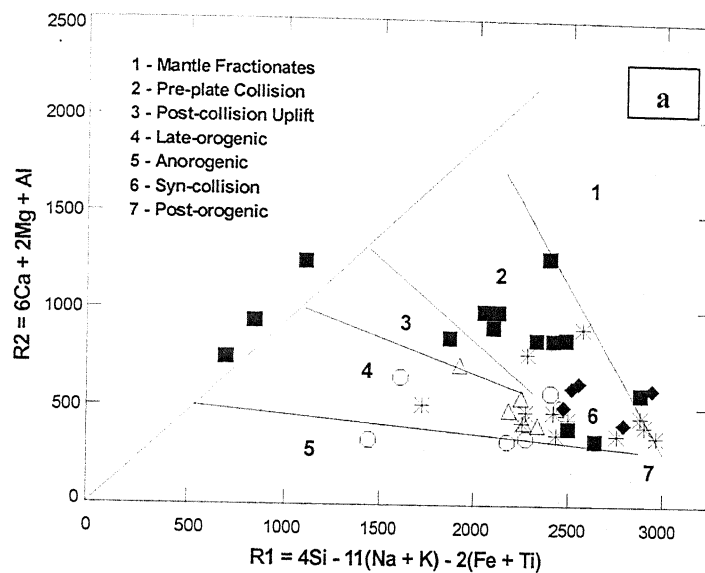
Present study : ○, Saxena, 1961 : ◆, Rahman & Zainuddin, 1993 : △, Mondal, 1995 : ■, Basu, 1986 : *

Fig. 4.8. Discrimination diagram for the granites of the study are (After Maniar and Piccoli, 1989). (a) SiO₂ vs K₂O, (b) SiO₂ vs Al₂O₃, (c) SiO₂ vs FeO / (FeO+MgO). IAG : Island Arc Granitoids, CAG : Continental Arc Granitoids, CCG : Continental Collision Granitoids, RRG : Rift Related Granitoids, CEUG : Continental Epeirogenic Uplift Granitoids, POG : Post Orogenic Granitoids, OP : Oceanic Plagiogranites.

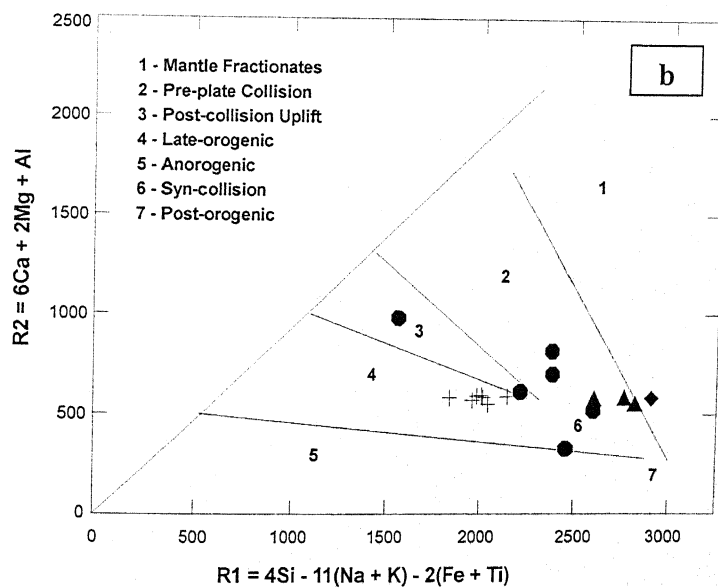


Present study : \circ , Saxena, 1961 : \blacklozenge , Rahman & Zainuddin, 1993 : \triangle , Mondal, 1995 : \blacksquare , Basu, 1986 : $*$

Fig. 4.9. Shands Alumina Saturation Index diagram for granites of the study area (After Maniar and Piccoli, 1989).

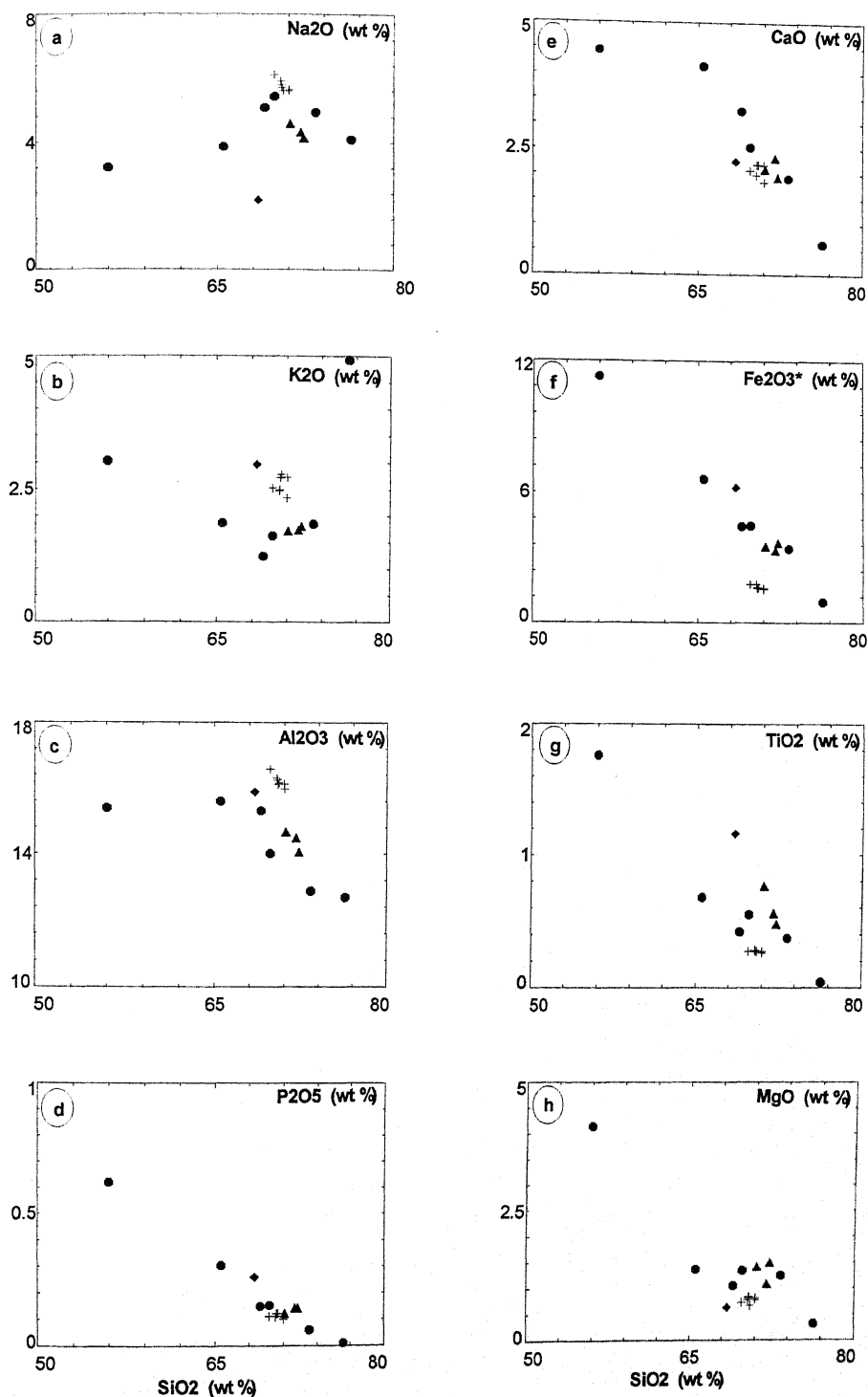


Present study : \square , Saxena, 1961 : \blacklozenge , Rahman & Zainuddin, 1993 : \triangle , Mondal, 1995 : \blacksquare , Basu, 1986 : $*$



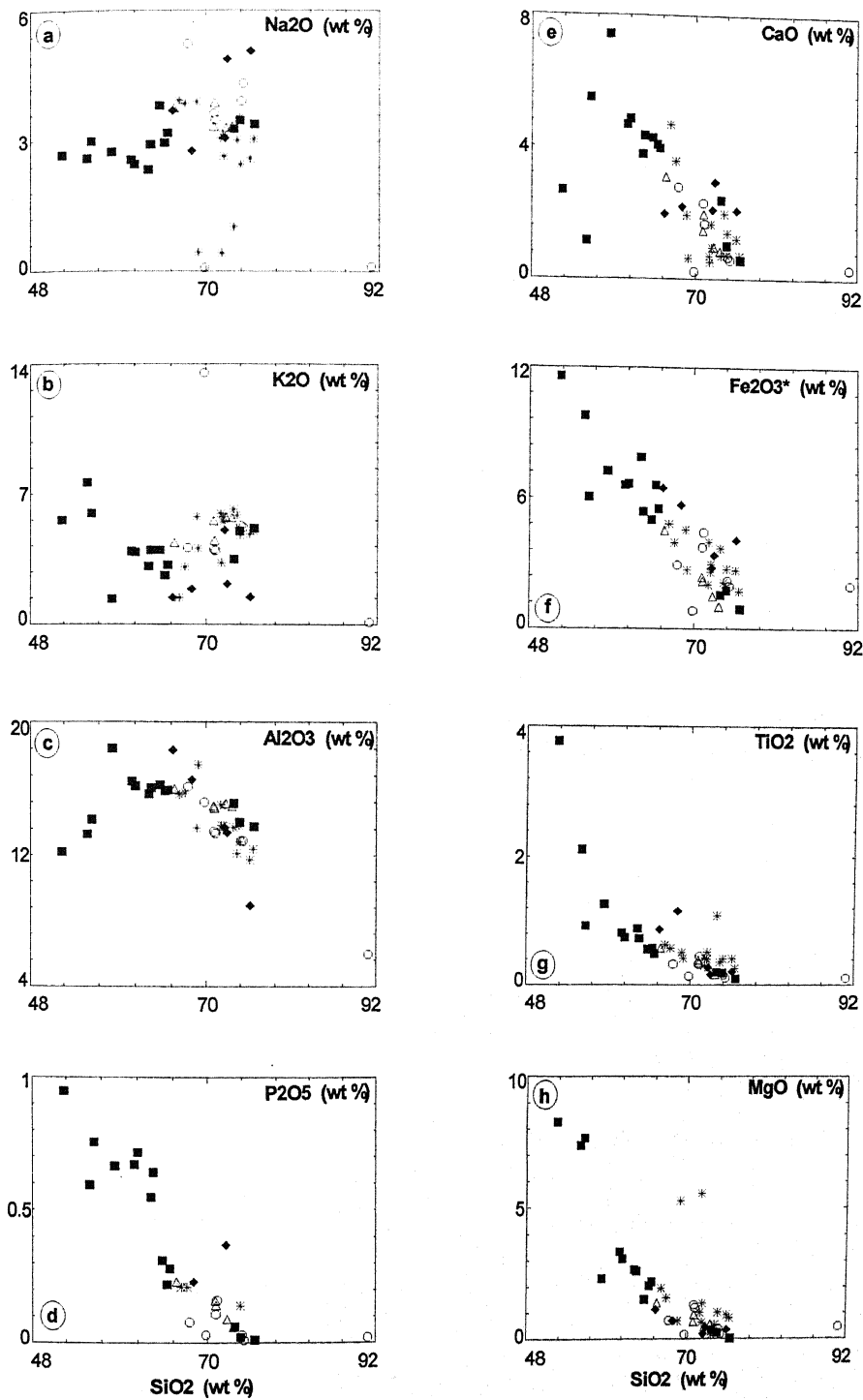
Present study : \bullet , Sarkar, 1995 : \blacktriangle , Saxena, 1961 : \blacklozenge , Sharma, 1995 : $+$

Fig. 4.10 Ri vs R_2 multicatic plots of (a) granites and (b) gneisses of the study area (After De La Roche, 1980, Modified by Batchlor and Bowden, 1985).



Present study : ●, Sarkar, 1995 : ▲, Saxena, 1961 : ◆, Sharma, 1995 : +

Fig. 4.11a-h. Harkers variation diagrams of SiO_2 vs Na_2O , K_2O , Al_2O_3 , P_2O_5 , CaO , Fe_2O_3 , TiO_2 and MgO for the gneisses of the study area.



Present study : \circ , Saxena, 1961 : \blacklozenge , Rahman & Zainuddin, 1993 : \triangle ,
Mondal, 1995 : \blacksquare , Basu, 1986 : $*$

Fig. 4.12a-h. Harkers variation diagrams of SiO_2 vs Na_2O , K_2O , Al_2O_3 , P_2O_5 , CaO , Fe_2O_3 , TiO_2 and MgO for the granites of the study area.

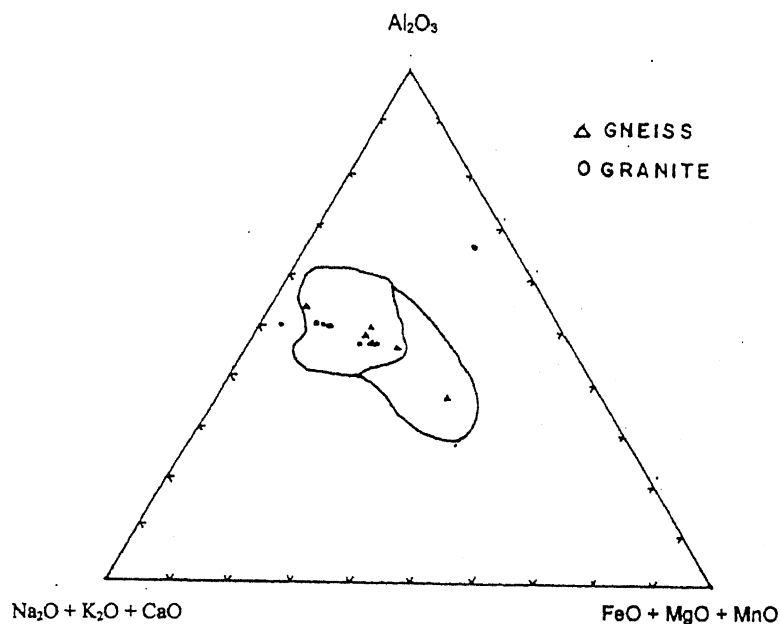


Fig. 4.13 (a) $\text{Al}_2\text{O}_3 - (\text{Na}_2\text{O} + \text{K}_2\text{O} + \text{CaO}) - (\text{FeO} + \text{MgO} + \text{MnO})$ Triangular diagram showing the different modes of magma formation of granites and gneisses of the study area. Delineated boundary showing Granites of cotectic minimum composition.

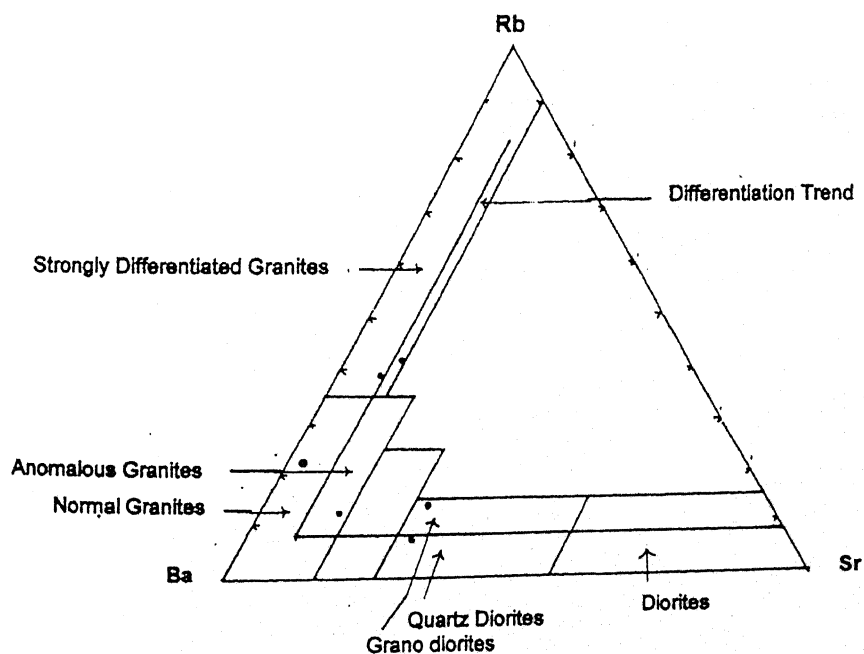


Fig. 4.13 (b) Rb - Ba - Sr ternary diagram after El-Bouseilly and El-Sokkary (1975).

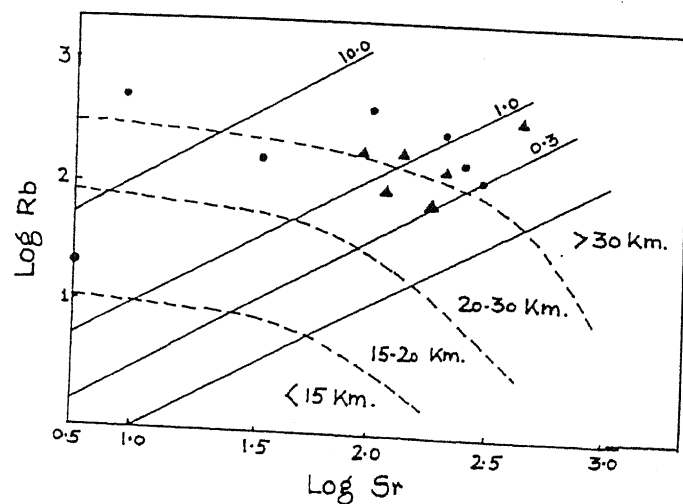


Fig4.14.(a) Rb-Sr (log-log) plots of gneisses and granites with grids for crustal thickness (after Condie, 1973).

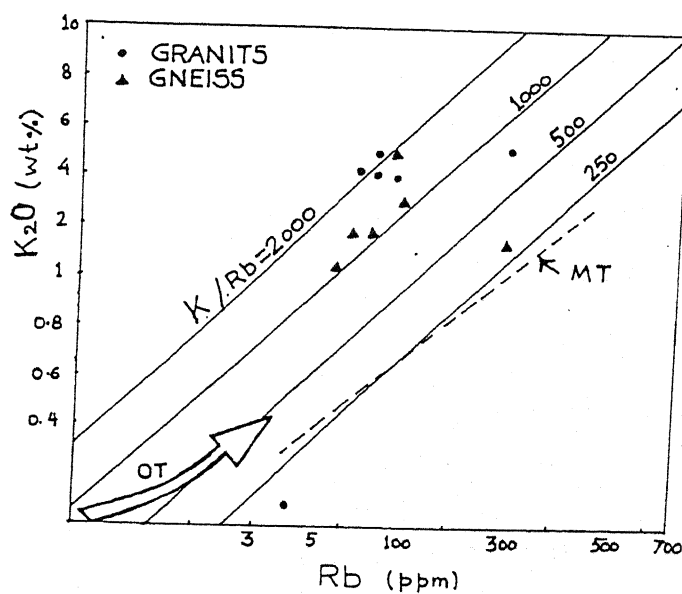


Fig4.14 (b) K - Rb relationship of the gneisses and granites of the study area. MT-main trend and OT-ocenic trend after Shaw (1968).

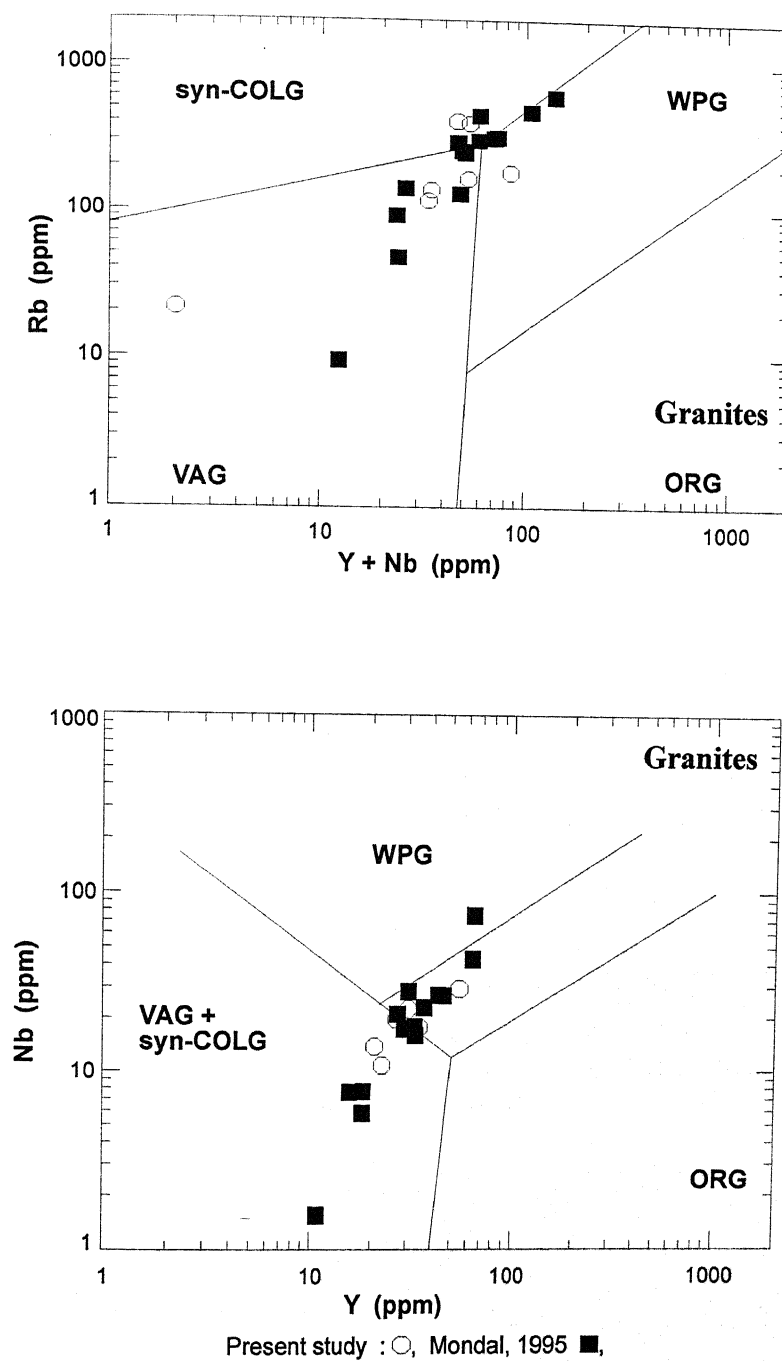


Fig. 4.15 Discrimination diagrams for the granites for the study area (After Pearce et. al., 1984. (a) Rb - (Y + Nb) and (b) Nb - Y. VAG : Volcanic Arc Granites, syn. COLG : syn. Collisional Granite, WPG : Within Plate Granite, ORG : Oceanic Ridge Granites.

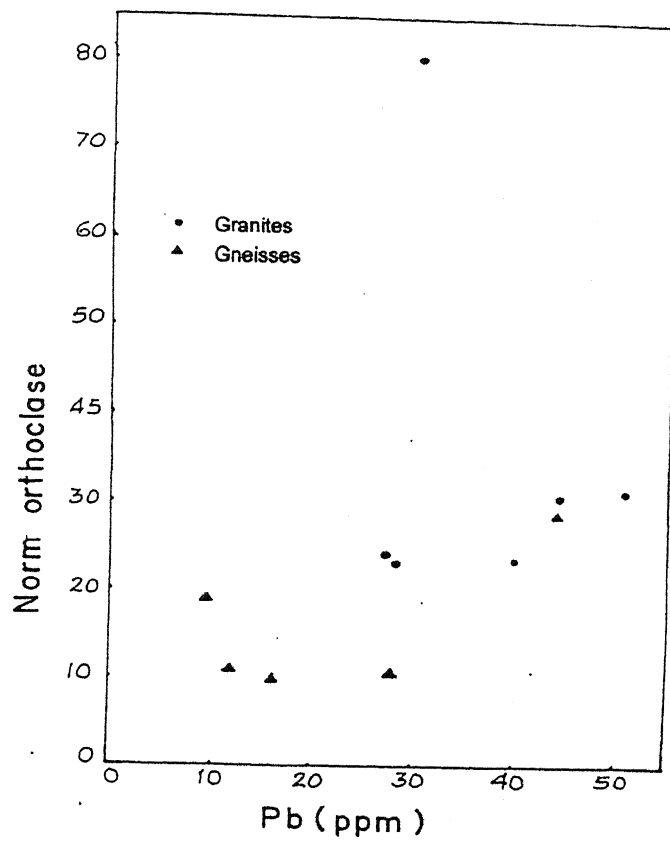


Fig.4.16 (a) Variation diagram of Normative orthoclase vs Pb (ppm) for gneisses and granites of the study area.

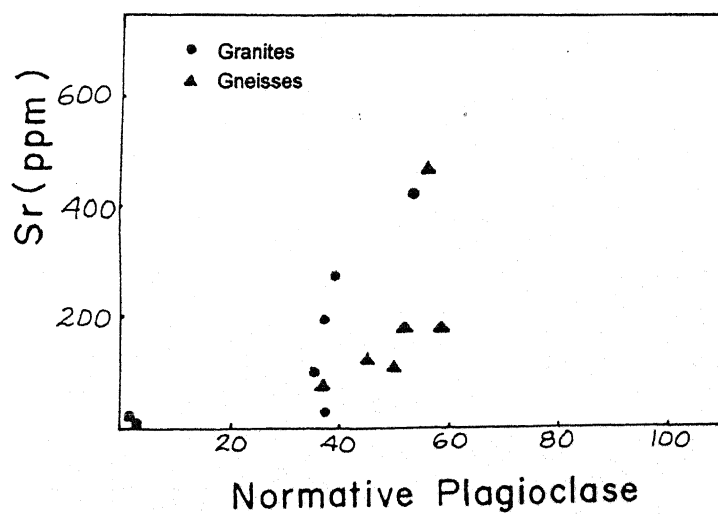
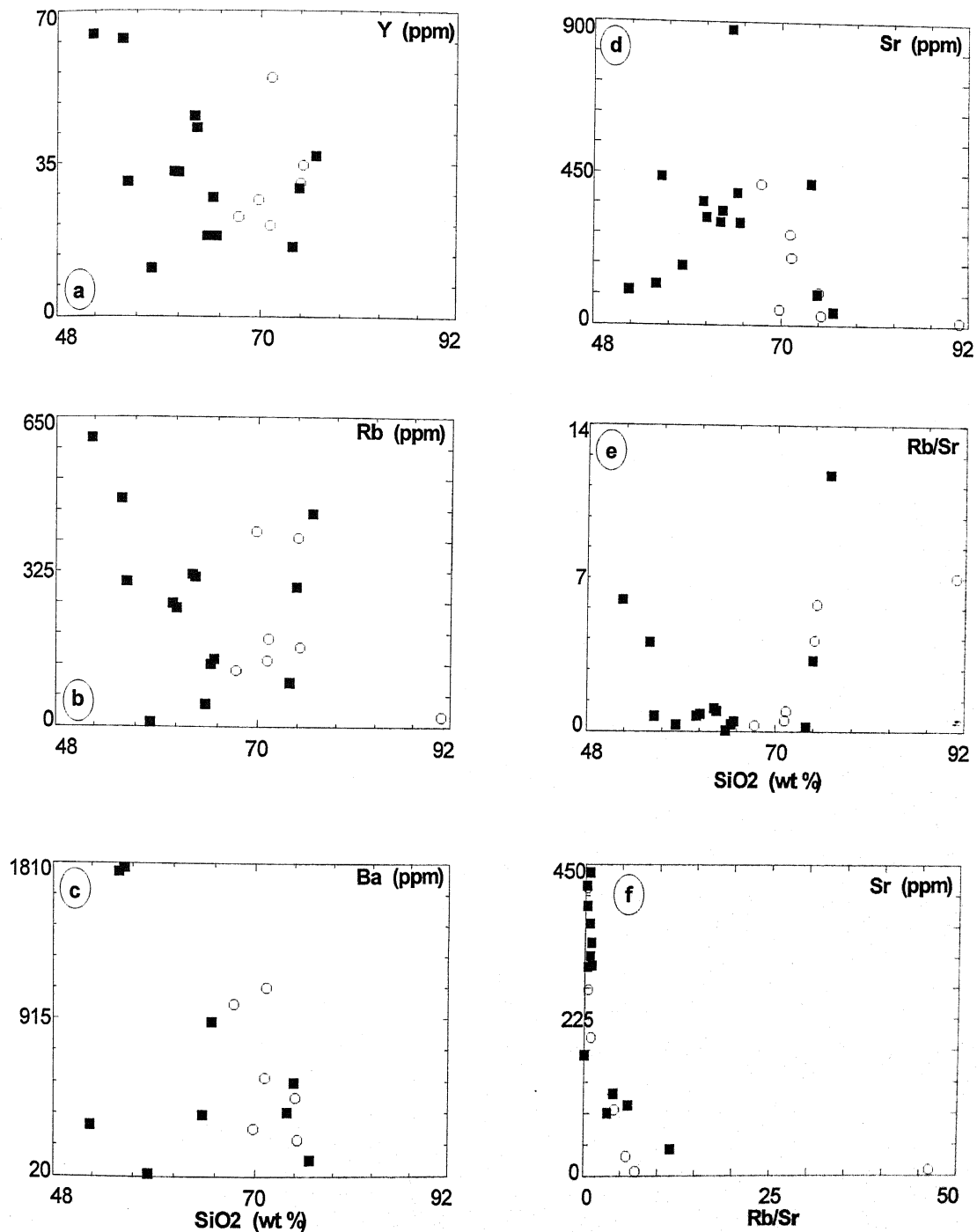
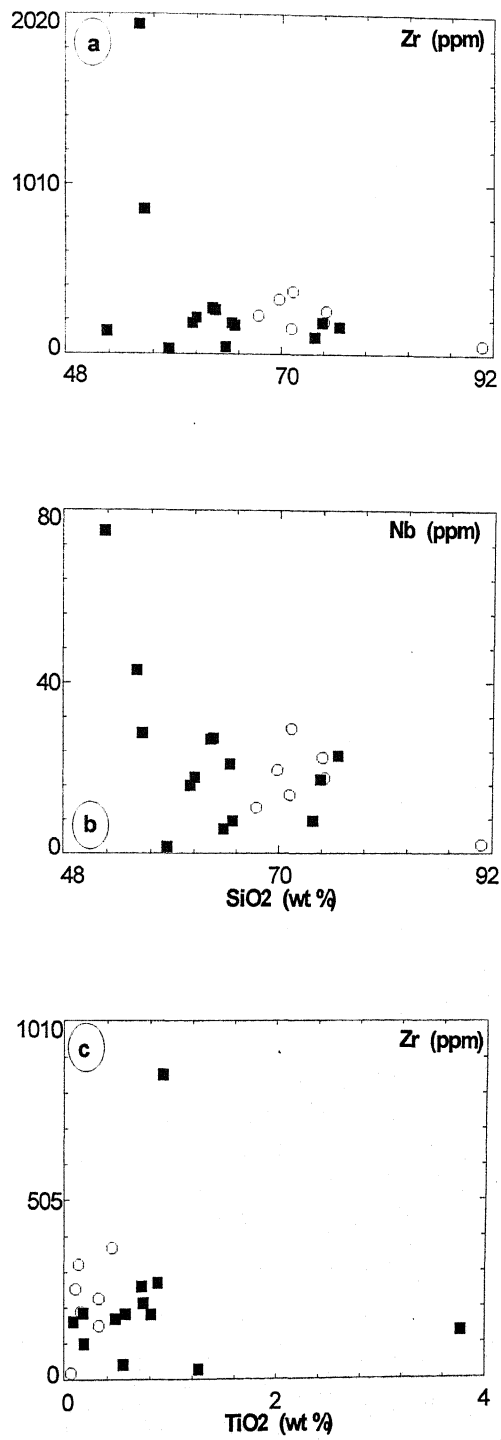


Fig. 4.16 (b) Variation diagram of Sr. (ppm) against model plagioclase for gneisses and granites of the study area.



Present study : ○, Mondal, 1995 ■,

4.17. Harkers variation diagrams of SiO₂ vs Y, Rb, Ba, Sr, Rb/Sr, and Rb/Sr vs Sr. for granites of the study area.



Present study : ○, Mondal, 1995 ■,

Fig. 4.18. Harkers variation diagrams of SiO₂ vs Zr, Nb and TiO₂ vs Zr of granites of the study area.

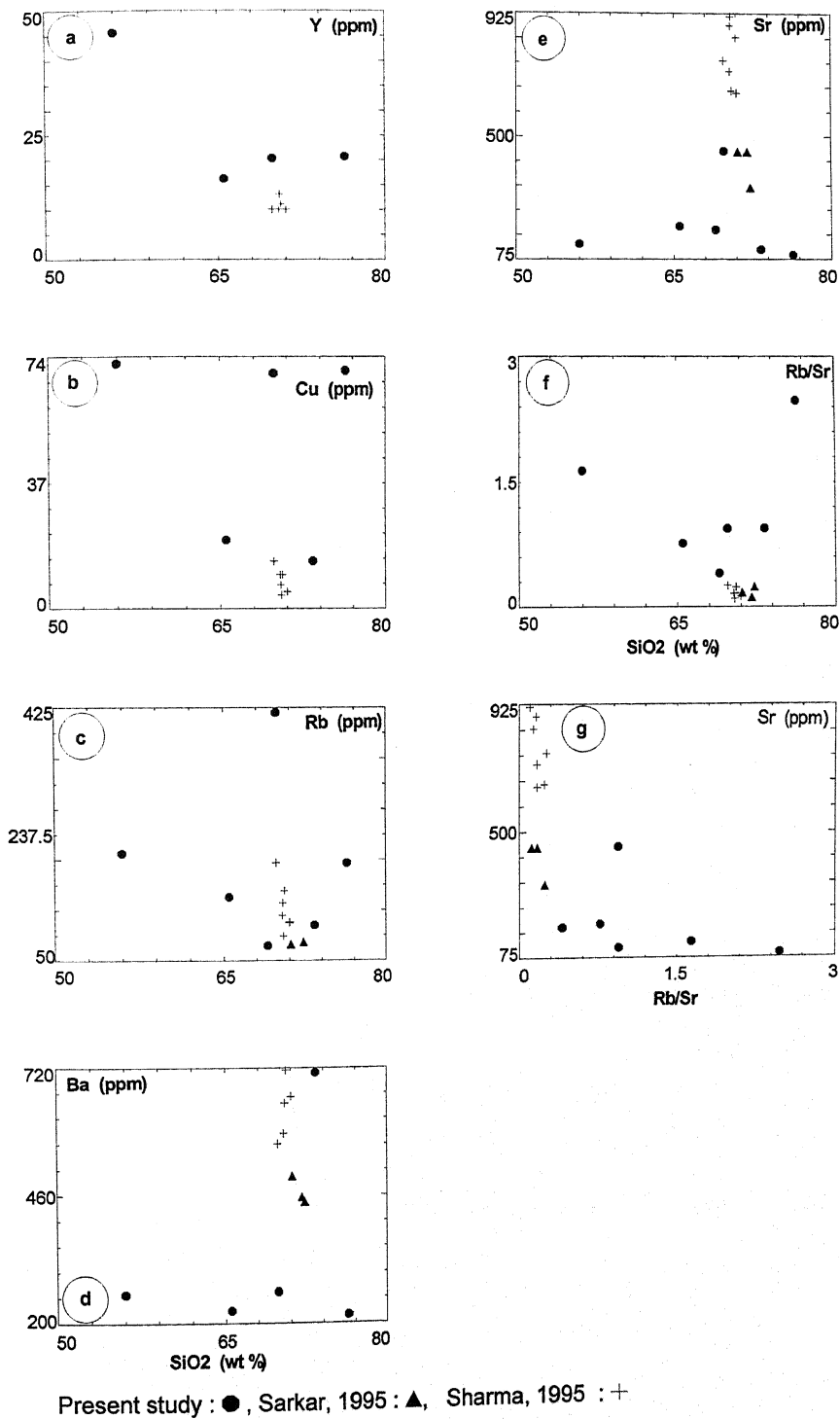


Fig. 4.19. Harker's variation of SiO_2 vs Y, Cu, Rb, Ba, Sr, Rb/Sr and Rb/Sr vs Sr for gneisses of the study area.

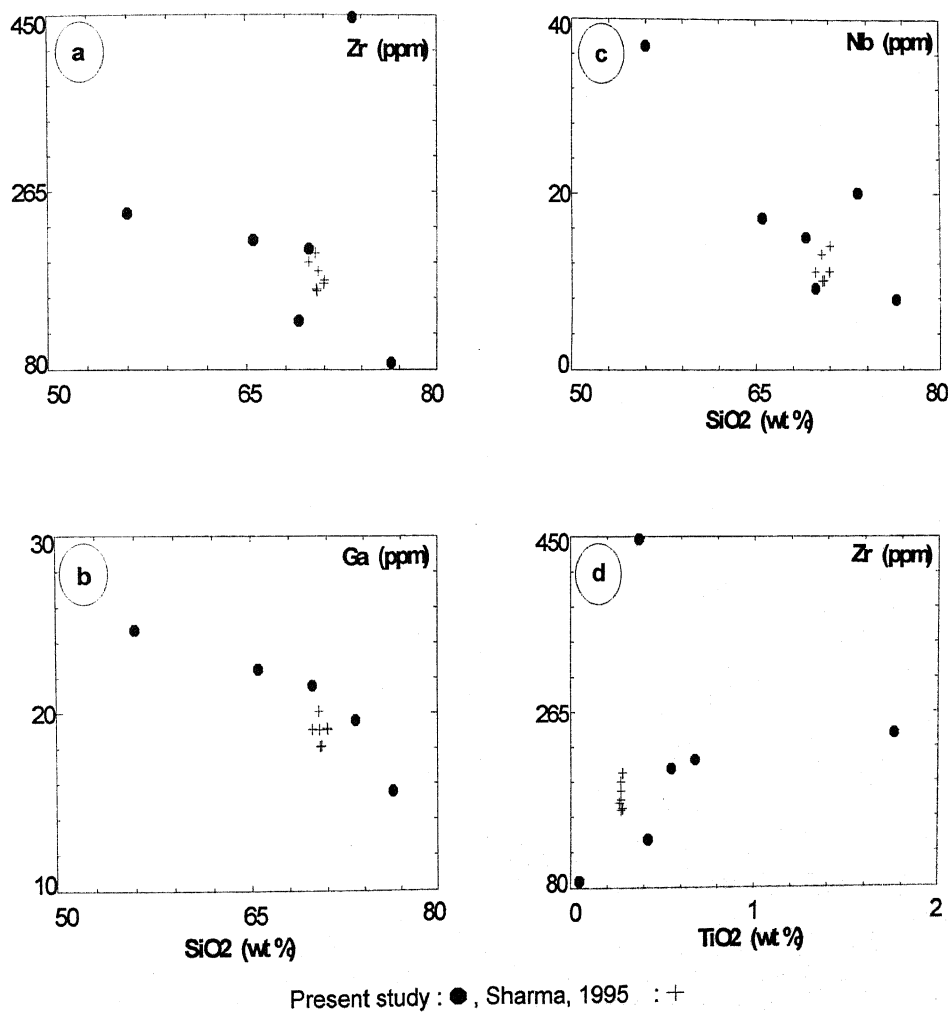


Fig. 4.20. Harker variation diagrams of SiO₂ vs Zr, Ga, Nb, and TiO₂ vs Zr. for gneisses of the study the area.

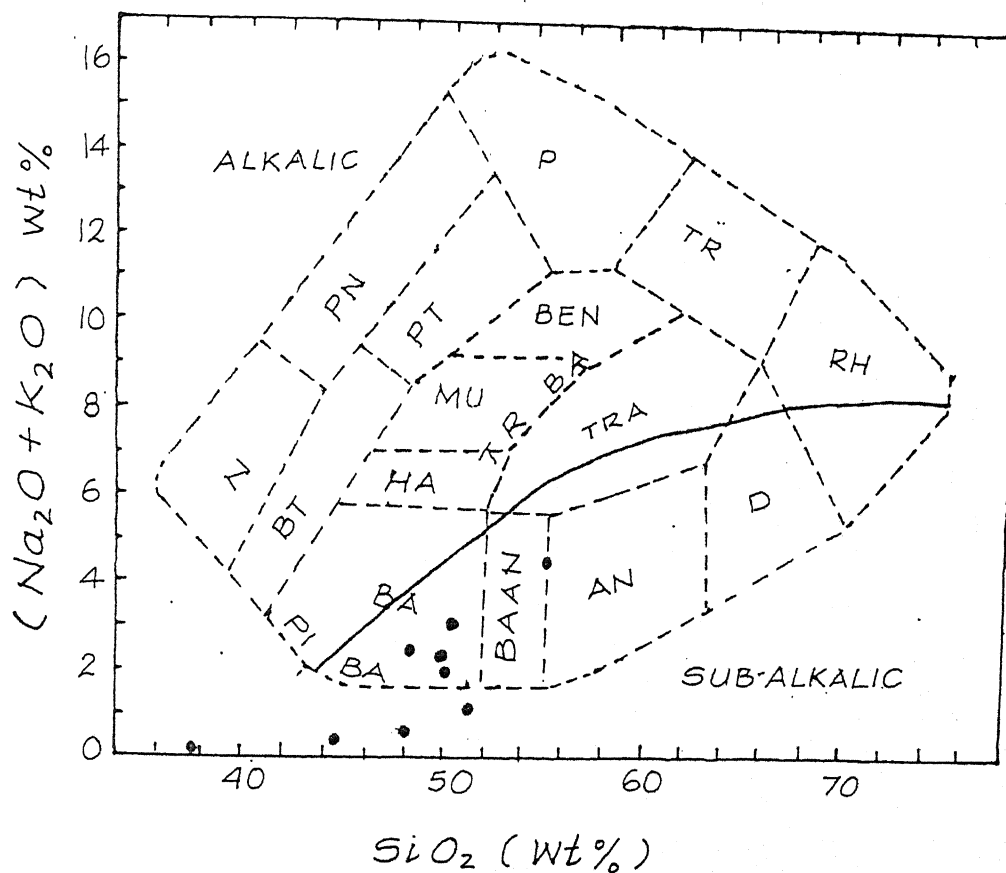


Fig. 4.21. Nomenclature of normal (i.e. non-potassic) igneous rocks from the study area after Cox et al. (1979). The dividing solid line between alkali and sub-alkalic magma series is from Miyashiro (1978). N : Nephelinites, PN : Phonolitic nephelinite, P : Phonolites, TR : Trachytes, RH : Rhyolites, BT : Basanite and tephrites, PT : Phonolitic tephrites, BEN : Benmoreites, MU : Mugearites, HA : Hawaiites, BA : Basalts PI : Picrites, TRBA : Trachybasalts, TRA : Trachyandesites, BAAN : Basaltic andesite, AN : Andesites, D : Dacites.

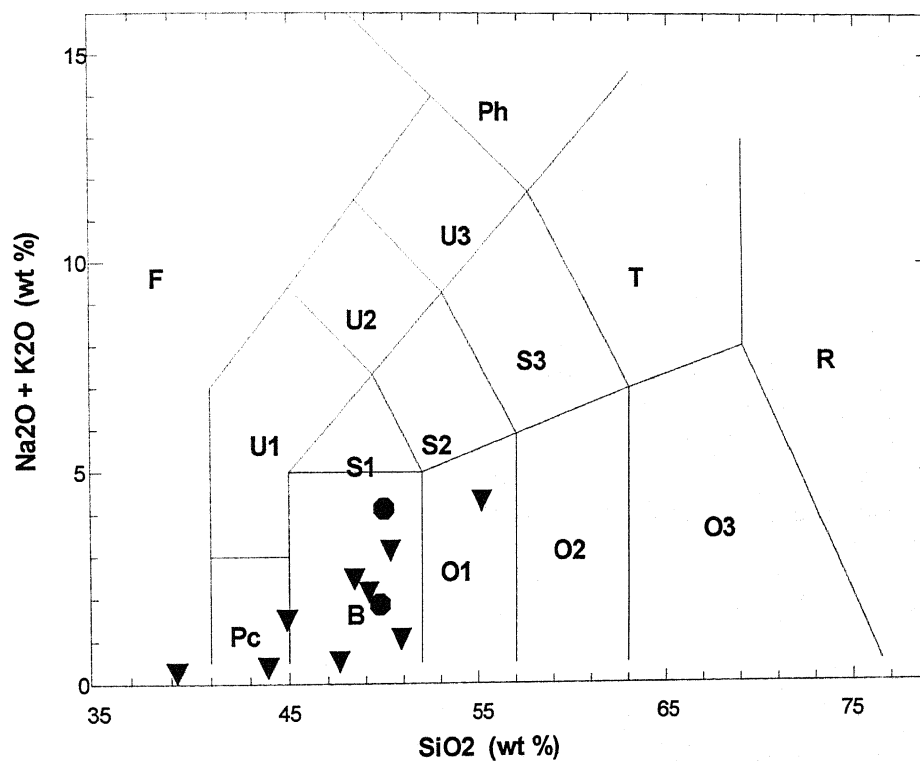


Fig. 4.22. Classification of the mafic and ultramafic rocks based on total alkalis versus silica (TAS), after La Bas and Streckeisen (1991). Pc : Picrobasalt, U1 : Tephrite/Basanite, U2 : Phonotephrite, U3 : Tephriphonolite, Ph : Phonolite, B : Basalt, S1 : Trachybasalt, S2 : Basaltic trachyandesite, S3 : Trachyandesite, T : Trachite/Trachydacite, O1 : Basaltic andesite, O2 : Andesite, O3 : Dacite, R : Rhyolite

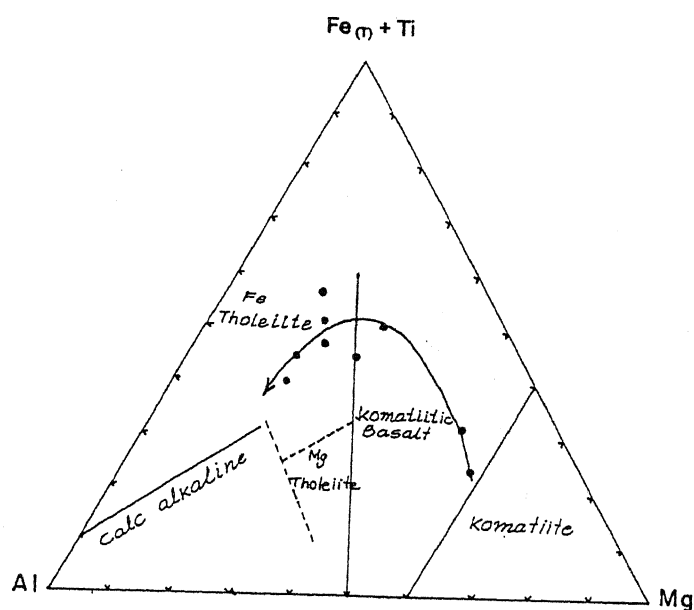


Fig. 4.23 (a) The classification of mafic and ultramafic rocks according to their cation percentage of Al , $(Fe_{total} + Ti)$ and Mg showing the tholeiite, calc-alkaline and komatiite fields after Jensen, (1976).

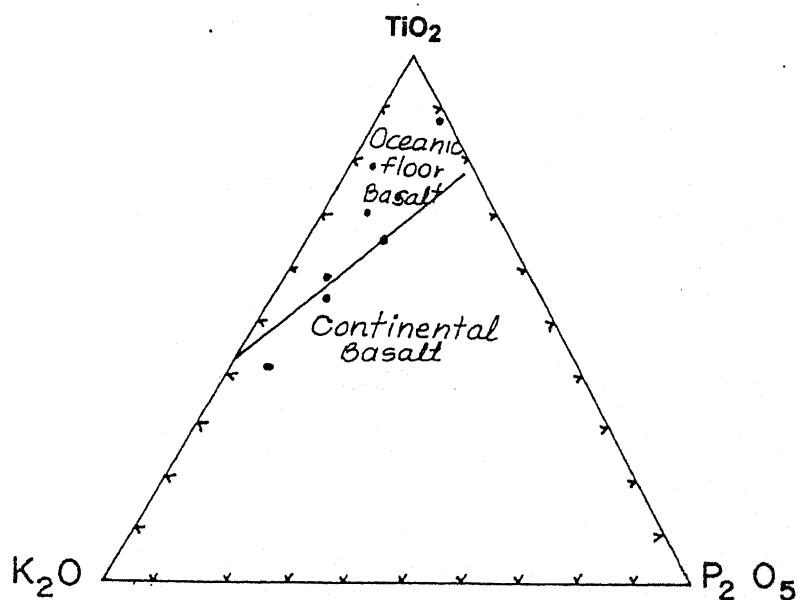


Fig. 4.23 (b) Major element trending diagram to distinguish continental and oceanic basalts (after Pearce et. al., 1975) show the maximum concentration of mafic and ultramafic samples of the area in the ocean floor domain.

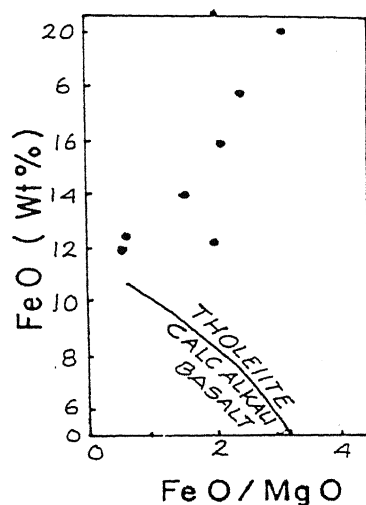


Fig.4.24 (a) FeO - FeO/MgO variation diagram (Miyashiro and Shido 1967) showing abyssal tholeiite affinity of the mafic and ultramafic rocks of the area.

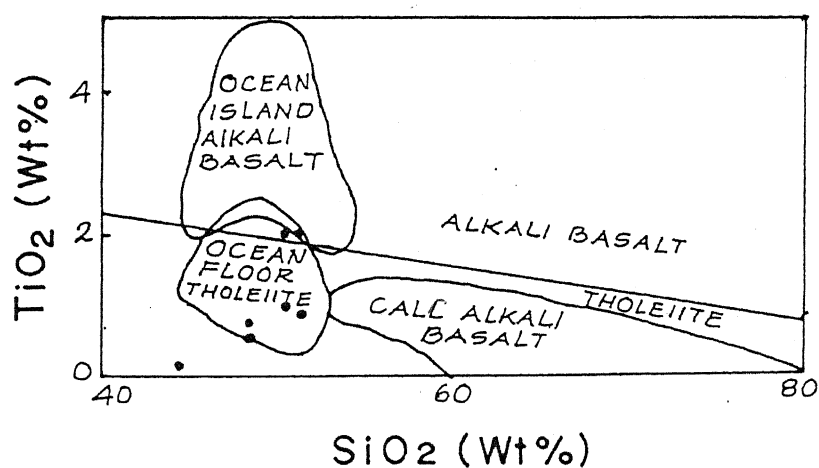


Fig.4.24 (b) TiO₂ - SiO₂ variation diagrams (Macdonald & Katsura 1964; Whitehead & Good fellow 1978) for the mafic and ultramafic rocks of the area.

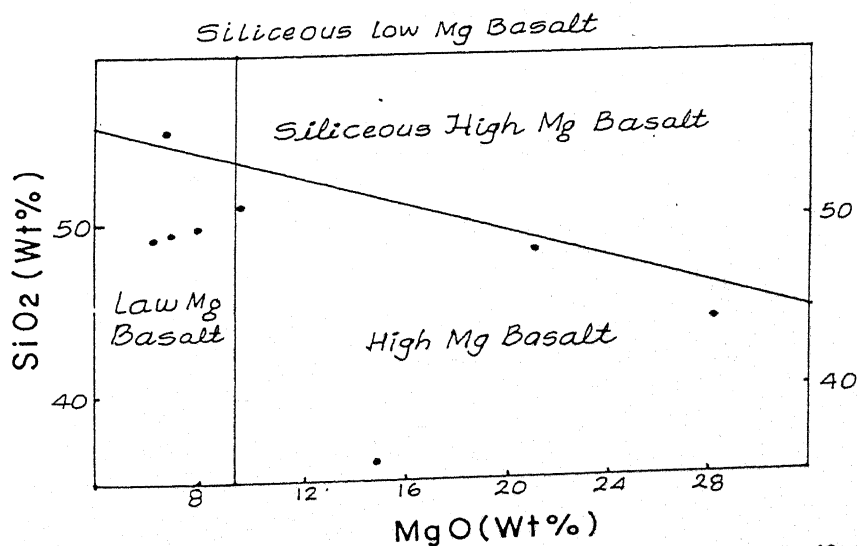


Fig.4.24 (c) SiO₂ - MgO diagram of Redman and Keays (1985) has been used to classify the mafic and ultramafic rocks of the area.

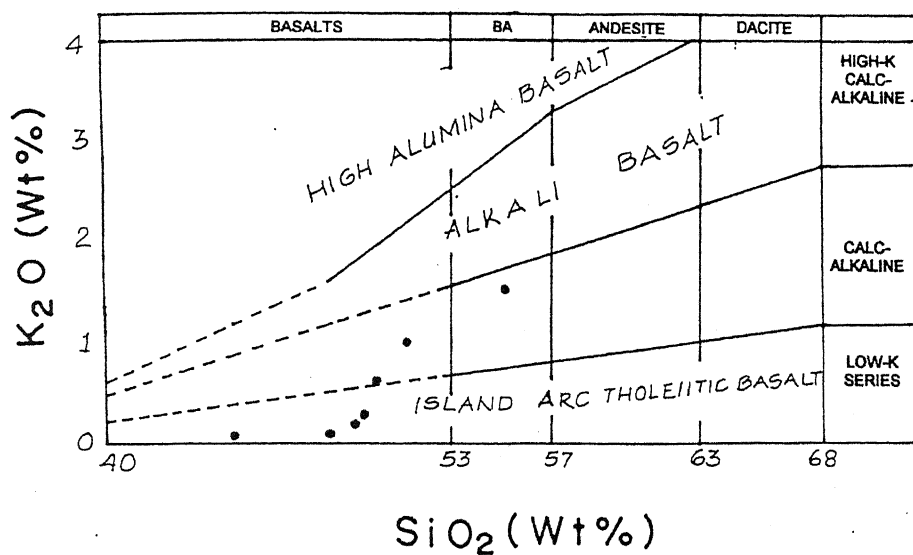


Fig. 4.25 (a) Plot of wt.% K_2O versus wt.% SiO_2 showing the major subdivision of the island arc volcanics rock suits.

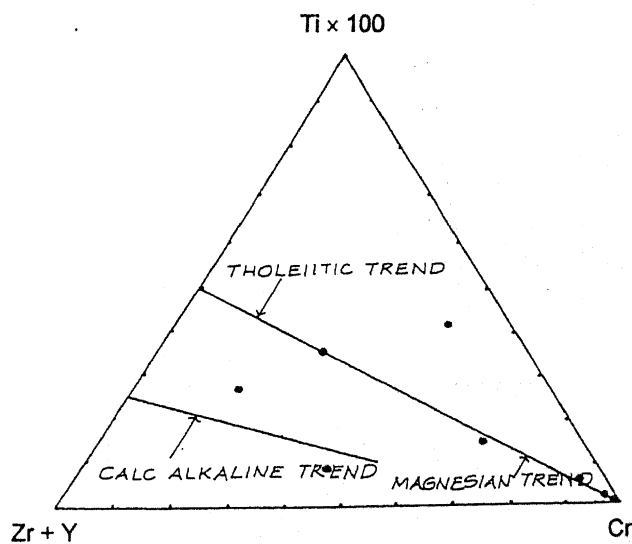


Fig. 4.25 (b) Triangular $(Zr + Y) - 100 Ti - Cr$ diagram showing the major differentiation trend of mafics and ultramafic the study area (Davis et. al., 1979).

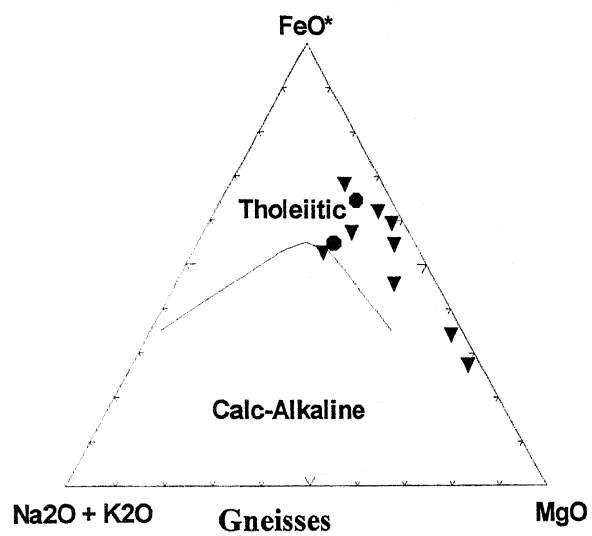


Fig. 4.26 (a) A-F-M diagram plots for the mafic and ultramafics of the study area (after Irvine and Baragar, 1971).

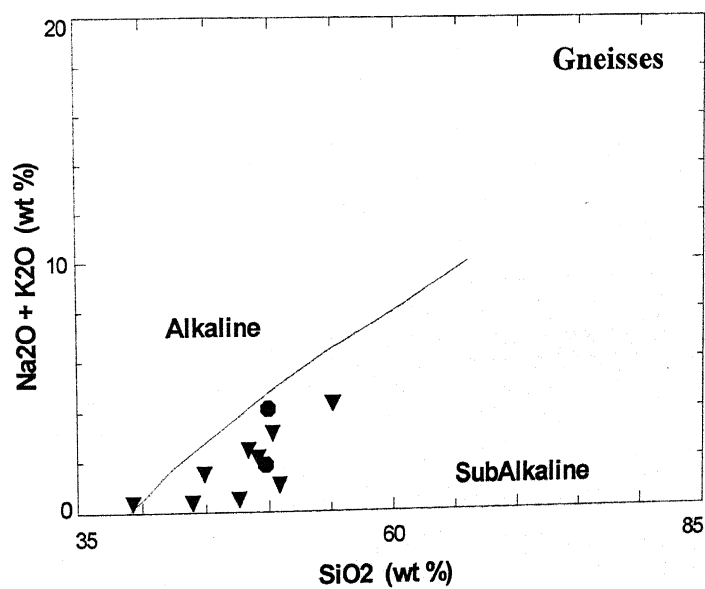


Fig. 4.26 (b) Total alkalis vs Silica diagram for mafic and ultramafic rocks of the area with lines separating field of alkaline sub-alkaline (after Irvine and Baragar, 1971).

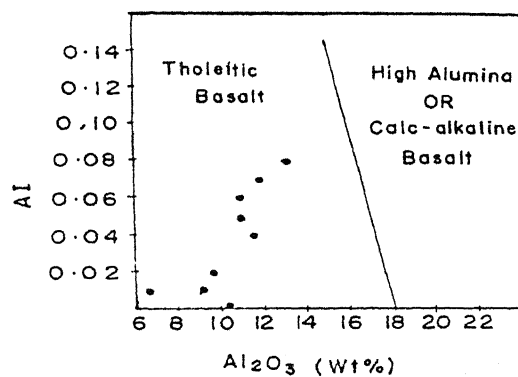


Fig. 4.27 (a) Diagram of Alkali Index (A.I) versus wt.% Al_2O_3 for the Classification of tholeiitic and high-alumina (calc-alkaline) basalts (after Middlemost 1975).

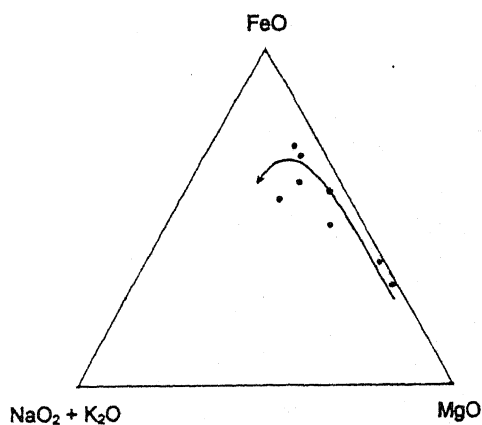


Fig. 4.27 (b) AFM diagram indicates the tholeiitic characters of the mafic and ultramafic rocks of the study area with progressive iron-environment compatible towards tholeiitic trend.

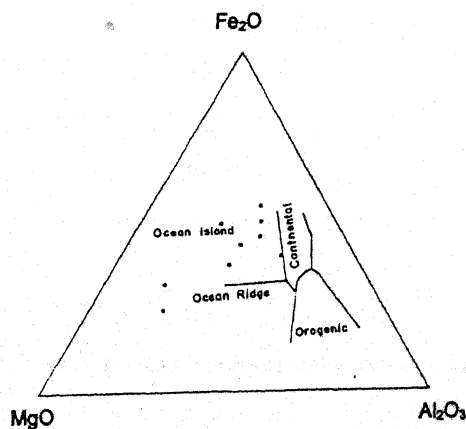


Fig. 4.27 (c) $\text{FeO} - \text{MgO} - \text{Al}_2\text{O}_3$ diagram (Pearce et. al., 1977) for mafic and ultramafic rocks

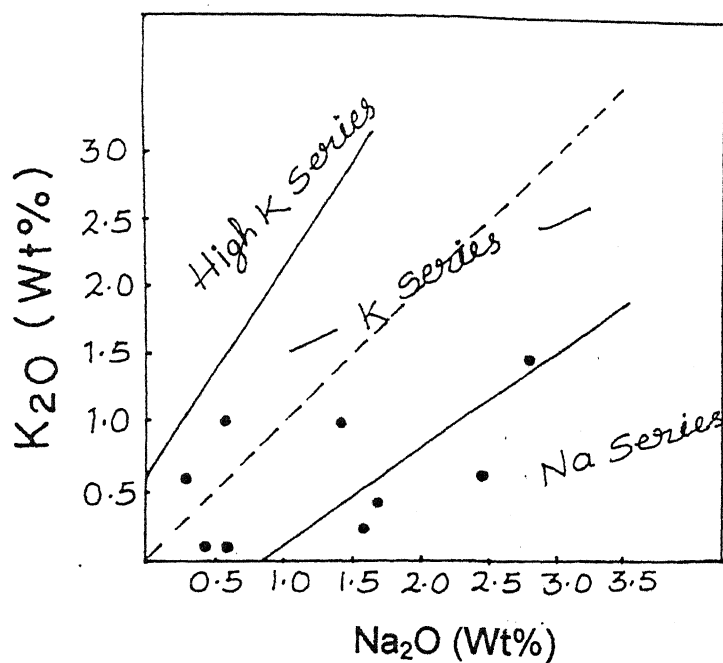


Fig. 4.28 (a) K_2O versus Na_2O (wt.%) diagram showing the subdivision of the alkali magma series into high-K, K, and Na sub-series (Middlemost 1975).

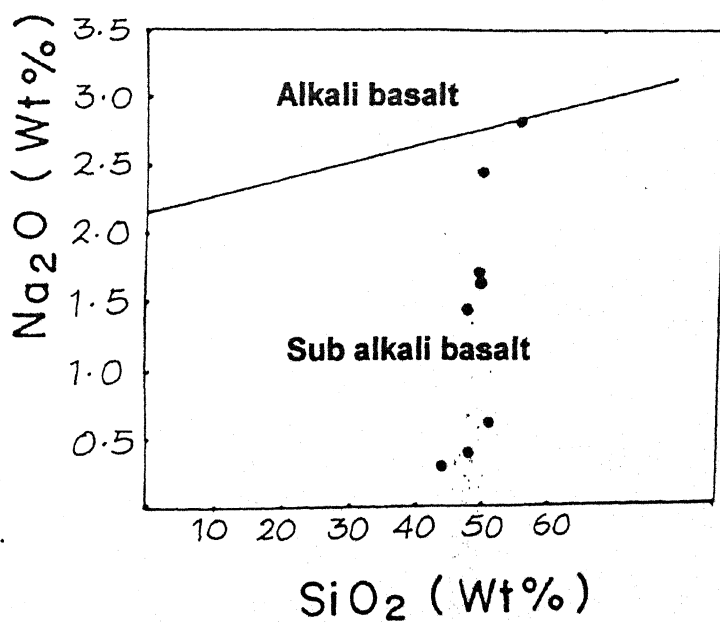


Fig. 4.28 (b) Classification of alkali and sub-alkali basalts in terms of wt.% Na_2O versus wt.% SiO_2 (after Middlemost 1975).

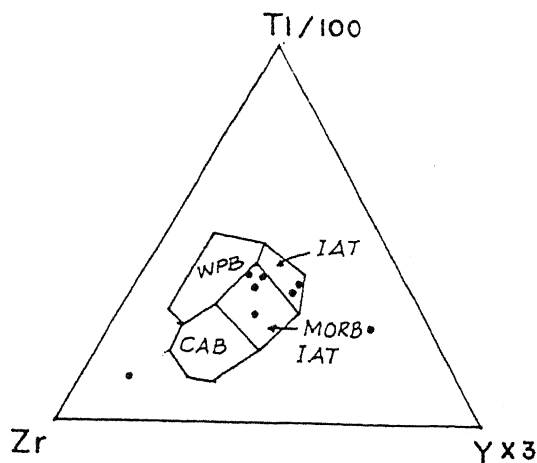


Fig. 4.29 (a) Ti/100 - Zr-Yx3 tectonomagmatic discrimination diagram for mafic and ultramafics rocks of the area (after Pearce and Cann, 1973). IAT : Island Arc Tholeiite, WPB : Within Plate Basalt, MORB : Mid-Oceanic Ridge Basalt, CAB : Calc-alkaline Basalt.

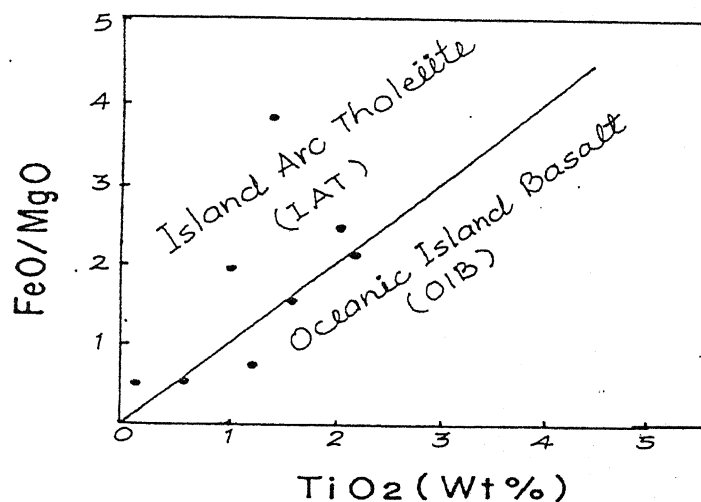


Fig. 4.29 (b) FeO/MgO vs. TiO₂ diagram (after Jelinek et. al., 1980) for the mafic and ultramafics rocks of the area.

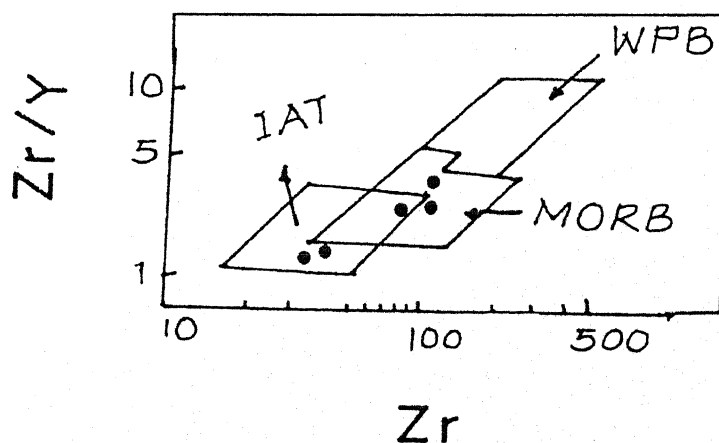


Fig. 4.29 (c) Zr/Y vs. Zr diagram (after Pearce and Norry, 1979) showing plots for the mafic and ultramafics rocks of the area. WPB : Within Plate Basalt, IAT : Island Arc Tholeiite, MORB : Mid Oceanic Ridge Basalt.

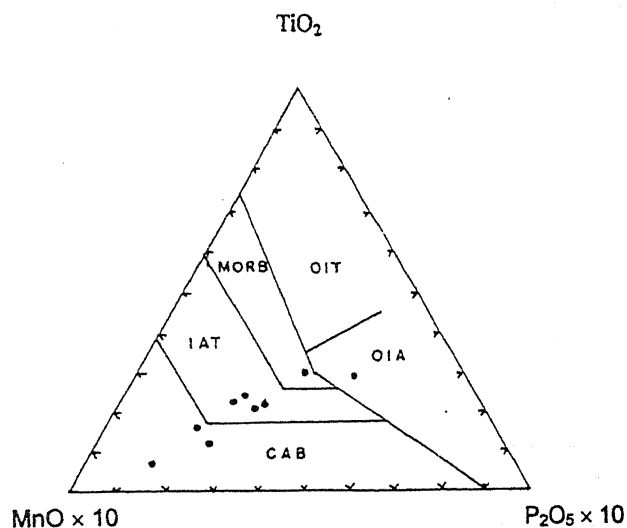


Fig. 4.30 (a). TiO_2 - MnO - P_2O_5 tectonomagmatic discrimination diagram for mafic and ultramafic rocks of the study area (after Mullen, 1983). OIT : Oceanic Island Tholeiite, MORB : Mid Oceanic Ridge Basalt, IAT : Island Arc Tholeiite, OIA : Oceanic Island Alkalic, CAB : Island Arc Calc-alkaline Basalt.

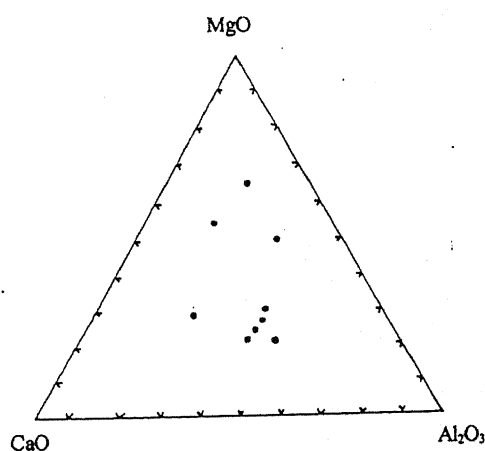


Fig. 4.30 (b). MgO - CaO - Al_2O_3 triangular diagram for mafics and ultramafics of the study area.

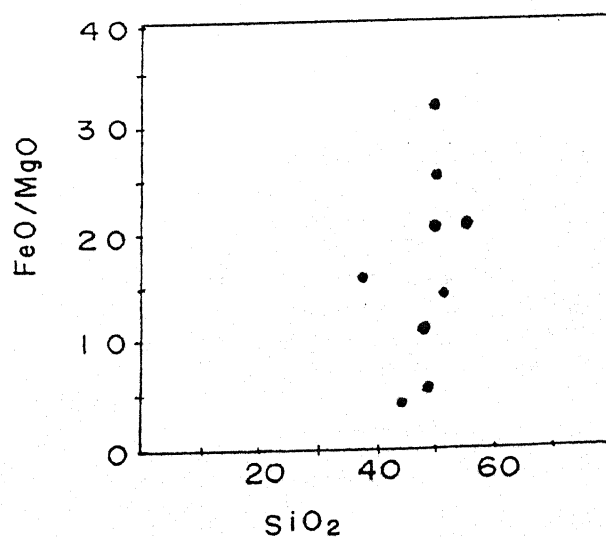


Fig. 4.30 (c). SiO_2 vs FeO/MgO variation diagram for mafics and ultramafics of the study area.

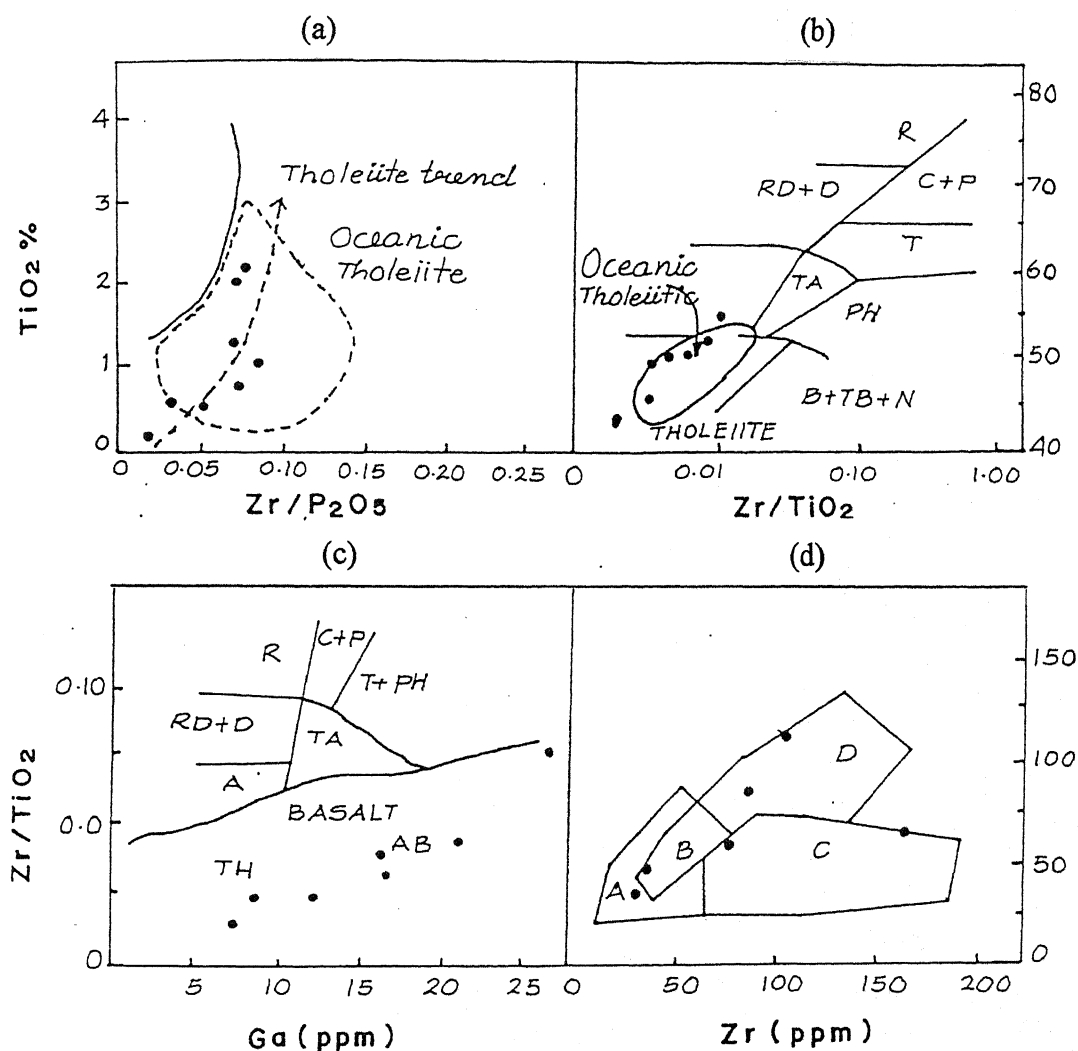


Fig. 4.31 Plots of the mafic and ultramafic rocks in various discrimination diagrams principally based on immobile minor and trace element. The classification boundaries are as proposed (a) Winchester & Floyd (1977), (b) and (c) Floyd & Winchester (1978) and (d) Pearce & Cann (1973). In (b) and (c) AB : Alkali Basalt, B+TB+N : Basanites, Trachy Basanites, Nephelinites, A : Andesites, D+RD : Dacites and Rhyodacites, R : Rhyolites, TA : Trachyandesites, T : Trachytes, Ph : Phonolites, Ph+T : Phonolites Trachytes, C+P : Comendites and Pantellerites, TH : Tholeiites and in (d) A&B : Island Arc Basalts, B&C : Calc-alkalic Basalts, B&D : Ocean Floor Basalts,

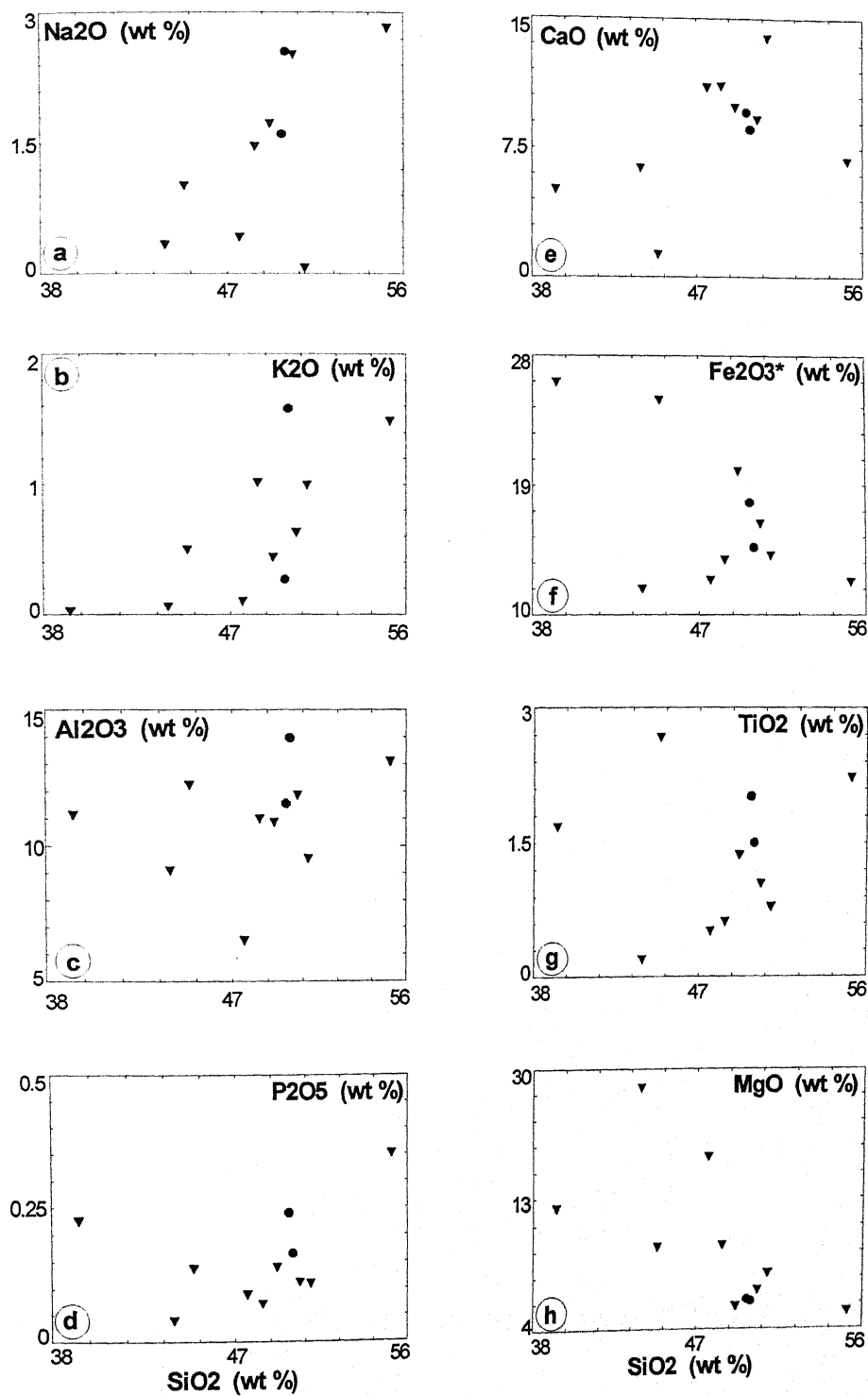


Fig. 4.32 a-h. Harkers variation diagram of SiO_2 vs Na_2O , K_2O , Al_2O_3 , P_2O_5 , CaO , Fe_2O_3 , TiO_2 and MgO .

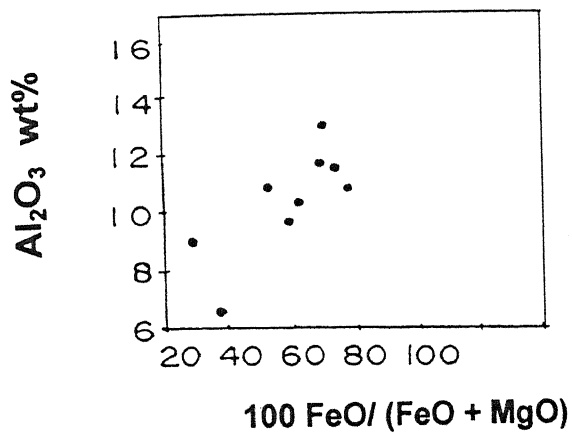


Fig. 4.33 (a) Al_2O_3 vs $\text{FeO} / (\text{FeO} + \text{MgO})$ diagram for mafic and ultramafics rocks of the study area.

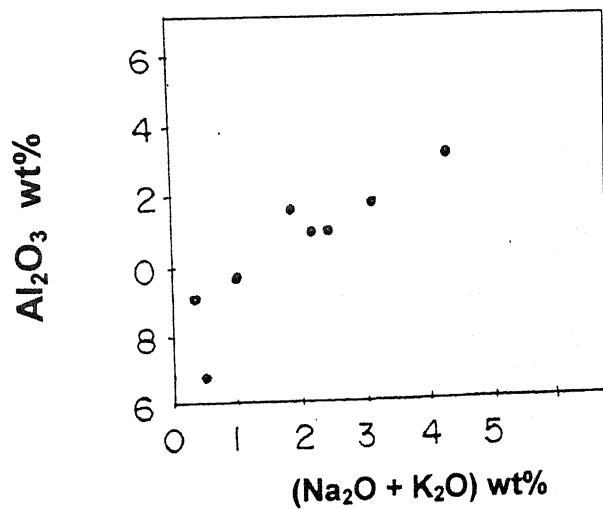


Fig. 4.33 (b) Alumina vs total alkalis diagram of mafic and ultramafic of studies area.

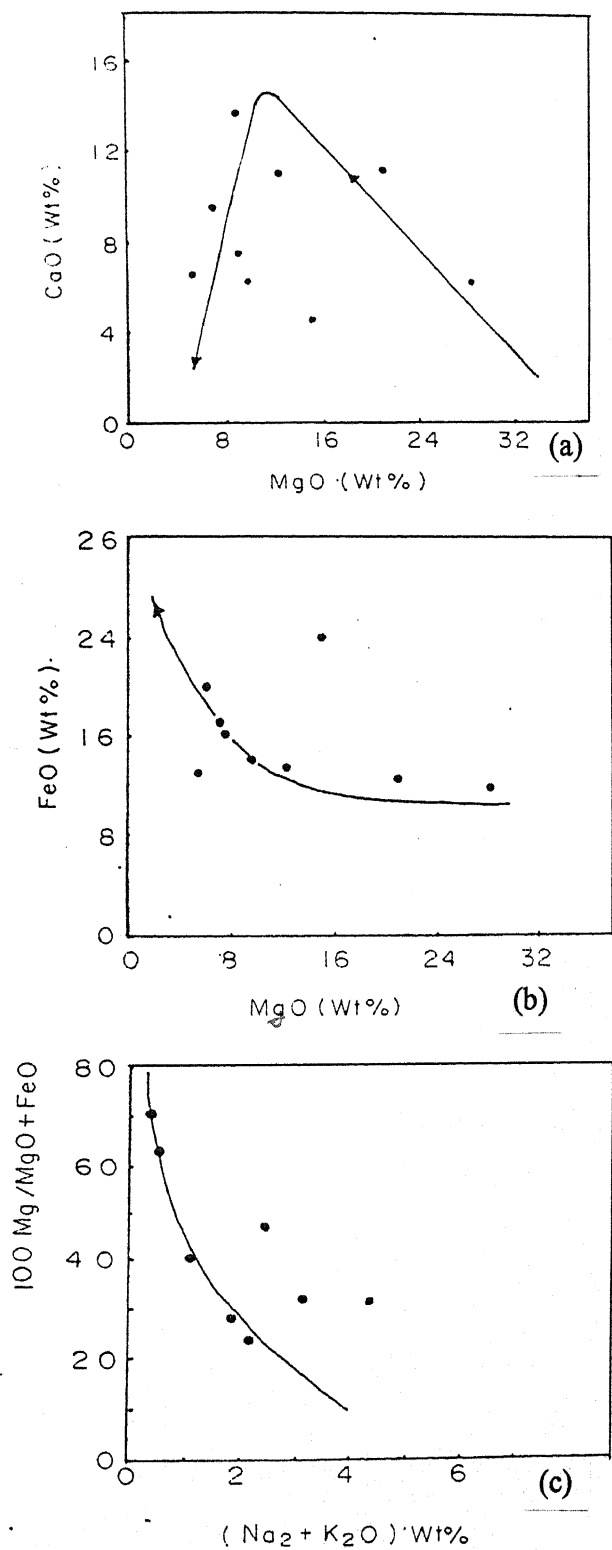


Fig. 4.34 (a) MgO vs CaO, (b) MgO vs FeO, (c) $100 \times \text{Mg} / (\text{MgO} + \text{FeO})$ vs $(\text{Na}_2\text{O} + \text{K}_2\text{O})$ diagram for mafics and ultramafics of the study area.

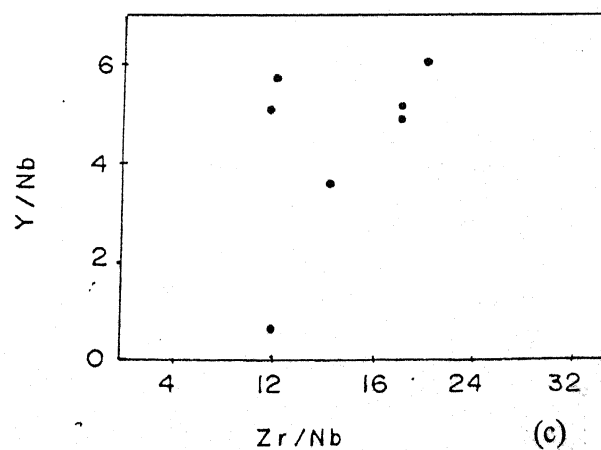
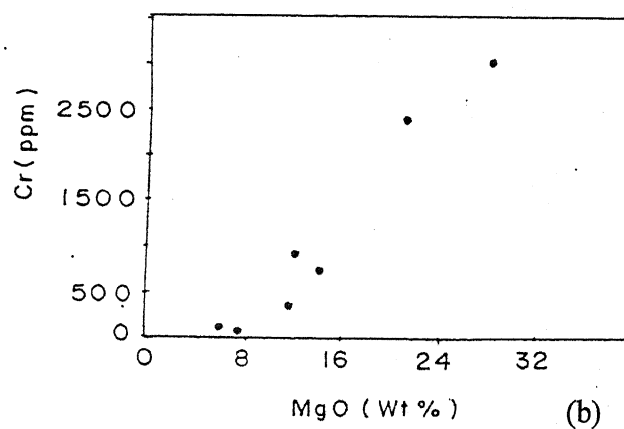
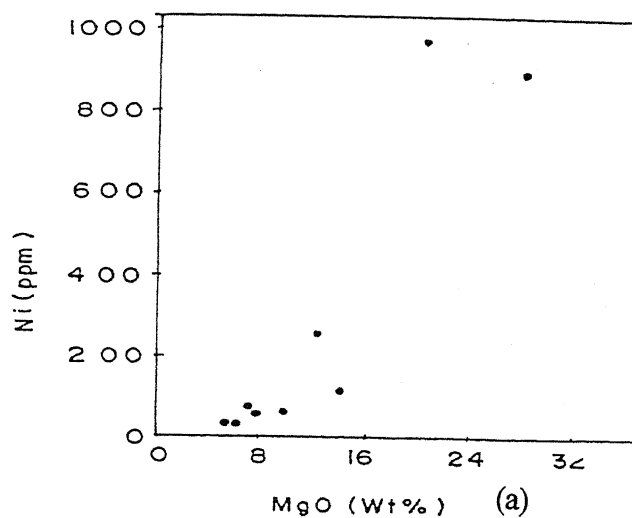


Fig. 4.35. The relation diagram (a) MgO vs Ni, (b) MgO vs Cr for the mafics and ultramafics of the study area, (c) Zr/Nb vs Y/Nb diagram for mafics and ultramafics of the study area.

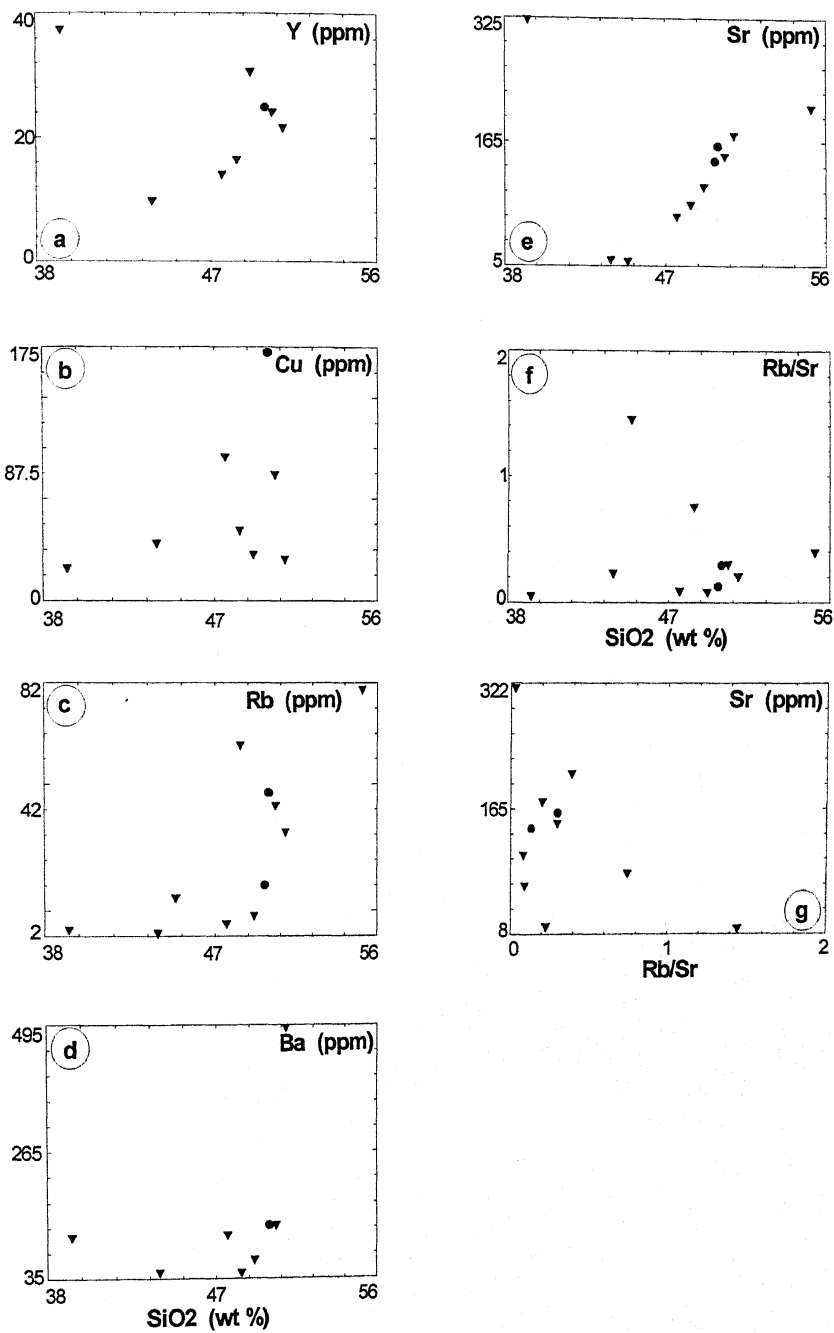


Fig. 4.36 Harkers variation diagrams of SiO_2 vs Y, Cu, Rb, Ba, Sr, Rb/Sr and Pb/Sr vs Sr.

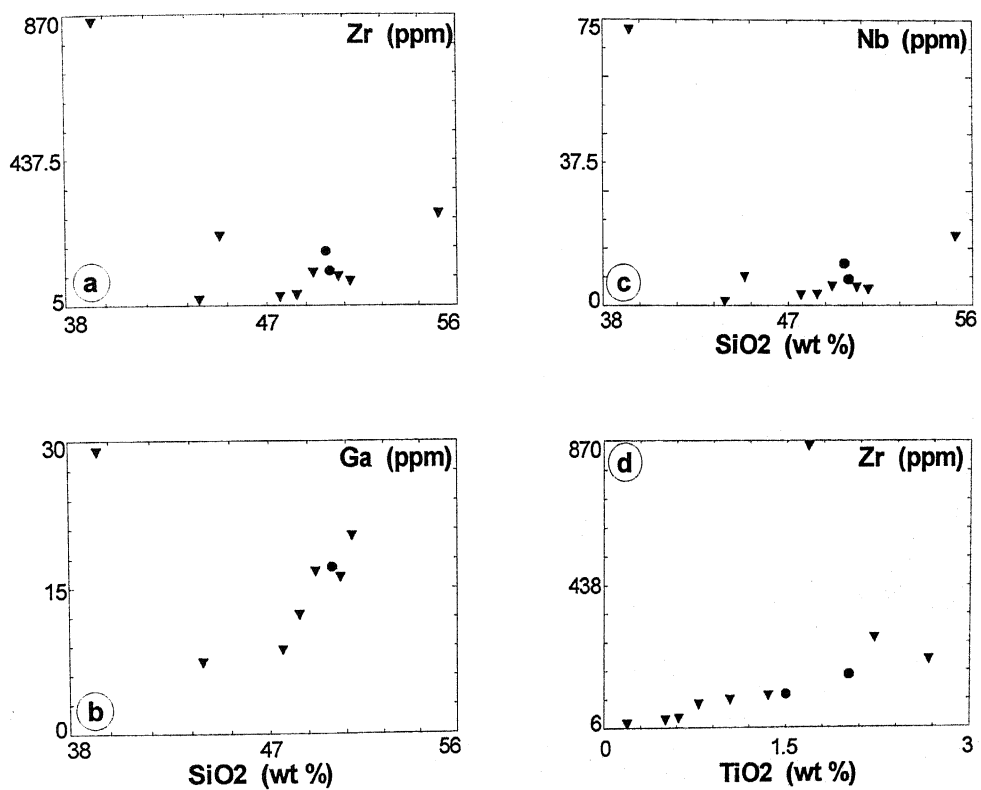


Fig. 4.37. Harkers variation diagrams of SiO₂ vs Zr, Ga, Nb, and TiO₂ vs Zr.

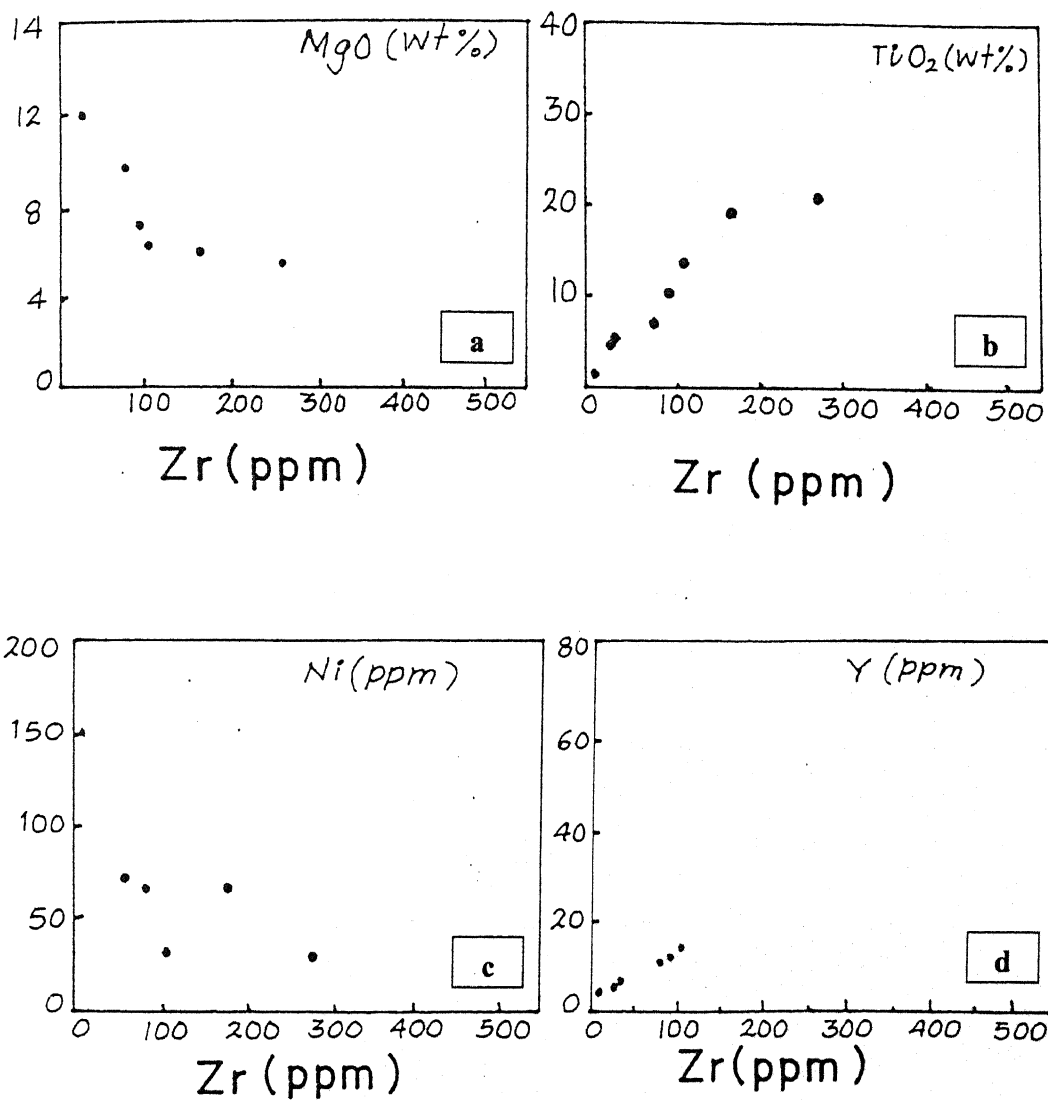


Fig. 4.38 Binary plots of (a) Zr vs MgO, (b) Zr vs TiO₂, (c) Zr vs Ni and (d) Y Zr vs Y.

MINERALOGY & PHASE PETROLOGY

5.1 Mineralogy

The detailed textural study of the different rock types of the study area reveals the presence of a number of mineralogical assemblages. The coexisting minerals listed in the chapter iii have been analysed by the electron microprobe techniques. In this chapter an attempt has been made of discuss critically the range in chemical composition of the minerals and effect of other elements and substitution.

5.1.1 Electron microprobe technique

An electron microprobe is an electron microscope designed for the non-destructive X-ray microanalysis and imaging of solid materials. It is essentially a hybrid and imaging instrument combining the capabilities of both the scanning electron microscope (SEM) and an x-ray fluorescence spectrometer (XRF), with the added features of fine spot focus using (-1μ micrometer), optical microscope imaging, and precision-automated sample positioning. The analyst makes measurements while observing the sample (with the optical microscope or with a secondary/black scattered electron image) and selecting specific analysis location (using the precision sample stage).

The technique is capable of high spatial resolution ($-1\mu\text{m}$) and relatively high spatial sensitivity ($< 0.5\%$ for major elements) and detection limits (-100ppm for trace element). It can also acquire digital secondary electron and back scattered electron and cathodoluminescence images as well as digital x-ray maps. It is normally equipped with upto 5 wavelengths – disperse spectrometers. Most of the elements of the periodic table from beryllium to uranium can be analysed by this technique.

5.1.2 Samples preparation

The volume of samples is typically a few cubic microns at the surface, corresponding to a weight of a few picograms and are therefore sensitive to surface contamination. Samples should be prepared as clean, flat, polished solid mounts up to 1 inch in diameter or as uncovered petrographic thin section and must be stable in a 10-5 Torr vacuum environment and under electron bombardment. For best results, samples must be polished to within a $0.05\mu\text{m}$ flat surface. After preparation, samples are coated with an approximately 200 Angstrom (10 nm) layer of carbon using a carbon or other conductive material in an evaporator.

5.1.3 Advances of EPMA in mineralogy

The compositional variation within a minerals grain and in the different domains of chemical equilibrium can be detected only by the electron microprobe analyses techniques, while the analysis of minerals separated from rocks by rapid methods (Shapiro and Brannock 1962) yield only the bulk composition of them minerals. Further, minerals present in lesser amount in rocks cannot be separated in sufficient amount for analysis by this method.

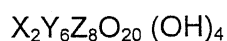
Minerals from various types of reaction coronas and those occurring as inclusions can be easily analyzed microprobe techniques not by wet methods of analysis.

The standards used for microprobe analyses were: Wollastonite for Si and Ca, pure metals for Fe, Mn, In, Corundum for Al, periclase for Mg, narsukite for Na and Ti, Cr_2O_3 for Cr and K-feldspar glass for K.

5.1.4 Biotite

Biotite is an important ferromagnesian mineral in, gneisses, amphibolites, granites, metamytonites and metavolcanics etc. The microprobe analyses and structural formulae based on 22 oxygen of the biotite from the investigation area are presented in table 5.1. The bulk composition of the biotite can be represented (Fig 5.1) in terms of four end members: phlogopite - $\text{K}_2\text{Mg}_6 (\text{Si}_6\text{Al}_2\text{O}_{20}) (\text{OH})_4$; annite - $\text{K}_2\text{Fe}_6 (\text{Si}_6\text{Al}_2\text{O}_{20}) (\text{OH})_4$; eastonite - $\text{K}_2\text{Mg}_5\text{Al} (\text{Si}_5\text{Al}_3\text{O}_{20}) (\text{OH})_4$; and siderophyllite $\text{K}_2\text{Fe}_5\text{Al} (\text{Si}_5\text{Al}_3\text{O}_{20}) (\text{OH})_4$.

The general formula of trioctahedral biotite can be expressed as:



Where,

X= K, Na, Ca

Y=Mg, Fe, Al^{IV} , Mn, Cr, Ti

Z= Si, Al^{IV}

The Y cations occur in six-fold coordination forming octahedral layer, which is sandwiched between two inwardly pointed sheets of tetrahedral layer. The structural formula of biotite is too similar to similar rock types from other areas. The Y site cations are ranging from 5.46 to 7.44 p.f.u but do not correspond to 6p.f.u. This deficiency and excess of cations on Y position reveal the heterovalent substitution in octahedral layers. According to Foster (1960) additional positive charges carried by trivalent and tetravalent cations proxy for divalent cations in the octahedral group of octahedral biotite.

The deficiency can be accommodated in two different ways (a) positive charge on the octahedral layer, it can be neutralized by an equivalent increase in the negative tetrahedral charge (increase in the replacement of Si by Al^{IV}) by $+2 n\text{R}^{+3} = (2n\text{R}^{+2}) + (-n$

Si⁴⁺) or (b) neutralized by negative charge associated with occupied octahedral position ($+2 nR^{+3} = (-3nR^{+2}) + (-n \text{ octahedral position})$).

The excess of cations in Y position reveals that the divalent cations in X position are substituted by Y cations viz. Fe, Mg and Mn etc. Those samples which have deficiency of cations in Y position is not substituted by X cations, even the alkalies shows deficiency which reveals that they are substituted by Trace elements like Cr, Ti, Li etc.

The deficiency in alkali i.e. $\sum X$ is less than 2.0 indicating that these cations might have been substituted by the cations in Y. Sometimes the Y cations also showing deficiency, it means that this X site cations were substituted by trace elements which usually found in X cations viz. Rb, Ba, Cs etc. But the alkali deficiency in biotite (trioctahedral) of metamorphics is not abnormal (Guidotti, 1974)

It has been shown by many petrologists (Butler 1965, Nagar and Atherton 1970) that the composition of biotite is sensitive to host rock composition and coexisting minerals.

There is a wide range of X_{mg} (0.112-0.441). This X_{mg} is low in biotite of Granites, than that of metamorphic rocks of the study area. In the triangular diagram of Mg-(Fe+Mn)-R⁺³ in octahedral sheet of biotite based on Foster, 1960, the analysed biotite lies in a distinct band.

Alumina-content of biotite

The Al₂O₃ plays an important role in mica chemistry. The Al₂O₃- content of biotite varies from 14.11 to 18.32-wt%. Al^{VI} content in biotite ranges from 0.2571 to 0.5661p.f.u. in the metamorphics and granites of the study area.

TiO₂- content of biotite

Among all the oxides present in biotite, TiO₂ variation reflects its significant feature. The TiO₂ concentration increases with increase in the grade of metamorphism from green schist to granulite facies (Engel and Engel, 1960; Guidotti, 1974 Lal; 1991).

The analysed biotites of the study area shows wide range of TiO₂- content 0.291 to 3.26 wt% but the TiO₂ contents of biotite are randomly distributed in all types of rocks.

The analysed samples of biotites are plotted on the quadrilateral diagram outlined by four end-members- phlogopite, annite, eastonite and siderophyllite (Fig-1). All the samples fall in the biotite field, and more concentrated towards annite corner which suggests that magnesium is replaced by ferrous iron and also by trivalent ions (Fe⁺³, Al), and aluminum replaces silicon in tetrahedral sites usually beyond the ratio Al: Si = 2:6.

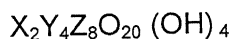
5.1.5 Muscovite

Muscovite is one of the common micas in NMG rocks and meta-volcanosedimentary rocks of the study area.

The microprobe analysed and structural formulae based on 24 oxygen of muscovite of study area are presented in Table 5.2.

The bulk composition of muscovite (dioctahedral) can be represented in terms of four end members; Muscovite – $K_2Al_4(Si_6Al_2)O_{20}(OH)_4$, Ferro-muscovite- $K_2Fe^{+3}Al_3(Si_6Al_2)O_{20}(OH)_4$, Phengite – $K_2(Mg, Fe^{+2})Al_3(Si_7Al)O_{20}(OH)_4$ and Ferro-phengite- $K_2(Mg, Fe^{+2})Fe^{+3}Al_2(Si_7Al)O_{20}(OH)_4$.

The general formulae of dioctahedral muscovite can be expressed as :



Where X=K, Na, Ca

Y = Mg, Fe, Al^{VI} , Mn, Ti, Cr.

Z= Si, Al^{IV} .

The analysed muscovite samples were plotted on the diagram outlined by four end-members: Muscovite- $K_2Al_4(Si_6Al_2)O_{20}(OH)_4$, Ferro-muscovite- $K_2Fe^{+3}Al_3(Si_6Al_2)O_{20}(OH)_4$, Phengite- $K_2(Mg, Fe^{+2})Al_3(Si_7Al)O_{20}(OH)_4$ and Ferro-phengite- $K_2(Mg, Fe^{+2})Fe^{+3}Al_2(Si_7Al_2)O_{20}(OH)_4$ (Fig 5.2). All the samples plots near the corner of ferro muscovite, which reveals that in the muscovite-phengite series Mg, Al^{VI} substitutes Fe^{+2} .

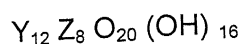
Alumina-content of Muscovite

The Al_2O_3 plays an important role in muscovite chemistry. The Al_2O_3 content of muscovite varies from 35.462 wt% as highest and minimum of 34.224 wt%. Al^{VI} content ranges from 4.8100 to 4.9771 p.f.u. In above paragraph also discussed that the muscovite and phengite series is related to the substitution of (Mg, Fe^{+2}), Si, Al^{VI} , Al^{IV} , and Ferromuscovite ferrophengite is derived from muscovite and phengite respectively replacement of one of the Al^{VI} ions by Fe^{+3} (Fig 5.2).

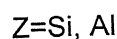
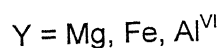
5.1.6 Chlorite

Chlorite is an important ferromagnesian mineral in metamorphic rocks of the study area. The microprobe analyses and structural formulae based on 28 oxygen of the chlorite from the investigated area are presented in table 5.3

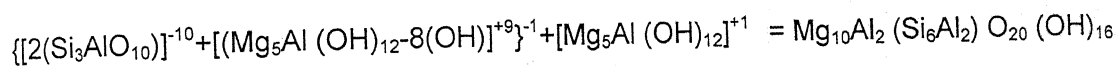
The general formulae of chlorite can be expressed as:



Where,



It consists of alternate talc-like. $Y_6 Z_8 O_{20} (OH)_4$ and brucite type $Y_6 (OH)_{12}$ sheets structure. The negative charges of talc-like layer is balanced by positively charged of brucite-like layer as shown by the following equation:



Talc like layer

Brucite-like layer

Chlorite

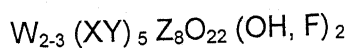
Al_2O_3 play an important role in chlorite chemistry and substitution occurs in both talc and brucite layers; silicon is replaced by aluminum $Si_5 [Al_3]^{+4}$ in Z site.

Magnesium in Y site is replaceable principally by aluminum in both the talc and brucite components (W.A. Deer, R.A. Howie and J. Zussman, 1962) but Al^{VI} content is normal (2.4377 p.f.u) and Mg content is low (0.9708 p.f.u.) So here in the analysed sample Fe+2 replaces Mg, Fe content is quite high (8.4963 p.f.u.).

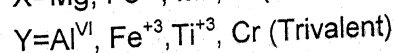
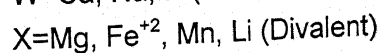
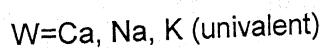
5.1.7. Amphiboles

Amphibole is an important ferromagnesian mineral observed in all rock types of the study area. The microprobe analyses and structural formulae based on 24 oxygen of the amphiboles are presented in table 5.3.

The general formulae of amphiboles can be expressed as :



Where,



The analysed samples of amphiboles are plotted on the chemical variation diagram of the calcium-rich amphiboles expressed as the numbers of (Na+K) and $[Al]^{IV}$ atoms p.f.u. The samples were plotted in the near hornblende field (Fig 5.3).

The amphibole analyses are also plotted on amphibole diagram (Na/(Na+Ca) vs Si atoms p.f.u) after Leake, 1978 showing the range in chemical composition (Fig 5.4).

The analysed amphiboles are plots in the fields of actinolite, actinolite-hornblende and hornblende in the calcic amphibole. Silica content in amphiboles ranges from 7.08 to 7.87 p.f.u. So the substitution of silica by aluminum (Al^{IV}) ranges from 0.132 to 0.920 p.f.u. The Al^{VI} content in amphiboles of the study area ranges from 0.0135 to 0.7486 p.f.u. All this substitution is limited to approximately 1Al atom per formulae unit $\text{Mg} = \text{Fe}$ replacement is important for paragenesis of amphiboles. Other important substitution occur in the amphiboles are $\text{Al}=\text{Si}$, $(\text{Mg}, \text{Fe})=\text{Al}$, $\text{Na}=\text{Ca}$ etc.

The end-members tremolite, common hornblende, and tschermakite involve increasing substitutions in the (XY) and Z positions of the type $\text{Mg Si}=\text{Al}$.

The edenite and paragasite formulae can be regarded as derived from tremolite and common hornblende respectively by the addition of Na on the A site and the substitution of Al for Si. The end members common hornblende, tschermakite, edenite and pargasite, and intermediate compositions can be collectively termed hornblendes. In these calcic amphiboles Ca occupies W site; Ca also predominant over Na. Fe^{+2} cations in Y site ranges from 0.8755 to 1.9565 per formula unit, and Mg ranges from 2.9521 to 4.0930 per formula unit.

Ca in amphibole analyses ranges from 1.8586 to 2.2432 per formula unit while Na ranges from 0.0574 to 0.3106 p.f.u.

5.1.8 Opaque Minerals

Opaques are important minerals observed in all rock types of the study area as essential and accessory constituents.

The microprobe analyses and structural formulae based on 4oxygen. The opaques are presented in table 5.5. According to trivalent ion (Fe^{+3}) magnetite series includes magnesioferrite (Mg), Magnetite (Fe^{+2}), Franklinite (Zn), Jacobsite (Mn) and Trevorite (Ni). Haematites and ilmanites are also characterized by microprobe analyses.

The ideal composition of hematite is Fe_2O_3 , but a small amount of MnO and FeO may be found, while any appreciable SiO_2 and Al_2O_3 probably represent impurities.

The formula of ilmanite may be expressed as $(\text{Fe}, \text{Mg}, \text{Mn}) \text{TiO}_3$ with only a limited amount of Mg and Mn. The magnetite series may be expressed as $\text{Fe}^{+2}\text{Fe}^{+3}_2\text{O}_4$. Silica (0.0277p.f.u) and aluminum (0.1058p.f.u) in sample S_{2a} and KT9 respectively.

Fe contains in opaque ranges from 2.4377 to 3.9979 per formula unit and Mn ranges from 0.0005 to 0.0024per formula unit while Zn ranges from 0.0004 to 0.0094p.f.u. Cr content ranges from 0.0008 to 0.0014p.f.u. and V ranges from 0.0001 to 0.0002 p.f.u. Ti content found in two samples as 0.009 and 0.0365p.f.u.

5.2 Phase petrology

It has been realised that the mineral assemblages of metamorphic rock may reflect the approach of chemical equilibrium during the formation. The distribution of elements in the coexisting minerals should be systematic if they attained chemical equilibrium. These crystallized minerals also show a systematic chemical variation in their composition. Such variation in their mineral chemistry indeed reflects the physical condition of metamorphism and the mineral paragenesis reflects a unique phase compatibility relation, in the P-T space.

The analysis of co-existing minerals and the phase compatibility relationships in pertinent system have been used to provide data about nature and tendency of equilibrium and also help to deduce the P-T-X conditions during metamorphism. Thus, we can find out unique pigeonhole on the basis of mineral parageneses depicted in the petrogenetic grids, which provide informations about the metamorphic evolution. Today the concept of petrogenetic grid is too advanced in comparison to Bowen (1940), who first proposed the concept of grid with univariant reaction curves bounding all the conceivable divariant mineral assemblages for a particular bulk chemical composition.

In this chapter an attempt has been made to discuss the mineral parageneses, P-T conditions and phase compatibility relationships of different assemblages obtained from the petrography, textural relationship and mineral chemistry of the gneisses, amphibolites, mafics and ultramafics and B.M.Q. meta-volcano-sedimentaries of the study area. The phase petrology and involved metamorphic reactions of different metamorphism are discussed in the following paragraphs.

A detailed study of the metamorphosed pelitic, psammitic and mafic rocks of the study area indicate progressive increase in the grade of metamorphism from north to south across the Babina-Mauranipur transect. Owing to the problems of the multiphase metamorphism & deformation, an attempt has been made first time in entire Bundelkhand massif to delineate the type of metamorphism and metamorphic conditions of each episode in Newer Metamorphic Group (NMG) and also in the Older Metamorphic Group (OMG) of the area.

A metamorphic zone is characterized by the presence of specific index minerals or a set of minerals formed under a definite pressure, temperature conditions from an appropriate rock composition. The investigated area comprises two groups of rocks of which were subjected multi episode of metamorphism:

5.2.1 Phase relationship in older metamorphic group

The rocks of OMG, exposed around Babina, Gora, Prithivipur and Mauranipur comprise biotite gneisses, granite-gneisses, tonalite gneisses, trondhjemite gneisses, hornblende-biotite gneisses and amphibolites. These Achaean rocks were tectonically deformed, metamorphosed and subsequently emplaced by different episodes of granitoids and finally subjected to low-grade retrograde metamorphism. The detailed petrographic study on different foliation planes with chronological events of deformations revealed at least two phases of metamorphism in OMG. The early phase metamorphism was very high-grade as evident by complete absence of prograde muscovite chlorite, kyanite and epidote minerals and presence of cordierite, sillimanite, perthite, and diopside. The presence of tonalite-gneisses and their intermingled relationship with other gneisses in the field, points that regional metamorphism was coterminous with TTG. The geochronological study suggests the formation of TTG around 3300 Ma (Mondal et al 2002}. Since the crystallized minerals of the metamorphics are aligned on S_1 and S_2 planes developed during the D_1 & D_2 deformations and have similar structural trend as that of TTG, it can be concluded that a tectonothermal event should be required at Mid-Archaeon for the metamorphism of OMG. Basu (2001) and Sharma (1988) has also been suggested similar view. The second episode of metamorphism in the TTG & granite gneisses of OMG is mainly confined to the shear zones and is low grade to very low grade may be possibly contemporaneous to east-west trending shear zone and may be considered as a retrograde event. The mylonitised and sheared rocks have been recorded from the gneisses, granite, migmatites, amphibolites and hornblende, biotite gneisses. During the mylonitisation, the chlorite-biotite microcline-albite-quartz and chlorite-biotite-epidote, chlorite-chloritoid-magnetite assemblages were developed in shear zones trending in E-W direction along the mylonites foliation planes related to D_4 deformation (Table 2.6).

The first phase of metamorphism possibly initiated at deformation D_1 . In general, rocks associated with the F_1 , F_2 , and F_3 folds observed in the gneisses are responsible for the development of gneissic foliation in the pelitic, psammitic and mafic rocks which are defined by the orientation of flaky minerals and elongated plagioclase and needles of magnetite. This episode of metamorphism is further subdivided into two stages (i) formation of gneisses and amphibolites (ii) anatexis migmatite, granite-gneisses, granulites, tonalite, and trondhjemite. The detailed mineral assemblages of gneisses and amphibolites are listed in chapter-III.

- (i) Biotite-K-feldspar-perthite-quartz.
- (ii) Biotite-plagioclase-K-feldspar-antiperthite quartz.
- (iii) Garnet-biotite-K-feldspar-quartz.

Assemblages in amphibiotites and hornblende biotite gneisses:

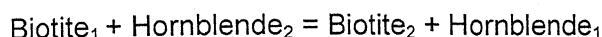
- (i) Hornblende - clinopyroxene - biotite - plagioclase - K-feldspar - quartz.
- (ii) Hornblende - biotite - K - feldspar - plagioclase - quartz.
- (iii) Hornblende - clinopyroxene - plagioclase - quartz.
- (iv) Hornblende - plagioclase - K - feldspar - quartz.
- (v) Hornblende - garnet - plagioclase - K - feldspar - quartz.

The TTG, which includes both tonalite and Trondhjemite-rocks, contain significant amount of K-feldspar, antiperthite, plagioclase, perthite, biotite, and quartz with minor amount of ilmanite, apatite, zircon, sphene, spinel etc. The muscovite and clinopyroxene are completely absent in TTG. The hornblende has been noticed in minor amount in most of the TTG rocks.

The biotite-gneisses consist mainly of biotite, quartz, plagioclase and K-feldspars. The zircon and apatite are present in the significant amount in all the rock samples. The perthite and antiperthite texture are also present in the gneisses. The garnet and sillimanite reported by earlier workers from the Kabrai area (Saxena 1961) could not be obtained in the present investigated area. The absence of the garnet and sillimanite may be possibly due to composition variation. It is very significant that muscovite as prograde or retrograde phase is completely absent from the gneisses.

The mineral assemblages of these rocks can be portrayed in AKF diagram and explained through six components in the KFMASH system. The AKF diagram shows three phases fields of garnet, biotite and K-feldspar (Fig 5.5b). The K-feldspar - biotite join defines the two-phase field for non-garnetiferous gneisses. The mineral assemblages of tonalite and trondhjemite gneisses may be treated in K_2O , FeO , MgO , SiO_2 , CaO , Al_2O_3 and H_2O (CNKF MASH) system and portrayed in the AFM diagram (Reinhardt Projection) with FeO and MgO as separate component and as plagioclase. Thus the phase compatibility relationship can be better represented by AFM projection from plagioclase (Fig 5.6). The advantage of this projection is that the tie lines connecting hornblende, clinopyroxene and biotite composition of the three coexisting phases form triangle, enclosing the field of composition of three mineral associations having the fixed composition. The common presence of hornblende-clinopyroxene-biotite phase may be due to large field with variation in the bulk composition of rock and minerals in these three co-existing minerals may be considered as continuous reaction in the CFMASH system between hornblende and biotite at variable pressure and temperature. The presence of corroded biotite in the hornblende and clinopyroxene, and similarly presence of corroded hornblende in the biotite and clinopyroxene from the hornblende-biotite gneisses

discussed in the chapter III may be attributed to the break down of the biotite and hornblende by the following continuous reaction in CFMASH system and portrayed in AFM diagram (Fig 5.6).



The composition of the hornblende lies between the biotite - clinopyroxene lines (Fig.5.6). Therefore the appearance of hornblende may be due to the following reaction in the CNFMASH system and described in Fig 5.6:



The composition of the orthopyroxene lies on the tie line of the biotite - clinopyroxene in the A'-F-M projection (Fig 5.6) in the system KNCFMASH (Reinhardt 1967). The absence of this mineral from all the hornblende-biotite gneisses and biotite-gneisses may be due to either low silica content or due to strong retrograde metamorphism of hornblende biotite-gneisses or inappropriate fluid activity. The absence of garnet from these gneisses may be considered due to the non-availability of appropriate bulk composition and high K_2O and Al_2O_3 .

The enclaves of amphibolites are very common in the gneisses. Sometimes they are co folded with biotite gneisses. The petrography studies reveal that phlogopite, epidote, tremolite, chlorite, actinolite, etc. are completely absent. While diopside, calcite, plagioclase, hornblende are present as medium to coarse grained texture. The absence of garnet from the basic gneisses may be due to high MgO , K_2O and low Al_2O_3 . The common presence of plagioclase, hornblende, and diopside assemblages can be explained in three-phase field of ACF diagram (Fig 5.5a) in CFMASH system. The other compatible assemblages hornblende-plagioclase-magnetite \pm quartz and diopside - hornblende - magnetite \pm quartz can be also explained in ACF diagram in six component system of CFMASH system.

5.2.2 Phase relationships in newer metamorphic group

The rocks of this group comprises three important litho-units (i) mafic and ultramafic rocks, (ii) Quartzites and banded magnetite quartzite (BMQ) and (iii) Metavolcanic rocks and recrystallised mylonites. All these rocks are characterized by S_1 and S_2 schistosity and metamorphism has hardly been reached to lower amphibolite facies. The low-grade metamorphism has been encountered in the mafic and ultra mafic rocks exposed at the south of BMQ, while slightly higher-grade metamorphism has been noticed in the quartzite and BMQ. The low-grade metamorphisms specially, the thermal imprints have been recorded in the metavolcanic and mylonite rocks lying above the BMQ

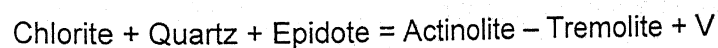
at the northern part of the NMG, where porphyritic granitoids are found as intrusives. In the preceding paragraphs phase relations of both the types of metamorphism have been discussed on the basis of mineral assemblages, field relationships low-grade regional metamorphism and low-grade thermal metamorphism.

5.2.3 Prograde regional metamorphism (M_2)

The first phase of metamorphism in the mafic and ultramafic, metasedimentary rocks was possibly initiated at the D_3 deformation (Table 2.6), which is characterized by the increase in load pressure and rise in geotherms. In general, this prograde metamorphism (M_2) in mafic, ultramafic and metasedimentaries observed at Babina is responsible to the development of the S_1 foliation. This is defined by the orientation of flaky minerals viz. muscovite, chlorite, talc, biotite, amphiboles and epidote.

The appearance of talc, chlorite, tremolite, actinolite in the ultramafic rocks and actinolite, commingtonite grunerite, hornblende, epidote, garnet, chlorite, biotite in the mafic rocks points that metamorphism has reached upto the green-schist to lower amphibolite facies conditions. The mafic and ultramafics along with Banded-magnetite-quartzite is known to all but no attempt was made to evaluate the metamorphic zone and the reaction isograd of different phases of metamorphism in the entire Bundelkhand craton. In the present study geothermometry for the pressure-temperature conditions metamorphism, demarcation of metamorphic zones type of metamorphism and metamorphism phase relationship have been discussed for first time each metamorphic episode and is correlated with the experimentally determined curves.

The ultramafic-mafic rocks occur at the contact of sheared gneisses. The beginning of the chlorite and talc from the lower unit of the ultramafic and also from shear zone may be define by the following reactions in CFMASH system and portrayed in ACF diagram (Fig 5.7a)



By these reactions, progressive regional metamorphism possibly proceeded to higher temperature. The transition of the green schist facies to subgreen schist facies is marked by the first appearance of diagnostic assemblage, actinolite + epidote in the presence of chlorite+ albite + quartz in the basic rocks and tremolite-actinolite-talc-chlorite \pm epidote in the ultramafic rocks. The presence of chlorite-epidote – actinolite / tremolite-quartz assemblage clearly suggests the appearance of green schist facies.

Since no diagnostic mineral to delineate the chlorite-epidote subfacies and biotite-epidote subfacies of green schist facies classification has been discussed or proposed for the mafic and ultramafic rocks, both the subfacies have been considered here as lower green schist facies. The following mineral assemblages have been observed in the lower green schist facies:

- I. Epidote – chlorite – actinolite/tremolite – albite – magnetite – quartz
- II. Chlorite – actinolite – tremolite – magnetite \pm quartz \pm albite
- III. Actinolite – tremolite – talc – chlorite \pm quartz \pm serpentine \pm biotite
- IV. Talc – tremolite \pm quartz
- V. Talc – chlorite \pm quartz \pm magnetite \pm phlogopite

All the above assemblages have been reported for the first time from the ultramafic rock found immediately at the contact of gneisses in Babina-Mauranipur transect.

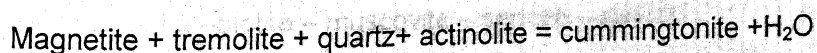
With further increase in temperature, the prograde metamorphism proceeded by the appearance of hornblende mineral in the assemblages : epidote-hornblende-chlorite-albite-quartz and actinolite-tremolite-chlorite-quartz-magnetite. The appearance of hornblende can be attributed to the following reaction in the six-component system (CFMASH system) and can be portrayed in ACF diagram (Fig 5.7b).



The aforesaid terminal reaction can be explained in ACF diagram (Fig 5.7b) for the beginning of almandine-albite-epidote zone of green schist facies. In this zone, following mineral assemblages have been obtained from the study area.

- I. Epidote – hornblende – chlorite-quartz \pm magnetite
- II. Epidote-actinolite-tremolite-hornblende-albite-magnetite \pm quartz
- III. Actinolite / tremolite – chlorite-hornblende – magnetite – quartz.

The appearance of cummingtonite, grunerite in the presence of the tremolite / hornblende and sometimes clinopyroxene marks the beginning of amphibolite facies metamorphism. The beginning of this transition zone has been demarked at the base limit of the BMQ. The appearance of the cummingtonite, actinolite, and clinopyroxene minerals may be attributed to the following reactions in the CFMASH system and may be explained in ACF diagram (5.8a).



The following mineral assemblages have been reported from this transitional facies:

- I. Actinolite – tremolite – cummingtonite-magnetite-quartz.
- II. Cummingtonite-magnetite – quartz
- III. Chlorite – cummingtonite – actinolite / tremolite – quartz
- IV. Hornblende – actinolite – cummingtonite – chlorite – magnetite

The presence of assemblages garnet – hornblende plagioclase – quartz, hornblende- garnet-cummingtonite-magnetite-quartz and hornblende-actinolite / tremolite – plagioclase – quartz from the upper part of the iron formation suggest that metamorphism has reached up to staurolite – biotite subfacies of amphibolite facies. These assemblages have been portrayed in the ACF diagram (Fig 5.8b) and defined in CFMASH system.

5.2.4 Phase relationship in recrystallised mylonites and metavolcanics

The northern part of the NMG comprises a thick sequence of metamorphosed mafic and felsic volcanic rocks along with thick mylonites of shear zone. The medium grained porphyritic granite has been found as intrusive in this tectonic unit. Due to the emplacement of the plutonic granites along the shear zones, the earlier signatures of deformation of shear zone and the metamorphism have almost disappeared. The mylonites and shear zone were subjected to recrystallization after the thermal effect.

As a result, sheared unit comprises a very heterogeneous bulk composition and mineralogy as well. The entire sequence is characterized by different type of hornfelsic texture viz. radiating plagioclase and actinolite, mortar texture at places. The overgrowth textures of the feldspar quartz, and hornblende have been also recorded.

A careful study reveals that this unit has a mild effect of the low-pressure temperature metamorphism in general. The following mineral assemblages have been obtained which are portrayed in the ACF and AFM diagrams (Fig 5.9 a, b, c) in the CFMASH and KFMASH systems.

- (i) Andalusite – epidote – chlorite – quartz – albite
- (ii) Epidote – chlorite – chloritoid – quartz
- (iii) Epidote – actinolite – chlorite – quartz
- (iv) Andalusite – chloritoid – epidote – muscovite – quartz
- (v) Chlorite – biotite – muscovite – sericite – quartz

Table 5.1 : Microprobe analyses and structural formulae of Biotite.

Sample No	1	2	3	4	5	28 (I)	28 (II)
SiO ₂	38.55	37.58	36.61	35.11	35.30	24.898	23.656
TiO ₂	3.26	2.88	3.14	3.09	3.15	0.291	0.599
Al ₂ O ₃	15.53	15.50	14.85	14.11	14.72	18.322	17.438
FeO	21.77	21.63	23.48	23.13	23.01	36.928	39.510
MnO	0.32	0.36	0.41	0.47	0.39	0.770	0.785
MgO	7.97	8.60	7.43	7.24	7.33	2.636	2.916
CaO	0.02	0.02	0.03	0.02	0.04	0.123	0.124
Na ₂ O	0.16	0.10	0.20	0.19	0.00	-	-
K ₂ O	9.79	9.91	9.61	9.77	9.65	1.837	1.10
Total	97.37	96.59	95.75	93.12	93.60	85.805	86.130
<div> <div>←</div> <div>11 Oxygen basis</div> <div>→</div> <div>←</div> <div>22 Oxygen basis</div> <div>→</div> </div>							
Si	2.90	2.86	2.84	2.82	2.81	4.5877	4.4129
Al ^{IV}	1.10	1.14	1.16	1.18	1.19	3.4133	3.5871
ΣZ	4.00	4.00	4.00	4.00	4.00	8.00	8.00
Al ^{VI}	0.28	0.25	0.20	0.16	0.20	0.5661	0.2571
Fe ⁺³	0.21	0.13	0.05	0.03	0.01	-	-
Ti	0.18	0.17	0.18	0.19	0.19	0.0403	0.0841
Mg	0.89	0.98	0.86	0.87	0.87	0.7241	0.8109
Mn	0.02	0.02	0.03	0.03	0.03	0.1202	0.124
Fe	1.15	1.24	1.47	1.53	1.53	5.6906	6.164
Σ	2.73	2.79	2.79	2.81	2.83	7.1413	7.4401
Ca	0.00	0.00	0.00	0.00	0.00	0.0242	0.0249
Na	0.02	0.01	0.03	0.00	0.00	-	-
K	0.94	0.96	0.95	0.98	0.98	0.4317	0.2618
Σ	0.96	0.97	0.98	0.98	0.98	0.4559	0.2867

Table 5.2 : Microprobe analyses and structural formulae of Muscovite

Sample No	28 (I)	28 (II)	27(I)	27(II)	27(III)
SiO ₂	49.246	48.043	45.468	47.499	49.699
TiO ₂	0.039	0.097	0.039	0.129	0.023
Al ₂ O ₃	35.462	35.289	34.224	34.865	35.396
FeO	2.717	3.227	2.834	3.069	3.015
MnO	0.020	-	0.009	0.026	0.057
MgO	-	0.080	0.200	0.169	0.262
CaO	0.100	0.087	0.173	0.178	0.057
Na ₂ O	0.103	0.364	0.132	0.121	0.023
K ₂ O	7.653	8.047	8.690	8.186	5.240
Total	95.341	95.234	91.769	94.242	93.692

24 Oxygen basis

Si	7.0085	6.9041	6.81925	6.9005	7.0855
Al ^{IV}	0.9915	1.0959	1.1808	1.0995	0.9145
ΣZ	8.00	8.00	8.00	8.00	8.00
Al ^{VI}	4.9012	4.8218	4.8100	4.8123	4.9771
Fe ⁺²	0.3232	0.3877	0.3551	0.3727	0.3589
Mn	0.0017	-	0.0009	0.0026	-
Mg	-	0.0164	0.0441	0.0357	0.0548
Ti	0.0034	0.0103	0.0036	0.0139	0.0017
ΣY	5.2295	5.2362	5.2137	5.2372	5.3925
Ca	0.0145	0.0129	0.0270	0.0270	0.0085
Na	0.0272	0.100	0.0378	0.0330	-
K	1.3888	1.4748	1.6620	1.5172	0.9526
ΣX	1.4305	1.5877	1.7268	1.5772	0.9611

Table 5.3 Microprobe analyses and structural formulae of Chlorite

Sample No	28
SiO ₂	21.660
TiO ₂	0.048
Al ₂ O ₃	18.930
FeO	42.578
MnO	0.832
MgO	2.731
CaO	0.109
Total	86.889
28 Oxygen basis	
Si	5.1680
Al ^{IV}	2.8320
ΣZ	8.00
Al ^{VI}	2.4377
Feldspar	8.4963
Mg	0.9708
Mn	0.1677
Carlsbad twinning	0.0272
Ti	0.0086
Σ	12.1083

Table : 5.4 : Microprobe analyses and structural formulae of Amphibole

Sample No	S2A	28	J3C	28(I)	S2A(I)	S2A(II)	J3C(I)	J3C(II)
SiO ₂	49.091	48.560	47.495	47.126	51.060	45.663	45.020	45.512
TiO ₂	0.444	0.306	0.414	0.653	0.262	0.523	0.723	0.736
Al ₂ O ₃	8.649	5.718	5.333	6.674	4.812	8.432	7.017	7.499
FeO	7.340	7.456	12.486	13.029	6.853	7.963	13.391	13.823
MnO	0.160	0.203	0.291	0.261	0.287	0.135	0.328	0.300
MgO	17.067	17.619	14.360	13.233	17.863	16.591	13.151	12.352
CaO	12.028	11.929	12.565	12.279	11.964	11.792	11.981	12.154
Na ₂ O	0.698	0.675	0.243	0.366	0.543	1.022	0.638	0.729
K ₂ O	0.115	0.075	0.201	0.370	0.064	0.21	0.538	0.511
Total	95.593	92.541	93.388	93.992	93.708	92.331	92.987	93.616
24 Oxygen basis								
Si	7.0791	7.5818	7.5598	7.1485	7.8064	7.1977	7.8680	7.2989
Al ^{IV}	0.9209	0.4182	0.4402	0.8515	0.1936	0.8023	0.1320	0.7011
ΣZ	8.00	8.00	8.00	8.00	8.00	8.00	8.00	8.00
Al ^{VI}	0.5492	0.6205	0.545	0.3417	0.6649	0.7486	0.0135	0.7015
Ti	0.0482	0.0355	0.0478	0.0745	0.0293	0.0615	0.0945	0.0886
Fe ⁺²	0.8852	0.9715	1.6555	1.6529	0.8755	1.0494	1.9565	1.8534
Mg	3.6689	4.0930	3.4066	2.9922	4.0699	3.8967	3.4246	2.9521
Mn	0.0195	0.0262	0.0382	0.0336	0.0367	0.0179	0.0483	0.0404
ΣY	5.171	5.7467	5.6931	5.10	5.6763	5.7741	5.5369	5.6360
Ca	1.8586	1.9926	2.1435	1.9957	1.9596	1.9910	3.2432	2.0885
K	0.0211	0.013	0.0382	0.0717	0.0110	0.0416	0.1491	0.1040
Na	0.1952	0.2022	0.0574	0.1077	0.1598	0.3106	0.2142	0.2254
ΣX	2.0749	2.2078	2.2391	2.17	2.1304	2.3432	2.6065	2.4179

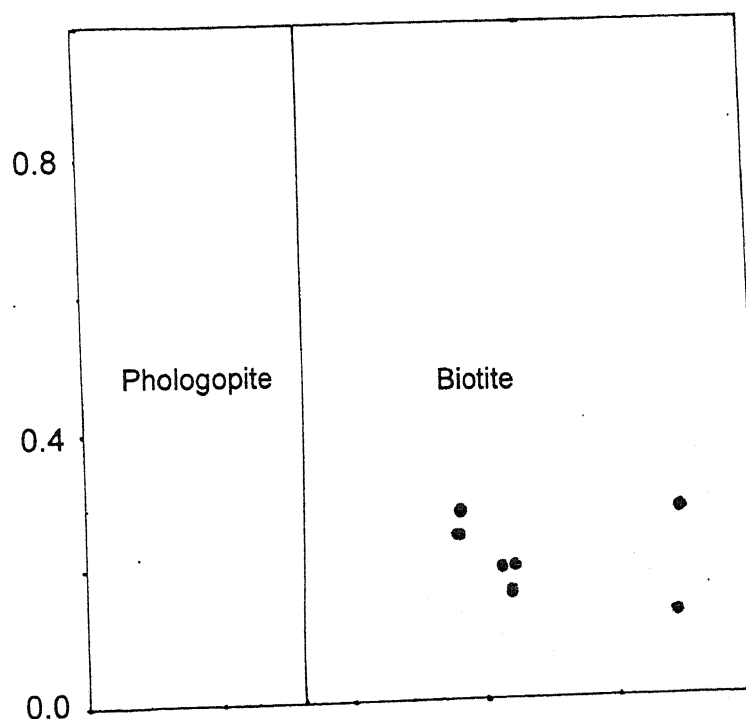
Table 5.5 : Microprobe analyses and structural formulae of Opaque Minerals

Sample No	S2A	KT9	28(I)	28(II)
SiO ₂	0.454	-	-	-
TiO ₂	-	0.989	-	0.021
Al ₂ O ₃	-	1.830	-	-
FeO	76.745	91.477	88.321	89.266
MnO	0.040	0.057	0.010	0.050
MgO	0.241	-	-	-
ZnO	0.046	0.260	0.010	0.020
Cr ₂ O ₃	0.027	0.037	0.019	0.01
V ₂ O ₃	0.002	0.004	0.001	0.002
Total	77.554	94.653	88.361	89.358

4 Oxygen basis

Si	0.0277	-	-	-
Al	-	0.1058	-	-
Fe	3.9165	3.7541	3.9979	3.9951
Mg	0.0219	-	-	-
Mn	0.0021	0.0024	0.0005	0.0023
Zn	0.0021	0.0094	0.0004	0.0008
Cr	0.0013	0.0014	0.0008	-
V	0.0001	0.0002	-	0.0001
Ti	-	0.0365	-	0.0009

SIDEROPHYLLITE
 $K_2Fe_5Al(Si_5Al_3O_{20})(OH)_4$



ANNITE
 $K_2Fe_6(Si_6Al_2O_{20})(OH)_4$

Fig 5.1 The EMPA data of the biotite are plotted in the four end member phlogopite, Annite, Siderophyllite and Eastonite. (Deer, Howie and Zussman , 1962). The data plots in the biotite field.

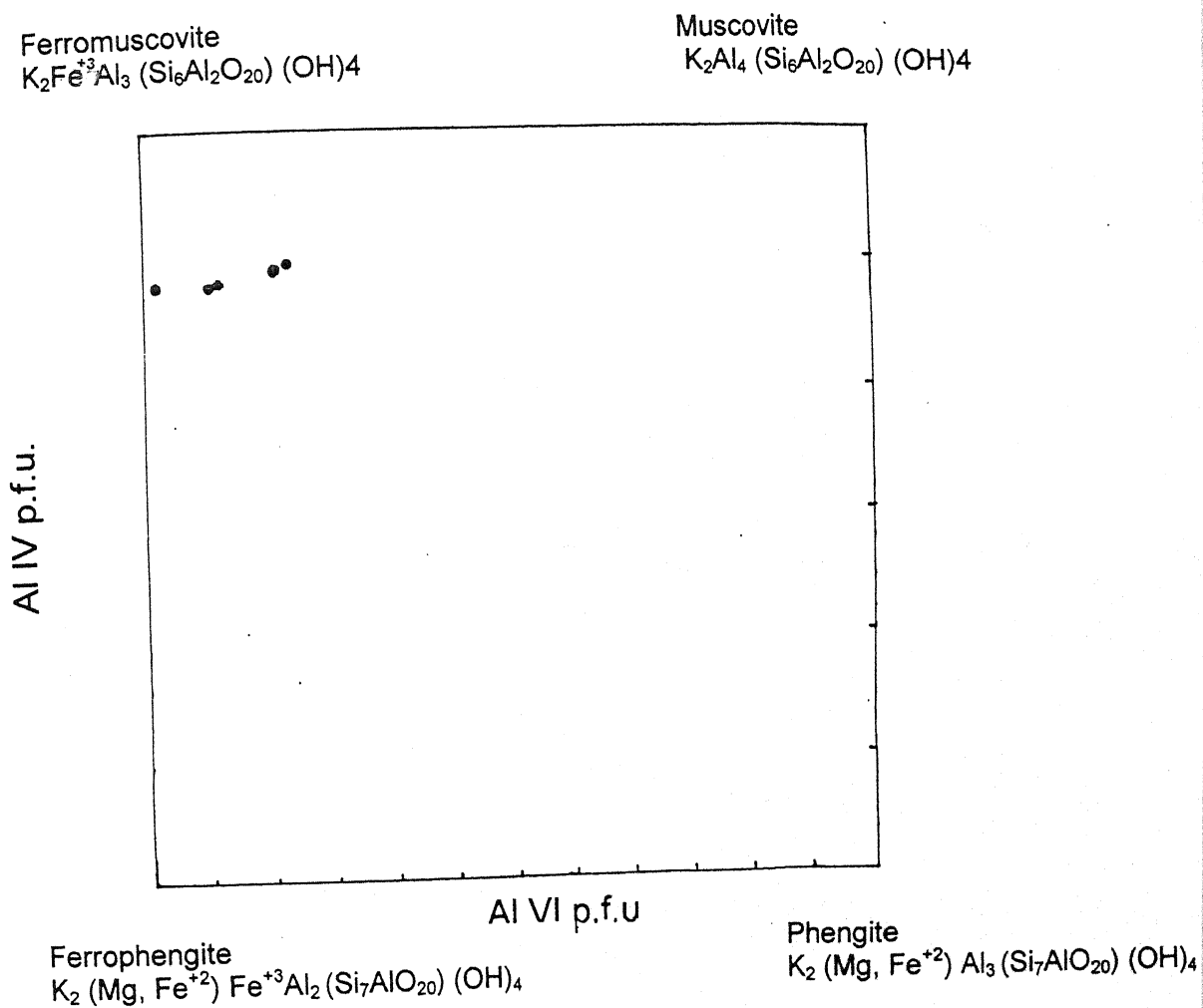


Fig 5.2 The EMPA data of muscovite of investigated area has been shown in Ferrophengite-phengite-muscovite and Ferromuscovite diagram (Deer, Howie and Zussman, 1962). The plotted data are closer to Ferromuscovite.

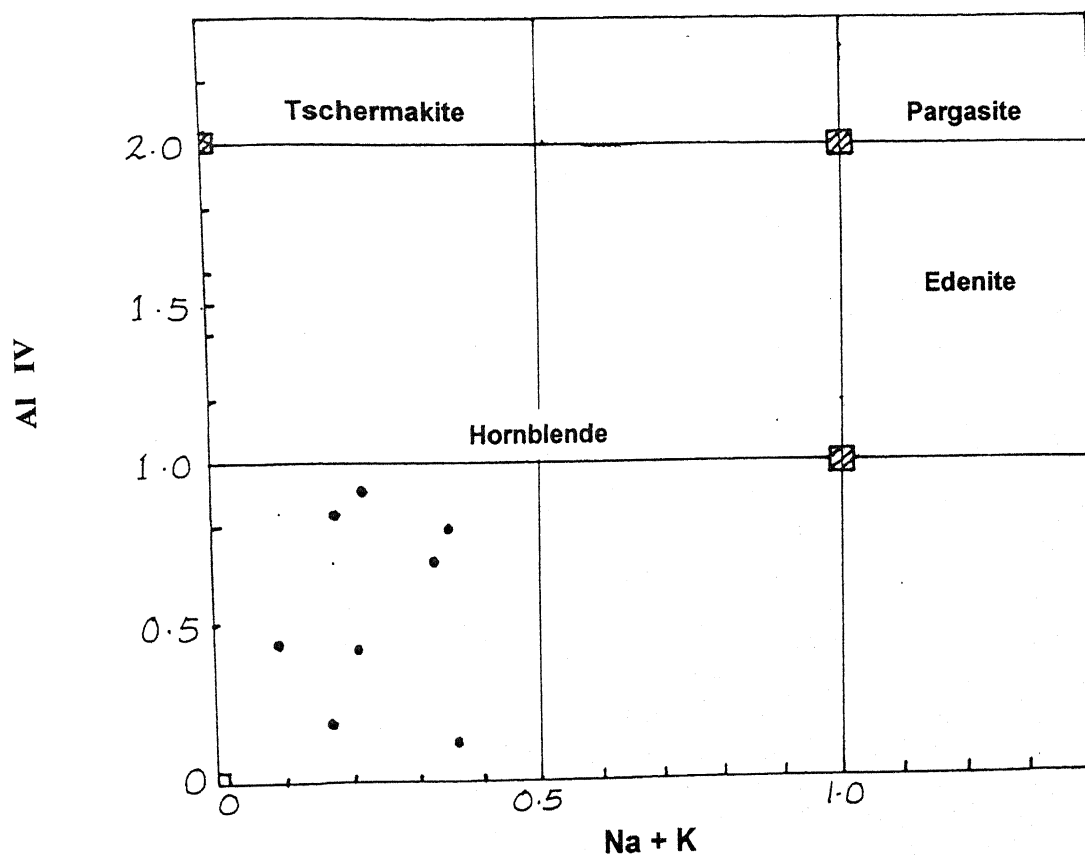


Fig. 5.3 The electron microprobe data of the investigated area are plotted in the amphibole diagram showing the range and composition of amphibole in the (Na + K) vs Al^{VI} diagram after Leake 1978.

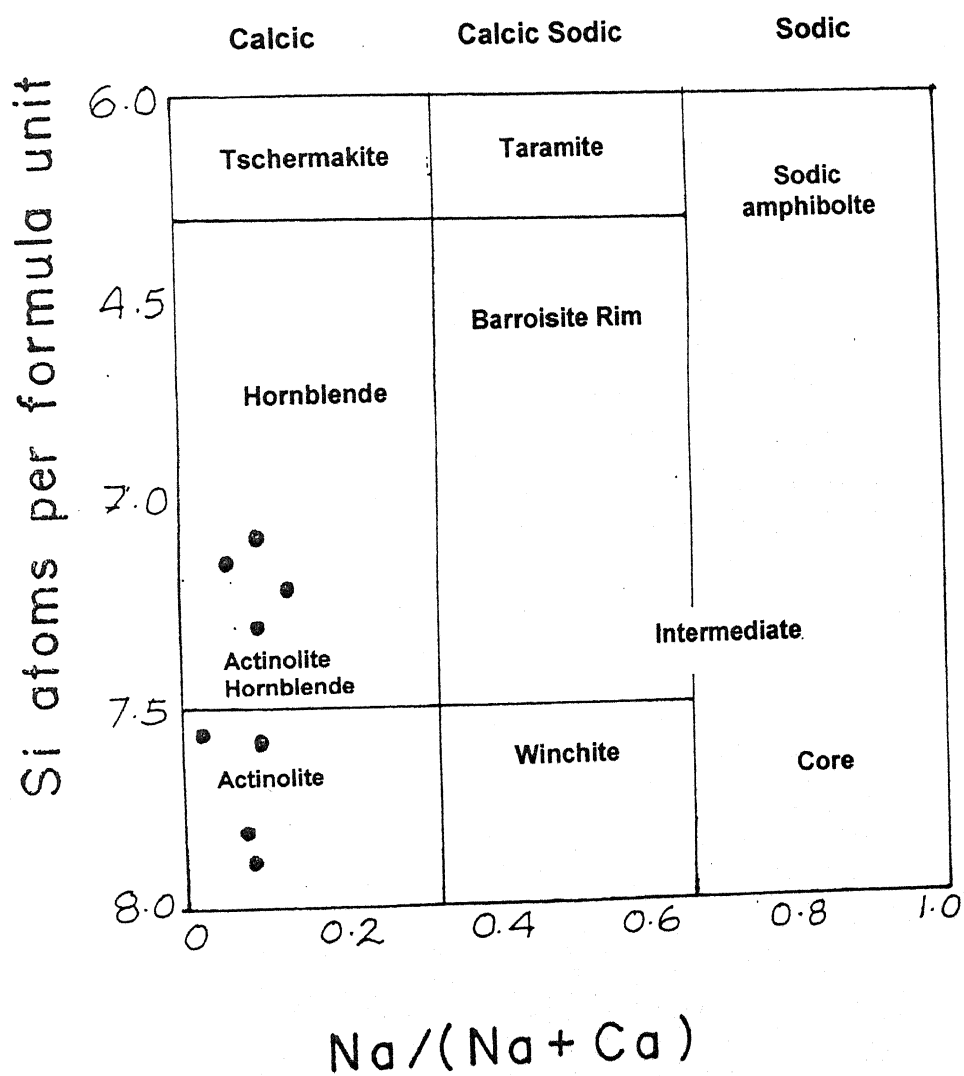


Fig 5.4 The EPMA data of amphibole from the investigated area is plotted on amphibole diagram (after Leake 1978). The plotted data showing that the amphiboles are initially actinolite in composition and systematically changes into actinolite-hornblende to hornblende.

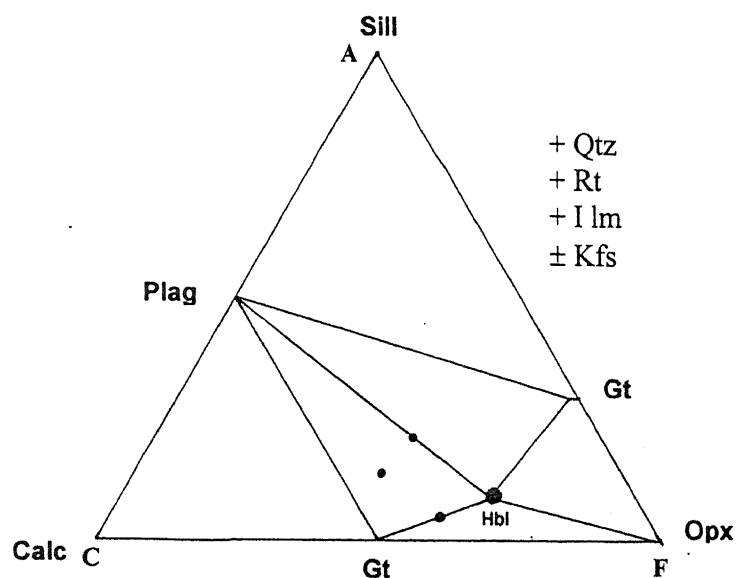


Fig 5.5 (a) The phase compatibility relation for amphibolites portrayed in ACF diagram. The solid circle represent the observed mineral assemblages, $A = (\text{Al}_2\text{O}_3 + \text{Fe}_2\text{O}_3) - (\text{Na}_2\text{O} + \text{MnO})$, $C = \text{CaO}$, and $F = (\text{FeO} + \text{MgO} + \text{MnO})$, $A + C + F = 100$ in mole percentage. Sill=Sillimanite, gt = Garnet, plag = Plagioclase, Hbl=Hornblende, Opx = Orthopyroxene, Qtz=Quartz, Rt= Rutile, Ilm = Ilmenite Kfs= K-feldspars.

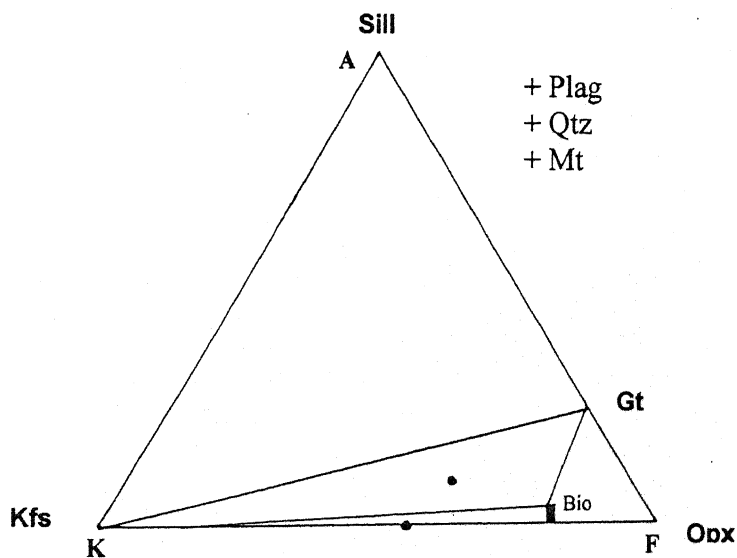


Fig 5.5 (b) Phase relations for biotite gneisses, tonalite, garnetiferous gneiss and TTG are shown in AKF diagram in the KFMASH system. The solid circles represent the observed mineral assemblages in these rocks of the study area. In the AKF diagram $A = (\text{Al}_2\text{O}_3 + \text{Fe}_2\text{O}_3) - (\text{K}_2\text{O} + \text{Na}_2\text{O} + \text{CaO})$, $K = \text{K}_2\text{O}$, $F = (\text{FeO} + \text{MgO} - \text{MnO})$, $A + K + F = 100$ in mole percent. Mt = Magnetite.

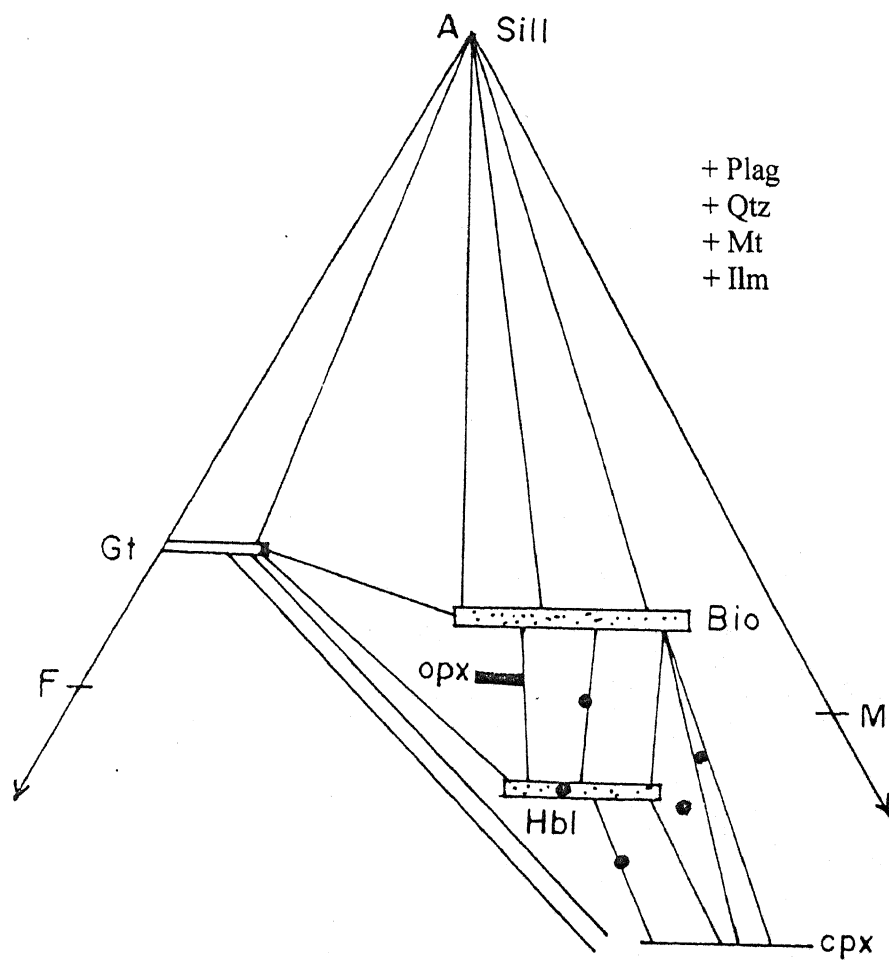


Fig 5.6. The phase relation for biotite-hornblende gneisses and amphibolites of OMG group are shown in A'FM projection diagram : The projection is from plagioclase in the tetrahedron AKFM in the system $\text{Na}_2\text{O} - \text{K}_2\text{O} - \text{CaO} - \text{FeO} - \text{Al}_2\text{O}_3 - \text{SiO}_2 - \text{H}_2\text{O}$ (NKCFMASH) proposed by Renard 1967). In the A'FM diagram $A' = (\text{Al}_2\text{O}_3 + \text{Fe}_2\text{O}_3) - (\text{K}_2\text{O} + \text{Na}_2\text{O} + \text{CaO})$, $F = \text{FeO}$ and $M = \text{MgO}$. The solid circles represent the observed mineral assemblages.

Sill = Sillimanite, G= Garnet, Bio= Biotite, Hbl = Hornblende, Cpx= Clinopyroxene, Opx= Orthopyroxene, Plag= Plagioclase, Qtz= Quartz, Mt= Magnetite, Ilm = Ilmanite.

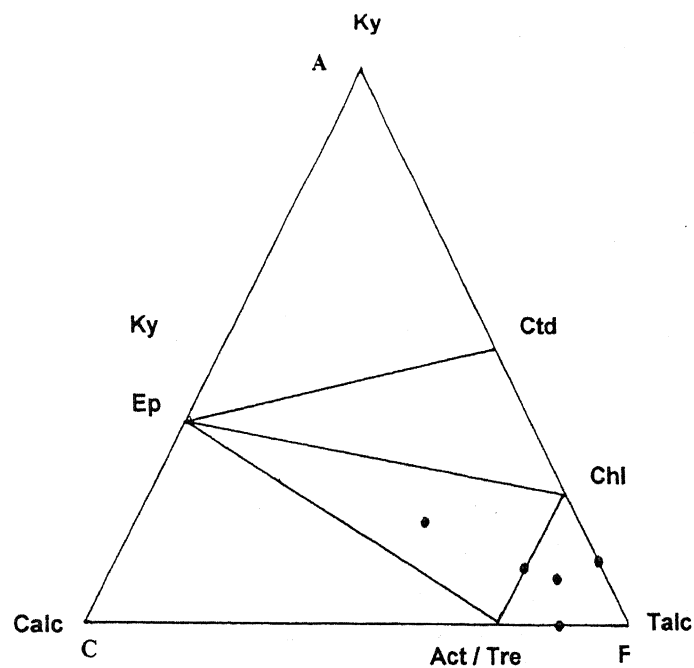


Fig 5.7 (a) Mineral assemblages of coexisting phases of mafics and ultramafics (low-grade metamorphites) are shown in CaO-MgO-FeO-Al₂O₃-SiO₂-H₂O (CFMASH) system through ACF diagram (Bowen 1940). The solid circles shown in bounded area by the tie lines represent the observed mineral assemblages.

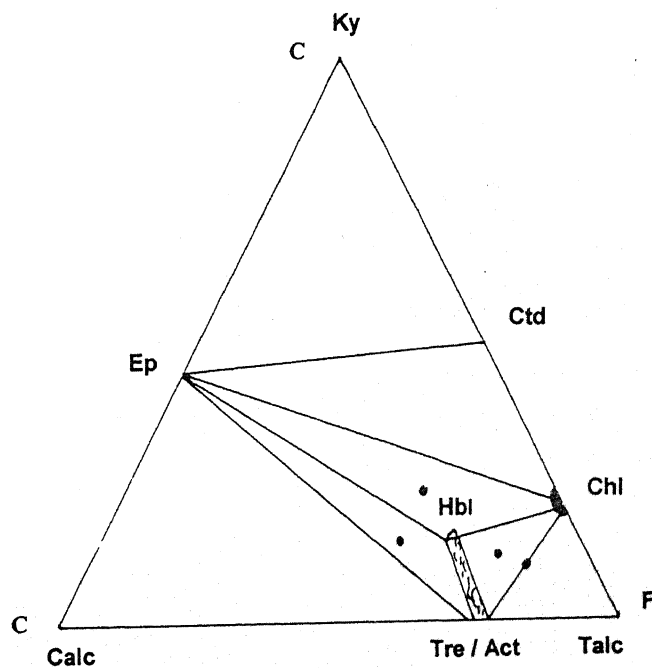


Fig 5.7 (b) The phase relationship for low-grade metamorphosed mafic and ultramafics are shown in ACF diagram. The solid circles represent the observed mineral parageneses in these rocks of study area. In the ACF diagram $A = (Al_2O_3 + Fe_2O_3) - (K_2O + Na_2O)$ and $F = (FeO + MgO + MnO)$ and $C = CaO$, $A + C + F = 100$ in mole percent.

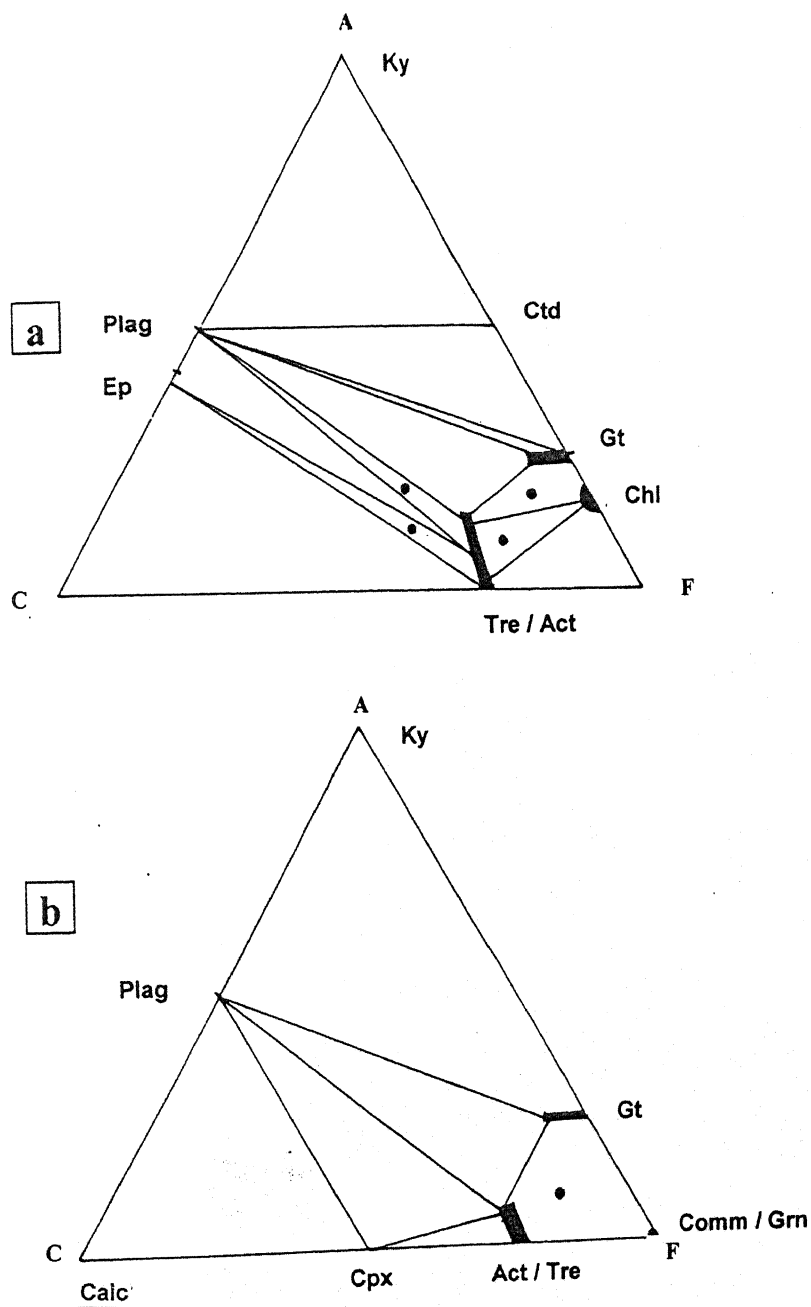


Fig. 5.8 The phase compatibility relations for metamorphosed low-grade schist portrayed in ACF diagrams (a and b) in the $\text{CaO-FeO-MgO-Al}_2\text{O}_3\text{-SiO}_2\text{-H}_2\text{O}$ (CFMASH) system. The solid circles represent the observed mineral parageneses in the study area, $A = (\text{Al}_2\text{O}_3 + \text{Fe}_2\text{O}_3) - (\text{Na}_2\text{O} + \text{K}_2\text{O})$, $C = \text{CaO}$ and $F = (\text{FeO} + \text{MgO} + \text{MnO})$, $A + C + F = 100$ in mole percentage.

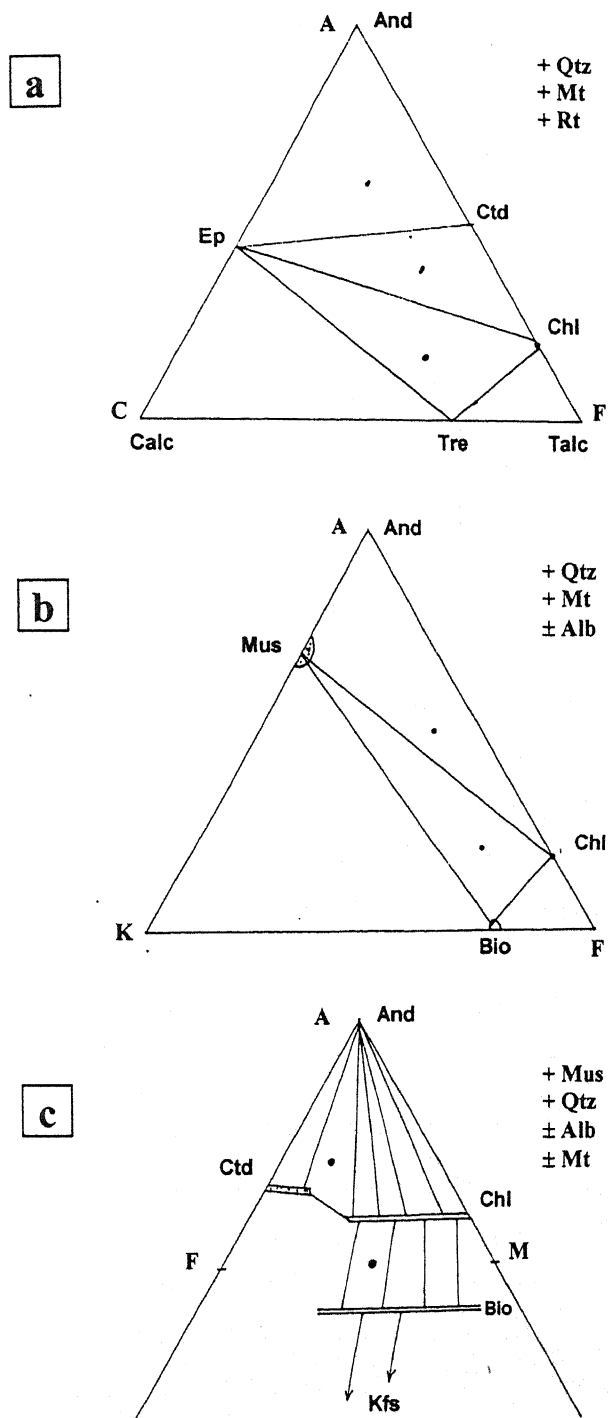


Fig 5.9 The phase relationship for mylonitised metavolcanics and recrystallised mylonites are shown in (a) ACF diagram (b) AKF diagram, and (c) AFM projection from muscovite. The solid circles represent the observed mineral assemblages in these rocks in the study area in the pertinent system. In the ACF, $A = (Al_2O_3 + Fe_2O_3)$, $C = CaO$ and $F = (FeO + MgO + MnO)$, in AKF diagram $A = (Al_2O_3 + Fe_2O_3)$, $K = K_2O$, $F = FeO + MgO + MnO$, $A + K + F = 100$ in mole percent. AFM projection $A = (Al_2O_3 + FeO - Na_2O - K_2O - CaO) / (Na_2O + K_2O + CaO)$, $F = FeO / (FeO + MgO)$ and $M = MgO / (MgO + FeO)$.

METAMORPHISM AND EARLY CRUSTAL EVOLUTION

A detailed study of the metamorphism of gneisses, TTG, quartzite, banded magnetite quartzite, mafic and ultramafic rocks of the area indicates a progressively increasing metamorphic grade from south to north. On the basis of structural trend, metamorphic conditions, mineral assemblages and field relationship, the metamorphites of the study area have been divided into two groups (1) Older metamorphic group and (2) New metamorphic group. Since the time of the first supracrustal formation, the Bundelkhand block was continuously subjected to deformations and thermal activities from the cratonic stage to continental growth. In the Bundelkhand craton, the early records is in the fragmented form due to these activities and the signatures of older events are either diminished or in the fragmentary form in most of the cratonic blocks. In spite of the problems of the superposition of the metamorphisms and deformation, an attempt has been made for the first time to delineate the metamorphic zones based on the index minerals and inferred assemblages from the OMG and NMG of the Bundelkhand craton.

6.1 Metamorphic zones

A specific mineral or a set of minerals formed under a definite P-T condition from an appropriate rock composition is characteristic of a metamorphic zone. Barrow (1912) mapped a sequence of zone of progressive metamorphism with the help of the first appearance of index mineral, in the order of increasing grade of metamorphism viz. chlorite, biotite, almandine, staurolite, kyanite and sillimanite. The present investigated area preserves an order of index minerals, chlorite, talc, biotite cummingtonite-grunerite, hornblende and almandine in the metamorphosed mafic and ultramafic rock sequences lying above the gneisses of the older metamorphic group (OMG). On the basis of texture, structure and mineral assemblages from petrographic studies following three metamorphic zones have been recorded in the area i.e. (i) Chlorite + biotite zone (lower green schist facies), (ii) almandine zone (upper green schist facies), and (iii) almandine- staurolite zone of green schist to lower amphibolite facies.

Due to lack of specific index minerals from chlorite and biotite zones of green schist, it has been considered as lower green schist facies in the present case. The common minerals of low-grade regional metamorphism are characterized by the abundance of green minerals viz. chlorite, epidote, actinolite, biotite, serpentine and talc. The mineral assemblages of these zones are as follows:

6.1.1 Chlorite - biotite zone (lower green schist facies)

1. Epidote – chlorite – actinolite – tremolite – albite – magnetite – quartz.
2. Chlorite – actinolite – tremolite – magnetite \pm quartz \pm albite.
3. Actinolite – tremolite – talc – chlorite \pm quartz \pm serpentine \pm biotite.
4. Talc – tremolite \pm quartz.
5. Talc – chlorite \pm quartz \pm magnetite \pm phlogopite.

6.1.2 Almandine zone (upper green schist facies) :

1. Epidote – hornblende – chlorite – quartz \pm magnetite.
2. Epidote – actinolite – tremolite – hornblende – albite – magnetite \pm quartz.
3. Actinolite / tremolite – chlorite – hornblende – magnetite – quartz.

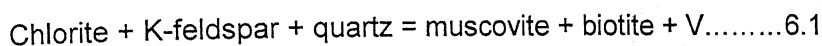
6.1.3 Staurolite – almandine zone (Lower amphibolite Facies)

This zone marks the beginning of the amphibolite facies and has the following mineral assemblages:

1. Actinolite – cummingtonite – tremolite – magnetite – quartz.
2. Cummingtonite – magnetite – quartz.
3. Hornblende – actinolite – cummingtonite – chlorite – magnetite.

The prograde metamorphism in metamorphic rock produces sequence of mineral assemblages that can be compared with metamorphic zones defined in ACF diagram in the CFMASH system. The characteristic assemblages in mafic and ultramafic rock are used for the identification of metamorphic facies and served as a reference frame for all rock composition. The diagnostic minerals for the different facies discussed in previous paragraphs and portrayed in figure 6.2. It is evident from observed assemblages that mafics and ultramafic rocks subjected to a prograde regional metamorphism on kyanite sillimanite type geotherm proposed by Winkler, (1979) and Miyashiro et al (1971). The diagnostic assemblage points that prograde metamorphism proceeded from the subgreen schist facies conditions to green schist facies and ultimately reached up to lower amphibolite facies environment. The transition of sub-greenschist to green schist facies is demarcated by the first appearance of diagnostic assemblage actinolite + epidote in the presence of chlorite, albite and quartz. The disappearance of prehnite and pyrophyllite could not be recorded from the mafic and ultramafics from the investigated area, which points that metamorphism, was above 300° C temperature below 6 Kbar pressure. The first occurrence of actinolite, epidote, chlorite, albite, quartz from mafic rocks and actinolite, chlorite, talc, \pm quartz from the ultramafic rocks define the beginning of green

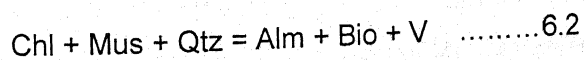
schist facies. The muscovite in general is phengite, which is the most common K-bearing mineral in the lower grade metamorphic rocks. It is also true that middle of green schist facies is characterised by the first appearance of biotite in the metamorphics replacing white mica. The appearance of biotite mineral can be defined by the following univariant reaction in the KFMASH system.



The first appearance of phlogopite (biotite) in prograde metamorphism & mafic and ultramafic rocks is characterized by green to light green in color. This is an indication of high Fe^{+3} in the biotite and due to continuous production of biotite, the potassium – white mica is depleted and ultimately diminished at 400°C to 450°C . The Stilpnomelane is another characteristic mineral of low-grade regional metamorphism, which has been reported from many low-grade iron rich ultramafics and sedimentaries. The presence of stilpnomelane in some of the thin sections of the study area is suggestive of regional metamorphism.

6.2 P-T Conditions

If it is assumed that mineral assemblages of different zones were formed at equilibrium, the P-T conditions of the metamorphism may be estimated either by the calibration of geothermobarometers of coexisting mineral phases in pertinent system or by comparing the natural assemblages with experimentally determined mineral equilibrium curves (Fig 6.1) or by both. The microscopic and other laboratory investigations of different metamorphic assemblages of the investigated area reveal that the rocks of NMG belong to green schist to lower amphibolite facies. The presences of index minerals like chlorite – talc, actinolite – talc, epidote – actinolite – chlorite, and hornblende – chlorite – actinolite – epidote in the mafic and ultramafics suggests that the area has undergone Barrovian type of the regional metamorphism (Fig.6.1). The inferred P-T conditions by the geothermometer model of Lal, 1991, for the above mineral assemblages yield 480 to 405°C temperature. The temperature conditions for the hornblende - chlorite – tremolite zone of upper green schist facies may be approximately estimated to be around 500°C comparing the experimental data on the reaction (6.2) suggested by Hirschberg and Winkler 1968, (Fig 6.2).



The experimental data for the first formation of biotite is attributed to the reaction: 6.1. The chlorite + sericite or chlorite + K-feldspars, reactants are not available. However, the appearance of biotite through the break down of Stilpnomelane in the presence of white mica from some of the BMQ is attributed to following reaction in FMASH system.

The stability of Stilpnomelane may be defined by experiment work for this reaction, which yields 350° C temperature and 4-7 Kb pressure (Winkler 1976).

The presence of garnet, cummingtonite, hornblende and plagioclase from some of the rocks of BMQ suggest that the regional metamorphism should have reached above the green schist facies conditions. Since the pelitic rocks (other than BMQ) are nearly absent from the entire sequence of NMG, the disappearance of the epidote and formation of the oligoclase in the presence of hornblende and coexistence of garnet, hornblende, chlorite may be considered as the beginning of amphibolite facies. Bucher and Frey (1994) suggested that reaction (6.3) consumed epidote and chlorite from the green schist facies and products anorthite component of plagioclase and tschermakite component of amphibole may be attributed to following the reaction.

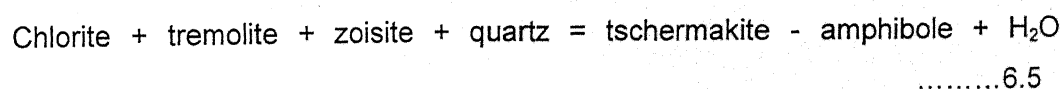


The product tschermakite component is consumed by the actinolite component of the amphibole. Similarly following reaction has been described for the formation edenite component of the amphibolite facies.



The combined effect of the reactions 6.3 and 6.4 suggest that the chlorite + epidote assemblage gradually disappears, plagioclase becomes increasingly calcic and amphibole systematically changes its compositions from actinolite to alkali and aluminum – bearing green hornblende as indicated by the mineral chemistry of amphibole (Table 5.4 and Fig 5.3).

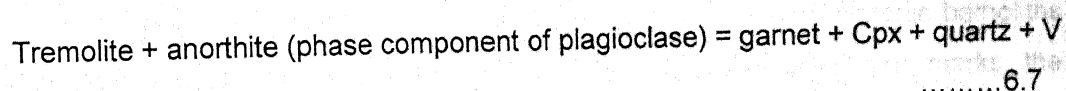
Garnet grew initially at the expense of chlorite, which can be explained by following reaction in CFMASH system. Decompositions of chlorite and epidote mineral contributed the bulk of the component of calcic garnet. Garnet may also appear at the transition phase of the amphibolite facies.



and



In metapelitic rocks of low-grade metamorphism the garnets are generally rich in manganese. The strong fractionation of Mn into garnet makes the mineral appear in mafic schists at temperature as low as 450°C. Winkler suggested that the following reaction consumes chlorite and epidote and produces garnet.



6.3 Evolution of Early Supracrustal Rocks of Bundelkhand Massif

It is merely described that Bundelkhand massif complex mainly comprises multiphase granitoids (Jhingran, 1958; Sharma, 1982; Sarkar et al; 1984; Basu, 1986) an intrusion of early Proterozoic age (Mondal et al.; 2002) and remnants of metamorphics of low and high- grade rocks of Archean. Five phases of granite emplacements have been suggested for this massif by Rahman and Zainuddin (1993), Mondal and Zainuddin (1996) and many others. The hornblende- bearing granitoids characterized by metaluminous composition is attributed to the oldest phase (Phase I) and is followed by biotite granites. It is supposed that granitic magma was perhaps generated by the partial melting of the early formed alkali felsic crust i.e. TTG (Mondal et al; 2002). The coarse grained porphyritic granite belongs to the third phase of emplacement intrusive into the older phases of granitoids. The leucogranites attributed to fourth and fifth phases of granite emplacement and are the youngest phase, characterized as paraluminous and monzo-to-syno-granites (Mondal and Zainuddin 1997). It is suggested (Mondal et. al; 2002) that the first three major phases of above granitoids were emplaced around 2500 Ma within a short time span. The discrimination diagrams (Fig 4.8, 4.10 and 4.15) and geochemical behaviors discussed in the previous chapter suggest that Bundelkhand granitoids are assigned to subduction and collision related mechanisms. Sharma and Rahman (1996) and Mondal et.al (2002) also indicated similar opinion and suggested that this event may be related to as continental welding and an event of cratonic growth and it's stabilization phase in Bundelkhand.

The granitoids occur over about 70% of total area of craton, therefore more attempts have been made for the evolution of Bundelkhand granitoids. The early geological records are nearly meager or nearly absent due to huge emplacement of granitoids. It is a fact that no serious attempt has been made for early geological history of the craton viz. what was before the granitoids and how was the continental crust. Perhaps Basu (1986) first described in detailed about the older xenoliths/enclaves (metasedimentaries and metamafigs) from the Bundelkhand craton. Later on Basu (2001) suggested that the older metamorphics present as a lensoidal body are aligned in specific orientation within the Bundelkhand granite. Sharma and Rahman (1995) first time described a complex evolutionary history of the Bundelkhand region extending from early Achaean to palaeoproterozoic in a systematic chronological order with little documents. They divided the cratonic history of Bundelkhand into three parts: (i) the highly deformed older gneissic-greenstone crust comprising amphibolites, quartzite, banded – magnetite – quartzite and calc-silicates rocks emplaced by syn-to-late alkaline to tonalitic granites around 3200 Ma, and 2700Ma. (ii) Undeformed multiphase granitoid plutonic batholiths (2500-2400Ma) emplaced into the early crust (granite-greenstone) and marks the

cratonization of Bundelkhand blocks and (iii) mafic dyke swarms, marked the tectonic rifting and extension as last phase of magmatism in the tectonically stabilized Craton.

This is established that the primitive continental crust gradually and gradually thickened and enlarged during the Archaean by rapid intrusive and extrusive mafic and ultra mafic activities. At the early Proterozoic time the continents were started to stabilize on the earth. As a result, about three quarters of the present area and volume of continents were formed by this time (Condie, 1983).

It has been also postulated by many workers (Windley 1983 and Condie, 1973) that first continents appeared in the Archaean were possibly small plates, which eventually converged to form the larger continent. Most of the exposed rocks of Archaean age in shield are metamorphics, reflecting the removal of the upper Archaean crust that once overlaid them. In many instances, these ancient metamorphic rocks preserve the faint signatures of sedimentary and volcanic features also, such as cross bedding, ripple marks, pillow structure (Gillen 1985). It is also supposed that tectonic activity then (at Archaean) may have been more marked, i.e. orogenic cycles completed relatively more rapidly than in more recent periods of earth history.

The Phanerozoic was a period of earth's history when large continents broke up, drifted apart and collided. Modern plate tectonic processes probably seems to become established during the Proterozoic but its mechanism in Archean can't be ignored (Condie 1973). Mountain chains and metamorphic belts were formed in collision zones and progressively younger orogenic belts were attached to the Precambrian cores or cratons as nucleous. Thus continents started to grow outwards as sedimentary basin around the early phase of cratonic event (Micro-continent/Proterozoic cratons) and subsequently, they closed, compressed and collided. Archean mountain belts contain metamorphics of mafic & ultramafic. The tectonic activities are related to high heat flow, which is the driving force of the earth's activity and heat generation. This was very high in the early stage and started to decline during the Proterozoic.

The recent geological studies (Gillen, 1985) reveal that Precambrian shield rocks were formed in two different metamorphic environments. The first is so called "greenstone belt" which was deformed and metamorphosed at relatively low grade and, secondly, the contrasting gneissic terrain, which is made up of granulites, granite-gneisses and migmatites that were formed at high temperature and pressure. The gneisses of these high-grade terrains were intensively deformed and crystallized at moderate to high pressure and temperature at the nucleous of the Achaeen shield. The greenstone belts have been reported from most of the cratonic areas of world, which were formed during the period 3500-3000/2700Ma ago. This belt is usually considered as a

long, narrow synform and marginal basin containing thick sequences of metamorphosed mafic and ultramafic, volcano sedimentaries and overlying sediments (Gillen, 1985). There are three major litho-units in all the green stone belts: (a) upper part: gray rocks, conglomerates, sandstones, banded ironstones (b) Middle part: andesitic volcanic rocks (c) lower part : basic to ultrabasic lavas. The ultra mafics lavas were probably derived from the mantle and are komatiitic in composition and characterised by spinifex texture. Mafic rocks of greenstone belt are mainly basalt, andesite and dacite, similar in composition to lavas of modern island arcs. The sedimentary of green stone belts were derived from granite-gneisses and volcanics.

In the Indian shield, the green stone has been reported from Dharwar, Singhbhum and Rajasthan cratons. Recently, it is assumed that Bundelkhand craton is another nucleus in the north of Sonata, which has its own continental growth and Precambrian crustal evolution. The available geo-chronological data, field evidences, various discrimination diagrams and geo chemical behaviors of major and trace elements discussed in previous chapters suggest that crustal growth of Bundelkhand craton occurred between middle Archaean to early Proterozoic i.e. 3300-2500 Ma and was related to green stone belt.

In the older metamorphic group of rocks tight to isoclinal, coaxial folds (F_1 & F_2) were developed possibly during the deformation D_1 and first phase of metamorphism that is followed by D_2 deformation (F_3 open fold) marks the post metamorphism. The first phase of metamorphism (M_1) was high-grade as evidenced by the complete absence of muscovite, chlorite, talc, kyanite, staurolite, tremolite and epidote from the gneisses and pelitic rocks of the study area. These rocks (OMG) are characterized by granulose texture where clinopyroxene, hornblende, perthite, biotite, sillimanite, orthopyroxene, garnet etc minerals were developed. M_1 metamorphism can be further be subdivided into two stages (i) formation of gneisses and amphibolites and (ii) migmatite stage anatexis, granulites, tonalite and trondhjemitic.

The TTG contains significant amount of K-feldspar, plagioclase, biotite and quartz, and minor amount of ilmenite, apatite, zircon, and sphene. The biotite gneisses contain biotite, quartz, plagioclase and K-feldspar with significant amount of zircon and apatite. Mishra and Sexena (1952) reported garnet and sillimanite from Kabrai area but it could not be found in the study area, possibly due to composition variation. It is worth mentioning that prograde muscovite, chlorite, staurolite, actinolite could be recorded from these rocks. Mineral assemblages in gneisses are biotite – K-feldspar – antiperthite + quartz, biotite-plagioclase – K-feldspar – quartz and in amphibolites and hornblende-gneisses are hornblende – clinopyroxene – biotite – plagioclase – K-feldspar – quartz and

hornblende – clinopyroxene – plagioclase – K-feldspar – quartz. The P–T conditions reveal that all the above mineral assemblages were developed between 650° C to 750° C temperature and 6 to 7 kbar pressure (Fig.6.2).

The observed mineral assemblages, petrochemistry and field relations from the study area are similar to other older crust. The geochronological study points that high-grade gneisses and granulite comprising meta-sediments and ultrabasic to basic igneous rocks along with tonalitic gneisses were crystallized at 3500-3200 M.a. It can also be inferred that the crystallized minerals of older metamorphics aligned on S_1 and S_2 planes in the gneisses and the mesoscopic structures viz. F_1 and F_2 folds formed during D_1 belong to pre-tectonic M_1 metamorphism while F_3 folds developed in the D_2 deformation post date the M_1 .

The signature of second phase of metamorphism (M_2) is well preserved in the NMG exposed along the gneisses terrain. The field relationship shows that mafics and ultramafics are trending ENE–WSW to E–W parallel to the banded iron formation. The foliation planes generally striking ENE–WSW, steeply dip north westerly while towards the south of these schistose rocks, exposures of OMG rocks are observed trending WNW–ESE. Thus it can be concluded that they have an angular relationship with each other. The NMG rock comprises mafics and ultramafics, banded magnetite quartzites and metavolcanics. In NMG rocks tight to open folds trending in E–W direction were observed especially in metasedimentary rocks, axial surface trending NW–SE to NE–SW plunging towards north. The S_1 and S_2 schistosity developed in NMG are related to D_1 and D_2 deformations. Intense schistosity at the contact between meta-sedimentary and metavolcanics within NMG indicate synistral shearing.

The first phase of metamorphism in mafics and ultramafics and metavolcanosedimentaries is possibly initiated at the D_4 deformation due to load pressure and rise in temperature. Tight to open F_1 folds developed in mafics and ultramafics and metasedimentaries are the responsible for the development of S_1 foliation, which is defined by the flaky minerals viz. muscovite, chlorite, talc, biotite amphibole and epidote. The appearance of talc, chlorite tremolite, actinolite in the ultramafic rocks and actinolite, hornblende, epidote, garnet, chlorite and biotite in the mafic rocks points that metamorphism has reached up to the green schist to lower amphibolites facies conditions.

The minerals assemblages observed in the NMG are epidote–chlorite–actinolite / tremolite–albite–magnetite–quartz; chlorite–actinolite–tremolite–magnetite±quartz ± albite; actinolite–tremolite–talc–chlorite ± quartz ± serpentine ± biotite; talc–tremolite ± quartz and talc–chlorite ± magnetite ± phlogopite are related to green schist facies.

The field relationship, textural study, phase relationship and geochemical studies reveal that the exposed metamorphic rocks of the study area have been divided into two groups: (i) older metamorphic group (OMG) (3500 to 3200Ma), which comprises TTG gneisses, migmatites, amphibolites, hornblende-biotite gneisses and granite- gneisses, and (ii) Newer Metamorphic Group (NMG) (3200-2600Ma) which comprises mafic-ultramafics, banded magnetite quartzite, quartzite and meta-volcanics. These two groups of rocks were invaded by granite intrusions of different episodes (2500-2300Ma), is known as Bundelkhand acid magmatism. In the later phase major quartz reefs, trending NE-SW offsetting the above said older litho-units, were emplaced around 2000-2300Ma. The last phase episode in the craton is related to an evidence of extensional tectonic and thermal relaxation that is marked by the emplacement of mafic dykes trending in NW-SE around (1800- 1600 Ma?).

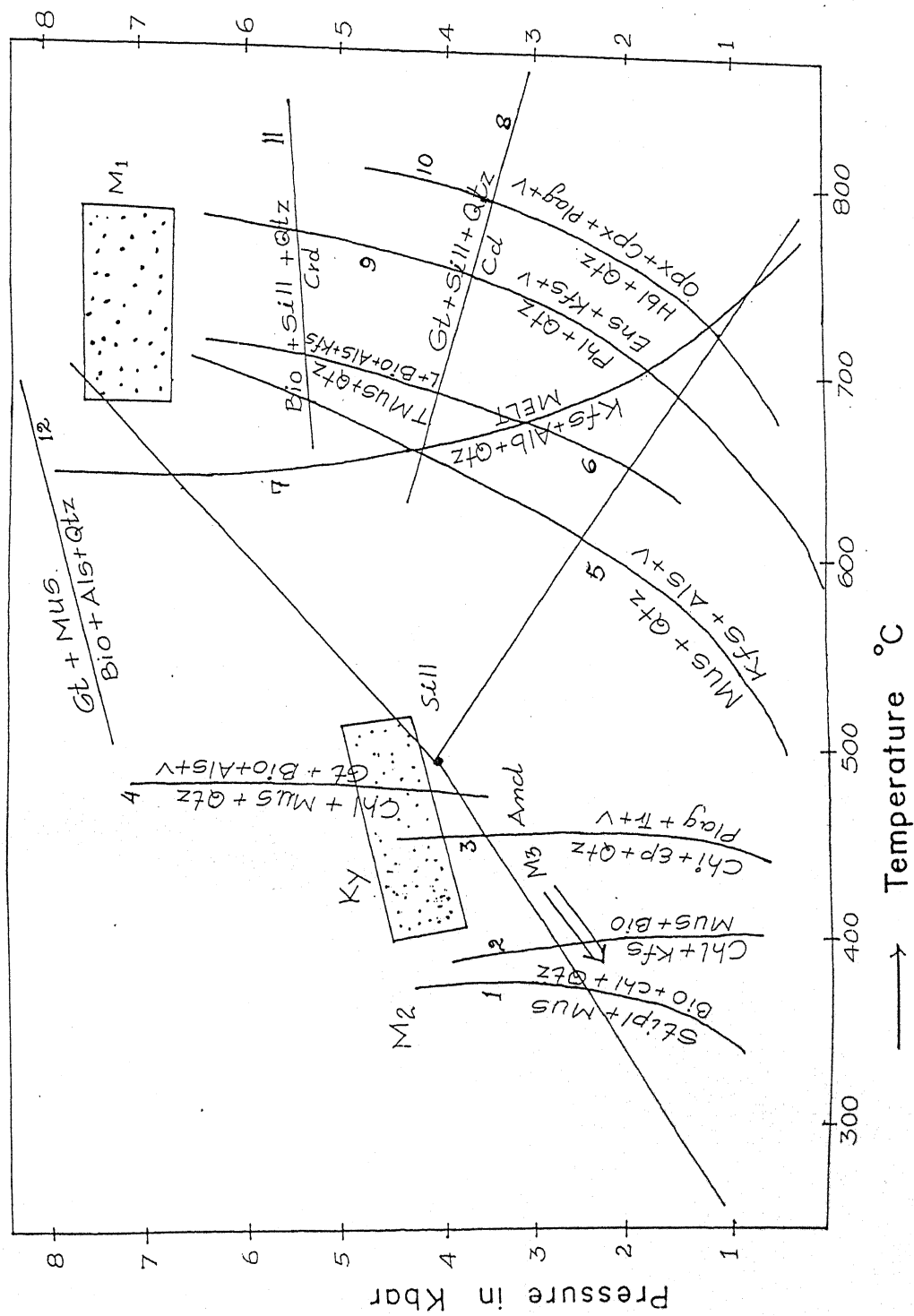


Fig 6.1 P-T conditions diagram showing experimentally determined equilibria to the present study. The triple point and stability of aluminosilicate is after Bohlen et al. (1991). The experimentally determined equilibria are: 1. Nitsch 1970, 2 and 3 - Winkler 1976, 4- Hirschberg and Winkler 1968, 5- Chatterjee and Johannes 1974, 6- Thomson 1982, 7- Ebadi and Johannes 1991, 8- Holdaway and Lee 1977, 9- Valley et al. 1990, 10- Spear 1981, 11- Thompson 1982 and Holdaway and Lee 1977, 12- Thompson 1982. The shaded area represents the P-T for the metamorphism M₁ and M₂ for the OMG and NMG group of rocks respectively. The arrow represents the retrogression.

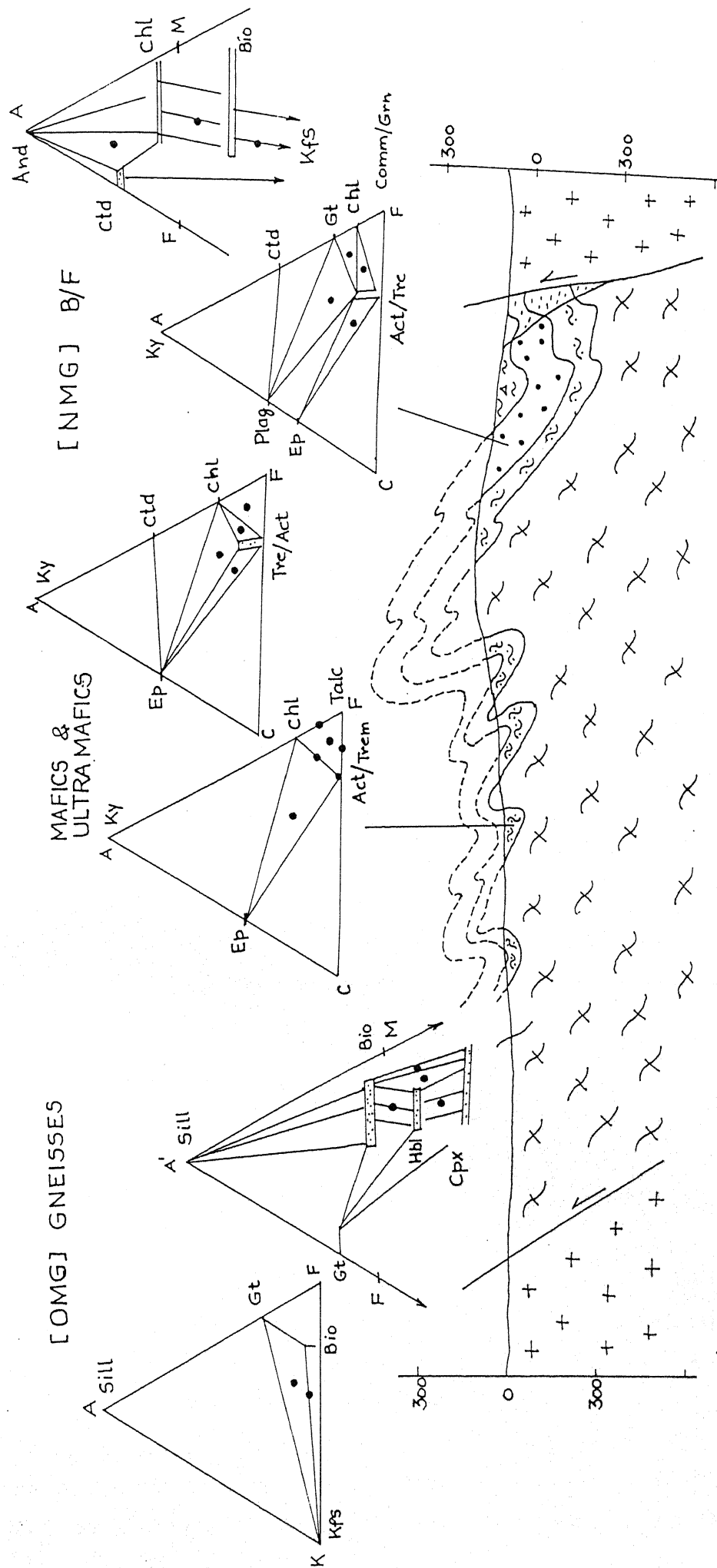


Fig 6.2 A geological cross action along X-Y line of geological map of the investigated area Fig 2.b. The different observed mineral assemblages are shown in pertinent system. The solid circles of the different triangles represent the observed mineral assemblage of the M₁ and M₂ episodes of metamorphism.

CONCLUSIONS

The Bundelkhand massif represents one of the oldest nuclei of the northern part of the Indian Peninsula, which comprises extensive outcrop of granite- gneisses and granitoids in association with meta-sedimentaries and meta-volcanics of older supracrustal mass. The relationship of different episodes of metamorphite and granitoid rocks has been depicted on the basis of available geochronology and evidences from petrological, geochemical and phase petrological studies along the Babina-Mauranipur transect of the Bundelkhand.

The Bundelkhand craton is delineated from Aravalli-Rajasthan craton by Great Boundary Fault (GBF) in the west and is delineated from Bastar-Chhotanagpur craton by E-W trending Son Narmada Lineament (SNL) in the south and southeast. The northern boundary of the craton is probably deep faulted and is covered by Indo Gangetic alluvium. The craton comprises rocks of **Bundelkhand massif** of Archean, Bijawar and Vindhyan Supergroup of Proterozoic and Malwa Traps of Cretaceous-Eocene. The **Bundelkhand massif** is exposed as semicircular out crop, which comprises mainly granitoids of different episodes, low to high-grade metamorphics of pelitic, mafic and ultramafic composition, BMQ and emplacement of dolerite dykes and quartz reefs. The faded signatures of relics of greenstone-granite-gneissic terrain represent the investigated area. The detailed studies of regional structures, rock types and their field relationship reveal that metamorphics of Bundelkhand can be classified into Older Metamorphic Group and Newer Metamorphic Group.

The Bundelkhand craton is known as the classical terrain for the Early Proterozoic rocks, which are widely exposed and have destroyed most of the early geological records. On the basis of the presence of granitoids, the present stratigraphy of Bundelkhand has been classified as Pre-Bundelkhand granitoids, syn Bundelkhand granitoids and Post-Bundelkhand rocks.

The rocks of Pre-Bundelkhand granitoids comprise Older Metamorphic Group (OMG) and Newer Metamorphic Group (NMG). The former (OMG) occur as sporadic bodies in E-W linear trend at the low land areas and comprise TTG, biotite gneisses, migmatites and amphibolites. The Newer Metamorphic Group of rocks are exposed at slightly elevated E-W trending detached hillocks and comprise mafics and ultramafics, banded iron formation and meta-volcanics. Metamorphosed mafics and ultramafics unit of NMG contain mainly actinolite-chlorite schist, hornblende-epidote-chlorite schist, talc-

chlorite schist, garnet-chlorite-actinolite schist, tremolite-talc-actinolite schist; banded iron formation having banded magnetite schist and meta-volcanics composed mainly of felsic and mafic compositions.

The structural studies of gneisses and migmatites point out that rocks of OMG have experienced six phases of deformation while the rocks of NMG have experienced four phases of deformation. Tight to reclined F_2 folds of the gneisses formed during D2 deformation are co-axial and co-planar with tight to isoclinal and reclined F_1 folds formed during the D1, which is the oldest structure. Tight to open F_3 folds have NW-SE to NE-SW trending axial plane and plunging towards north formed during the D3 deformation have been recorded from NMG and OMG. Bands of BIF are trending ENE-WSW direction and steeply dip towards north. In meta-sedimentaries and meta-volcanics indicate sinistral shearing. These are present as lensoidal bodies in gneisses.

The vast granitic batholith of Bundelkhand Granitoids has been found as multiple acidic intrusives in these metamorphites (OMG and NMG). Hornblende granite is found as earliest phase of magmatism in the region, which is followed by biotite granite. The leucogranite is the last phase of granitoids in the massif. Coarse-grained porphyritic granite is found as an intrusive into foliated biotite. The fine-grained leucogranite is the youngest phase of batholiths in this massif and is intrusive into all the older granites. Bundelkhand granitoids are subjected to three phases of deformation. E-W trending dextral and sinistral shear zones and S-C fabrics are observed in granitoids, besides the gneiss and low grade metamorphics (OMG and NMG). The presence of shear indicators viz. rotation of porphyroblasts, S-C fabrics, sheath folds from gneisses and migmatites, intrafolial folds and "S" type folds of BMQ, S-C fabrics in the granites and also from E-W trending mylonites and ultra mylonite zone indeed indicates that a north-south compression was prevailed after the granitic emplacement. The presence of recrystallized mylonites and emplacement of porphyritic granitoids into the E-W trending mylonites zones point that the compressive forces were active during the batholithic acidic magmatism.

The NE-SW bearing quartz-reefs, emplaced in the massif are found to displaced the older rock units sinistrally. At many places, displacement is recorded along NW-SE trend and is related to D5 phase of deformation. Dolerite dykes in the form of swarms, emplaced along NW-SE direction and having displaced the NE-SW quartz reefs, are related to D6 phase of deformation.

On the basis of regional field relationship, structural data, deformation, relationship with metamorphism and magmatism, geochronological data, a geochronostratigraphy has been proposed for the first time. It is suggested that the high-grade metamorphics of

OMG viz. TTG, gneisses and amphibolites were formed during the first episode of metamorphism and during 3200Ma. The low-grade metamorphics, comprising mafics, ultramafics, meta-sedimentaries and metavolcano sedimentaries have been grouped under NMG (3200 – 2600Ma) and are related to second episode of Metamorphism. These metamorphics are further intruded by the different episodes of granites (2500-2300). Quartz reefs (NE-SW trending) between 2300-2000 Ma and NW-SE trending mafic dykes 2000-1800 Ma.

The rocks of older metamorphic group have been divided into (i) gneisses, TTG, migmatites, granite-gneisses, and (ii) amphibolites and hornblende-biotite gneisses. Biotite-gneisses, TTG, migmatites, and granite-gneisses observed in the investigated area are medium-to-coarse-grained, gray to light gray in colour and show gneissic structure. The following minerals assemblages have been obtained:

- (i) K-feldspar – perthite – plagioclase – biotite – quartz (K-feldspar < plagioclase)
- (ii) K-feldspar – perthite – plagioclase – quartz
- (iii) K-feldspar – perthite – antiperthite – biotite – quartz (plagioclase < K-feldspar)
- (iv) K-feldspar – biotite – quartz
- (v) K-feldspar – plagioclase – biotite – quartz
- (vi) K-feldspar – plagioclase – biotite – hornblende – quartz (plagioclase > K – feldspar.)

The amphibolites and hornblende – biotite gneisses show the medium-to fine-grained, dark greenish black in colour, very hard and compact. On the basis of minerals constituents, these rocks have been classified into (i) hornblende plagioclase gneisses, (ii) hornblende – biotite gneisses, and (iii) hornblende – biotite – diopside gneisses.

The rocks of Newer Metamorphic Group are the metamorphosed products of viz; (i) Mafics and Ultramafics, (ii) Banded Iron Formation and (iii) meta-volcanics and metamytonites.

- (i) The mafic and Ultramafic rocks are generally observed in highly weathered form and are characterised by grayish green to dark dirty greenish with white tint in colour. Schistosity is marked by the alignment of chlorite, tremolite, actinolite and talc minerals. The mineral assemblages obtained from these rocks are:
 - (a) Hornblende - magnetite – quartz
 - (b) Hornblende ± tremolite – actinolite – chlorite – quartz
 - (c) Tremolite ± phlogopite – chlorite – magnetite – quartz

- (d) Garnet – chlorite – actinolite – epidote – quartz.
 - (e) Talc – chlorite \pm serpentine – magnetite \pm quartz \pm phlogopite
 - (f) Chlorite – talc – tremolite \pm actinolite \pm hornblende \pm phlogopite
- (ii) Band Iron Formation (BIF) generally occurs along E-W direction in the investigated area. The metamorphosed ferruginous rocks show alternate bands of quartzite and magnetite; at places hematite bands are also recorded. In few places, cummingtonite-grunerite bands of whitish green colour were also recorded. Quartzites of light pink to pinkish white in colour, fine grained and massive compact nature are also observed. The following assemblages have been obtained.
- (a) Magnetite – quartz
 - (b) Stilpnomelane – chlorite – magnetite – quartz
 - (c) Magnetite – epidote – actinolite – quartz
 - (d) Cummingtonite – hornblende – garnet – chlorite – magnetite – quartz.
 - (e) Cummingtonite – grunerite – magnetite – quartz
 - (f) Muscovite -sericite – biotite – quartz
 - (g) Chlorite – epidote – quartz
 - (h) Magnetite – actinolite – tremolite – epidote – chlorite – quartz
 - (i) Garnet – chlorite – muscovite – microcline – magnetite – quartz.
- (iii) Meta-mylonite and meta-volcanics exposed in the north of iron formation (BMQ) show medium to fine-grained, (at places porphyroblastic) texture. These rocks have been divided into two litho-units on the basis of diverse physical appearance, texture and mineral compositions. (i) The felsic and mafic volcanics are found in association with mylonites and ultramylonites, which are light gray to pink in colour, massive, hard and compact. The elongated thread like phenocrysts of K-feldspars along foliation plane show the signature of rotation of crystals to some extent. (ii) The meta-mylonite and ultra-mylonites, which are generally observed just at the contact of BMQ, are medium-to fine-grained, dark gray to light pink or whitish green in color, with patches of whitish spots of feldspars and epidote. The following mineral assemblages in these rocks have been observed in the study area are :
- (a) Hornblende – chlorite – biotite – quartz – K-feldspars.
 - (b) Actinolite – hornblende – K-feldspars – plagioclase
 - (c) K-feldspar – quartz – chlorite – magnetite – epidote \pm biotite

- (d) Chlorite – epidote – K-feldspar – andalusite – quartz
- (e) Chlorite – chloritoids – muscovite – K-feldspar – quartz – magnetite.

Megascopically, the granites of the investigated area are varying in grain size from coarse to fine grained, leucocratic to mesocratic, hard and compact in nature. The phenocrysts of feldspar are very frequent in fine-grained leucogranite. In hand specimen feldspar, quartz, biotite and rarely hornblendes can be identified. In the deformed granites, the bands of quartz – feldspar masses show preferred orientation with alternate ferromagnesian minerals bands in biotite rich variety. Biotite is common in all types of granite but hornblende may or may not be present except in hornblende granite.

Twenty-five representative rock samples of gneisses and granites and mafics, ultramafics of petrological interest from investigated area were chosen for analysis.

Based on Na_2O vs K_2O diagram, ternary (An-Ab-Or) diagram, Q-A-P triangular diagram, P-Q diagram the analyzed gneisses show tonalite, trendhjemite affinity while granites show granite, granodiorite and adamellite affinity. A vs B, TAS, A – F – M, and SiO_2 vs $(\text{Na}_2 + \text{K}_2\text{O})$ diagrams show that the gneisses and granites are sub-alkaline in nature.

Alumina content of gneisses (14.25 wt%) and granites (12.95 wt%) are greater than the total alkalis ($\text{K}_2\text{O} + \text{Na}_2\text{O}$); average value being 6.84 wt% and 8.26 wt% in gneisses and granites respectively.

The tectonic environment of the granite of the study area is classified according to different discrimination parameters proposed by Mamiar and Piccoli (1989) and it has been noted that the chemical signatures of granites of the study area do not follow a single and firm tectonic environment but all the data are related to orogenic granites and also Shand's alumina saturation index diagram points that majority of the granites are related to metaluminous characters which suggest that granites of the study area were resulted from magmatic origin. Discrimination diagram of Pearce et al; (1984) suggests that granites of the study area are related to syn-collision type tectonics.

The milli-cationic parameters proposed by De La Roche's suggest that granites of the study area should be related with syn-continental collision tectonic. Majority of the granites of study area were formed due to remobilization and partial melting of the biotite gneisses as evident by Triangular $\text{Al}_2\text{O}_3 - (\text{Na}_2\text{O} + \text{K}_2\text{O} + \text{CaO}) - (\text{FeO} + \text{MgO} + \text{MnO})$ diagram. Rb Vs Sr (log-log) diagram, suggests that granite melt might have been generated at depth around 23 to 35km and temperature of about 750°C.

Trace element analyzed by El Bouseily and El Sökkary (1975) in Rb-Ba-Sr ternary diagram reveals that granites of the study area are related to magmatic source and have been emplaced and crystallized at different depth with varying physicochemical conditions. Ba/Rb ratio characterizes the change from normal granite to strongly differentiated type.

The very high value of Rb (209ppm) from the leucogranitoids suggests that these granites were subjected late stage differentiation. The high Rb/Sr ratio of the gneisses may be due to chemical variation during metasomatism of feldspar minerals. It appears to be the dominant controlling factor for the abundance for Sr, which is evident from the positive correlation shown by gneisses of the study area when plotted against normative plagioclase. The granite of the study area has also positive correlation. The positive correlation shown by Pb with normative orthoclase in gneisses suggests that the elements preferentially occupy in the lattice of K-feldspar in the rock.

Mafics and ultramafics of the investigated area are classified by the various schemes of classification : TAS, AFM and $\text{TiO}_2 - \text{K}_2\text{O} - \text{P}_2\text{O}_5$ diagrams, which represent basaltic nature for these rocks. K_2O Vs SiO_2 diagram depicts that the mafic and ultramafic rocks of the study area are characterized by calc-alkaline and low- K series and are related to island arc tholeiite basaltic trend. TAS diagram proposed by Irvine and Baragar (1971) and Na_2O vs. SiO_2 diagram of Middle Most (1975) suggest sub alkaline characters for the mafic and ultramafics rock of study.

The triangular diagram $(\text{Fe}_{\text{T}} + \text{Ti}) - (\text{Al}) - (\text{Mg})$ and A: $(\text{Na}_2\text{O} + \text{K}_2\text{O}) - \text{F}: (\text{FeO}) - \text{M}: (\text{MgO})$ suggest that initially the magma was komatiitic in characters which was subsequently changed into tholeiitic magma. The fractionation of komatiitic magma may be responsible for the development of tholeiitic character in the late stage of crystallization.

The triangular $(\text{TiO}_2 - \text{K}_2\text{O} - \text{P}_2\text{O}_5)$ shows that the mafic and ultramafics are tholeiites of ocean floor basalt. It is also supported by the $\text{TiO}_2 - \text{SiO}_2$ diagram of Whitehead and Good fellow (1978). Similar tholeiitic trend is also shown by the $\text{FeO} - \text{FeO} / \text{MgO}$ diagram of Miyashiro and Shido (1975) and Alkali Index Vs Al_2O_3 .

Based on $100\text{Ti} - \text{Zr} - \text{Y}_{\text{X3}}$ diagram proposed by Pearce and Cann (1973), Zr/Y Vs Zr diagram (Pearce and Norry 1979), $\text{FeO}_t / \text{MgO}$ Vs TiO_2 diagram (Jelinek et.al. 1980) and $\text{TiO}_2 - \text{MnO} \times 10 - \text{P}_2\text{O}_5 \times 10$ diagram (Muller 1983) suggest that majority of the mafics and ultramafics are of island arc tholeiitic type.

The positive correlation trends in different variation diagram suggest that the Komatiitic magma of the early stage fractionated in simple way and subsequently changed to tholeiitic composition. It is evident from the MgO Vs FeO, Ni, and Cr diagrams.

Biotite is an important ferromagnesian mineral in, gneisses, amphibolites, granites, metamytonites and metavolcanics of the study area. The composition of the biotite shown in the quadrilateral diagram of four end members phlogopite – $K_2 Mg_6 (Si_6 Al_2 O_{20}) (OH)_4$, annite – $K_2 Fe_6 (Si_6 Al_2 O_{20}) (OH)_4$, eastonite – $K_2 Mg_5 Al (Si_5 Al_3 O_{20}) (OH)_4$ and siderophyllite – $K_2 Fe_5 Al (Si_5 Al_3 O_{20}) (OH)_4$ represent near the annite composition which suggest, that magnesium is replaced by ferrous iron and also by trivalent ions (Fe^{+3} , Al) and aluminum replaces silicon in tetrahedral sites usual beyond the ratio Al:Si = 2:6 The deficiency and excess of cations on Y positions reveal the heterovalent substitution in octahedral layers. The deficiency in alkali i.e ΣX less than 2.0 indicating that these cations might have been substituted by the cations in Y. The deficiency Y cations also indicates in substitution of Y cations by trace elements found in X cations viz. Rb, Ba, Cs etc.

All the analysed muscovite samples plotted on the quadrilateral diagram outlined by four en-members: muscovite - $K_2 Al_4 (Si_6 Al_2) O_{20} (OH)_4$, Ferro-muscovite – $K_2 Fe^{+3} Al_3 (Si_6 Al_2) O_2 (OH)_4$, Phengite- $K_2 (Mg, Fe^{+2}) Al_3 (Si_7 Al) (OH)_4$ and ferro-phengite- $K_2 (Mg, Fe^{+2}) Fe^{+3} Al_2 (Si_7 Al_2) O_2 (OH)_4$ (Fig 2), reveal that in the muscovite-phengite series Mg, AlVI substitutes Fe^{+2} . Ferromuscovite is derived from muscovite by replacement of one of the Al^{VI} ions by Fe^{+3} .

Silica content in amphiboles ranges from 7.08 to 7.87 p.f.u. So the substitution of Silica by aluminum (Al^{IV}) ranges from 0.132 to 0.920 p.f.u. Al^{VI} content in amphiboles of the study area ranges from 0.0135 to 0.7486 p.f.u. so all the substitution is limited to approximately 1Al atom per formulae unit. In calcic amphiboles Ca occupies W site; Ca is also predominant over Na. Fe^{+2} cations in Y site ranges from 0.8755 to 1.9565 p.f.u. and Mg ranges from 2.9521 to 4.0930 per formula unit. Ca in amphibole analyses contains 1.8586 to 2.2432 per formula unit while Na ranges from 0.0574 to 0.3106 p.f.u.

The phase petrology and involved metamorphic reactions of different metamorphics of pelitic, psammatic and mafic rocks of the study area indicate progressive increase in the grade of metamorphism from north to south across the Babina-Mauranipur transect. An attempt has been made for the first time in entire Bundelkhand massif to delineate the type of metamorphism and metamorphic conditions of each episode from Newer Metamorphic Group (NMG) and also from the Older Metamorphic Group (OMG) of the area.

The TTG, which includes both tonalite and trondhjemite rocks, contain significant amount of K-feldspar, antiperthite, plagioclase, perthite, biotite, and quartz with minor amount of ilmenite, apatite, zircon, sphene and spinel. The muscovite and clinopyroxene are completely absent in TTG. The hornblende has been noticed in minor amount in most of the TTG rocks.

The biotite-gneisses consist mainly of biotite, quartz, plagioclase and K-feldspars. The zircon and apatite are present in the significant amount in all the rock samples. The perthite and antiperthite texture are also present in the gneisses. The garnet and sillimanite reported by earlier workers from the Kabrai area (Saxena, 1961) could not found in the present investigated area. The absence of the garnet and sillimanite may be possibly due to composition variation. The muscovite of prograde or retrograde phase is completely absent from the gneisses.

In the OMG rocks, the first phase of metamorphism possibly initiated at deformation D1 and culminated in the advanced stage of partial melting and granulite formation. The following assemblages have been obtained in the KFMASH system.

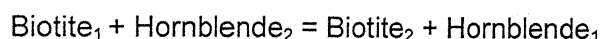
- (i) Biotite-K-feldspar-perthite-quartz.
- (ii) Biotite-plagioclase-K-feldspar-antiperthite quartz.
- (iii) Garnet-biotite-K-feldspar-quartz.

Assemblages in amphibiotites and hornblende biotite gneisses:

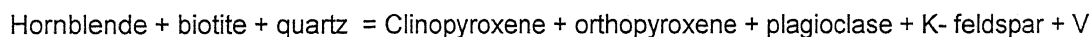
- (i) Hornblende - clinopyroxene - biotite - plagioclase - K-feldspar - quartz.
- (ii) Hornblende - biotite - K - feldspar - plagioclase - quartz.
- (iii) Hornblende - clinopyroxene - plagioclase - quartz.
- (iv) Hornblende - plagioclase - K-feldspar - quartz.
- (v) Hornblende - garnet - plagioclase - K - feldspar - quartz.

The AKF diagram shows three phases fields of garnet - biotite and K - feldspar. The K- feldspar - biotite join defines the two-phase field for non-garnetiferous gneisses. The mineral assemblages of tonalite and trondhjemite gneisses can be represented in K_2O , FeO, MgO, SiO_2 , CaO, Al_2O_3 and H_2O (CNKF MASH) system and portrayed in the AFM diagram (Reinhardt Projection) with FeO and MgO as separate component and as plagioclase. The advantage of A'FM projection is that the tie lines connecting hornblende, clinopyroxene and biotite composition of the three coexisting phases form triangle, enclosing the field of composition of three mineral associations. The common presence of hornblende-clinopyroxene-biotite phase may be due to large field with variation in the bulk

composition of rock. These three co-existing phases may be considered as continuous reaction in the CFMASH system in A'FM diagram. Because of this, the assemblage biotite- hornblende- clinopyroxene is stable at wide range of pressure, temperature and composition. The presence of corroded biotite in the hornblende and clinopyroxene, and similarly presence of corroded hornblende in the biotite and clinopyroxene from the hornblende-biotite gneisses may be attributed to the break down of the biotite and hornblende by the following continuous reaction in CFMASH system.



The composition of the hornblende lies between the biotite - clinopyroxene lines. Therefore, the appearance of pyroxene may be due to the following reaction in the CFMASH system.



The composition of the orthopyroxene lies on the tie line of the biotite - clinopyroxene in the A'-F-M projection in the system KCFMASH. The absence of this mineral from the hornblende-biotite gneisses and biotite-gneisses may be due to either quartz deficient mineral or due to strong retrograde metamorphism of gneisses or inappropriate fluid activity. The absence of garnet from these gneisses may be considered due to the non-availability of appropriate bulk composition and high MgO, K₂O and Al₂O₃.

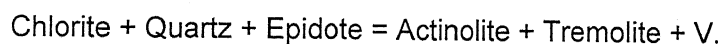
The enclaves of amphibolites are very common in the gneisses. Sometimes they are cofolded with biotite gneisses. The petrographic studies reveal that phlogopite, epidote, tremolite, chlorite and actinolite are completely absent while diopside, calcite, plagioclase, hornblende are present as medium to coarse grained texture. The common presence of plagioclase - hornblende - diopside assemblages can be explained in three-phase field of ACF diagram in CFMASH system. The other compatible assemblages viz hornblende - plagioclase - magnetite \pm quartz and diopside - hornblende - magnetite \pm quartz have been explained in ACF diagram in six component system of CFMASH system.

The low-grade metamorphism has been encountered in the mafic and ultra mafic rocks exposed south of BMQ, while slightly higher-grade metamorphism has been noticed in the quartzite and BMQ. The low-grade metamorphisms specially, the thermal imprints have been recorded in the metavolcanic and mylonite rocks tectonically lying above the BMQ at the northern part of the NMG, where porphyritic granitoids are found as intrusive. The first phase of metamorphism in the mafic and ultramafic and metasedimentary was possibly initiated at the D₃ deformation, which is characterized by the increase in load pressure and rise in geotherms. In general, this prograde metamorphism (M₂) in mafic,

ultramafic and metasedimentaries observed at Babina is responsible to the development of the S_1 foliation. This is defined by the orientation of flaky minerals viz., muscovite, chlorite, talc, biotite, amphiboles and epidote.

The appearance of talc, chlorite, tremolite, actinolite in the ultramafic rocks and actinolite, cummingtonite-grunerite, hornblende, epidote, garnet, chlorite, biotite in the mafic rocks points that metamorphism has reached upto the green-schist to lower amphibolite facies conditions.

The beginning of the chlorite and talc from the lower unit of the ultramafic and also from shear zone may be defined by the following reactions in CFMASH system and portrayed in ACF diagram. By these reactions, progressive regional metamorphism possibly proceeded to higher temperature.



The transition of the green schist facies to subgreen schist facies is marked by the first appearance of diagnostic assemblage, actinolite + epidote in the presence of chlorite + albite + quartz in the basic rocks and tremolite-actinolite-talc-chlorite \pm epidote in the ultramafic rocks. The presence of chlorite – epidote – actinolite / tremolite – quartz assemblage clearly suggests the appearance of green schist facies.

Since no diagnostic minerals have been discussed and proposed, for the mafic and ultramafic rocks to delineate the chlorite-epidote subfacies and biotite- epidote subfacies of green schist facies classification, both the subfacies have been considered here as a lower green schist facies. The following minerals assemblages have been observed in the lower green schist facies:

- (i) Epidote – chlorite – actinolite/tremolite – albite – magnetite – quartz
- (ii) Chlorite – actinolite – tremolite – magnetite \pm quartz \pm albite
- (iii) Actinolite – tremolite – talc – chlorite \pm quartz \pm serpentine \pm biotite
- (iv) Talc – tremolite \pm quartz
- (v) Talc – chlorite \pm quartz \pm magnetite \pm phlogopite.

All the above assemblages have been reported for first time from the ultramafic rock found immediately at the contact of gneisses in Babina-Mauranipur transect. With further increase in temperature, the prograde metamorphism proceeded by the appearance of

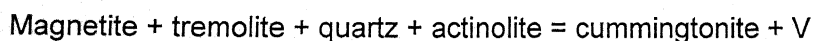
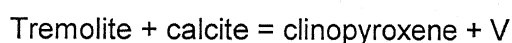
hornblende mineral in the assemblages: epidote-hornblende-chlorite-albite-quartz and hornblende-actinolite-tremolite-chlorite-quartz-magnetite. The appearance of hornblende can be attributed to the following reaction in the six-component system (CFMASH system) and can be portrayed in ACF diagram.



The aforesaid terminal reaction can be explained in CFMASH system and ACF diagram for the beginning of almandine-albite-epidote zone of green schist facies. In this zone, following mineral assemblages have been obtained from the study area.

- (i) Epidote – hornblende – chlorite – quartz \pm magnetite
- (ii) Epidote – actinolite – tremolite – hornblende – albite – magnetite \pm quartz
- (iii) Actinolite / tremolite – chlorite – hornblende – magnetite – quartz.

The appearance of cummingtonite, grunerite in the presence of the tremolite/hornblende and sometimes clinopyroxene mark the beginning of amphibolite facies metamorphism. The beginning of this transition zone has been demarked at the base limit of the BMQ. The appearance of the cummingtonite, actinolite, and clinopyroxene minerals may be attributed to the following reactions in the CFMASH system and may be explained in ACF diagram.



The following mineral assemblages have been reported from this transition facies:

- (i) Actinolite – tremolite – cummingtonite – magnetite – quartz
- (ii) Cummingtonite – magnetite – quartz
- (iii) Chlorite – cummingtonite – actinolite / tremolite – quartz
- (iv) Hornblende – actinolite – cummingtonite – chlorite – magnetite.

The presence of assemblages garnet-hornblende-plagioclase-quartz, hornblende-garnet-cummingtonite-magnetite-quartz and hornblende-actinolite / tremolite – plagioclase – quartz from the upper part of the iron formation suggest that metamorphism has reached up to staurolite – biotite subfacies of amphibolite facies. These assemblages can be portrayed in the ACF diagram and defined in CFMASH system.

The northern part of the NMG comprises a thick sequence of metamorphosed mafic and felsic volcanic rocks along with thick mylonites of E-W trending shear zone. The

medium grained porphyritic granite has been found as intrusive in this tectonic unit. Due to the emplacement of the plutonic granites, along the shear zones, the earlier signatures of deformation and crystallization of rocks of shear zone are almost destroyed. Not only this, due to thermal heat during emplacement of granitoids, the mylonites rocks of shear zone were subjected to recrystallization.

As a result, sheared unit comprises a very heterogeneous bulk composition and mineralogy as well. The entire sequence is characterizes by different types of hornfelsic textures viz. radiating plagioclase and actinolite, mortar texture at places. The overgrowth textures of the feldspar quartz and hornblende have been also recorded.

The following mineral assemblages have been obtained in the CFMASH and KFMASH systems.

- (i) Andalusite – epidote – chlorite – quartz – albite
- (ii) Epidote – chlorite – chloritoid-quartz
- (iii) Epidote – actinolite – chlorite – quartz
- (iv) Andalusite – chloritoid – epidote – muscovite – quartz.

In the investigated area an order of index minerals chlorite, talc, biotite, cummingtonite, grunerite, hornblende almandine in metamorphosed mafic and ultramafic and BMQ sequences lying above the gneisses have been identified on the basis of texture, structure and mineral assemblages in the CFMASH system. The lower green schist facies (Chlorite biotite zone), upper green schist facies (almandine zone) and lower amphibolite facies (almandine-staurolite zone) have been recognized for the first time in the NMG rocks. The mineral assemblages of these zones are as follows :

(A) Chlorite-biotite zone (Lower green schist facies)

- (i) Epidote – chlorite – actinolite – tremolite – albite – magnetite – quartz
- (ii) Chlorite – actinolite – tremolite – magnetite \pm quartz \pm albite
- (iii) Actinolite – tremolite – talc – chlorite \pm quartz \pm serpentine \pm biotite
- (iv) Talc – tremolite \pm quartz
- (v) Talc – chlorite \pm quartz \pm magnetite \pm phlogopite.

(B) Almandine zone (Upper green schist facies)

- (i) Epidote – hornblende – chlorite – quartz \pm magnetite.
- (ii) Epidote – actinolite – tremolite – hornblende – albite – magnetite \pm quartz.
- (iii) Actinolite / tremolite – chlorite – hornblende – magnetite – quartz.

(C) Staurolite – almandine zone (Lower amphibolite facies)

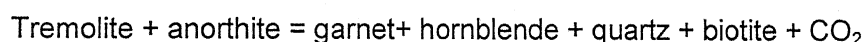
This zone marks the beginning of the amphibolite facies and has the following mineral assemblages :

- (i) Actinolite – cummingtonite – tremolite – magnetite – quartz.
- (ii) Cummingtonite – magnetite – quartz.
- (iii) Hornblende – actinolite – cummingtonite – chlorite – magnetite.

The first appearance of actinolite, epidote, chlorite, albite, quartz from the mafic and ultramafic rocks defines the beginning of the green schist facies. The appearance of biotite replacing the white mica has been defined by the invariant reaction



The appearance of hornblende in the mafics and ultramafic rocks at the expense of chlorite and epidote in the presence of the quartz has been defined by the following reaction :



P-T conditions estimated by geothermometry (proposed by Lal et al; 1991) yield 400°C-550°C for all the rocks. This temperature estimate suggests that the rocks of the NMG are metamorphosed regionally in the green schist to lower amphibolite facies conditions.

The gneisses contain significant amount of K-feldspar, plagioclase, biotite, quartz and minor amount of ilmenite, apatite, zircon and sphene. The phase petrology relation points that assemblages in gneisses (biotite - K-feldspar – antiperthite – quartz; biotite – plagioclase – K-feldspar – quartz) and in amphibolite, hornblende gneisses (Hornblende-clinopyroxene-biotite-K-feldspar-plagioclase-quartz and Hornblende-clinopyroxene-biotite-K-feldspar-quartz) reveal that they were formed above 650° C and 6-7 kb pressure in upper amphibolite to lower granulite facies conditions. The observed mineral assemblages, petrochemistry, field relationship and P-T conditions point that the high grade gneisses and granulite metasediments and mafic to ultramafic rocks were recrystallised around 3200Ma along with tonalitic gneisses. It is also inferred that crystallized minerals of OMG were aligned in S1 and S2 plane in the gneisses and mesoscopic structure viz. F1 and F2 folds were formed during the D1 deformation episode, which is pre-tectonic to M1 episode of metamorphism while the F3 folds were developed during the D1 deformation and are post-date the M1 episode of metamorphism.

The signatures of the M2 episode of metamorphism are well observed in the NMG, which are trending in ENE-WSW to E-W parallel to the bands of BMQ, mafic, ultramafic

and volcanic rock sequence. A discordant relationship between the NMG and OMG has been marked on the basis of change in the structural trend, grade of metamorphism, mineral chemistry and mineral assemblages. The NMG rocks comprise tight to open folds in the E-W direction has been correlated with OMG rock formed during the D3 deformation. The presence of the relicts of E-W trending linear pattern of rocks of NMG within the OMG represents a large scale folding after the metamorphism (M_2). The presence of E-W trending mylonites structures and the offset relations as well as sinistral displacement of shear are due to another shear trends NE-SW. The presence of E-W and NE-SW trends mylonitised ultramylonite suggest that atleast two phases of the shearing have taken place after the crystallization of the granitic batholith. It is indeed worth to describing that mylonites trending in the E-W direction are comparatively thicker and prominent in the investigated area. The presence of post tectonic growth of K-feldspars, quartz and chlorite and augen type structure from E-W shears indicate that they were further subjected to recrystallisation possibly during the late phase of the granitic emplacement.

Thus, the field relationship, texture, geochemistry, and the phase relationship studies suggest that Bundelkhand massif is a complex terrain, which has undergone polyphase deformation, multiple episodes of magmatism and different episodes of metamorphism during Pre-Bundelkhand granitoid episode. In the study area the metamorphic rocks are expose in a raft form within the granitoid massif suggesting that Pre-Bundelkhand granitoid received two phases of metamorphism and atleast three phases of deformation. The relicts of older metamorphics in the study area have been divided into (i) Older Metamorphic Group (OMG) (3500 to 3200Ma), which comprises TTG gneisses, migmatites, amphibolites, hornblende-biotite gneisses and granite-gneisses, and (ii) Newer Metamorphic Group (NMG) (3200-2600Ma) which comprises mafic-ultramafics, banded magnetite quartzite, quartzite and meta-volcanics. Due to the difference in the degree of metamorphism and structural trend two different names have been proposed. These metamorphic rocks were invaded by granite intrusions of different episodes (3200–3100Ma) and (2500-2300Ma), and are known as granite-gneisse and Bundelkhand acid magmatism respectively. Further major quartz reefs, trending NE-SW offsetting the Granitoid and NMG litho-units were emplaced in the late phase around 2000-2300Ma. The last episode in the craton is marked by the emplacement of NW-SE trending mafic dykes (1800-1600 Ma?), which is an evidence of extensional tectonics and thermal relaxation in the region.

REFERENCES

- Agarwal, B.N.P., Das L. K., Chakraborty, K. and Sivaji CH, (1995); Analysis of the Bonguer anomaly over Central Indian; a regional perspective, Mem. Geol. Soc. Ind. V.31, pp 469-493.
- Ahrens, L.H., Pinson, W.H. and Kearns, M.M., (1952): Association of rubidium and potassium and their abundance in common igneous rocks and meteorites, *Geochim. Cosmochim. Acta*, V.2 pp.229-242.
- Alam, S. and Zainuddin, S.M. (1981): Petrology of Bundelkhand granites near Mahoba distric hamirpur, up, j, Goel, Soc, India, V. 22, pp502-504.
- Arth, J.C. (1976): behavior of trace elements during magmatic process. A summary of theoretical models and their applications, *J. Res.U.S.Geol. Surv.*, V.4, pp 41-47.
- Baker, D.K., (1973): Volcanism at destructive plate margins. *J. Earth Sci. Leeds* V.8 pp. 183-195.
- Banerjee, D.M., (1982): Lithotectonic phosphate mineralisation and regional correlation of Bijawar Group of rocks in Central India, In: *Geology of Vindhyanchal*, Ed. K. S. Valdia, S. B. Bhatia and V. K. Gaur, Hindustan Pub. Corporation, pp. 47-54.
- Banerjee, P.K., (1987): On the correlation of lineament with 'Metallogeny' in Indian – A brief critique. In; *Recent Researches in Geology*, V 13, pp. 16-23.
- Barker, F. and Arth, J.G. (1976): Generation of trondhjemite-tonalitic liquids and Archean bimodal trondhjemite-basalt suites, *Geology* ,4,596-600.
- Barrow, G. (1912): Proceeding, Geological Association, 23, p. 268.
- Basu, A.K., (1970-71): A report on geological mapping around Jhararghat, Jhansi dist., U.P. Unpublished Progress Report, G.S.I.
- Basu, A.K., (1986): Geology of parts of the Bundelkhand Granite Massif. *Rec. Geol. Surv. Ind.* 117 (2), pp. 61-124.
- Basu, A.K., (2001): Some characteristics of the Precambrian crust in the northern part of Central India. *Geol. Surv. Ind. Spl. Pub. No.55*, pp. 182-204.
- Batchelor, R.A. and Bowden, P. (1985) : Petrogenetic interpretation of granitoid rock series using multicationic parameters. *Chem. Geol.*, V. 48, pp. 43-55.
- Beckinsole, R.D.,; Drury, S.A. and Holt, R.W., (1980): 3360 Myr. Old Gneisses from south Indian Craton, *Nature (London)*, V.283, pp. 469-470.

- Bhattacharya, A.R. (1985): Some unusual strain relations in elliptical deformed xenoliths and feldspar porphyroblasts, *Z. geol. Wiss. Berlin*. V.6., pp.689-697.
- Bhattacharya, A.R., (1986): Wavelength-amplitude Characteristics of polyphase folds in the Precambrian Bundelkhand Complex, India, *Tectonophysics*, V.128, pp.121-125.
- Bohlen, S.R., Mantana, A. and Kerric, D.M., (1991): Precise determination of the equilibrium kyanite-sillimanite and kyanite-andalusite and a revised triple point for Al_2SiO_5 polymorphs. *American Mineral.*, 76, pp. 677-680.
- Bose, M.K., (1997): *Igneous Petrology*. The World Press Private Limited, Calcutta.
- Bowen, N.L., (1940): Progressive metamorphism of siliceous limestone and dolomite. *Jour. Geol.* 48; 225-274.
- Bucher, K.; Frey, M., (1994): *Petrogenesis of Metamorphic Rocks*. Springer-Verlag Berlin Heidelberg.
- Butler, B.C.M. (1965): Composition of mica in metamorphic rocks (eds) Pitcher, W.S., Flinn, G.W., control of metamorphism, *Edinberg*, 291-98.
- Chatterji, G.C., Ray, D.K. and Banerjee, P.K. (1971): Stratigraphic sub-division and nomenclature of the Precambrian rocks of India. *Rec. Geol. Surv. Ind.*, V. 101, Pt. 2, pp. 1-14.
- Chatterjee, N.D. & Johannes, W., (1974). Thermal stability and standard thermodynamic properties of synthetic 2M, muscovite, $\text{KAl}_2(\text{AlSi}_3\text{O}_{10}(\text{OH})_2$. *Contrib. Mineral. Petrol.*, v.48, pp.89-114.
- Condie, K.C. (1973) : Archaean magmatism and crustal thickening. *Geol. Soc. Am. Bull.* v. 84, pp. 2981-2992.
- Condie, K.C., (1983): *Plate tectonic and crustal evolution*. 2nd edtn., Pergamon Press, 310 p.
- Cox, K.G., (1980): A model for flood basalt volcanism. *J. Petrol.* V.21, pp.629-659.
- Cox. K.G., Bell, J.D. and Pankhurst, R.J., (1979): *The interpretation of igneous rocks*. Chapman and Hall, London 450 p.
- Crawford, A.R. (1970): Precambrian geochronology of Rajasthan and Bundelkhand, northern India. *Canadian Jour. Earth Sc.*, V. 7 pp. 91-110.
- Crawford, A.R. and Compston, W., (1970): The Age of the Vindhyan System, *Quart. Jour. Geol. Soc.*, London.

- Das, A.S. (1959-60): – A report on geological mapping of the Bundelkhand Granites and Gneisses in parts of Jhansi district. U.P. and intervening parts of Tikamgarh district, Madhya Pradesh. Unpublished Progress Report, G.S.I.
- Davis, J.F., Grant, R.W.E and Whitehead, R.E.S., (1979): Immobile trace elements and Archaean volcanic stratigraphy in the Timmings mining area. Ontario. Can J. Earth Sci. V16, pp 305-311.
- Debon, F. and Le Fort, P. (1982): A chemical – mineralogical classification of common plutonic rocks and associations. Trans. Royal Soc. Edinburg, (Earth Sci), v. 73, pp. 135-149.
- Debon, F., Sheppard, S.M.F. and Sonet, J. (1986): The four plutonic belts of the Transhimalaya-Himalaya: A chemical, mineralogical, isotopic and geochronological synthesis along a Tibet-Nepal section. Jour. Petrol. v. 27, pp. 219-250.
- Deer, W.A. Howie, R.A. and Zussman, J., (1962): Rock-forming minerals, p. 270 Longmans.
- De La Roche, H., Leterrier, P., Grandclaude, P. and Marchal, M., (1980): A classification of volcanic and plutonic rocks using R1-R2 diagrams and major element analyses –its relationship with current nomenclature. Chem. Geol., V.29, pp. 183-210.
- Dhoundial, D.P. Paul, D.K. Sarkar Amitabha, Trivedi, J.R. Gopalan, K. and Potts, P.J. (1987): Geochronology and geochemistry of Precambrian granitic rocks of Goa, SW India, precamn. Res., v.36, (287-302).
- Didier, J., (1973): Granites and their Enclaves. Elsevier Scientific Publishing Co., Amsterdam.
- Ebadi, A. and Johannes, W., (1991): Beginning of melting and compositions of first melt in system Qtz-Ab-Or-H₂O-CO₂. Contribution Minerl. Petrol. 106, pp. 286-295.
- El Bouseilly, A.M. and El Sokyary, A.A. (1975): The relation between Rb, Ba and Sr in granite rocks. Chem. Geol., v. 16, pp. 207-219.
- Engel, A.E.J. and Engel, C.G., (1960): Progressive metamorphism and granitization of major paragenesis, northwest adirondock Mountain, N.Y. pp II. Mineralogy, Bull. Geol. Soc. Am. V.71, pp, 1-58.
- Fermor, L.L., (1936): An attempt at the correlation of the ancient schistose formations of Peninsular India. Mem. Geol. Surv. Ind., V.70.

- Floyd, P.A. and Winchester, J.A. (1978): Identification and discrimination of altered and metamorphosed volcanic rocks using immobile elements. *Chem. Geol.* V. 21, pp.291-306
- Foster, M.D., (1960): Interpretation of the composition of trioctahedral micas. *U.S. Geol. Surv. Prof. Pap.* 354-B. 11-46.
- Gillen, C., (1985): *Metamorphic Geology : An introduction to tectonic and metamorphic processes.* London, George Allen & Unwin.
- Goyal, A.N., (1968): – Archaean Protocontinental growth and early Crustal history of the Canadian Shield XXIII International Geological Congress, V. 1. pp. 69-89.
- Goyal and Jain, S.C., R.S., (1972-73): *Geology of parts of Lalitpur district.* U.P. Unpublished progress report, GSI.
- Guidotti, C.V., (1974.) Transition from staurolite to sillimanite zone, Rangeley Quadrangle, Maine. *Bull. Geol. Soc. Am.* V 85, pp 475-490.
- Gupta, A. and Bhattacharya, A., (1991): Correlation of Landsat and Aeromagnetic Lineament systems of parts of the Indian Peninsular Shield and their geodynamic significance. First International Seminar and Exhibition on "Exploration Geophysics in Nineteen Nineties" Extended abstracts.V.I., pp. 41-52.
- Hackett, C.A., (1870): *Geology of Gwalior and vicinity*, *Rec. Geol. Surv. Ind.*, V. III, Pt. 2, pp. 33-62.
- Haldar, D. Ghosh, R.N. Ghosh, D.B. (1981): An Archean mafic-ultramafic suite in the Bargodha – Solda sector. M.P. and U.P. In *Archean of central India* eds. S.K. Banerjee, S.K. Rao and S.V. Choudhary, *Geol. Surv. India. Spl. Pub.No.* 3. pp. 81 – 85.
- Hanson, G.N. (1978): The application of trace elements to the petrogenesis of igneous rocks of granite composition. *Ibid.* pp. 26-43.
- Hanson, G.N. (1980) : Rare earth elements in petrogenetic studies of igneous rocks. *Ann. Rev. Earth Planet. Sci.*, 8, pp. 371-406.
- Harker, A. (1909) : *The natural history of igneous rocks.* Methuen, London, pp. 384.
- Harpur, J.R (1963) : Petrographic classification of granite rocks by partial chemical analysis. *Tanganyika Geol. Surv. Rep.*, v. 10, pp. 80-86.
- Heier, K.S., (1965): *Metamorphism and differentiation of the crust.* *Geol. Foren. Forh.* Stockholm, V.86, pp. 249-256.

- Heier, K.S., and S.R. Taylor, (1959): The distribution of Li, Na, K, Rb, Cs, Pb and Ti in southern Norwegian Precambrian alkali-feldspars: *Geoch. Cosmo. Acta*, v.15, pp. 284-304.
- Hirschberg, A. and Winkler, H.G.F., (1968). Stabilisbeziehungen zwischen Chlorit, Cordierit and Almandin bei der Metamorphose. *Contrib. Mineral. Petrol.*, V18, pp.17-42.
- Holdaway, M.J. and Lee, S.M, (1977): Fe-Mg cordierite stability in high-grade pelitic rocks based on experimental, theoretical and natural observations. *Cont. Min. Pet.*
- Irvine, T.N. and Baragar, W.R.A. (1971) : A guide to the chemical classification of the common volcanic rocks. *Canad. Jour. Earth, Sci.*, v. 8, pp. 523-548.
- Jakes, P. and Gill, J.B., (1970): Rare earth element and the island arc tholiitic series. *Earth planet science. Lett.*9, pp.17-28.
- Jain, S.C. and Goyal, R.S., (1973-74): Geology of parts of Jhansi district. U.P. Unpublished progress report, GSI.
- Jain, S.C. Nair, K.K. and Yedekar, D.B., (1995): tectonic Evolution of the Son-Narmada – Tapti lineament zone. In: *Geoscientific studies of the Son-Narmada – Tapti lineament zone. Geol. Surv. Ind. Spl. Pub.* 10, pp. 188-197.
- Jelinek, E., Soncek, J., Bluck, B.J., Bowers, D.R. and Treloar, P.J., (1980). Nature and significance of Beobachites in the Ballantrac ophiolite, S.W. Scotland. *Trans. Roy. Soc. Edin. Earth Sci.*, V.71, pp150-179.
- Jensen, L.S.,(1976). A new cation plot for classifying subalkalic volcanic rocks. *Ont. Dep. Mines Misc. Paper.*, V66, 22pp.
- Khan, A.U., Bhartiya, S.P. and Kumar, G. (1996): Cross faults in Ganga basin and their surface manifestations. *Geol. Surv. Ind., Spl. Pub.* 21. (2) pp. 215-220.
- Kumar, B., Srivastava, R.K., Jha, D.K., Pant, N.C., Bhandaree, B.K., (1990): A revised stratigraphy of the rocks of type area of the Bijawar Group in Central India. *Ind. Minls.* V.44, No.4, pp. 303-314.
- Jhingran, A.G., (1958): The problem of Bundelkhand Granites and Gneisses : Presidential Address, Section Geology and Geography, 45th. *Ind. Sc. Cong.*, Madras.
- Lameyre, J. and Bowden, P.(1982):Plutonic rock type series: Discrimination of granitoid series and related rocks ,*Jour. volco..Geoth.Res.*, V14, pp169 -186.
- Lal R.K. (1991) Empirical Calibration of the Ti-contents of biotite and muscovite for geothermometry and their application to low to high-grade metamorphic rocks. III Indo Soviet Symp " Experimental Mineralogy and Petrology . New Delhi. P 18

- Leake, B.E., (1978): Nomenclature of amphiboles, *Mineral. Mag.*, V42, pp 533-561.
- Le Bas, M.J. and Streckeisen, A.L., (1991): The IUGS systematics of igneous rocks. *Jour. Geol. Soc.*, London, 148; 825-833.
- LeMaitre, R.W (ed) (1989): A classification of Igneous Rocks and Glossary of Terms (with P.Bateman, A. Dudek, J. Keller et al). Blackwell Scientific Publication, Oxford, 193 pp.
- Macdonald, G.A. & Katsura, T. 1964 : Chemical Composition of Hawaiian lavas. *J.Petrol.* 82-133.
- Mahadevan, T.M., (1994): Deep Continental Structure of India : A Review, *Geol. Soc. India, Mem.* 28.
- Mallet, F.R. (1869): Vindhyan rocks in Bundelkhand. *Mem Geol. Surv. Ind.*, 7.
- Mani, G., (1969): Report on the reconnaissance for phosphorite and systematic mapping of Bijawar group in Sagar and Chhattarpur districts, M.P. Unpublished report, *Geol. Surv. Ind.*
- Mani, G., and Bhattacharya, S.N., (1969-70): Report on the Investigation for copper-ore in Hirapur – Tighara – India area, Sagar, Chhattarpur and Tikamgarh district. U.p. Unpublished Progress report G.S.I.
- Maniar, P.D. and Piccoli, P.M. (1989) : Tectonic discrimination of granitoids. *Geol. Soc. Am. Bull.* v. 101, pp. 635-643
- Martin, H. (1986): Petrogneisses of Archean trondhjemites, tonalite and grandiorities from eastern Finland : Major and trace element geochemistry. *J. Petrol.*V., 28 pp.921-953.
- Martin, H. (1993): The mechanisms of petrogneisses of the Archean continental crust – Comparison with modern processes. *Lithos*, 30, pp 373-388.
- Mathur, P.C., (1954): A note on granitisation of quartzites in Bundelkhand. *Sc. and Cult.*, 20 (5), pp. 242 – 243.
- Mathur, S.M., (1960): A note on the Bijawar series in the eastern party of the type area, Chhattarpur district, M.P. *Rec. Geol. Surv. Ind.*, V.86, pp.539-544.
- Medlicott, H.B. (1859): On the Vidhyan rocks, and their associates in Bundelkhand. *Mem. Geol. Surv. Ind.*, V. II, Pt. 1, pp. 1-95.
- Middlemost, E.A.K. (1985) : The potassic rocks. Their nomenclature, origin and evolution with examples from Australia. IAVCET Scientific Assembly Abst.
- Middlemost, Eric A.K., (1975): Magmas and magmatic rocks. Longman Group Ltd., L.Y. 266p.

- Mishra, D.C., Singh, B., Tiwari, V., Gupta, S.B. and Rao, M.B.S., (2000): Two cases of continental collision and related tectonics during the Proterozoic period in India – insights from gravity modeling constrained by seismic and magnetotelluric studies. *Precambrian Research*, 99, pp.149-169.
- Mishra, R.C., (1948): Hybrid gneisses in Bundelkhand Granites of Mahoba, Hamirpur Dist., U.P: *Proc. 35th Ind. Sc. Cong.* pp.114
- Mishra, R.C. and Mathur, P.C. (1952) Pre-Bundelkhand Granite rocks in Mahoba and Kabrai, Hamirpur U.P. *Proc. 22nd Nat. Acad. Sci. Ind.*
- Mishra, R.C. and Saxena, M.N (1952): Geology of the Kabrai area. *Pro. 22nd Nat. Acad. Sci., Ind., V.22.*
- Mishra, R.C. and Saxena, M.N (1959): A Keratophyre-like rock from Mata Tila Dam site. *Geol.Min.Met. Sc. Ind.* 40(2), pp. 115-119.
- Mishra, S., Deomurari, M.P., Wiedenbeck, M., Goswami. J.N., Ray, S., Saha, A.K., (1998): $^{207}\text{Pb}/^{206}\text{Pb}$ zircon ages and the evolution of the Singbhum Craon, eastern India: an ion microprobe study. *Precambrian Res.* V.93, pp.139-151.
- Mishra, R.C., and Sharma, R. P., (1974): Petrochemistry of Bundelkhand Granites and associated rocks of Central India. *Indian Mineralogist*, V. 15, pp. 43-50.
- Mishra, R.C., (1975): New data on the geology of the Bundelkhand Complex of Central India. *Recent Researches in Geology*, V. II, pp. 311-346, Hindustan Publishing Corpn., India.
- Miyashiro. A & Shido, F., Ewing, M., (1971): Metamorphism in the mid-Atlantic ridge near 24° and 30° N, *Phil Trans Roy Soc London A268*: 589-603.
- Miyashiro. A & Shido, F., (1975): Tholeitic and Calc-alkalic series in relation to the behaviour of titanium, vanadium, chromium and nickel. *Am. J. Sci.* V.275, pp 265-277.
- Miyashiro. A., (1975): Classification, characteristics and origin of ophiolites. *Jour. Geol.* 83, pp 249-281.
- Miyashiro. A., (1978): Nature of alkali volcanic series. *Contrib. Mineral. Petrol.* 66, pp 91-104.
- Mondal, M.E.A., (1995): Petrological and geochemical study of the granite rocks of Bundelkhand massif in the Jhansi, Lalitpur area, U.P., India. Ph.D. thesis, Aligarh Muslim University, Aligarh.

- Mondal, M.E.A., Sharma, K.K., Rahman, A., Goswami, J.N., (1998): Ion microprobe $^{207}\text{Pb}/^{206}\text{Pb}$ zircon ages for the gneisses-granitoids rocks from Bundelkhand massif : Evidence for the Archean components. *Curr. Sci.* V.74, pp70-75.
- Mondal, M.E.A., Zainuddin, S.M., (1996): Evolution of the Archean – Paleoproterozoic Bundelkhand massif, central India-evidence from granitoids geochemistry. *Terra Nova* V.8, pp.532-539.
- Mondal, M.E.A., Zainuddin, S.M., (1997): Geochemical characteristics of the granites of Bundelkhand massif, central India. *Jour. Geol. Soc. India* V.50, pp.69-74.
- Mondal, M.E.A., Goswami, J.N., Deomurari, M.P. and Sharma, K.K. (2002): Ion microprobe $^{207}\text{Pb}/^{206}\text{Pb}$ ages of Zircons from the Bundelkhand massif, northern India, implications for crustal evolution of the Bundelkhand-Aravalli Proto Continent. *Precambrian Research*. V 117, pp 85-110
- Moorbath, S. & R.N. Thompson (eds) 1984. The relative contributions off mantle, oceanic crust and continental crust to magma genesis. *Phil Trans. R. Soc. Lond.* A310, 437-780.
- Moorbath, S., Taylor, P.N. and Jones, N.W. (1986) : Dating the oldest terrestrial rocks – Facts and Fiction. *Chem. Geol.*, v. 57, pp. 63-86
- Moorbath, S., Taylor, P.N. and Jones, N.W. (1986): Dating the oldest terrestrial rocks – Fact and fiction. *Chem. Geol.*, V. 57pp. 63-86.
- Mukherji, A., and Senthappan, M. (1973-74): Geology of the area around Gaurari-Palar-Garhmau, Jhansi dist., U.P. Unpublished Progress Report, G.S.I.
- Mukherji, A., (1973-74): Geology of parts of Kharaha – Maror Area, Jhansi dist. U.P. & Tikagarh dist., M.P. Unpublished Progress Report, G.S.I.
- Mullen, E.D., (1983): $\text{MnO}/\text{TiO}_2/\text{P}_2\text{O}_5$: a minor element discrimination for basaltic rocks of ocean environments and its implication for petrogenesis. *Earth Planet. Sci. Lett.*, V.62, pp. 53-62.
- Nagar, M.H. and Atherton, M.P. (1970): the composition and metamorphic history of some aluminium silicate bearing rocks from the aureoles of the Donegal granites, *Jour. Petrol.* 11, 3, pp. 549-589.
- Nitsch, K.H., (1970): Experimentelle Bestimmung der oberen Stabilitätsgrenze von Stilpnomelan, *Fortschr Mineral* 47, Beiheft, 1; 48-49.
- O'Connor, J.J. (1965) : A classification for the quartz-rich igneous rocks based on feldspar ratios. *U.S. Geol. Surv. Prof. Pap.* pp. 525.

- Pandey, B.K., Chabria, T. and Gupta, J.N., (1995): Geochronological characterization of the Proterozoic terrains of Peninsular India : relevance to the first order target selection for uranium exploration. *Expl. and Res. Atomic Minerals*, V.8, pp. 187-213.
- Pascoe, E.H., (1950): A manual of the Geology of India and Burma. V. I., Geol. Surv. Ind. Calcutta.
- Pati, J.K. and Shukla, R. (1999): the specialized thematic study of older enclaves (Migmatites gneisses and Supracrustals) within the Bundelkhand granitoids complex in Southern U.P. *Geol. Surv. India. Records*, V 132 pp. 132-137.
- Pati, J.K., and Mangain, V. D., (1996): A note on the occurrence of Orbicular Rocks in Bundelkhand Grnaitoid Complex. *Geol. Soc. India*, Vol. 48, pp. 345-348.
- Pati, J.K and Raju, S., (2001): Petrochemistry of pillowed metabasalts from the Bijawar Group, Central India. *Indian Jour. of Geol.* V.73. No. 2. PP 77-92
- Pearce, J.A., Harris, N.B.W. and Tindle, A.G. (1984) : Trace element discrimination diagrams for the tectonic interpretation of granitic rocks. *Jour. Petrol*, v.25, pp. 956-983.
- Pearce, J.A. and Cann, J.R., (1973): Tectonic setting of basic volcanic rocks determined using trace elements analyses. *Earth Planet. Sci. Lett.*, V.99, pp 290-300.
- Pearce, J.A., and Norry, M.J., (1979): Petrogenetic implication of Ti, Zr,Y and Nb variations in volcanic rocks. *Contrib.Mineral. Petrol.*, V. 69,pp. 33-47.
- Pearce, T.H., Gorman, B.E. and Birkett, T.C., (1977): The relationship between major element chemistry and tectonic environment of basic and intermediate volcanic rocks. *Earth Planet Science. Lett.* 36. pp. 121-132.
- Pearce, J.A., Harris, N.B.W. and Tindle, A.G., (1984): Trace Element Discrimination Diagrams for the Tectonic Interpretation of Granite Rocks. *Journal of Petrology*, Vol. 25. Part 4, pp. 256-983.
- Pearce, T.H., Gorman, B.E. and Birkett, T.C.(1975). The TiO_2 - K_2O - P_2O_5 diagram: a method of discriminating between oceanic and non-oceanic basalt. *Earth Planet. Sci. Lett.*, V.24, pp 419-426.
- Prakash, Ravi, Singh, J.N. and Saxena, P.N., (1970): Geology of the pyrophyllite and diaspore deposits of Jhansi dist. U.P., Monograph I, Part I, Directorate of Geology and Mining, U.P., pp. 1-50.

- Prakash, Ravi, Singh, J.N. and Saxena, P.N., (1975): – Geology and mineralization in the southern parts of Bundelkhand in Lalitpur dist., U.P. Jour. Geog. Soc. Ind., V.16(2), pp. 143-156.
- Prasad, M.H., Hakim, A., and Rao, B.K. (1999): Metavolcanic and metasedimentary inclusions in the Bundelkhand Granitic Complex in Tikamgarh District, Madhya Pradesh. Jour. Geol. Soc. Ind., V. 54, pp. 359-368.
- Radhakrishna, B.P. and Naqvi, S.M. (1986) : Precambrian continental crust of India and its evolution. J. Geol., vol. 94, pp. 145-166.
- Radhakrishna, B.P., (1989): Suspected tectono-stratigraphic terrane elements in the Indian Sub-continent. Jour. Geol. Soc. India, V. 34 pp. 1-24.
- Rahman, A. and Zainuddin, S.M. (1993): Bundelkhand Granites : an example of collision related Precambrian magmatism and its relevance to the evolution to the Central Indian Shield. Jour. Geol., V.101, pp. 413-419.
- Ramakrishna, T.S. (1995): A geophysical view of crustal structure along the Jaipur-Raipur transect in continental crust of northwestern and central India. Eds. S.Sinha-Roy and K.R.Gupta, Geol. Soc. Ind., Mem.31, pp.329-343.
- Rankama, K. and Sharma, Th.G (1950) : Geochemistry : The Univ. of Chicago Press, Chicago, Illinois, U.S.A.
- Rao, G.V., (1968): Base Metal Mineralization in Bundelkhand Gneisses in Gwalior and Shivpuri districts. Abstracts; Int. Seminar of Tectonics and Metallogeny of Southeast Asia and Far East, Calcutta. Geog. Surv. Ind. Misc. Pub., No. 34.
- Redman, B.A. and Keays, R.R., (1985): Archean basic volcanism in eastern goldfields province, Yilgarn block, Western Australia, Precambrian Research, 30, pp. 113-152.
- Roday, P.P. and Singh, S, (1998): Palaeostress analysis of heterogeneous fault sets in the Central Indian Bundelkhand Granitoids: separation into homogeneous subsets, stress ratios and comparison with finite strains. In : The Indian Precambrians. Edt. B.S. Paliwal, Scientific Publishers (India), Jodhpur, pp. 44-60.
- Roday, P.P. Diwan, P. and Singh, S., (1995): A kinematic model of emplacement of quartz reef and subsequent deformation pattern in the Central Indian Bundelkhand batholith. Proc. Indian Acad. Sci. (Earth Planet. Sci.), V. 104 (3) pp. 465-488.
- Roday, P.P. Diwan, P. and Singh, S., and Pal, A., (1993): A two-stage model for the development of Karitoan shear zones, Lalitpur district, U.P., Central India. Jour. Geol. Soc. Ind., 42, pp.481-492.

- Roday, P.P. and Maheshwari, G. and Vaghmarey, N.H., (1990): $R_{i-\mu i/\mu m-Ci}$ dependent oblateness of deformed pebbles in Baraitha conglomerate, Central India and tectonic implication. Proc. Ind. Acad. Sci. (Earth Planet Science) V.99, No. 2. pp.321-338.
- Rogers, J.J.W., Callahan, E.J., Dennen, K.O., Fullagar, P.D., Stroh, P.T. and Wood, L.F., (1986): Chemical evolution of Peninsular gneiss in the western Dharwar craton, southern Indian. Jour. Geol., 94, pp. 233-246.
- Rogers, J.J.W., and Greenberg, J.K., (1990): Late-orogenic, Post-orogenic, and Anorogenic Granites : Distinction by Major-Element and Trace-Element and Chemistry and possible origins. The Jour. Of Geol., V. 98, 3, pp 291-310.
- Rollinson, H.R., Windley, B.F., Ramakrishnan, M. (1981): Contrasting high and intermediate pressure of metamorphism in the Archean Sagur schists of south India. Cont. Min. Tetrol. 72, pp. 265-281.
- Rudnick, R.L. and Taylor, S.R. (1986): Geochemical Constraints on the Origin of Archean Tonalitic – trondhjemitic Rocks and Implication for Lower Crustal Composition. In : J.B. Dawson D.A. Carswell, J. Illall and K.H. Wedepohl (eds.), The Nature of the Lower Continental Crust. Geol. Soc. Publ., V. 24 pp. 179-191.
- Sarkar, A. Trivedi, J.R. Gopalan, K. Singh, P.N. Das, A.K. and Paul, D.K. (1984): Rb/Sr geochronology of Bundelkhand granitic complex in the Jhansi – Babina-Talbehat Sector. U.P.; CEISM seminar volume, Indian J. Earth. Sci., .pp 64-72.
- Sarkar, A., Bhalla, J.K., Paul, D.K. Potts, P.J., Bishni, P.K., Gupta, S.N. and Srimal, N (1989): Geochemistry and geochronology of the early Proterozoic Bundelkhand granitic complex, Centralm India. Symp. Precamb. Granitoids, Helsinki, Finland, Geol. Surv. Finland, Spl. Paper 8. pp 117.
- Sarkar, A., Paul, D.K. and Potts, P.J. (1996): Geochronology and geochemistry of the Mid-Archaeon trondhjemitic gneisses from the Bundelkhand craton, Central India. Recent Researches in Geology, v.16, Ed. A.K. Saha, pp 76-92.
- Sarkar, A., (1997): Geochronology of mafic dykes from the Bundelkhand Craton, Central India; Abs., International Conference on Isotopes in the solar system, P.R.L. Ahmedabad, pp.98-99.
- Sarkar, A., Sarkar, G., Paul, D.K. and Mitra, N.D (1990): Precambrian geochronology of the central Indian Shield- A review. Geol. Surv. India, Spec. Publ. no. 28, pp 453-482.

- Sarkar, Amitabha, Bhalla, J.K., Bishui, P.K., Gupta, S.N., Singhai, R.K. and Upadhyay, T.P. (1995): Tectonic discrimination of granite rocks : Situation on the Early Proterozoic Bundelkhand complex, Central India. Ind., Minerals.
- Saxena, M.N., (1957): – Structural study of Bundelkhand granites and associates rocks. Indian Mining Journal, V. 5, p. 9.
- Saxena, M.N., (1961): Bundelkhand granites and associated rocks from Kabrai and Mau Ranipur areas of Hamirpur and Jhansidist., India, Res. Bull. Punj. University, 12 (I &II): 85-107.
- Shapiro, L., and W.W. Brannock, (1962): U.S. Geological Survey Bulletin, 1144A.
- Sharma, K. K, (1998): geological evolution and crustal growth of the Bundelkhand craton and its relict in the surroundings regions, Northern Indian Shield. In : The Indian Precambrian. Ed. B.S. Paliwal, Scientific Publishers (India), Jodhpur, pp. 33-43.
- Sharma, K.K. and Rahman, A., (1995): Occurrence and petrogenesis of the Loda Pahar trochjemitic gneiss from Bundelkhand craton, central India: Remnant of an early crust. Curr. Sci., V.69, pp.613-617.
- Sharma, K.K. and Rahman, A., (1996): Bundelkhand craton, Northern India Shield Geochemistry, petrogenesis and tectonomagmatic environments. Deep Continental Studies News Letter, DST, New Delhi, V. 6, pp12-19
- Sharma, K.K., (2000): Evolution of Archean Palaeoproterozoic Crust of the Bundelkhand Craton, Northern Indian Shield. Research Highlights in Earth System Science. DST's Spl. V.1, (Eds. O.P Verma and T.M. Mahadevan) Indian Geological Congress, pp.95-105
- Sharma, R.P., (1982): Lithostratigraphy, structure and petrology of the Bundelkhand group. In: Geology of Vindhyanchal, Eds. K.S. Valdia, Bhatia, S.b. and Gaur V.K., pp. 30-46.
- Sharma, R.S., (1988). Patterns of metamorphism in the Precambrian rocks of the Aravalli Mountain Belt. In Precambrian of the Aravalli Mountain, Rajasthan, India; (ed.) A.B. Roy., Mem. Geol. Soc. India, v.7, pp 33-75.
- Shastri, V.V., Bhabdari, L.L. Raju, T.R., and Datta, A.K., (1971): Tectonic framework and subsurface stratigraphy of the Ganga Basin : Jour. Geol. Soc. Ind. V. 12, No. 3.
- Shaw, D.M., (1968): A review of K/Rb fractionation trends by covariance analysis. Geochim, Cosmochim. Acta., V 32 ,pp. 573-602.
- Shaw, H.R., (1965): Comment of viscosity, crystal setting and convection in granitic magmas. Am. J.Sci., V.263, pp120-152.

- Shukla, R. and Pati, J.K. (1999): The specialized Thematic study of older enclaves (migmatites gneiss and supracrustals) within the Bundelkhand granitoid complex in southern U.P. *Geol. Ind. Records*, V. 132. pp. 132-136.
- Singh, V.P. and Kumar, (1970): A report on the preliminary geological investigation of the calcite deposits of Khajraha in Jhansi district. Directorate of Geology and Mining, U.P. (Unpublished).
- Sinha-Roy, S.; Gupta, K.R., (1995): Continental crust of Northwestern and Central India. *Geol. Soc. India, Mem.* 31.
- Spear, F.S., Selverstone, J., Heckmott, D. Crowleg, P. and Hodges, K.V. (1981) P-T path from garnet zonig. A new technique for deciphering tectonic processes in crystalline terrains, *Geology* V.12, pp.87-90.
- Spray, A., (1969): *Metamorphic textures*, Pergamon press, Oxford.
- Srivastava, K.K., (1970-71): The Geology around Babina, Jhansi dist., U.P. Unpublished Progress Report, G.S.I.
- Streckeisen, A.L. (1967) : Classification and nomenclature of igneous rocks. *Neues. Jahr. Mineral. Abhandl*, v. 107, pp. 144-240.
- Tarney, J., Wood, D.A., Saunders, A.D., Varet, J. and Cann, J.R., (1979): Nature of mantle heterogeneity in the North Atlantic : evidence from Leg 49. In : M. Talwani (Editor). *Results of Deep Sea Drilling in the Atlantic. Maurice Ewing Series. 2.* American Geophysical Union. pp 285-301.
- Taylor, R.G. (1979) : *Geology of tin deposits, Developments in Economic Geology-11.* Elsevier Scientific Publishing Company, Amsterdam. 543p.
- Taylor, S.R. and McLennan, S.M., (1985): *The Continental Crust: Its Composition and Evolution.* Blackwell, Oxford, 312pp.
- Taylor, S.R., Emelens, C.H. and Exley, C.S., (1956): Some anomalous K/Rb ratio in igneous rocks and their petrological significance : *Geochim. Cosmochim. Acta*, V.10, pp. 224-229.
- Taylor, S.R., Heier, K.S. and Sverdrup, P.L. (1960) : Contribution to the mineralogy of Norway. No. 5. Trace element variations in three generations of feldspars from Landsverk I Pegmatite, Evje, Southern Norway, *Norsk. Geol. Tidsskr.* v. 40, pp. 135-156.
- Thompson, A.B., (1982): Dehydration melting of pelitic rocks and generation of H₂O undersaturated granitic liquid. *American Jour. Sci.*, V.282, pp.15657-1595.

- Valdiya, K. S. (1982); Tectonic perspective of the Vindhyaachal region. In;Valdiya, K. S.,et.al. Eds. Geology of Vindhyaachal, Hindustan Publishing Corporation, India, pp.148-161.
- Valley, J.W., Bohlen, S.R., Essene, E. & Lamb, W., (1990): Metamorphism in the Adirondock II. The role of fluids. Jour. Petrol. 31.
- Verma, R.K. and Banerjee P., (1992): Nature of the continental Crust along the Son-Narmada Lineament inferred from gravity and deep seismic sound data. Tectonophysics, V.202, pp. 375-397.
- Viljoen, M.J. and Viljoen, R.P., (1970): The geochemical evolution of the granite rocks of the Barberton region. Geological Soc. S. Africa, Sp. Pub. No. 2, pp. 189-219.
- Whitehead, R.F.S. & Goodfellow, W.D. (1978): Geochem of volcanic rocks from the Tatagouche Group Bathurst New Brunswick. Canada. Can J. Earth, Sci. V.15, pp207-219.
- Whitney, J.A., (1975): The effects of pressure, temperature, and H₂O on phase assemblage in four synthetic compositions. J. Geology, V. 83, pp1-31.
- Wilson, A.F, (1873-74): Progress report of mapping in Central India. Unpublished report, Geol. Surv. India.
- Wilson, M., (1989): Igneous petrology : Aglobal tectonic approach. Chapman & Hall, Madras.
- Wilson, M., (1997): Igneous Petrogenesis. Chapman & Hall.
- Winchester, J.A. and Floyd, P.A. (1977): Geochemical discrimination of different magma series and their differentiation products using immobile elements. Chem. Geol V. 26, pp.325-344.
- Windley, B.F. (1983): Metamorphism and tectonic of the Himalaya. Jour. Geol. Soc., London, 140, pp 849-865.
- Winkler, H.G.F, (1976): Petrogenesis of metamorphic rocks (4th ed.). Springer Verlag., N.Y.
- Winkler, H.G.F, (1979): Petrogenesis of metamorphic rocks (3rd ed.), Springer, 348.
- Yedekar, D.B. Jain, S.C., Nair, K.K. and Dutta, K.K., (1990): The Central Indian Collision Suture. In, Precambrian of central India. Geol. Surv. Ind. Sp. Pub., 28.
- Yedekar, D.B., Reddy, P.R, and Divakar Rao, V., (2000): Deep Continental Studies in Central India. Ind. Geol. Cong., pp. 50-75.
- Zainuddin, S.M, Rahman, A. and Mondal, M.E.A (1992): Geochemical fingerprints of Bundelkhand granites as an indicator of minor Indian plate collision during

Precambrian. In : Geology in South Asia-1, Eds. R. Ahmad and A.M. Sheikh, pp. 161-168.

Zainuddin, S.M, Rahman, A. and Mondal, M.E.A (1992): Tectonic evolution of Bundelkhand granite and its implication to paleoplate configuration. Abs. First South Asia Geol.Cong., Islamabad , Pakistan.